Universitat Autònoma de Barcelona

Carbon export from the upper water column of the polar oceans by using natural radionuclides

Montserrat Roca Martí

Carbon export from the upper water column of the polar oceans by using natural radionuclides

Montserrat Roca Martí

Tesi doctoral 2017

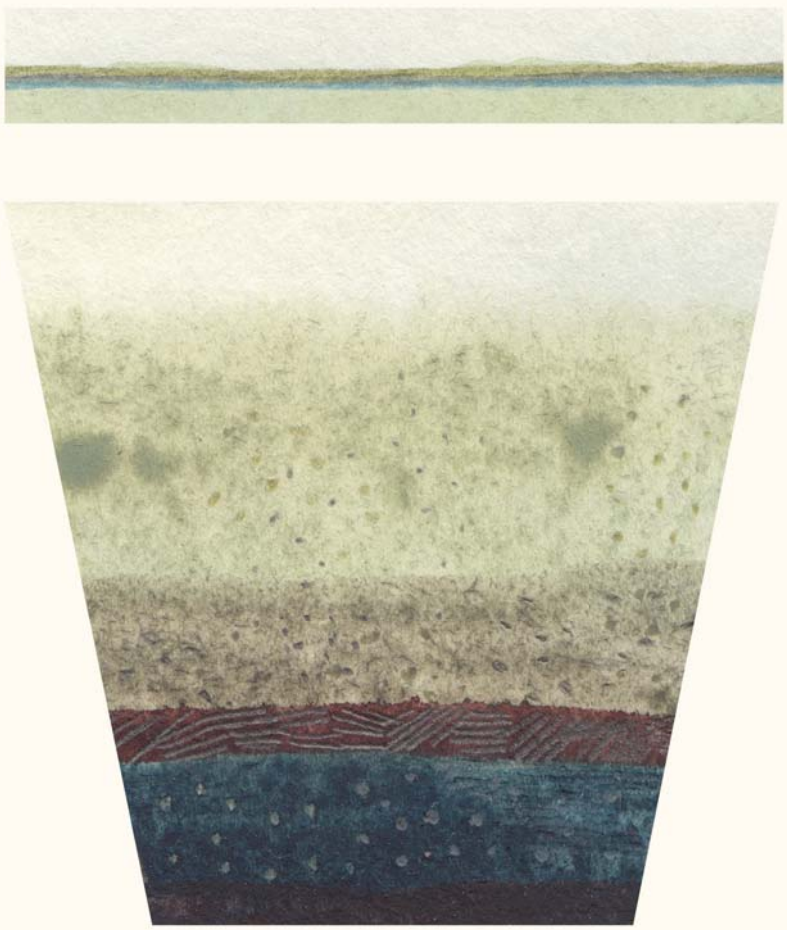

Director
Dr. Pere Masqué Barri

Universitat Autònoma de Barcelona
Institut de Ciència i Tecnologia Ambientals

UNIVERSITAT AUTÒNOMA DE BARCELONA

INSTITUT DE CIÈNCIA I TECNOLOGIA AMBIENTALS

Carbon export from the upper water column of the polar oceans by using natural radionuclides

Montserrat Roca Martí

TESI DOCTORAL

Doctorat en Ciència i Tecnologia Ambientals

Juny 2017

Director:

Dr. Pere Masqué Barri

Aquesta tesi doctoral ha estat finançada mitjançant una beca del Programa de Formación de Profesorado Universitario (FPU) del Ministerio de Educación (AP2010-2510), des del desembre de 2011 fins al desembre de 2015 i de fons del grup de recerca consolidat MERS (2014 SGR-1356) de la Generalitat de Catalunya i del Laboratori de Radioactivitat Ambiental de la Universitat Autònoma de Barcelona. Així mateix, la recerca que es presenta s'ha realitzat en el marc dels següents projectes d'investigació:

- Export and remineralization rates of particulate organic carbon in Southern Ocean eddies (Eddy Pump). Ministerio de Ciencia e Innovación (CTM2011-14027-E).
- Carbon export from the upper water column under different sea-ice regimes in the Arctic Ocean (CARICE). Ministerio de Ciencia e Innovación (CTM2011-28452).
- IPY-GEOTRACES in the Arctic Ocean: Radionuclides as tracers of the role of sea ice in the transport, dispersion and accumulation of particulate material and associated species in the Arctic Ocean. Ministerio de Educación y Ciencia (POL2006-00449).

Coberta dissenyada per Pau Gasol

S'alça un sol rogenc,
llença un crit al vent
i ens desperta en les nits
arraulits vora el mar.
Un futur incert
repta un cor valent,
contemplant orenetes
que passen volant.

Iceberg, Nòmades

Agraïments

Sou moltes les persones amb qui m'he creuat en el transcurs d'aquests cinc anys i escaig de doctorat. Amb vosaltres he compartit una infinitat d'hores a la universitat, a alta mar, a països estrangers o breus estones en algun racó de món. Al vostre costat he viscut moments inoblidables que n'estic segura que m'acompanyaran d'ara endavant i molt sovint em dibuixaran un somriure. Totes m'heu ajudat a escriure aquestes línies ara i aquí. Us estic profundament agraïda!

Els culpables que han fet possible el meu pas pel Laboratori de Radioactivitat Ambiental sou vosaltres Pere i Jordi. Mil gràcies per la vostra confiança i recolzament en tot moment, per haver-me donat totes les eines que teníeu a l'abast i sobretot per fer-me descobrir aquest món tan apassionant de l'oceanografia. Pere, sempre recordaré la conversa que vam tenir abans de començar mentre li preparaves l'arròs bullit a la Mekdi... qui ho havia de dir on acabaria desembocant! Moltes gràcies per donar-me aquesta oportunitat amb lletres majúscules. Gràcies també per rebre'm per segona vegada a l'ECU, ens tornem a veure a l'octubre! Jordi, ja fa uns quants anys de la xerrada que vam tenir al banc de davant de la peixera quan encara feia Ciències Ambientals en la que vas obrir-me les portes del laboratori, moltes gràcies! Gràcies pel teu suport i per generar un ambient de feina tan bo. Ha sigut divertit treballar amb música de fons de *era una chica muy mona que vivía en Barcelona*... i amb dies de *team building* alguns en forma de barbacoa i picanya a casa teva.

Companys i amics del LRA, com diria el Quim Masferrer, sou molt bona gent! Ha sigut un autèntic plaer treballar amb tots i cadascun de vosaltres. Joan Manuel, moltes gràcies per haver tingut la paciència d'ensenyar-me com funcionava el laboratori (quan encara estàveu a la quarta planta), quan la destresa amb pipetes i vasos de precipitats encara no m'acompanyava. Gràcies per haver-me donat tants cops de mà, per endolcir els divendres amb els *Gordi Fridays* i pels bons moments lluny de la UAB acompanyats de *Little Creatures*, *banksias* i *kookaburras*. Núria, vam coincidir poc temps al laboratori però la teva energia encomanadissa em va enamorar des d'un bon principi! Gràcies pels consells, pel cap de setmana a Zürich i per aguantar els tan repetits *Thank you Chairman* de New Orleans i *marinòlegs* d'Heraklion! Patricia, gràcies pel suport dels primers dies amb el full de càlcul de Po/Pb en aigua i pel curset accelerat de "què has de saber abans d'embarcar-te al Polarstern". Viena, se'm fa difícil posar ordre a totes les aventures que hem passat juntes, diria que gairebé ha sigut una pel·lícula d'acció! Han estat un total de 6 mesos compartits navegant pels oceans polars amb tot el que això comporta: milers de litres d'aigua de mostres, trepitjar gel marí i el continent glaçat, albatros, pingüins i óssos, *Zillertals*, BBQ's a coberta, atac babuí, rescat amb amfibi militar i un llarg etcètera. Gràcies per haver-me ensenyat tot el que sé i per ser-hi sempre! Em fa molta il·lusió que ens retrobem a l'octubre i que les aventures de *Zipi* i *Zape* continuïn.

Valentí, tens un positivisme que s'enganxa! Gràcies pel teu humor, pels moments de *fotris* compartits i per haver fet del despatx més que un lloc de feina. Espero que et deixis veure el pèl sovint! Teresa, que ja quasi ho tenim! Deixa marge per agafar el vol de tornada a terres angleses que hem de celebrar-ho juntes a l'estil Hernani. Giada, vas arribar més tard que jo i ja ets doctora des de fa dies, ets una crac! M'ha agradat molt compartir aquests anys amb tu. Encara somnio amb aquells croissants farcits de crema de pistatxo i xocolata negra de la Puglia... vas ser una amfitriona genial! Maxi, el teu pas pel LRA no ha estat pas discret i els teus *Aupa Ekipo* i *power* m'han animat i m'han fet riure en molts moments. Gràcies per ser com ets! Vam fer un bon tàndem a la campanya MedSeA. El trajecte en furgoneta UAB-Cádiz fent nit a Sangonera la Seca ja prometia... Gràcies també per acollir-nos a Euskadi, va estar molt i molt bé! Vinga, una empenta més i ho celebrem amb uns bons *txotx*! Almu, t'escric en català perquè ja ets tota una experta dels pronoms febles. Has aportat al grup aquella *xispa* que només podia venir d'una tia amb sabor andalús com tu! Gràcies per les abraçades de la més mimosa del grup (però sense bata, eh!) i per convidar-nos a Huelva aquest estiu, ara sí que sí, quines ganes! Ester, ets un gran exemple d'esforç i dedicació. Però, a més, gràcies a tu hem anat de *bodorrio* junts i els teus apunts dels *musts* de Cabo de Gata m'han portat a l'autèntic Bar de Jo, gràcies! Ari, sóc fan del turbo que portes dins! Gràcies per traspuar energia i ganes de fer coses a tota hora. Espero que ens en quedin moltes per fer. Sarah, gràcies per la teva ajuda amb les mostres de Geovide quan vas entrar, per estar sempre pendent de tot i pel teu suport en aquesta recta final en forma d'ànims i subministrament de xiclets. Gràcies als jovenets del grup, Marc i Aaron, quin amor! Que duri l'entusiasme i gaudiu molt del temps que teniu per endavant al LRA. Durant aquests anys molts d'altres heu passat una temporada al LRA o heu vingut a visitar-nos. Pepe Mas, muchas gracias por tu espontaneidad y por tu apoyo en distintas fases de la tesis. Carolina, no m'hagués cregut que faria classe amb la meva professora de problemes de Física de les Radiacions, va ser un plaer! A més, sospito que tens part de culpa que a hores d'ara estigui escrivint aquests agraïments... gràcies! Alba, no saps com m'has ajudat amb els teus trucs del Word, moltes gràcies, aquesta tesi també és teva! Marta, Esther, Xènia, Marc Cerdà, Mercè, Tania i Diana gràcies pels moments compartits.

Vull agrair el suport dels companys d'unitat de l'ala nord i del personal de l'administració de l'ICTA. Gràcies al Manel per estar sempre disposat a muntar invents, al Pedro i al Jose del servei d'informàtica, a la Dra. Núria per l'ajuda amb els informes mèdics de les campanyes i al Chuck, del servei de llengües, per fer-me adonar que no puc posposar més el curs de submarinisme. Gràcies també al Jordi Mompart per llançar-me dosis de bon rotllo quan topem pel passadís i al Jordi de la pizzeria per alegrar-nos els divendres.

Michiel you deserve a very special thank you. I really appreciate your support since the very beginning and in every important step in my PhD. I feel very fortunate to have participated in two Polarstern cruises (with a fully equipped container on board!) and worked for about three months at AWI. You have always been an excellent supervisor and co-worker. Your countless comments on every manuscript and conference contribution have made a big difference in the final result. Ingrid, I am very grateful to you for your kind assistance with the cruises preparation and ICP-MS analyses. There is not enough *pa amb tomàquet i pernil* to compensate all your efforts! Thanks also to all the other members of the Geochemistry group, flatmates from the AWI guesthouse in Bürgermeister-Smidt-Straße and visitors to make the time spent in Bremerhaven much more enjoyable. Danke sehr!

I sincerely acknowledge the crew and scientific party of the R/V Polarstern ANT-XXVIII/3, R/V Polarstern ARK-XXVII/3, B/O Ángeles Alvariño MedSeA and R/V Aurora Australis Voyage 2 for the support at sea and for creating an amazing atmosphere during the expeditions. Special thanks to the in situ pump guys, Matt Donnelly, Daniel and Matt Corkill, for your help with the deployment of the pumps. My first PhD experience, sailing from Cape Town to Punta Arenas stopping in South Georgia in such a multidisciplinary cruise, could not have been better. It was the first time I saw a CTD rosette, sediment traps, amphipods, deep-sea sponges and foraminifera, and I worked in a floating laboratory. I learnt a lot from all of you, thank you! Thanks also to the Red Mafia for the awesome time spent together. This same year, during the IceArc cruise I met the white of the Arctic. I am grateful to all the people that helped Viena and me in taking so many ice cores. Charlie, Marie it was nice to work together! Thanks for your help with the under ice and aerosol sampling, and for your kindness that brought me at your place two years later. It was great to spend some time between sediment, seawater, ice and precipitation samples in the *Zillertal* with Karl, JP, Daniel, Xiaotong, Eva, Carmen, Mar, Raquel and many others. I also want to thank the helicopter team to let me enjoy the Arctic beauty from the sky. Un año más tarde tuve la suerte de participar en una campaña en nuestro mar, el Mediterráneo. Muchas gracias a todos los tripulantes por ser tan accesibles y por hacernos sentir como en casa desde el primer día. Gracias a los cocineros por cargarnos de energía de la buena y a Miguel y a los de máquinas por compartir vuestra manera de ver las cosas y las experiencias vividas en el mar. Thanks also to the small family of scientists on board B/O Ángeles Alvariño for the great team we built and for those moments of dancing in the lab and on the bow. Finally, a few months ago I had the unique opportunity to participate in a Southern Ocean expedition, but this time further south reaching Antarctica by Christmas time. My deepest thanks to the biogeochemistry team, the best people I have ever worked with on board: Delphine, Seb, Julie, Lavy, Mar, Cristina, Matt and Viena. Thanks also to the CTD team, support staff and watercraft operators for all your support even bringing us cups of tea during the long nights of filtration. I would like to express my gratitude to King Neptune and

associates to consider myself worthy of exploring the southern waters. Rick thanks for your daily smiles and kind words. Andy and Margie thanks for let us discover the Tasmanian version of paella and for fully equipping us for our journey to Maria Island. Jay and Lavy thanks for offering your place and delicious food while in Hobart.

Thank you very much to all the co-authors: Morten, Christine, Wee, Astrid, Christian, Mar, Ilka, Jana, Ben, Meri, Patricia, Viena, Michiel, Jordi and Pere. Thanks for sharing your knowledge with me. Without you this thesis would not have been possible. Clara, Volker, Dieter, Mariana, Catherine, Carmen, Haucke, Eva-Maria, Marcel and Dorothea, many thanks for providing valuable comments on earlier drafts. I would also like to thank the crew of the R/V Polarstern ARK-XXII/2 and the scientists on board for their cooperation. I especially acknowledge the hard work of Oliver Lechtenfeld for collecting and processing the ^{210}Pb and ^{210}Po samples on board.

Thanks Sylvain, Rachel and Viena for providing me the opportunity to collaborate in your own works, widening my research experience in the use of natural radionuclides as tools for studying ocean-related processes.

Lluís Camarero i col·laboradors us vull agrair l'oportunitat que m'heu donat per treballar en un àmbit completament diferent, els llacs d'alta muntanya. Gràcies per haver-me transmès la vostra passió per la feina i l'entorn i per haver-me rebut amb els braços oberts tant a Senet com al Centre de Recerca d'Alta Muntanya.

Família Masqué Salgado, gràcies per acollir-me a Perth i per les estones de platja, cangurs, dutxes al jardí després d'anar a córrer i les teves delícies Gloria. Em va agradar tant l'experiència que ben aviat em tornareu a tenir per aquí baix. Thanks also to the colleagues from the School of Science and Centre for Marine Ecosystems Research of the Edith Cowan University for hosting me on my Endeavour Fellowship programme. I look very forward to working with you.

Finalment, m'agradaria agrair el suport incondicional del meu entorn més enllà de l'àmbit laboral. Als Nòmades us vull donar les gràcies per ser la banda sonora d'aquesta tesi i per les estones compartides. Hi ha algun testimoni que afirma haver sentit cantar a *grito pelado* les vostres cançons des del despatx C3/348 a altes hores de la jornada laboral... I als altres amics de Ciències Ambientals, Elisa, Raquel, Carla, Marta, Sandra, Núria, Ander... encara que no ens veiem tant com voldríem gràcies per fer-vos sentir tan a prop. Gràcies també als amics de Sentmenat, Cal Camilo i la Trama. Marina i mama II, gràcies per ser-hi sempre, us estimo molt! Moltes gràcies a tota la meva família: del Vallès, del Bages, de la Selva, del Maresme i més enllà.

Papa i mama gràcies pel vostre recolzament en cada pas. Vaig començar aquest camí sota el mateix sostre que vosaltres amb *tupper* sota el braç i encara que ara no ens veiem tan sovint (tot i que els dijous no fallen!) us tinc presents en tot moment. Gràcies per ser els millors pares que podia tenir. A les meves germanetes, Raquel i Mònica, i cunyats, Marc i Pep, gràcies per ser l'hòstia i haver fet tanta feina i tan ben feta durant aquests anys, la Gala, el Jofre, l'Estel i l'Ariadna.

I per últim, Narcís, m'has acompanyat des del principi de l'aventura després d'aquelles vacances al Camí de Cavalls quan vas decidir construir un caiac de fusta que, avui, estem a punt d'estrenar. Gràcies per fer-me sempre costat i fer-ho tot tan fàcil. Gràcies per la teva paciència quan he desaparegut del mapa i he sigut xicota de mitja jornada. Gràcies per fer-me veure el futur amb optimisme, encomanar-me les ganes de fer coses i fer-me feliç. Menorca ens espera i com diria *Mishima* tot torna a començar.

Table of contents

List of figures

List of tables

List of acronyms

ACC	Antarctic Circumpolar Current
APF	Antarctic Polar Front
AW	Atlantic Water
Chl-a	chlorophyll *a*
CTD	conductivity-temperature-depth
DIC	dissolved inorganic carbon
E_Z	euphotic zone
HPLC	high-performance liquid chromatography
ICP-MS	inductively coupled plasma-mass spectrometry
ICP-OES	inductively coupled plasma-optical emission spectrometry
IPY	International Polar Year
ISP	in situ pump
LHC	lower halocline
MLD	mixed layer depth
NPP	net primary production
NSS	non-steady state
PAR	photosynthetically active radiation
PML	polar mixed layer
POC	particulate organic carbon
PON	particulate organic nitrogen
PPZ	primary production zone
PW	Pacific Water
SIS	sea-ice sediments
SPF	Southern Polar Front
SS	steady state
ST	sediment trap
TPheo	total pheopigments
UHC	upper halocline
WMLD	winter mixed layer depth
WW	winter water

Preface

The polar oceans, the Arctic and Southern Oceans, have a major role in the Earth's energy budget and are important sinks for atmospheric carbon dioxide (CO_2), accounting together for about 20 to 35% of the global oceanic uptake [*Takahashi et al.*, 2002; *Bates and Mathis*, 2009; *Gruber et al.*, 2009]. This carbon uptake is caused by surface-water cooling, subduction, deep water formation and the biological pump, which transforms CO_2 into organic matter in surface waters and pumps a fraction of it to the deep ocean [*Wassmann et al.*, 2004; *Bates and Mathis*, 2009; *Hauck et al.*, 2013]. Both oceans are undergoing accelerated changes in response to global warming, with uncertain implications for the export of carbon to deep waters [*Reid et al.*, 2009]. A major challenge to polar research is to predict how climate change will affect the marine ecosystem functioning and the carbon uptake at high latitudes, as underlined by the International Arctic Science Committee (IASC) and the Scientific Committee on Antarctic Research (SCAR). Besides the physical processes, the efficiency of the biologically-mediated sequestration of atmospheric CO_2 and the processes involved are not well understood [*Buesseler and Boyd*, 2009]. This is especially the case of the Arctic and Southern Oceans, which are the less explored waters of the planet partly due to the logistical difficulties imposed by the sea-ice and snow covers.

The scientific community has made considerable observational efforts in the Arctic and Southern Oceans during the last decade, which are clearly illustrated by the International Polar Year 2007-2008 (IPY) [*http://www.ipy.org/*]. The IPY consisted of an extensive programme that performed multidisciplinary research in the polar oceans with an unprecedented spatial coverage involving tens of thousands of scientists all over the world. Another example is the international programme GEOTRACES [*http://www.geotraces.org/*], which has conducted more than twenty polar expeditions since 2006 with the aim to improve the knowledge of the biogeochemical cycles of trace elements and isotopes in the marine environment. Furthermore, a new fleet of research icebreakers equipped with advanced technology is underway, which shall enhance multidisciplinary polar research in the near term.

The disequilibrium in seawater between the radionuclide pairs, $^{234}Th/^{238}U$ and $^{210}Po/^{210}Pb$, which belong to the natural ^{238}U decay chain, are used to study the export of particulate organic carbon (POC) in the water column since the 1990s [see reviews by *Cochran and Masqué*, 2003; *Buesseler et al.,* 2006; *Verdeny et al.*, 2009]. These tracers allow quantifying particle export fluxes at high spatial resolution over time scales of weeks to months, respectively, which are of special interest to follow the development of phytoplankton blooms and obtain estimates of seasonal export of carbon.

Relevant information on the nature of the POC fluxes and the processes that play a role in shaping the biological pump can be obtained using complementary techniques (e.g. sediment traps) and the analysis of ecologically relevant parameters (e.g. primary production and plankton community composition).

The limited baseline data on ecosystem dynamics in the Arctic and Southern Oceans, the rapid impacts of climate change on polar marine systems, together with their relevance within the global carbon cycle, have motivated this thesis. This work represents an attempt to contribute to the knowledge of the particle and carbon export fluxes driven by the biological pump in the polar oceans, as well as the processes that control these fluxes in the upper water column.

Thesis structure

This dissertation is structured into six chapters:

Chapter 1 is a general introduction to the topic of the biological pump and the polar oceans. First, the role of the global ocean as a carbon sink is described with reference to the different pathways that drive the uptake of atmospheric carbon dioxide. Second, the functioning of the biological pump and the main mechanisms that control the transport of particulate organic carbon (POC) from surface to deep waters are presented. Third, the general characteristics of the Southern and Arctic Oceans are described in terms of circulation, sea-ice conditions, nutrient regime, primary and export production and recent changes observed. Finally, a brief overview of the methods that are used to measure the export of POC in the water column is provided, with a special focus on the disequilibrium between the natural radionuclide pairs $^{234}Th/^{238}U$ and $^{210}Po/^{210}Pb$ as proxies for POC export.

Chapter 2 is devoted to describing the methods used for the determination of the core of the data presented in this thesis, namely ^{238}U, ^{234}Th, ^{210}Pb, ^{210}Po and POC in seawater and marine particles collected using sediment traps, in situ pumps and Niskin bottles. This includes the details on the collection and handling of the samples and the analytical and measurement techniques performed on board and at the home laboratories. Specific procedures for ancillary data used in each of the individual studies (Chapters 3-5) are found in the methods section of the respective chapters.

In **Chapter 3** the export and transfer efficiency of POC in the upper water column is evaluated under the decline of a vast diatom bloom developed in the Atlantic sector of the Southern Ocean in summer 2012. The POC export was measured by using the $^{234}Th/^{238}U$ proxy and sediment traps during three weeks at high spatial resolution. The results are compared to other phytoplankton blooms (natural and iron-fertilized) occurred in the Southern Ocean and discussed together with data on chlorophyll *a*, POC and net primary production (NPP) in the upper water column and pigments in sinking particles. This study was published in Deep Sea Research II in 2017 (online in 2015)[1].

Chapter 4 is dedicated to estimate the export of POC and its relation to NPP in the central Arctic during the record sea-ice minimum in 2012 by using both the $^{234}Th/^{238}U$ and $^{210}Po/^{210}Pb$ pairs. The phytoplankton community structure, sea-ice conditions and information on particle export and composition obtained during the same expedition from sediment traps and imaging techniques are used to interpret the POC export estimates. A compilation of radionuclide-derived export data

from the Arctic Ocean is presented to contextualize the results. This work was published in Journal of Geophysical Research in 2016[2].

Chapter 5 is a pan-Arctic study of the distribution of ^{210}Pb and ^{210}Po in the water column of the Arctic Ocean during the 2007 sea-ice minimum. The data on total and particulate fractions of both radionuclides are discussed in parallel to the hydrography, seasonal primary production and other physical and biological parameters and export production estimates reported in previous works. This study has been recently submitted for publication to Deep Sea Research I[3].

Chapter 6 summarizes the most significant conclusions of this dissertation and suggests research directions for further understanding of the biological pump in the polar oceans in the present and future scenarios.

---

[1] Roca-Martí, M., Puigcorbé, V., Iversen, M.H., Rutgers van der Loeff, M., Klaas, C., Cheah, W., Bracher, A., Masqué, P (2017). High particulate organic carbon export during the decline of a vast diatom bloom in the Atlantic sector of the Southern Ocean. *Deep Sea Research Part II: Topical Studies in Oceanography*, 138, 102-115. doi: 10.1016/j.dsr2.2015.12.007.

[2] Roca-Martí, M., Puigcorbé, V., Rutgers van der Loeff, M., Katlein, C., Fernández-Méndez, M., Peeken, I., Masqué, P (2016). Carbon export fluxes and export efficiency in the central Arctic during the record sea-ice minimum in 2012: a joint ^{234}Th/^{238}U and ^{210}Po/^{210}Pb study. *Journal of Geophysical Research: Oceans*, 121, 5030-5049. doi: 10.1002/2016JC011816.

[3] Roca-Martí, M., Puigcorbé, V., Friedrich, J., Rutgers van der Loeff, M., Rabe, B., Korhonen, M., Cámara-Mor, P., Garcia-Orellana, J., Masqué, P. Distribution of ^{210}Pb and ^{210}Po in the Arctic water column during the 2007 sea-ice minimum: particle export in the ice-covered basins. Submitted to *Deep Sea Research Part I: Oceanographic Research Papers.*

Chapter 1

Introduction and objectives

1.1 The ocean carbon sink

Atmospheric concentrations of the greenhouse gases carbon dioxide (CO_2), methane (CH_4), and nitrous oxide (N_2O) have all dramatically increased since 1860, after the advent of the Industrial Revolution, leading to global warming [*IPCC*, 2013]. CO_2 emissions from fossil-fuel combustion, cement production and anthropogenic land-use change (e.g. deforestation) are the largest contributors to human-induced climate change, with average emissions of 9.2 Pg C yr^{-1} between 2002 and 2011 (Figure 1.1) [*IPCC*, 2013]. The ocean has constituted a net sink for anthropogenic CO_2 since the beginning of the industrial era, significantly reducing the rate of global warming [*Sabine et al.*, 2004]. At present, despite great year-to-year variability, the land biosphere and the oceans absorb about 60% of the anthropogenic emissions of CO_2, in roughly equal measures [*Mikaloff Fletcher et al.*, 2006; *Le Quéré et al.*, 2009; *Rhein et al.*, 2013].

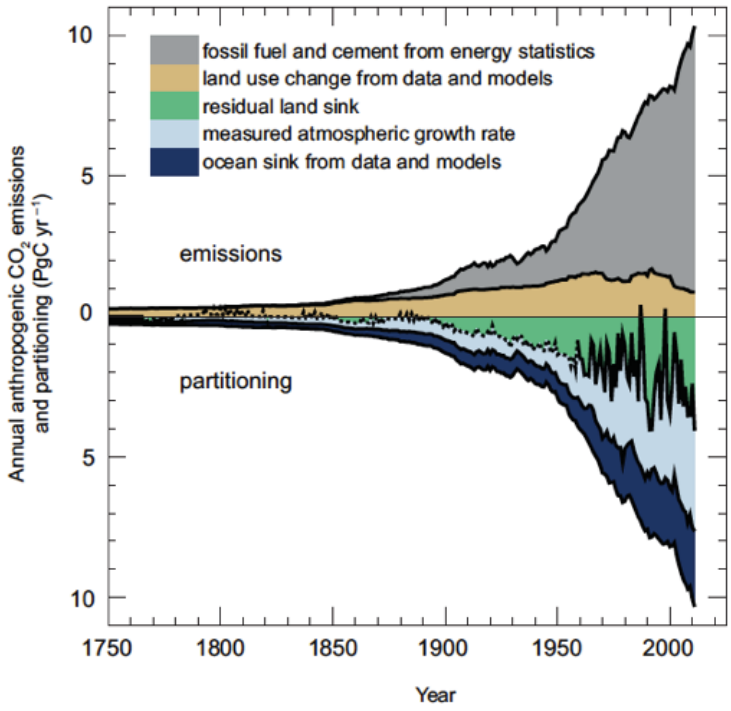

Figure 1.1: Annual anthropogenic CO_2 emissions (Pg C yr^{-1}) from fossil-fuel combustion, cement production and land-use change and their partitioning among the atmosphere, land and ocean from 1750 to 2011 [from *Stocker et al.*, 2013]. Pg C = petagrams of carbon (10^{15} g C).

The ocean takes up CO_2 from the atmosphere by two major mechanisms [*Reid et al.*, 2009]. First, the "solubility pump" refers to the absorption of CO_2 by gas exchange across the air-sea interface, which increases with decreasing water temperature, and the downward transport of CO_2-rich waters into the ocean interior where deep waters are formed [*Volk and Hoffert*, 1985]. Second, the "biological pump", or "soft tissue pump", involves the transport of photosynthetically-produced

organic matter from the upper ocean to depth by particle export, advection or mixing of dissolved organic matter, and the active transport of carbon by vertically migrating zooplankton and fish [*Volk and Hoffert*, 1985; *Ducklow et al.*, 2001; *Passow and Carlson*, 2012; *Turner*, 2015]. These mechanisms regulate the distribution of dissolved inorganic carbon (DIC, i.e. $CO_2 + HCO_3^- + CO_3^{2-}$), in the ocean water column, which presents lower concentrations in surface than in deep waters. It is worth noting that there is a third mechanism, "the carbonate pump", that contributes to this vertical gradient [*Gruber and Sarmiento*, 2002], although with an opposite effect on the capacity of the ocean to take up CO_2 from the atmosphere. The carbonate pump, also referred to as "carbonate counter pump", corresponds to the biologically-mediated incorporation of carbon into calcium carbonate shells and skeletons in the ocean surface and subsequent sinking to depth [*Volk and Hoffert*, 1985]. Although the production of calcium carbonate removes carbon from the DIC pool in surface waters, it also releases CO_2 to surrounding waters and, therefore, reduces the CO_2 invasion that would occur in a non-calcifying system [*Frankignoulle et al.*, 1994; *Passow and Carlson*, 2012; *Zeebe*, 2012; *Salter et al.*, 2014]. The biological pump contributes the most to the vertical gradient of DIC in the ocean [*Gruber and Sarmiento*, 2002], and modelling studies have projected that in the absence of this pump atmospheric CO_2 would increase by almost 200 ppm (50% higher than present day) [see references in *Parekh et al.*, 2006].

1.2 The biological pump

Current estimates of the global export driven by the biological pump range from 5 to 12 Pg C yr^{-1} [*Burd et al.*, 2016], with faecal pellets and marine snow aggregates as the main vehicles (Figure 1.2) [*Fowler and Knauer*, 1986; *Ebersbach et al.*, 2011; *Laurenceau-Cornec et al.*, 2015]. Marine snow consists of "all kinds of primary particles that are glued together including inorganic particles, detritus, phytoplankton, other microorganisms and feeding webs" [*Kiørboe*, 2001]. The transfer of organic matter from the surface to the deep ocean is controlled by a combination of biological, chemical and physical processes (Figure 1.3), which exhibit great variability over spatial and temporal scales [*Burd et al.*, 2016]. The principal factors that shape the biological pump are described in the following lines, with special emphasis on the sinking of particulate organic carbon (POC), the largest source of organic carbon to the deep ocean (>80% of global export) [*Hansell et al.*, 2009]. Note that apart from carbon, the biological pump modulates the distribution of many other elements in the ocean, including nutrients and particle-reactive elements.

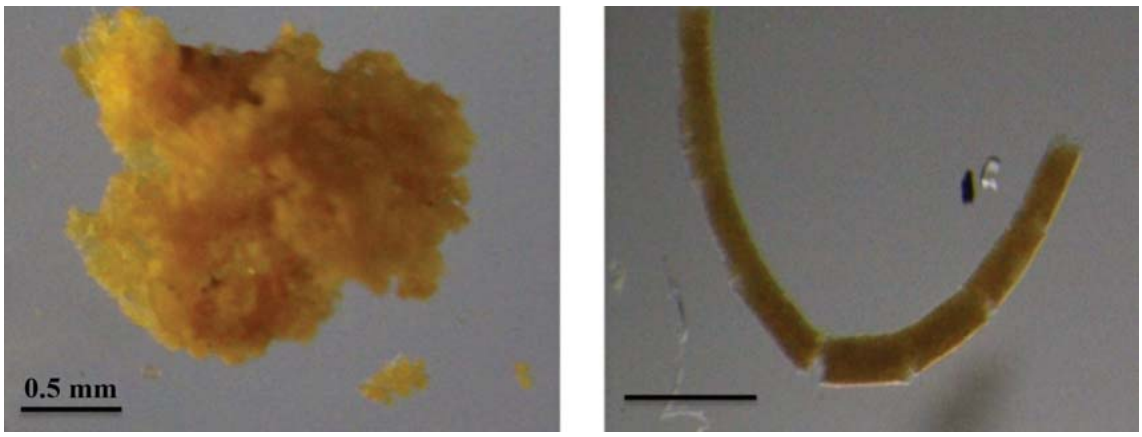

Figure 1.2: Microscopy images of sinking particles collected using a marine snow catcher [*Riley et al.*, 2012] in the Southern Ocean [from *Cavan et al.*, 2017]. The left panel is a phytodetrital aggregate and the right panel is a chain of krill faecal pellets. Scale bars are 0.5 mm.

New production sets up the maximum amount of biogenic carbon that can be potentially exported from the euphotic zone (E_Z) [*Platt et al.*, 1989]. New production depends on the availability of light and the supply of nutrients to the euphotic zone by processes such as advection, vertical mixing and nitrogen fixation [*Dugdale and Goering*, 1967]. In contrast, regenerated production is based upon nutrient recycling within the euphotic zone. *Eppley and Peterson* [1979] postulated that, over sufficiently large time and space scales, new production should balance the export of particulate organic matter to the deep ocean. According to this, they suggested that the fraction of primary production that is exported from the euphotic zone could be expressed as the ratio of new production to total production (new + regenerated), known as the "f-ratio". When the actual export production can be measured, the ratio between export and primary production is called the "e-ratio" [*Downs*, 1989] or the "ThE-ratio" [*Buesseler*, 1998], depending on the method used to estimate the export production, sediment traps or the disequilibrium between ^{234}Th and ^{238}U in seawater, respectively. These parameters illustrate the export efficiency, or in other words the strength of the biological pump, in the upper ocean, usually at the base of the euphotic zone or at 100 m depth [*Buesseler and Boyd*, 2009]. The export efficiency is low in much of the global ocean (<10%), even though it can be substantially greater during diatom blooms due to a rapid removal of diatoms via aggregation or incorporation into faecal pellets and subsequent settling [*Buesseler*, 1998; *Boyd and Trull*, 2007].

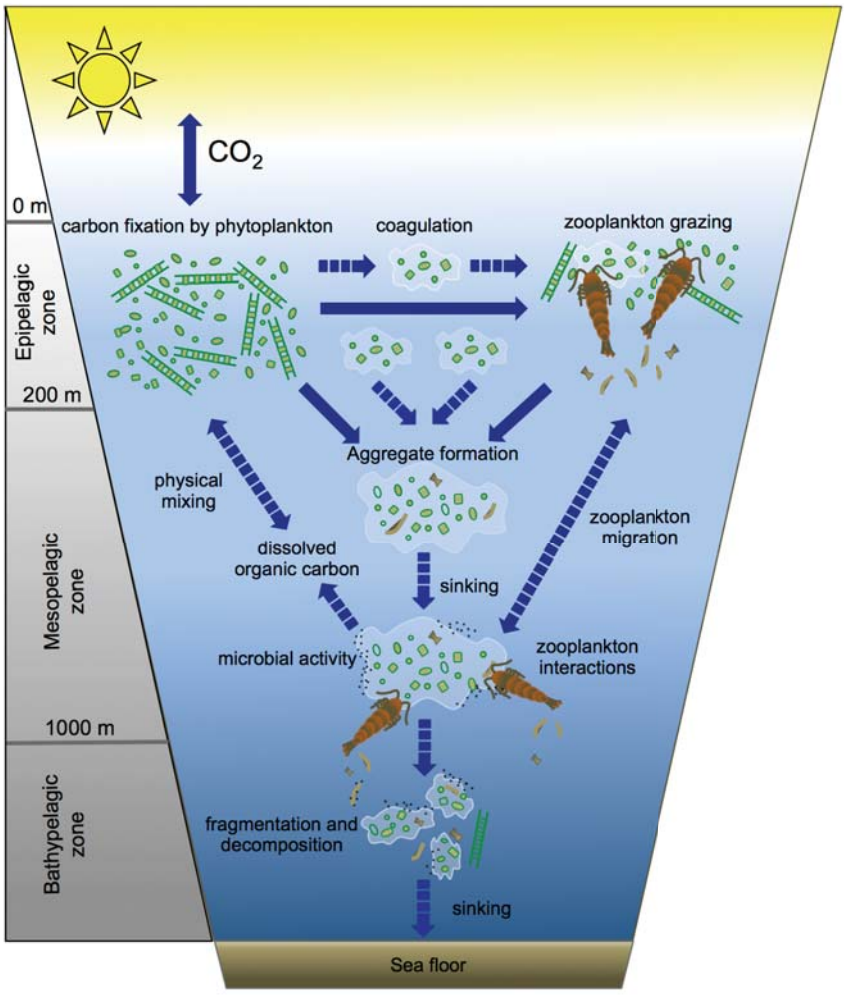

Figure 1.3: Diagram of the principal components of the biological pump [from *Puigcorbé*, 2016]. Dissolved inorganic carbon is transformed into organic biomass in the euphotic zone and a fraction of it is pumped to the deep ocean, either in particulate or dissolved phase. Several physical and biological processes (e.g. coagulation, mixing, gravitational settling, and ecosystem structure and food-web interactions) modulate the magnitude of the carbon export at the base of the euphotic zone and its transfer to deeper waters. Not drawn to scale.

Most of the POC that escapes the euphotic zone is remineralized and returned to the dissolved phase in the mesopelagic zone (i.e. depths immediately below the E_Z down to 1000 m) [*Schlitzer*, 2002]. Generally, less than 10% of the POC leaving the surface is transported to bathypelagic depths (i.e. >1000 m), and only ~1% reaches the abyssal seafloor, where it is consumed, respired or buried in the sediments [*Ducklow et al.*, 2001; *Lutz et al.*, 2002]. Given the global thermohaline circulation, the remineralization depth of the sinking flux is a key parameter in determining when DIC is returned back to the ocean surface and, hence, the time scale of carbon removal from the atmosphere. This results in storage of carbon for periods from decades to a century in the mesopelagic zone (export flux), from centuries to a millennium in the bathypelagic zone (sequestration flux) or for even longer periods in the sediments [*Passow and Carlson*, 2012].

The efficiency of the biological pump can be represented by the fraction of shallow export that is transferred to a certain depth, which is named transfer efficiency.

The attenuation of POC fluxes is sharpest in the upper twilight zone (i.e. 100–300 m below the E_Z), where the main controlling factor is the ecosystem structure, including the phytoplankton community composition and particle transformations by bacteria and zooplankton [*Boyd and Newton*, 1999; *Lam and Bishop*, 2007; *Buesseler and Boyd*, 2009; *Guidi et al.*, 2009; *Lam et al.*, 2011; *Henson et al.*, 2012]. Regarding the phytoplankton community, diatoms have an important contribution to the transport of POC to depth, potentially enhancing the sinking velocity of particles by two mechanisms: (i) the production of transparent exopolymer particles, which promotes the formation of aggregates [*Passow et al.*, 1994]; and (ii) the opal content of diatom frustules, which increases the density of organic matter and may offer protection against degradation, similarly to calcite and dust [*Armstrong et al.*, 2002; *Klaas and Archer*, 2002; *De La Rocha and Passow*, 2007; *Honjo et al.*, 2008; *Iversen and Robert*, 2015]. However, some studies have found that communities dominated by picophytoplankton (<2 μm) show higher transfer efficiencies than those dominated by microphytoplankton (>20 μm), which include diatoms [*Guidi et al.*, 2009; *Lam et al.*, 2011; *Henson et al.*, 2012]. This is ascribed to a more refractory particle pool produced by small-celled communities due to extensive recycling in the euphotic zone, which limits further remineralization in subsurface waters. Moreover, a high degree of particle reprocessing increases particle density, which, apart from size, regulates the sinking velocity of particles and, as a consequence, the attenuation of POC in the water column [*Bach et al.*, 2016]. Besides phytoplankton, both, prokariotes (i.e. bacteria and archaea) and zooplankton, solubilize, consume and fragment sinking organic particles in the mesopelagic zone decreasing the POC flux [*Steinberg et al.*, 2008; *Iversen et al.*, 2010; *Giering et al.*, 2014; *Mayor et al.*, 2014; *McDonnell et al.*, 2015; *Belcher et al.*, 2016]. Yet, zooplankton can also strengthen the POC flux by repackaging particles into faecal pellets and actively transporting surface particles to depth via vertical migration [*Wilson et al.*, 2008, 2013; *Buesseler and Boyd*, 2009; *Hansen and Visser*, 2016]. Some abiotic processes also play a significant role in shaping the attenuation of POC, such as aggregation by coagulation and disaggregation due to turbulence [*Burd and Jackson*, 2009]. In addition, temperature has a major influence on respiration rates and, therefore, on remineralization [*Iversen and Ploug*, 2013; *Marsay et al.*, 2015].

The diversity of processes that are involved in the biological pump, as well as the connections among them, are generally poorly understood [*Boyd and Trull*, 2007; *Buesseler and Boyd*, 2009; *Anderson and Tang*, 2010; *Burd et al.*, 2010, 2016; *Sanders et al.*, 2014]. Progress requires field programmes to constrain such processes and model how the downward transport of organic material varies regionally and temporally. This would be fundamental in order to predict future changes in the efficiency of the biological pump.

1.3 The polar oceans

Polar regions are showing the most rapid rates of warming in recent years [*Anisimov et al.*, 2007; *Reid et al.*, 2009]. On-going impacts of climate change on the terrestrial and marine cryosphere cause climate feedbacks and have cascading effects on marine systems [*Anisimov et al.*, 2007; *Doney et al.*, 2012]. In consequence, the components of the biological pump in the Arctic and Southern Oceans are subject to great changes.

1.3.1 Southern Ocean

The Southern Ocean plays a key role in driving the global thermohaline circulation through water-mass formation, ventilation and transport by the Antarctic Circumpolar Current (ACC) (Figure 1.4) [*Orsi et al.*, 1999; *Rintoul et al.*, 2001; *Sloyan and Rintoul*, 2001; *Marshall and Speer*, 2012]. At the Antarctic continental margin, dense water formed by air-sea-ice interactions sinks into the abyss mixing with ambient waters, and forms the Antarctic Bottom Water, which spreads out into the deep ocean. The eastward flow of the ACC, driven by strong westerly winds, encircles Antarctica and connects the Southern Ocean to the Atlantic, Indian and Pacific Oceans. The ACC is characterized by pronounced horizontal gradients in hydrographic and biogeochemical parameters (i.e. fronts) [*Orsi et al.*, 1995]. In the Antarctic Polar Front (APF), also referred to as the Antarctic Convergence, Antarctic Surface Water downwells and mixes with warmer water to the north to form Antarctic Intermediate Water [*Longhurst*, 2007]. In contrast, in the Antarctic Divergence, the southern boundary of the ACC, the warm and saline Circumpolar Deep Water, derived mainly from the North Atlantic, upwells as a result of wind-driven divergence of surface waters. The East Wind Drift, or Antarctic Coastal Current, follows the Antarctic coastline flowing counter to the ACC due to the polar easterlies. Two major clockwise gyres are found in the Weddell and Ross Seas.

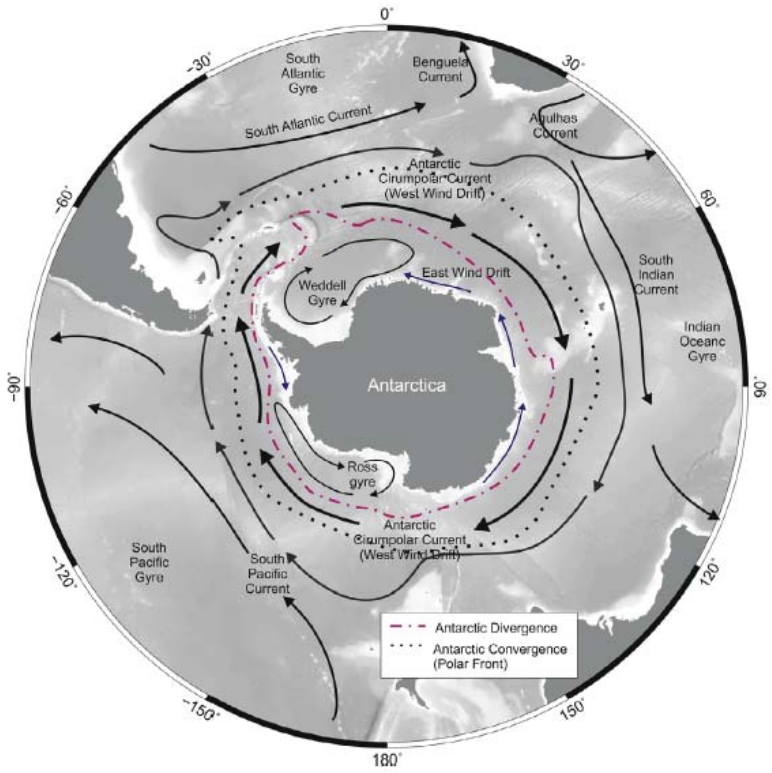

Figure 1.4: Major currents in the Southern Ocean and sub-Antarctic [from *Hunt et al.*, 2016].

Sea ice covers the Southern Ocean from about 60°S to the continent in winter, retreating during summer by a factor of 6, with an average extent of 3 million km² in February (Figure 1.5) [*Arrigo*, 2014]. Most of the sea ice consists of first-year ice that freezes in winter and melts every summer, being generally less than one-meter thick [*Worby et al.*, 2008]. The Southern Ocean has undergone substantial warming throughout the entire water column since the second half of the 20th century [*Gille*, 2002, 2008; *Purkey and Johnson*, 2010]. However, the Antarctic sea-ice extent has increased slightly over the past three decades, obscuring dramatic regional changes linked to large-scale climate variability patterns such as the El Niño-Southern Oscillation and the Southern Annular Mode, and the interaction between the two [*Stammerjohn et al.*, 2008; *Maksym et al.*, 2012]. In the Antarctic Peninsula and the Bellingshausen and Amundsen Seas, the sea-ice extent and the length of the sea-ice season have declined, whereas the opposite has been observed in the Ross Sea (Figure 1.5) [*Stammerjohn et al.*, 2008, 2012; *Turner et al.*, 2009; *Maksym et al.*, 2012; *Moreau et al.*, 2015]. Furthermore, a rapid retreat of ice shelves occurs in the west Antarctica and Antarctic Peninsula, as well as in some glaciers grounded well below the sea level in east Antarctica, due to basal melting and iceberg calving [*Rignot et al.*, 2013; *Rintoul et al.*, 2016].

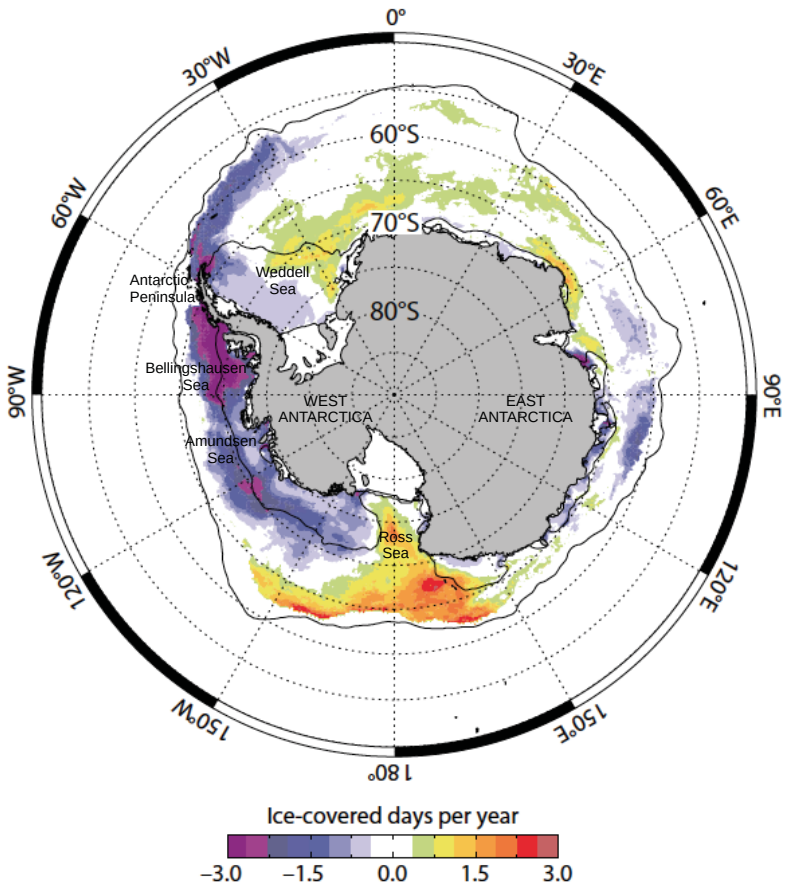

Figure 1.5: Changes in the length of the ice-covered season, expressed as increase/decrease of days per year with sea-ice cover, for 1979-2010 in the Southern Ocean, adapted from *Maksym et al.* [2012]. Black solid lines mark the summer (minimum) and winter (maximum) average sea-ice extent for the same period.

The Southern Ocean is a major sink for atmospheric CO_2, accounting for about 15–20% of the global oceanic uptake [*Takahashi et al.*, 2002; *Gruber et al.*, 2009]. The biological pump and downward advective fluxes, coupled with cold surface waters and strong winds, counteract the outgassing of CO_2 by upwelling [*Hauck et al.*, 2013], which brings nutrient-rich waters to the ocean surface. In the Southern Ocean the biological utilization of nutrients and CO_2 is inefficient, forming the largest high nutrient-low chlorophyll area of the world's oceans [*Falkowski et al.*, 1998; *Watson and Orr*, 2003; *Sigman et al.*, 2010]. This Antarctic paradox was attributed to limiting concentrations of iron, unfavourable light conditions, heavy zooplankton grazing, or a combination of these factors [see details and references in *Löscher et al.*, 1997]. Yet, since the "Iron Hypothesis" [*Martin*, 1990], the former has been highlighted as the main controlling factor of phytoplankton growth in the Southern Ocean [*de Baar et al.*, 1990; *Martin et al.*, 1990; *Moore et al.*, 2013]. This hypothesis was based on the concurrence of low atmospheric CO_2 concentrations and great atmospheric dust-Fe inputs over the Southern Ocean during the last glacial maximum, suggesting that iron could have enhanced productivity and contributed to decrease atmospheric CO_2 levels. In light of this, several in situ experiments of iron fertilization in the Southern Ocean have been

conducted since 1999 with the aim of elucidating the role of iron in phytoplankton growth and the subsequent export of carbon: SOIREE [*Boyd et al.*, 2000], EisenEx [*Gervais et al.*, 2002], SOFeX [*Coale et al.*, 2004], EIFEX [*Hoffmann et al.*, 2006] and LOHAFEX [*Martin et al.*, 2013]. All of these experiments induced phytoplankton blooms, demonstrating that iron is the principal limiting factor in the Southern Ocean, but, overall, they could not determine whether iron fertilization is a feasible mitigation measure for climate change [*Buesseler et al.*, 2008a; *Smetacek and Naqvi*, 2008; *Assmy et al.*, 2009].

Estimates of total primary production in waters south of 50ºS averaged 1950 ± 70 Tg C yr^{-1} over 1998-2006 according to a satellite-based primary production algorithm [*Arrigo et al.*, 2008b]. Natural blooms occur near land masses (Figure 1.6), such as the Kerguelen islands [e.g. *Blain et al.*, 2007] and the Antarctic continental shelves [e.g. *Smith and Gordon*, 1997], associated with the seasonal sea-ice retreat [e.g. *Smith and Nelson*, 1986], but also in land-remote areas, such as the vicinity of the APF [e.g. *Bathmann et al.*, 1997]. These distribution patterns of primary production are consistent with an iron-limited system [*Moore and Abbott*, 2000]. Iron can reach the Southern Ocean surface water through different pathways, such as atmospheric inputs, upwelling, lateral advection, sediment resuspension, subglacial runoff, and melting of icebergs and sea ice [*Lefèvre and Watson*, 1999; *Fitzwater et al.*, 2000; *Lannuzel et al.*, 2007; *Bowie et al.*, 2009; *Raiswell and Canfield*, 2012; *Death et al.*, 2014; *Winton et al.*, 2016]. Iron-replete waters in the Southern Ocean trigger the bloom of large-sized phytoplankton, especially diatoms [*de Baar et al.*, 2005]. Pico- and nanophytoplankton (2-20 μm) contribute to the bulk of phytoplankton biomass in iron-depleted waters, where large diatoms (>20 μm) are also present in heavily silicified forms, such as *Fragilariopsis kerguelensis* and *Thalassiothrix antarctica* [*Assmy et al.*, 2009]. These species are endemic to the Southern Ocean and are major contributors to the siliceous ooze that accumulates in the sediments underlying the iron-limited ACC [*Assmy et al.*, 2013 and references therein], known as the opal belt, with the majority of the accumulation occurring south of the APF [*Geibert et al.*, 2005; *Tréguer and De La Rocha*, 2013]. Antarctic krill (*Euphausia superba*), which occupies a key position in the Antarctic ecosystem, is mainly sustained by the more productive sectors of the Southern Ocean, while other herbivores, such as salps, prevail in less productive areas [*Flores et al.*, 2012].

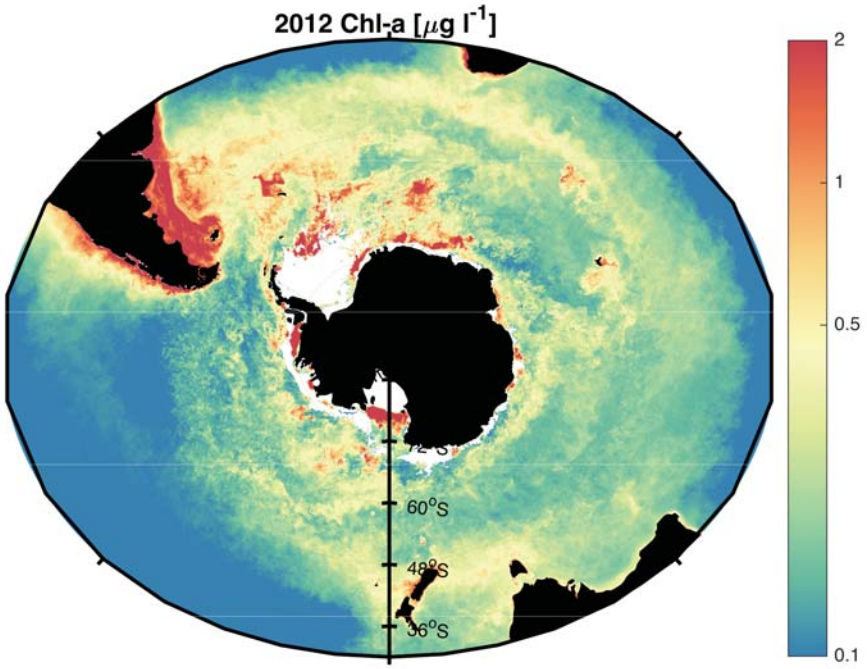

Figure 1.6: Annual mean of satellite-derived sea-surface Chl-a in the Southern Ocean in 2012. Chl-a was derived from the Moderate Resolution Imaging Spectrometer (MODIS) on board NASA's Aqua satellite [*https://oceandata.sci.gsfc.nasa.gov/MODIS-Aqua/L3SMI/*]. Elaborated by Sébastien Moreau.

The estimates of POC export fluxes in the Southern Ocean show great variability, ranging from 0 to 90 mmol C m^{-2} d^{-1} at 100 m depth (average: 12 ± 12 mmol C m^{-2} d^{-1}) from October to April according to in situ measurements derived from ^{234}Th and sediment traps [*Le Moigne et al.,* 2013b; *Maiti et al.*, 2013]. The majority of organic export occurs in pulses usually only once or a few times a year in response to phytoplankton blooms [*Honjo et al.*, 2014]. Nevertheless, the strength and efficiency of the biological pump during the development of blooms remain unclear [*Buesseler and Boyd*, 2009]. In the Southern Ocean, both high (30-50%) and low (<10%) export efficiencies have been reported for natural high-productive events [*Buesseler*, 1998; *Boyd and Trull*, 2007; *Jacquet et al.*, 2011; *Planchon et al.*, 2015]. Iron-fertilized blooms in the Southern Ocean also showed great variability in the fraction of production being exported from the ocean surface. As an example, during SOFeX-South (66°S) the export efficiency was low (<10%) [*Buesseler et al.*, 2005], while during EIFEX it was approximately 60%, indicating a very strong biological pump [*Smetacek et al.*, 2012]. A number of factors may explain the differences observed in export efficiencies, including phytoplankton community composition and study time frame. Diatoms are key exporters of carbon from the ocean surface to deep waters and sediments, and, hence, play an essential role in reducing the CO_2 content in the atmosphere [*Smetacek*, 1999]. Previous studies have shown that very low macronutrient concentrations, specifically of silicic acid, prevent the development of diatom blooms in benefit of flagellates, resulting in low POC export fluxes from the ocean surface [*Jacquet et al.*, 2011; *Martin et al.*, 2013]. Further, diatoms in the Southern Ocean contribute differently to POC

export according to their life-cycle strategy in which the degree of silicification is relevant [*Assmy et al.*, 2013; *Quéguiner*, 2013]. Moreover, since export lags production, the time scale of the studies may often be too short to quantitatively estimate the strength of the biological pump during bloom events [*Charette and Buesseler*, 2000; *Buesseler et al.*, 2004]. Besides this, packaging of slowly sinking phytoplankton cells into large faecal pellets may increase the export and transfer efficiencies in the Southern Ocean [*Le Moigne et al.*, 2014; *Cavan et al.*, 2015], although faecal pellets can be attenuated to a large extent by zooplankton transformations and microbial degradation [*Mayor et al.*, 2014; *Iversen et al.*, 2017].

In the Antarctic Peninsula, where warming is much more rapid than in the rest of Antarctica [*Vaughan et al.*, 2003], shifts in phytoplankton biomass and primary production [*Montes-Hugo et al.*, 2009; *Moreau et al.*, 2015], and in the food web, from phytoplankton to grazers and top predators [*Moline et al.*, 2004; *Montes-Hugo et al.*, 2009; *Schofield et al.*, 2010; *Borges Mendes et al.*, 2017], have been reported related to on-going physical environmental changes. During the 21st century, air and seawater temperatures in the Southern Ocean are projected to rise, Antarctic sea-ice to shrink, stratification of the upper water column to increase, and the westerly winds to strengthen and move to the south [*IPCC*, 2013]. Although it is challenging, given the gaps in our present understanding, several authors have proposed how components of the biological pump may be affected by this physical forcing. Poleward intensification of the westerly winds would lead to more divergence [*Russell et al.*, 2006] and, therefore, could increase the upwelling of nutrients and primary production [*Arrigo et al.*, 2008b]. Ocean stratification could reduce the input of nutrients into the euphotic zone, but, in the opposite direction, could provide an optimal irradiance environment for phytoplankton [*Sarmiento et al.*, 1998; *Montes-Hugo et al.*, 2009]. A reduced sea-ice extent could influence, either positively or negatively, primary production as a consequence of the direct increase in open-water area [*Arrigo and Thomas*, 2004] or due to a decrease in iron input from sea ice [*Wang et al.*, 2014], respectively. Increased melt-water outflow from glaciers could enhance iron fertilization and, consequently, primary production [*Flores et al.*, 2012]. Yet, freshening of surface waters could result in changes in plankton community structure. Small cells and salps could be favoured at the expense of diatoms and krill, which, in turn, would impact the transfer of carbon to higher trophic levels and the ocean interior [*Pakhomov et al.*, 2002; *Moline et al.*, 2004; *Flores et al.*, 2012]. However, some ecosystem models project an increase in the abundance of diatoms in the Southern Ocean over the 21st century, associated with an increase in export production [*Laufkötter et al.*, 2016].

1.3.2 Arctic Ocean

The Arctic is an enclosed ocean with about half of its area occupied by broad and shallow (50-300 m) continental shelves, which receive about 10% of the global river discharge [*Dai and Trenberth*, 2002]. It is comprised of the Amerasian and the Eurasian Basins, which are further divided by seafloor ridges into the Canada and Makarov Basins and the Nansen and Amundsen Basins, respectively (Figure 1.7). There are two gateways into the Arctic: the two-branched inflow of warm and saline Atlantic Water (AW) through western Spitsbergen and the Barents Sea, and the fresher and less dense Pacific Water (PW) inflow through the Bering Strait (50 m deep, 85 km wide) (Figure 1.7). The AW spreads into the entire ocean transporting a much larger volume of water and heat, whereas the PW is basically confined to the Amerasian Basin, strengthening the vertical stratification in this sector [see review by *Bluhm et al.*, 2015 and references therein]. The surface circulation in the Arctic Ocean is governed by the wind-driven Transpolar Drift, which transports water from Siberia to the Fram Strait, and the anticyclonic Beaufort Gyre in the Amerasian Basin. Along the coast, buoyant waters from continental runoff flow around the shelves in an anticlockwise direction [*Carmack et al.*, 2015]. Subsurface halocline waters are formed in the Fram Strait and the Barents Sea (lower halocline), but also in the Chukchi and East Siberian Seas (upper halocline, restricted to the Amerasian Basin) due to sea-ice formation, brine rejection and haline convection [*Rudels et al.*, 2004; *Anderson et al.*, 2013]. Below, the Arctic Circumpolar Boundary Current carries AW cyclonically along the continental slopes [*Rudels et al.*, 1999]. Deep Arctic waters form in the Greenland Sea by open ocean convection, and also in the Arctic via sinking plumes of brine-enriched water from the shelves to the basins [*Rudels et al.*, 2012]. Water outflows from the Arctic occur through the western Fram Strait and the Canadian Archipelago. The Fram Strait (2600 m deep, 580 km wide) is the major export pathway, draining about 5000 $km^3\ yr^{-1}$ of liquid freshwater and sea ice [*Serreze et al.*, 2006; *Haine et al.*, 2015]. The Arctic exports dense intermediate and deep waters to the south that contribute to the North Atlantic Deep Water, enforcing the Atlantic meridional overturning circulation [*Rudels*, 2009].

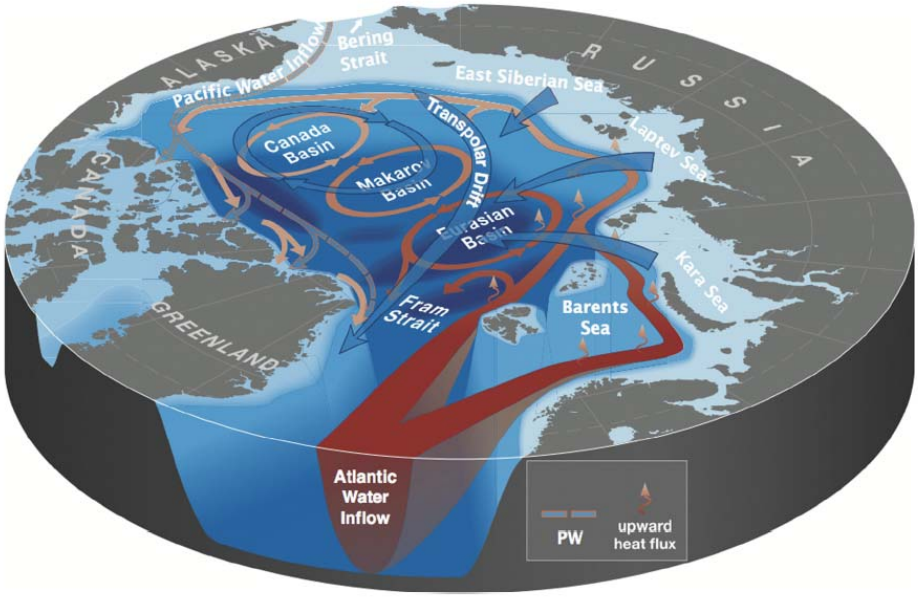

Figure 1.7: The main upper-ocean current patterns in the Arctic Ocean [from *Wassmann et al.*, 2015]. Cold and warm waters are shown in blue and red, respectively. Blue arrows with red border indicate the flow of Pacific Water (PW).

Sea ice covers the Arctic Ocean from about 60°N to the North Pole in winter, decreasing during summer by on average a factor of 2 in September when the mean sea-ice extent is of 6 to 7 million km^2 [*Vancoppenolle et al.*, 2013; *Meier*, 2016]. Since 2007, the Arctic sea ice is less than two meters thick and about 70% consists of first-year ice [*Tschudi et al.*, 2016; *http://psc.apl.uw.edu/research/projects/arctic-sea-ice-volume-anomaly/*]. Climate change is triggering an unprecedented decline in Arctic sea ice [e.g. *Stroeve et al.*, 2012; *Notz and Stroeve*, 2016]. During the last 10 years, the Arctic sea-ice extent has experienced two record minimums in September 2007 and 2012, related to anomalously high temperatures and southerly winds [*Comiso et al.*, 2008], or intense cyclone events [*Parkinson and Comiso*, 2013]. This rapid retreat is accompanied by thinning and volume-loss of sea ice (Figure 1.8) [*Haas et al.*, 2008; *Kwok et al.*, 2009; *Laxon et al.*, 2013; *Renner et al.*, 2014], allowing more sunlight to be transmitted through the sea ice and increasing the absorption of solar energy in the Arctic Ocean [*Nicolaus et al.*, 2012]. In parallel, increases in freshwater storage [*Rabe et al.*, 2014] and upper ocean stratification [*Korhonen et al.*, 2013] have been documented. This situation affects primary production [e.g. *Ardyna et al.*, 2014; *Arrigo and van Dijken*, 2015], sea-ice and upper-ocean ecosystems [e.g. *Wassmann*, 2011; *Wassmann et al.*, 2011] and pelagic-benthic coupling [e.g. *Wassmann and Reigstad*, 2011; *Grebmeier*, 2012].

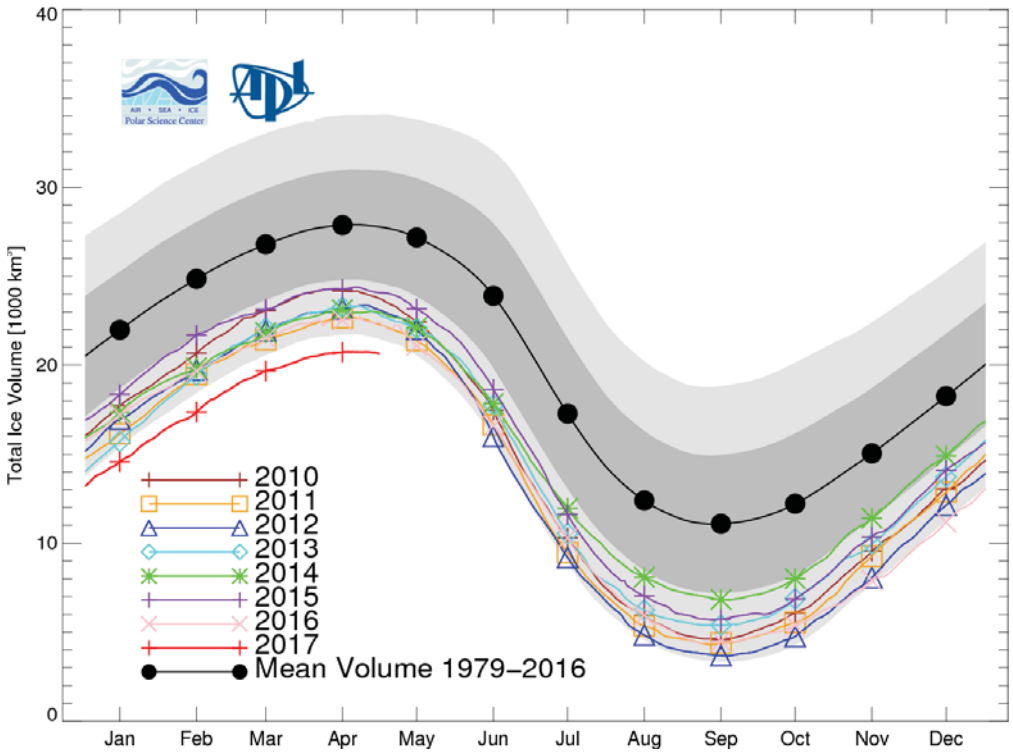

Figure 1.8: Total Arctic sea-ice volume from the Pan-Arctic Ice Ocean Modelling and Assimilation System [*Zhang and Rothrock*, 2003; *Schweiger et al.*, 2011], showing the volume of the mean annual cycle from 2010 to 2017. Shaded areas indicate one and two standard deviations from the mean over the period 1979-2016 [from *http://psc.apl.uw.edu/research/projects/arctic-sea-ice-volume-anomaly/*].

The Arctic Ocean is considered a significant sink for atmospheric CO_2, accounting for 5-14% of the global oceanic uptake, despite representing only ~3% of the global ocean area [*Bates and Mathis*, 2009; *Gruber et al.*, 2009]. Relevant processes regulating this air to sea flux include the cooling of surface waters during northward transport into the Arctic, brine rejection due to sea-ice formation and deep water formation, and primary production and export of organic carbon [*Bates and Mathis*, 2009]. In the Arctic, phytoplankton growth is co-limited by light and nutrient availability, primarily nitrate [*Popova et al.*, 2012; *Codispoti et al.*, 2013]. Favourable light conditions for photosynthesis occur within a narrow time window, mainly due to the constraints imposed by the annual light cycle and the sea-ice and snow covers [*Mundy et al.*, 2005; *Grenfell et al.*, 2006; *Wassmann and Reigstad*, 2011]. Sea-ice algae begin to grow in early spring, anticipating phytoplankton growth, due to their adaptation to low ambient irradiances [*Cota and Smith*, 1991]. Phytoplankton blooms usually occur after the sea-ice breakup, from April to September depending on the latitude, coinciding with increases in surface stratification and light availability [*Wassmann*, 2011]. The major inputs of nitrate and phosphate to the Arctic occur via the Barents Sea, whereas the Bering Strait represents the main conduit of silicate to the ocean [*Torres-Valdés et al.*, 2013]. Rivers are likely the second source of nutrients to the upper layers of the Arctic Ocean, delivering also significant amounts of dissolved and particulate organic matter [*Holmes et al.*, 2012; *Torres-Valdés et al.*, 2013].

Horizontal advection and winter mixing are the two main mechanisms that supply nutrients into the euphotic zone, while other processes, such as upwelling, storm-driven or tidal mixing and eddies, can be locally important [*Tremblay and Gagnon*, 2009; *McLaughlin and Carmack*, 2010; *Popova et al.*, 2012].

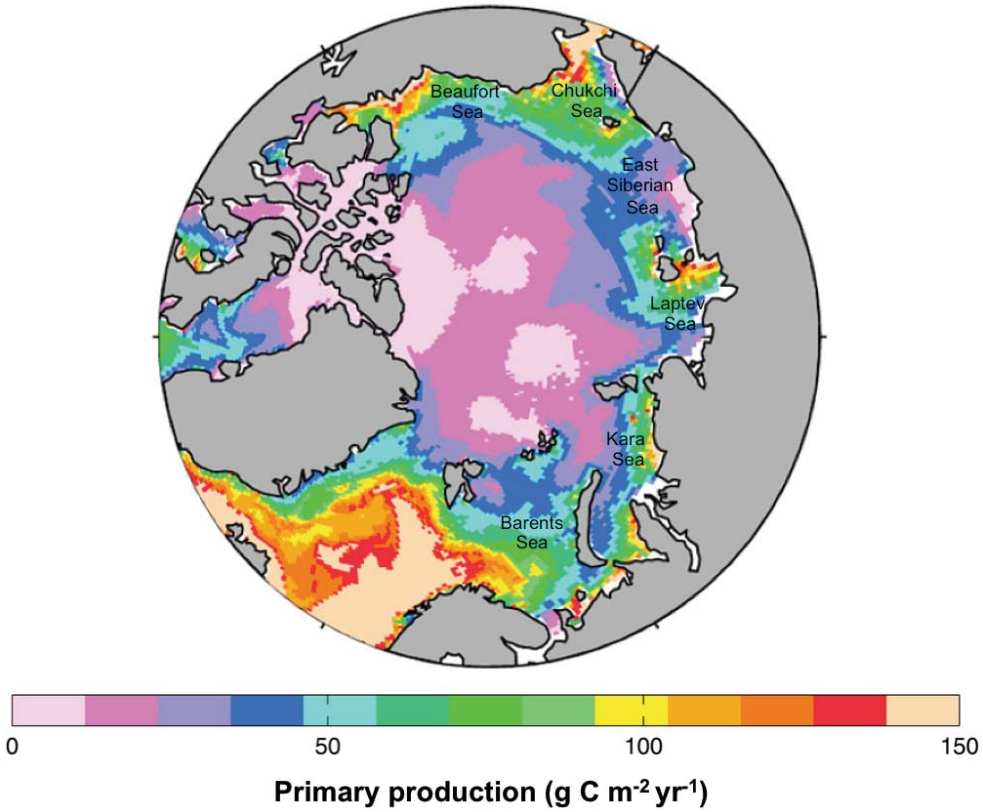

Figure 1.9: Total annual water column primary production in the Arctic Ocean in 1998 [adapted from *Popova et al.*, 2012] using a pan-Arctic biological/ice/ocean model [*Zhang et al.*, 2010].

Satellite-based estimates of total primary production in waters north of the Arctic Circle averaged 420 ± 30 Tg C yr^{-1} over 1998-2006 [*Pabi et al.*, 2008] using the same algorithm as *Arrigo et al.* [2008b] in the Southern Ocean. The highest primary production rates in the Arctic occur in the inflow shelves (i.e. the Chukchi and Barents Seas) [*Carmack and Wassmann*, 2006], reflecting the large supply of nutrients from the adjacent North Pacific and North Atlantic [*Carmack et al.*, 2006; *Popova et al.*, 2012]. The ice-covered central Arctic is characterized by oligotrophic conditions and very low primary production, whereas the interior shelves (i.e. Kara, Laptev, East Siberian and Beaufort Seas), which are influenced by the major Arctic rivers, show intermediate values (Figure 1.9). Despite the patchy distribution of sea-ice algae, their relative contribution to total primary production is estimated to be greater in the central basins (up to >50%) than in the shelf environment (<10%) [*Gosselin et al.*, 1997]. Algal blooms in the Arctic Ocean are dominated by diatoms, but flagellates and the haptophyte *Phaeocystis pouchetii* can also reach high biomass levels,

such as in the Greenland and Barents Seas [*Wassmann et al.*, 2006; *Tremblay and Gagnon*, 2009; *Vaquer-Sunyer et al.*, 2013; *Arrigo*, 2014]. Zooplankton biomass is overwhelmingly dominated by copepods, especially the large *Calanus* species [*Thibault et al.*, 1999; *Kosobokova and Hirche*, 2009], which overwinter at depth and ascend to surface waters in spring to feed. These copepods constitute a high-quality food source for fishes, sea birds and mammals, occupying a key position in the Arctic marine ecosystem [*Falk-Petersen et al.*, 2009; *Søreide et al.*, 2010].

POC export fluxes from the upper 25-200 m are widely heterogeneous in the Arctic, varying from 0 to >100 mmol C m^{-2} d^{-1} (average: 20 ± 30 mmol C m^{-2} d^{-1}) from May to September according to the ^{234}Th proxy [*Roca-Martí et al.*, 2016 and references therein]. The shelves clearly show higher vertical fluxes (reaching values >30 mmol C m^{-2} d^{-1}) compared to the basins (<5 mmol C m^{-2} d^{-1}), being generally higher in the Chukchi and Barents Seas than on the interior shelves, in consistency with the distribution of primary production [*Wassmann et al.*, 2004; *Cai et al.*, 2010; *Honjo et al.*, 2010; *Findlay et al.*, 2015b; *Randelhoff and Guthrie*, 2016]. Several studies have reported significant under-ice fluxes of biogenic matter in the shallow and the deep Arctic, indicating that these fluxes are not restricted to open waters [e.g. *Bauerfeind et al.*, 1997; *Fortier et al.*, 2002; *Lalande et al.*, 2007a, 2009a; *Juul-Pedersen et al.*, 2008; *Boetius et al.*, 2013]. The release of sea-ice algae, such as the chain-forming *Melosira arctica*, from melting ice can rapidly transfer organic carbon to the seafloor [*Leu et al.*, 2015]. The fraction of sea-ice algae and phytoplankton that sinks to the deep ocean largely depends on the match or mismatch between the autotrophs and the grazing impact of zooplankton [*Wassmann et al.*, 1996, 2004]. In general terms, the settling of autotrophic cells dominates in spring, whereas the sinking of faecal pellets dominates in summer and early autumn [*Wassmann et al.*, 2004]. Top-down control of zooplankton is commonly observed in the Arctic, reducing substantially newly produced biogenic matter and constraining the pelagic-benthic coupling [*Wassmann et al.*, 2004; *Olli et al.*, 2007; *Forest et al.*, 2011]. Although copepods contribute substantially to the carbon export in the Arctic by producing faecal pellets, they are also known to trigger the fragmentation of large particles and produce dissolved organic carbon at the expense of export [*Fortier et al.*, 2002; *Møller et al.*, 2003; *Juul-Pedersen et al.*, 2006; *Wexels Riser et al.*, 2007; *Sampei et al.*, 2009]. A recent model study reports a high annual mean export efficiency of >30% in Arctic waters [*Henson et al.*, 2015]. Nevertheless, measurements of primary production and downward POC fluxes are very scarce, especially in the interior basins, due to the logistical difficulties of conducting research in ice-covered waters [*Gustafsson and Andersson*, 2012; *Matrai et al.*, 2013]. Indeed, the temporal mismatch between the measurement of production and export, combined with the existence of a long lag period between both processes in the Arctic (30-40 days), makes the assessment of the export efficiency on a seasonal scale difficult [*Henson et al.*, 2015].

According to satellite-based estimates, annual net primary production (NPP) in the Arctic Ocean increased by 30% between 1998 and 2012, especially on the interior shelves, often associated with reduced sea-ice extent and a longer phytoplankton growing season [*Arrigo and van Dijken*, 2015]. Yet, satellite-derived estimates can be substantially underestimated since they do not take into account the productivity of under-ice phytoplankton and sea-ice algae [*Gosselin et al.*, 1997; *Fortier et al.*, 2002; *Lee et al.*, 2010; *Arrigo et al.*, 2012; *Fernández-Méndez et al.*, 2015]. Model projections indicate a mean warming of surface air in the Arctic region between 2.2 and 2.4 times the global average warming by the end of the 21st century, together with a continued loss of sea-ice volume, and a summer ice-free Arctic likely before 2050 [*IPCC*, 2013]. Under this scenario, future increases in primary production are expected, mainly along the shelf break and the adjacent continental shelves [*Arrigo et al.*, 2008a; *Ellingsen et al.*, 2008; *Wassmann et al.*, 2008; *Bates and Mathis*, 2009; *Slagstad et al.*, 2011; *Yool et al.*, 2015]. In spite of improved light conditions for photosynthesis, increases in new production will be constrained if nutrient supply to surface waters does not increase considerably [e.g. *Popova et al.*, 2012; *Slagstad et al.*, 2015; *Tremblay et al.*, 2015]. The decline in sea ice can increase nutrient availability by enhancing shelf-break upwelling, wind-driven mixing and eddy formation [*Carmack and Chapman*, 2003; *Zhang et al.*, 2010; *Barber et al.*, 2012; *Watanabe et al.*, 2014; *Harada*, 2016], but can also reduce the supply of nutrients to surface waters by ice-melt stratification [*Wassmann et al.*, 2008; *McLaughlin and Carmack*, 2010]. Stratification will be further promoted by increased river runoff and inputs from glacial ice melt and permafrost [*Haine et al.*, 2015; *Bring et al.*, 2016; *Carmack et al.*, 2016]. Therefore, the biological response to sea-ice retreat will depend on regional conditions [*Carmack et al.*, 2006; *Carmack and McLaughlin*, 2011; *Nishino et al.*, 2011; *Wassmann and Reigstad*, 2011; *Bhatt et al.*, 2014]. Besides primary production, the future composition of plankton and the match or mismatch between the timing of phytoplankton blooms and zooplankton production will also regulate the POC export fluxes to the deep ocean [e.g. *Honjo et al.*, 2010; *Leu et al.*, 2011]. Some studies project a future phytoplankton community based on the smallest cells (picophytoplankton) as warming and freshening strengthen stratification, and a higher retention of carbon in the upper ocean by zooplankton and/or bacteria [*Piepenburg*, 2005; *Grebmeier et al.*, 2006; *Kirchman et al.*, 2009; *Li et al.*, 2009; *Wassmann and Reigstad*, 2011]. Moreover, plankton and bacteria respiration rates are expected to increase faster than primary production rates in response to warming [*Kritzberg et al.*, 2010; *Vaquer-Sunyer et al.*, 2010]. Overall, it remains uncertain how the changes in NPP and plankton community will affect the sinking of POC from the ocean surface, and in turn contribute to the marine sequestration of CO_2 [*Honjo et al.*, 2010; *Anderson and Macdonald*, 2015].

1.4 Particle export measurements

Traditionally, the downward export of POC has been estimated using two approaches: the deployment of sediment traps and the use of particle-reactive radionuclides from the natural decay-series (i.e. the short-lived ^{234}Th and ^{210}Po, see Section 1.5) [*Eppley*, 1989]. Besides these techniques, bottle-incubation experiments (with ^{15}N as a tracer) and geochemical budgets have traditionally been used to estimate new production as the equivalent of export production by measuring nutrient uptake and seasonal changes in oxygen and nutrient stocks in the upper ocean, respectively [*Eppley*, 1989]. The drawbacks of the new production estimates include the use of stoichiometric ratios for conversion to carbon units [*Jenkins and Wallace*, 1992; *Tamelander et al.*, 2013], and the disregard of nitrification (i.e. oxidation of ammonium to nitrite/nitrate by bacteria) in the euphotic zone in nitrogen-based estimates [*Yool et al.*, 2007].

Sediment traps provide a direct measurement of the vertical flux of POC [e.g. *Honjo et al.*, 2008]. Moreover, some trap designs can supply very valuable information about the sinking-particle pool, such as the size distribution and abundance of different particle types [*Jannasch et al.*, 1980; *Asper*, 1987], particle sinking velocity [*Peterson et al.*, 2005] and remineralization rates [*Boyd et al.*, 2015]. Yet, sediment traps present several accuracy issues, especially in the upper 1000 m of the water column, related to hydrodynamics, the capture of zooplankton and the solubilization of material after collection [see review by *Buesseler et al.*, 2007]. These issues may be partly overcome by newly-developed designs (e.g. neutrally-buoyant sediment traps) [*Lampitt et al.*, 2008].

A growing body of research relies on modelling based on satellite remote sensing, which presents a great potential to measure the export of organic matter on a basin scale [*Sanders et al.*, 2014]. Export models use data derived from satellites (e.g. Chl-a and sea-surface temperature), models of primary production, and relationships derived from global observational datasets [e.g. *Dunne et al.*, 2005; *Henson et al.*, 2011; *Laws et al.*, 2011]. However, substantial differences among the models and with respect to in situ particle export measurements have been documented in several oceanic basins [*Maiti et al.*, 2013; *Stukel et al.*, 2015; *Puigcorbé et al.*, in revision]. Satellite-based export estimates shall improve in accuracy as our understanding and parameterization of the key biological processes affecting export move forward [*Burd et al.*, 2016]. Finally, new and emerging in situ imaging and optical techniques are promising tools to examine the abundance, type and size of particles that contribute to the export (Figure 1.10) [e.g. *Stemmann and Boss*, 2012; *Jackson et al.*, 2015].

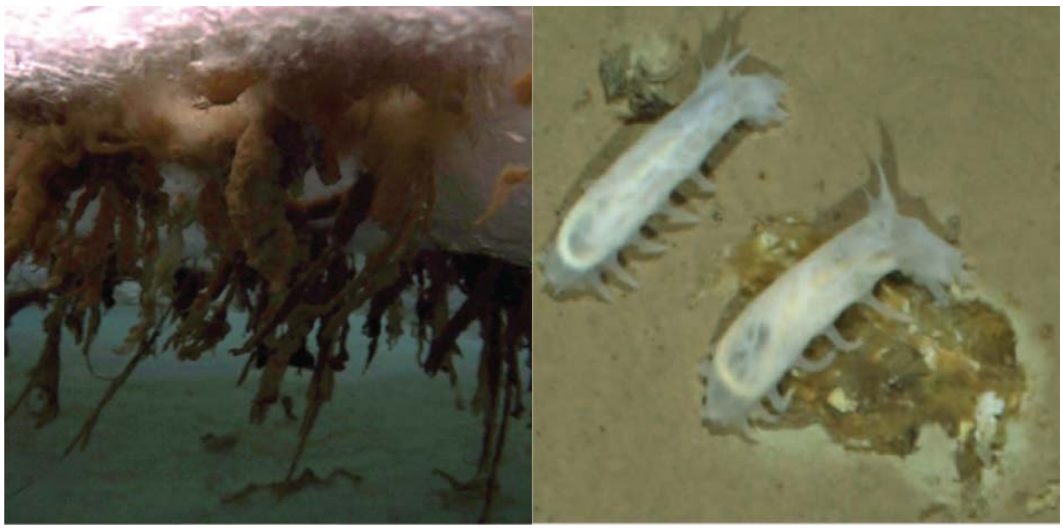

Figure 1.10: Images of *Melosira arctica* aggregations under the ice (left panel) and on the seafloor at more than 3500 m depth being grazed by holothurians (*Kolga hyaline*, right panel) in the central Arctic in 2012 [from *Boetius et al.*, 2013]. The cameras were placed on a remotely operated vehicle [*Nicolaus and Katlein*, 2013] and on an ocean floor observation system [*Soltwedel et al.*, 2009], respectively.

1.5 Radionuclides as proxies for particle export

Radionuclides from the natural decay-series ^{238}U, ^{232}Th and ^{235}U are suitable tools to study environmental processes and their temporal scales given their known rates of production and decay and element-specific chemical properties. The fractionation among members that belong to the same decay chain is the basis for the application of U- and Th-series radionuclides in environmental sciences [*Krishnaswami and Cochran*, 2008]. The radioactive disequilibrium in surface seawater between the daughter-parent pairs from the ^{238}U chain (Figure 1.11), $^{234}Th/^{238}U$ and $^{210}Po/^{210}Pb$, was reported around the decade of the 1970s [*Bhat et al.*, 1968; *Shannon et al.*, 1970], reflecting a preferential removal of the daughter isotopes by particle scavenging. This difference in particle reactivity between the daughter and parent isotopes allows the study of the production, transport and cycling of particles in the ocean [*Rutgers van der Loeff and Geibert*, 2008]. *Coale and Bruland* [1985, 1987] and *Nozaki et al.* [1997, 1998] showed that the scavenging of ^{234}Th and ^{210}Po was a function of phytoplankton biomass or primary production, triggering the use of both isotopes as tools to study the biological pump.

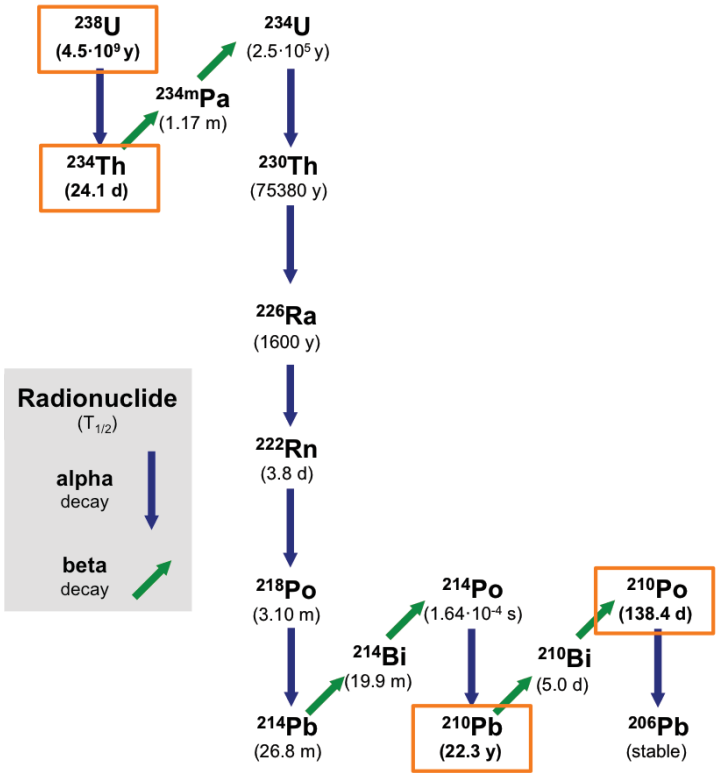

Figure 1.11: ^{238}U-decay series showing the α and β decay modes and the half-life of each radionuclide, adapted from *Rodellas* [2014].

The ^{234}Th/^{238}U and ^{210}Po/^{210}Pb pairs are suitable to quantify particle export fluxes over time scales of weeks to months, respectively, since the half-lives of the daughter isotopes are 24.1 days for ^{234}Th and 138.4 days for ^{210}Po. This time window is of special interest to follow the development of phytoplankton blooms and obtain estimates of seasonal export of carbon. The application of these pairs as proxies for POC export commenced in the 1990s [*Buesseler et al.*, 1992; *Shimmield et al.*, 1995], although ^{234}Th/^{238}U have been used to a major extent [*Benitez-Nelson and Moore*, 2006]. These proxies can provide a higher spatial resolution compared to sediment traps because they require sampling periods of only a few hours during oceanographic expeditions (see Chapter 2). Several authors have recommended the simultaneous use of ^{234}Th/^{238}U and ^{210}Po/^{210}Pb since they cover different time scales, and ^{234}Th and ^{210}Po have different biogeochemical behaviours, providing complementary information on POC export fluxes [*Friedrich and Rutgers van der Loeff*, 2002; *Verdeny et al.*, 2009; *Stewart et al.*, 2011]. Indeed, during the last ten years some studies have used both pairs together for that purpose [*Stewart et al.*, 2007a, 2011; *Verdeny et al.*, 2009; *Wei et al.*, 2011; *Le Moigne et al.*, 2013a; *Ceballos-Romero et al.*, 2016; *Maiti et al.*, 2016; *Roca-Martí et al.*, 2016].

1.5.1 $^{234}Th/^{238}U$ pair

Th-234 (half-life, $T_{1/2}$ = 24.1 days) is constantly produced by alpha decay of ^{238}U ($T_{1/2} = 4.5 \cdot 10^9$ years) in the water column of the oceans. Both isotopes are metals from the actinide series. Uranium occurs as dissolved uranyl-carbonate complexes (oxidation state +VI) in oxic seawater and is closely coupled to salinity [*Chen et al.*, 1986], showing activities of around 2.5 disintegrations per minute (dpm) per litre of seawater at a salinity of 35 (Figure 1.12A). Deviations from its conservative behaviour occur under anoxic conditions (oxidation state +IV) [*Choppin and Wong*, 1998], such as those that can be encountered in marine sediments. In clear contrast, thorium has only one stable oxidation state (+IV) in seawater and it is strongly adsorbed onto colloid and particle surfaces [*Santschi et al.*, 2006]. As a result, ^{234}Th activities in surface waters are usually lower than those expected from radioactive decay of ^{238}U due to the adsorption and removal of ^{234}Th by sinking particles (Figure 1.12A). With increasing water depth and decreasing particle concentration, the activities of ^{234}Th increase towards secular equilibrium with ^{238}U. Disequilibrium below the upper layer of the ocean has also been documented in some instances: an excess of ^{234}Th in subsurface waters due to remineralization or disaggregation of the particle pool exported from overlying waters [e.g. *Usbeck et al.*, 2002]; and a deficiency of ^{234}Th in the bottom nepheloid layer of the ocean as a consequence of sediment resuspension and scavenging [*Bacon and Rutgers van der Loeff*, 1989].

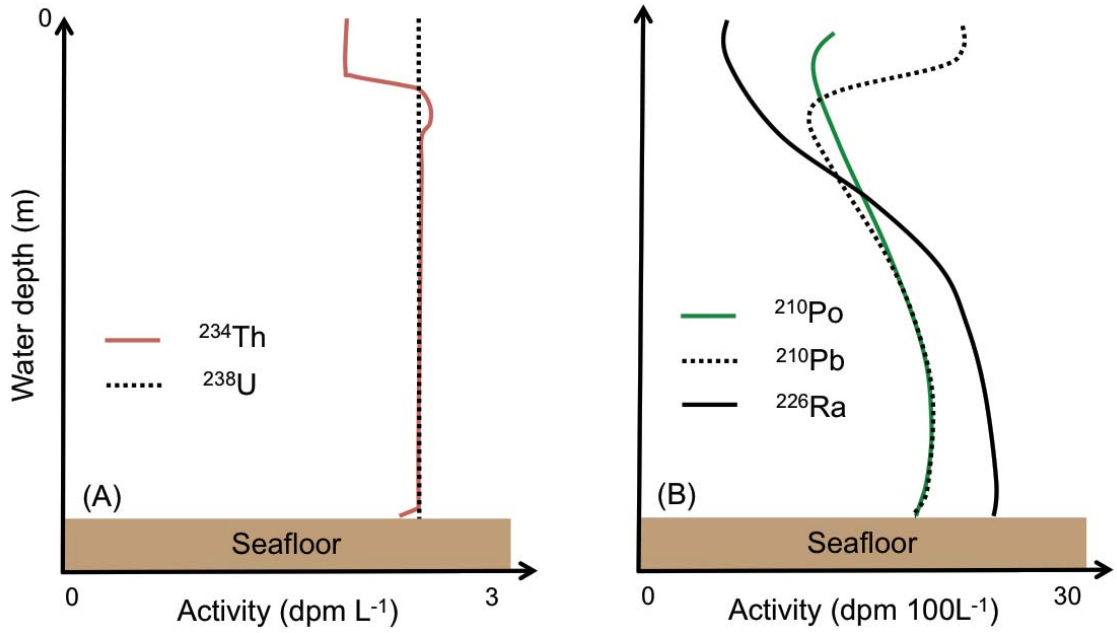

Figure 1.12: Schematic diagram of the distribution of ^{238}U and ^{234}Th (A) and ^{226}Ra, ^{210}Pb and ^{210}Po (B) in the water column of the ocean [based on *Rutgers van der Loeff and Geibert*, 2008]. Notice the different scales on the x-axis.

1.5.2 ^{210}Po/^{210}Pb pair

Pb-210 ($T_{1/2}$ = 22.3 years) in seawater is produced by decay of ^{226}Ra ($T_{1/2}$ = 1600 years) to ^{222}Rn ($T_{1/2}$ = 3.8 days) followed by a series of short-lived products (Figure 1.11). The distribution of ^{226}Ra resembles that of silicate and barium, which generally increase with increasing depth (Figure 1.12B), and is affected by biological cycling [*Ku and Luo*, 2008]. Pb-210 is also supplied to the ocean by atmospheric deposition. Rn-222 exhales from rocks and soils and produces ^{210}Pb, which becomes rapidly associated with aerosol particles that are subsequently removed by dry and wet deposition. The deposition of air-borne ^{210}Pb depends on the proximity to land masses and atmospheric circulation, and generally consists of the main source of ^{210}Pb to the ocean surface [*Church and Sarin*, 2008]. Due to this atmospheric input, the ^{210}Pb/^{226}Ra activity ratio in surface waters can be higher than one (Figure 1.12B) [*Chung*, 1987; *Cochran et al.*, 1990]. Po-210 ($T_{1/2}$ = 138.4 days) is produced by beta decay of ^{210}Pb via its short-lived daughter ^{210}Bi ($T_{1/2}$ = 5.0 days). Pb-210 and ^{210}Po present typical activities from about 2 to 20 dpm 100L^{-1}, depending on the region [*Verdeny et al.*, 2009; *Roca-Martí et al.*, 2016]. Unlike ^{210}Pb, the fraction of ^{210}Po supplied by atmospheric deposition to surface waters is small, typically corresponding to about 10-20% that of the ^{210}Pb flux [*Lambert et al.*, 1982]. This is ascribed to the short residence time of ^{210}Pb in the atmosphere, of about one to two weeks, which allows little ingrowth of ^{210}Po [*Turekian et al.*, 1977]. Pb and Po exhibit different oxidation states in seawater, but little is known about their speciation [*Stewart et al.*, 2008; *Powell et al.*, 2009]. Both display very strong binding to particle surfaces and have been used as particle tracers in the marine environment [e.g. *Bacon et al.*, 1976, 1988; *Cochran and Masqué*, 2003]. The removal of ^{210}Pb from the water column has been used to study processes of particle scavenging in the water column and sediment accumulation on the seafloor [e.g. *Cochran et al.*, 1990]. Additionally, ^{210}Po is incorporated into the cytoplasm of bacteria [*Cherrier et al.*, 1995; *Larock et al.*, 1996] and phytoplankton [*Fisher et al.*, 1983; *Stewart and Fisher*, 2003b], associating primarily with proteins. Po-210 is also preferentially assimilated by zooplankton with respect to ^{210}Pb [*Stewart and Fisher*, 2003a; *Stewart et al.*, 2005]. Yet, the mechanisms of biological uptake and bioaccumulation of ^{210}Po remain unclear [*Stewart et al.*, 2008; *Fowler*, 2011]. Because there is no known biological requirement for ^{210}Po, it is likely taken up as an analogue of some required element. Owing to its behaviour being similar to Se, it has been suggested that ^{210}Po acts as a sulphur-analogue or binds to sulphur ligands [*Stewart et al.*, 2008]. Thus, ^{210}Po is more strongly bound to biogenic particles than is ^{210}Pb. In consequence, the sinking of biogenic particles in the upper ocean creates a deficit of ^{210}Po that can be used to estimate POC export fluxes (Figure 1.12B) [see review by *Verdeny et al.*, 2009]. Similarly to ^{234}Th, ^{210}Po activities in subsurface waters can exceed those of ^{210}Pb due to particle remineralization or disaggregation of Po-bearing particles [*Bacon et al.*, 1988].

1.5.3 POC export by using $^{234}Th/^{238}U$ and $^{210}Po/^{210}Pb$

There are several scavenging models of ^{234}Th and ^{210}Po with different levels of complexity in the representation of particle and sorption dynamics (separation into dissolved and particulate pools vs. total fraction, incorporation of different particle-size classes, reversible vs. irreversible scavenging) [see review by *Savoye et al.*, 2006].

The one-box irreversible scavenging model can be applied when the total activities of the radionuclides of interest are measured, consisting of the simplest and most commonly used model. This model is the result of a balance between continuous production of the daughter isotope from its parent in seawater, the atmospheric input (in the case of ^{210}Po), radioactive decay and removal of the daughter driven by sinking particles, and its inputs or outputs by physical transport processes. Then, the temporal change of total ^{234}Th and ^{210}Po in the water column can be expressed as follows:

$$\frac{\partial A_D}{\partial t} = Ø + A_P\,\lambda_D - A_D\,\lambda_D - F_D \pm V \qquad (1.1),$$

where D stands for "daughter" (^{234}Th or ^{210}Po) and P for "parent" (^{238}U or ^{210}Pb, respectively). A is the total activity (dissolved + particulate), Ø the atmospheric flux of ^{210}Po, λ_D the decay constant of ^{234}Th (0.029 d^{-1}) or ^{210}Po (0.0050 d^{-1}), F_D the particulate export flux of the daughter isotope (dpm m^{-2} d^{-1}), and V the sum of the advective and diffusive fluxes.

The atmospheric flux of ^{210}Po is usually not considered [*Murray et al.*, 2005; *Stewart et al.*, 2007a; *Verdeny et al.*, 2008], since it represents only about 2% of the in situ production of ^{210}Po from ^{210}Pb in the upper water column of the open ocean [*Masqué et al.*, 2002]. Thus, when steady-state conditions can be assumed (i.e. $\frac{\partial A_D}{\partial t} = 0$), and physical transport processes ignored, the export fluxes of ^{234}Th and ^{210}Po can be calculated as follows:

$$F_D = \lambda_D(A_P - A_D) \qquad (1.2),$$

where ($A_P - A_D$) is the integrated daughter deficit with respect to its parent, down to a specific depth in the upper water column (dpm m^{-2}). This model is often valid for open-ocean stations with minimal advection and diffusion where particle export is not especially high [*Savoye et al.*, 2006]. When the steady-state assumption is not valid ($\frac{\partial A_D}{\partial t} \neq 0$), such as during the collapse and sinking of a phytoplankton bloom [*Buesseler et al.*, 1992], it is required to reoccupy the sampling stations within the half-life of the daughter isotope in order to apply the non-steady state model [*Savoye et al.*, 2006]:

$$F_D = \lambda_D \left[\frac{A_P(1-e^{-\lambda_D \Delta t}) + A_{D1} e^{-\lambda_D \Delta t} - A_{D2}}{1-e^{-\lambda_D \Delta t}} \right] \quad (1.3),$$

where Δt is the time interval between two visits of a single station and A_{D1} and A_{D2} the activities of the daughter isotope at the first and second visits, respectively. Note that this model assumes that the same water masses are sampled, the parent activity and daughter flux are constant over the time period between occupations, and physical transport terms are neglected.

In the application of ^{234}Th and ^{210}Po in coastal areas and other dynamic systems, physical transport processes should be incorporated, which are parameterized as:

$$V = \pm u \frac{\partial A_D}{\partial x} \pm v \frac{\partial A_D}{\partial y} \pm w \frac{\partial A_D}{\partial z} \pm K_x \frac{\partial^2 A_D}{\partial x^2} \pm K_y \frac{\partial^2 A_D}{\partial y^2} \pm K_z \frac{\partial^2 A_D}{\partial z^2} \quad (1.4),$$

where advective and diffusive components are included along the x, y and z directions. Velocities are denoted by u, v and w, $\frac{\partial A_D}{\partial x}$, $\frac{\partial A_D}{\partial y}$ and $\frac{\partial A_D}{\partial z}$ are the daughter activity gradients and K_x, K_y and K_z the diffusion coefficients.

Once the ^{234}Th and ^{210}Po downward fluxes at a specific depth are quantified, these fluxes can be converted to POC fluxes (F_C), or other elemental fluxes, by determining the POC/^{234}Th or POC/^{210}Po ratios (C/D) on the sinking-particle pool at the selected depth [*Buesseler et al.*, 1992; *Cochran and Masqué*, 2003]:

$$F_C = F_D(C/D) \quad (1.5).$$

The C/D ratio should be representative of the particle pool that originates the deficit of ^{234}Th or ^{210}Po observed in overlying waters. These particles are sampled by filtration or the use of devices that allow the capture of setting particles, typically sediment traps. Sediment traps are usually considered to be better in collecting the actual settling particles. However, the limitations that are associated with the deployment of traps can bias the nature and, therefore, the elemental concentrations of the sinking flux (see Section 1.4) [*Gustafsson et al.*, 2004; *Stanley et al.*, 2004]. When sediment traps are not available or there is not enough ship time, in situ filtration pumps are usually used, since they can filter several hundreds of litres of seawater in one or two hours. Particles are most often separated using a 53-μm pore-size screen, since particles larger than 53 μm are assumed to be those that sink. Nevertheless, several uncertainties arise from this size classification, the filtration device used, and the subsequent handling of the samples [e.g. *Lepore et al.*, 2009b; *Liu et al.*, 2009; *Durkin et al.*, 2015]. This, combined with regional, temporal and depth variations in C/D ratios, makes the determination of this parameter the greatest source of uncertainty in the application of radionuclides as proxies for POC export [see review by *Buesseler et al.*, 2006].

1.6 Objectives

The overall goal of this thesis is to provide insights into the particle export and the biological pump strength and efficiency in the upper water column of the polar oceans by using the $^{234}Th/^{238}U$ and $^{210}Po/^{210}Pb$ radionuclide pairs, accompanied by physical and biological information to gain understanding on the mechanisms that drive the export of POC.

This is addressed through four specific objectives:

1) Quantify the POC export in the upper water column of the Southern Ocean during the decline of a bloom at high spatial resolution covering time scales of days to weeks using the $^{234}Th/^{238}U$ proxy and sediment traps.

2) Estimate the magnitude of the POC export from the upper water column of the central Arctic from the beginning of the productive season until late summer by the joint application of the $^{234}Th/^{238}U$ and $^{210}Po/^{210}Pb$ pairs.

3) Analyse the distribution of the $^{210}Po/^{210}Pb$ pair on a pan-Arctic scale to investigate the processes governing the dynamics of particles and particle export in the shelf and basin environments of the Arctic Ocean.

4) Evaluate how ecologically relevant parameters, including primary production, phytoplankton community composition and sea-ice conditions, modulate the POC export from the mixed layer and its transfer to deeper waters.

Chapter 2

Analytical methods

This chapter is devoted to describing the sampling and analytical procedures used to determine radionuclide activities in seawater and particulate samples, as well as particulate organic carbon (POC) concentrations to estimate carbon export fluxes (see Chapters 3 and 4). The radiochemistry process was performed at the Universitat Autònoma de Barcelona (UAB) and the Alfred Wegener Institute (AWI). Both laboratories have participated in inter-calibration studies of ^{234}Th, ^{210}Pb and ^{210}Po in seawater and marine particles [*Church et al.*, 2012; *Maiti et al.*, 2012]. Analytical methods for ancillary measurements are included in the respective chapters (see Chapters 3-5).

2.1 Seawater samples

Th-234, ^{210}Pb, and ^{210}Po activities were determined from seawater samples collected using Niskin bottles attached to a conductivity-temperature-depth (CTD) rosette. In the Arctic Ocean in 2007 (Chapter 5), surface seawater samples (10 m) were taken from the ship seawater intake.

2.1.1 ^{238}U and ^{234}Th

The activity of ^{238}U was derived from salinity using the relationship given by *Owens et al.* [2011]:

$$^{238}\text{U}\ (\pm\ 0.047,\ \text{dpm L}^{-1}) = 0.0786 \times \text{salinity} - 0.315 \qquad (2.1).$$

This relationship is based on several oceanographic expeditions in open waters of the Atlantic and Southern Oceans and covers a salinity range from 32.69 to 37.10. Salinity data were obtained from the CTD measurements, ranging from 33.80 to 34.65 in the upper 750 m of the Southern Ocean around 51°S 13°W (see Chapter 3) and from 30.02 to 35.00 in the upper 400 m of the central Arctic Ocean (see Chapter 4). In this latter case, three sampling stations had salinities falling below the range used by *Owens et al.* [2011] from 10 to 30 m depth (n = 15). For these samples, the U-salinity relationship given by *Not et al.* [2012] was also applied:

$$^{238}\text{U}\ (\text{dpm L}^{-1}) = (0.0678 \pm 0.0004) \times \text{salinity} \qquad (2.2).$$

This relationship was determined from sea ice, surface seawater and sea-ice brine samples collected in the Arctic, covering a wide salinity range from 0 to 135. A difference of only 1.1% in ^{238}U activity, which is lower than its associated uncertainty (1.9-2.3%), was obtained using the two relationships, validating the use of Owens's relationship in the central Arctic Ocean.

Total ^{234}Th activities were determined from a total of 298 samples during two oceanographic expeditions in the Southern and Arctic Oceans in 2012 (Chapters 3 and 4, respectively). Four-litre samples were processed according to the MnO_2 co-precipitation technique [*Benitez-Nelson et al.*,

2001; *Buesseler et al.*, 2001a], using ^{230}Th as a chemical yield tracer to account for possible losses of ^{234}Th [*Pike et al.*, 2005]. Just after collection, the samples were acidified to pH 1-2 using nitric acid (~5 mL HNO_3 65%), and spiked with ^{230}Th (0.2 mL, 13.2 dpm mL^{-1}). The samples were shaken vigorously and allowed to equilibrate for at least ten hours. Then, the pH of the samples was raised to ~8.5 using ammonia (~6 mL NH_3 30%). Potassium permanganate (50 µL $KMnO_4$, 7.5 g L^{-1}) and manganese (II) chloride (50 µL $MnCl_2$, 30 g L^{-1}) were added to create a manganese dioxide (MnO_2) precipitate that scavenges thorium isotopes, but negligible amounts of uranium. After each reagent addition, the samples were shaken vigorously and allowed to stand for at least five hours prior to filtration. The precipitates were filtered through quartz-fibre filters (QMA, 25 mm, Whatman) (Figure 2.1) and dried overnight at 50°C. Then, the filters were mounted on plastic discs and covered with a layer of plastic film and a layer of aluminium foil (8.0 mg cm^{-2}) for beta counting.

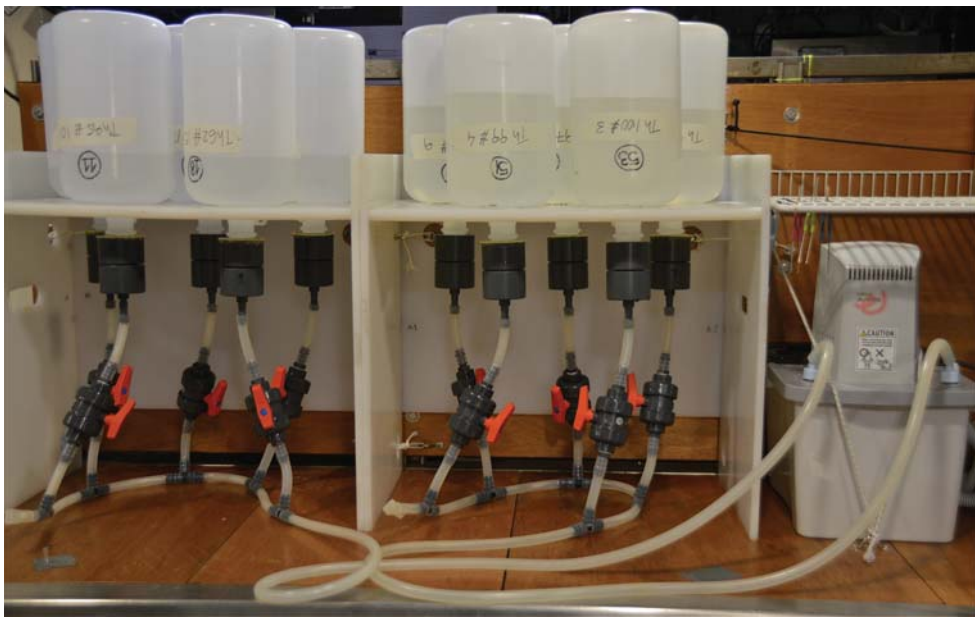

Figure 2.1: Filtration system for ^{234}Th with 4-L bottles connected to an Eyela aspirator vacuum pump.

The counting was done on board using low-background beta multi-counter systems (Risø National Laboratory, Denmark) (Figure 2.2), which allow the simultaneous measurement of five samples. The gas-flow counters were placed into a lead shielding that reduced the ambient background radiation down to ~0.20 counts per minute (cpm). Th-234 (E_{max} 199 keV) was measured via the detection of its high-energy beta-emitting daughter, ^{234m}Pa ($T_{1/2}$ = 1.17 minutes, E_{max} 2290 keV) [*Rutgers van der Loeff et al.*, 2006], with a counting efficiency of ~40%. The samples were counted in cycles of 60 minutes until the counting uncertainty was below 3%. Samples were re-measured after seven to ten months to quantify the background activity of other high-energy beta emitters present in the precipitate (e.g. ^{214}Bi) [*Benitez-Nelson et al.*, 2001], which amounted to 0.15 ± 0.04 cpm.

The detectors were calibrated by measuring ^{238}U standards (with ^{234}Th in secular equilibrium), which were mounted in the same geometry as the samples. Additionally, replicates of deep samples (1500-3000 m), where ^{238}U and ^{234}Th are expected to be in secular equilibrium, were collected during both expeditions to verify the detector calibration.

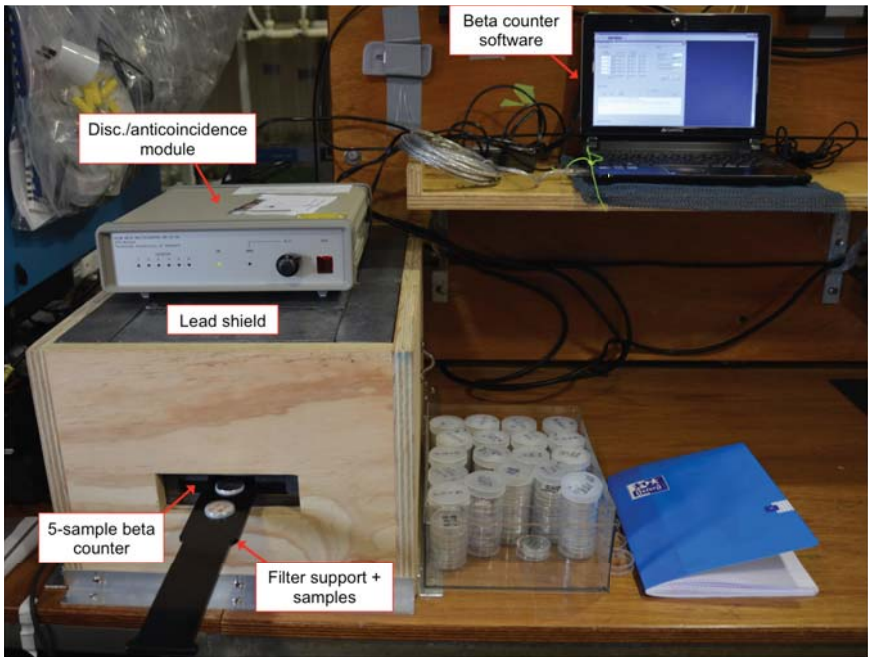

Figure 2.2: Low-background beta multi-counter system mounted on board with the main components identified. The discriminator/anticoincidence module receives the signals produced by beta particles from the individual counters and incorporates an automatically controlled high-voltage supply.

In order to calculate the chemical recovery of ^{234}Th, all samples were processed to determine ^{230}Th by inductively coupled plasma-mass spectrometry (ICP-MS, Thermo Finnigan MAT, Germany) using ^{229}Th as an internal standard. The precipitates were spiked with ^{229}Th (0.095 g, 217.8 dpm g^{-1}) and dissolved in 10 mL of 8 M HNO_3/10% H_2O_2 solution in beakers. The beakers were covered with parafilm and sonicated for 30 minutes before allowing them to rest for at least six hours. Prior to the ICP-MS analyses the samples were filtered through Acrodisc 0.2-µm syringe filters (13 mm, Pall Corporation) and reconstructed with 2.5% HNO_3/0.01% HF. This simple procedure has been tested and produces results that agree well within error with those obtained using anion-exchange column chemistry [*Puigcorbé*, 2016]. The average chemical recovery of the analytical process was 94 ± 7%, and the uncertainty of the $^{230}Th/^{229}Th$ ratios was below 2%. Thorium-234 activities were corrected for ingrowth and radioactive decay to the time of collection. The ^{234}Th activity uncertainties were calculated by propagating uncertainties associated with counting, detector background and calibration, ICP-MS measurements and ^{238}U activities, and were always <10%.

2.1.2 ^{210}Pb and ^{210}Po

Pb-210 and ^{210}Po activities were determined from a total of 246 samples during two oceanographic expeditions in the Arctic Ocean in 2007 and 2012 (Chapters 5 and 4, respectively). The samples from 2012, which represent one-third of the total, were pre-concentrated with cobalt-ammonium pyrrolidine dithiocarbamate (Co-APDC, see Chapter 4), whereas the remaining two-thirds from 2007 were pre-concentrated with iron hydroxides ($Fe(OH)_3$, see Chapter 5).

For the Co-APDC co-precipitation technique [*Fleer and Bacon*, 1984], total ^{210}Pb and ^{210}Po activities were determined from 11 L of seawater. The samples were immediately acidified after collection with hydrochloric acid (~12 mL HCl 37%) to pH below 2 and spiked with stable Pb (0.075 mL, 61.2 mg mL^{-1}) and ^{209}Po (0.050 mL, 42.2 dpm mL^{-1}) as chemical yield tracers. Cobalt (II) nitrate hexahydrate (12 mL $Co(NO_3)_2 \cdot 6\ H_2O$, 4.9 mg mL^{-1}) and APDC (40 mL, 2 g 100 mL^{-1}) solutions were added after at least one day of isotope equilibration. After each reagent addition, the samples were shaken vigorously and allowed to stand for a few hours prior to filtration. The samples were then filtered through 0.2-µm pore-size membrane-filters (142 mm, Whatman) and stored for later processing at the home laboratory. At the UAB, the filters were digested using concentrated HNO_3 (30 mL) and samples were reconstructed with 1 M HCl.

For the co-precipitation with $Fe(OH)_3$ [*Thomson and Turekian*, 1976; *Nozaki*, 1986], total and dissolved (<1 µm, see Section 2.2) ^{210}Pb and ^{210}Po activities were determined from 20 L of seawater using iron (III) chloride ($FeCl_3$) as a carrier. The samples were immediately acidified after collection and filtration, for the total and dissolved fractions, respectively, with concentrated HNO_3 (~20 mL), and spiked with stable Pb (0.10 mL, 98.7 $\cdot 10^{-5}$ mg mL^{-1}) and ^{208}Po (0.50 mL, 187.6 dpm mL^{-1}). After addition of $FeCl_3$ (3 mL, 50 mg mL^{-1}) and vigorous stirring, samples were allowed to equilibrate for about 24 hours. Pb and Po were then co-precipitated with $Fe(OH)_3$ by adjusting the pH to ~8.5 with NH_3. After a few hours, supernatants were removed carefully by centrifugation and decantation. The precipitates were transferred to plastic bottles and stored until further analyses at the home laboratory. At the AWI, the precipitates were dissolved in 0.5 M HCl adding ascorbic acid to complex the iron.

Pb and Po were separated by auto-deposition of Po onto silver discs (i.e. plating) at ~80°C during four to six hours (Figure 2.3) [*Flynn*, 1968; *Fleer and Bacon*, 1984]. The silver discs were then counted by alpha spectrometry using passivated implanted planar silicon (PIPS) alpha detectors (Canberra, USA) and silicon surface barrier (SSB) alpha detectors (EG&G Ortec, USA). These detectors are characterized by an excellent energy resolution and low background. In this case, the activities of ^{210}Po do not rely on the detector efficiency, but on the internal tracer added at the beginning of the

analytical process. The discs were usually measured long enough to achieve counting statistics below 5%.

Figure 2.3: Auto-deposition of Po isotopes onto silver discs using a hot plate that allows temperature and stirring control.

The alpha spectrum consisted of two single peaks ^{210}Po (5304 keV) and ^{209}Po (4882 keV), or ^{210}Po and ^{208}Po (5215 keV), depending on the spike used. Correction for interferences between the peaks of ^{210}Po and ^{208}Po are required (ΔE = 89 keV), whereas for ^{210}Po and ^{209}Po it is not (ΔE = 422 keV). The quantification of the ^{210}Po activity at the measuring time (A_{210}) is calculated as:

$$A_{210} = A_S \cdot \frac{N_{210}}{N_S} \qquad (2.3),$$

where A_S is the activity of the spike added to the sample, either ^{209}Po or ^{208}Po, and N_{210} and N_S are the net counts of ^{210}Po and the spike, respectively. The net counts are obtained by subtracting the detector background (~0.0012 cpm for ^{208}Po, ~0.0030 cpm for ^{209}Po and ~0.0005 cpm for ^{210}Po) and the corresponding blank to the total counts measured. For samples co-precipitated with Co-APDC, the solutions were re-plated and passed through an anion-exchange resin (AG 1-X8, Bio-Rad) to ensure the complete elimination of polonium from samples [*Rigaud et al.*, 2013]. Both sets of samples, those processed at the UAB (i.e. Co-APDC) and the AWI (i.e. $Fe(OH)_3$) were re-spiked with ^{209}Po (UAB: 0.050 g, 37.4 dpm g^{-1}; AWI: 0.32 g, 5.7 dpm g^{-1}) and stored for nine to eleven months in 9 M HCl, and for one to two years in 8 M HNO_3, respectively, for later determination of ^{210}Pb via ^{210}Po ingrowth. At that time, samples were plated and counted once more by alpha spectrometry.

The chemical recovery of stable Pb was determined by inductively coupled plasma-optical emission spectrometry (ICP-OES, Perkin-Elmer/Thermo Fisher Scientific, USA) in one or two aliquots collected from each sample. Two aliquots were taken before the first and last platings from the samples that passed through an anion-exchange resin, while only one aliquot was extracted after the last plating from the other samples. The average recovery was similar for both sets of samples with an average of 83 ± 7%. Pb-210 and ^{210}Po activities at the sampling time were calculated applying appropriate ingrowth, decay and recovery corrections following *Fleer and Bacon* [1984] and *Rigaud et al.* [2013]. The activity uncertainties, which account for counting, detector background, and spike activities, were on average 5% for ^{210}Pb and 9% for ^{210}Po in 2007 and 7% for ^{210}Pb and 16% for ^{210}Po in 2012. The greater uncertainties of ^{210}Po are due to the time elapsed between sampling and the first Po plating (>55 days and >80 days, respectively).

2.2 Particulate samples

Samples for the determination of ^{234}Th, ^{210}Pb, ^{210}Po, POC and particulate organic nitrogen (PON) in marine particles were obtained by using different devices, namely sediment traps (ST), in situ pumps (ISP) and Niskin bottles, depending on the oceanographic expedition.

In the Southern Ocean in 2012 (Chapter 3), sinking particles were collected using surface-tethered sediment traps (KC, Denmark) deployed for one to three days. The ST were attached to a drifting array with a surface buoy equipped with a GPS satellite transmitter, two surface floats and 12 buoyancy balls acting as wave breakers in order to reduce the hydrodynamic stress on traps. The ST array was equipped with two sets of four gimbal mounted collection cylinders (100 x 10.4 cm, Figure 2.4) positioned at nominal depths of 100–120 m and 300–320 m, respectively. At each depth, three cylinders were filled with an un-poisoned brine solution for biogeochemical analyses and one cylinder with a viscous gel to preserve sinking particles in their original shape. The content of one of the cylinders was homogenized and cleared of swimmers under a binocular microscope. Half of the volume was filtered through a pre-combusted QMA filter to analyse ^{234}Th, POC and PON on the same filter, as recommended by *Buesseler et al.* [2006], and the other half was filtered through a pre-combusted GF/F filter to analyse POC and PON.

Figure 2.4: Surface-tethered sediment trap, which mainly consists of four cylinders that capture settling particles, deployed during the ANT-XXVIII/3 expedition (see Chapter 3). Picture kindly provided by Morten H. Iversen.

In the Southern and Arctic Oceans in 2012 (Chapters 3 and 4), large (>53 µm) particles were collected using battery-operated ISP (Challenger Oceanic, UK) (Figure 2.5). ISP were deployed at four depths during 1.5 to 2 hours, filtering on average 1300 L. Particles were retained using 53-µm pore-size nylon-mesh screens (142 mm, Nitex). Particles were subsequently rinsed with filtered seawater (<0.2 µm), homogenized, and re-filtered through pre-combusted QMA filters to analyse ^{234}Th, POC and PON on the same filter. In the Arctic Ocean (Chapter 4), another aliquot was filtered through QMA filters to analyse ^{210}Pb and ^{210}Po. Swimmers observed by naked eye were picked from all samples.

For both types of samples, ST and ISP, the activity of ^{234}Th in particles was first measured on board and re-measured at the home laboratory seven to nine months later as described for seawater samples (see Section 2.1.1). The concentration of POC and PON was determined with an Elemental Analyser (EuroVector, Italy), pre-treating the filters with diluted HCl to remove carbonate [*Knap et al.*, 1996]. The results were corrected for POC and PON blanks, which on average represented less than 8% of the POC and PON measurements. At the UAB, the filters for ^{210}Pb and ^{210}Po determination were spiked with stable Pb (0.085 g, 53.3 mg g^{-1}) and ^{209}Po (0.050 g, 37.4 dpm g^{-1}), digested using a mixture of concentrated HNO_3, HF and HCl (5, 3 and 2 mL, respectively), evaporated to dryness and reconstructed with 1 M HCl. Samples were processed and measured by alpha spectrometry as seawater samples (see Section 2.1.2).

Figure 2.5: In situ pump employed during the ANT-XXVIII/3 and ARK-XXVII/3 expeditions (Chapters 3 and 4).

In the Arctic Ocean in 2007 (Chapter 5), 40 to 160 L of seawater were filtered through 1-µm pore-size Nuclepore filters (142 mm, Whatman) for the determination of ^{210}Pb and ^{210}Po in the particulate fraction. The filters were dried at room temperature and stored for later processing at the home laboratory. At the AWI, the filters were spiked with stable Pb (0.10 g, $97.8 \cdot 10^{-5}$ mg g^{-1}) and ^{208}Po (0.25 g, 144.3 dpm g^{-1}), and digested using a microwave with a mixture of concentrated HNO_3, H_2O_2 and HF (10, 2 and 0.3 mL, respectively). Subsequently, $FeCl_3$ (150 µL, 50 mg mL^{-1}) was added and Pb and Po isotopes were then co-precipitated and measured as seawater samples (see Section 2.1.2).

Chapter 3

High particulate organic carbon export during the decline of a vast diatom bloom in the Atlantic sector of the Southern Ocean

This chapter has been published as:
Roca-Martí, M., Puigcorbé, V., Iversen, M.H., Rutgers van der Loeff, M., Klaas, C., Cheah, W., Bracher, A., Masqué, P (2017). High particulate organic carbon export during the decline of a vast diatom bloom in the Atlantic sector of the Southern Ocean. *Deep Sea Research Part II: Topical Studies in Oceanography*, 138, 102-115. doi: 10.1016/j.dsr2.2015.12.007.

3.1 Aim

Carbon fixation by phytoplankton plays a key role in the uptake of atmospheric CO_2 in the Southern Ocean [*Hauck et al.*, 2013]. Yet, it still remains unclear how efficiently the particulate organic carbon (POC) is exported and transferred from ocean surface waters to depth during phytoplankton blooms. In addition, little is known about the processes that control the flux attenuation within the upper twilight zone.

This study focuses on the decline of a vast diatom bloom that occurred in the Antarctic Circumpolar Current (ACC) region of the Southern Ocean (around 51°S 13°W) during the late austral summer in 2012. The objectives were to evaluate the export efficiency and transfer efficiency of POC between 100 and 300 m, as well as identify the main mechanisms that had an influence on particle fluxes. Export fluxes of POC were quantified by means of two different techniques, the disequilibrium between the natural radionuclides ^{234}Th and ^{238}U and surface-tethered drifting sediment traps (ST), as recommended by previous studies given the uncertainties associated with each particle export measurement [e.g. *Puigcorbé et al.*, 2015; *Turner*, 2015]. Export fluxes were related to the evolution of chlorophyll *a* (Chl-a) and POC concentrations in the water column, as well as to pigments in sinking particles, following the decline of the bloom during three weeks. Net primary production (NPP) measured during the same cruise [*Hoppe et al.*, 2017] was used to assess the export efficiency.

3.2 Methods

3.2.1 Study area

Samples were collected from 29 January to 17 February 2012 during the ANT-XXVIII/3 expedition in the Atlantic sector of the Southern Ocean (7 January to 11 March, 2012; R/V Polarstern) [*Wolf-Gladrow*, 2013]. The sampling was carried out to study a massive bloom with high spatial and temporal resolution over an area of about 8000 km^2 located between the Antarctic Polar Front (APF) and the Southern Polar Front (SPF) [*Strass et al.*, 2017]. Time-series measurements of ^{234}Th, POC, particulate organic nitrogen (PON), Chl-a, other pigments and NPP were carried out at a station located in the centre of the study area at 51.21°S 12.67°W (hereafter "central station", indicated by a 'C' in front of the station number). The location and sampling dates of the stations sampled for ^{234}Th, POC and PON fluxes are given in Figure 3.1 and Table 3.1.

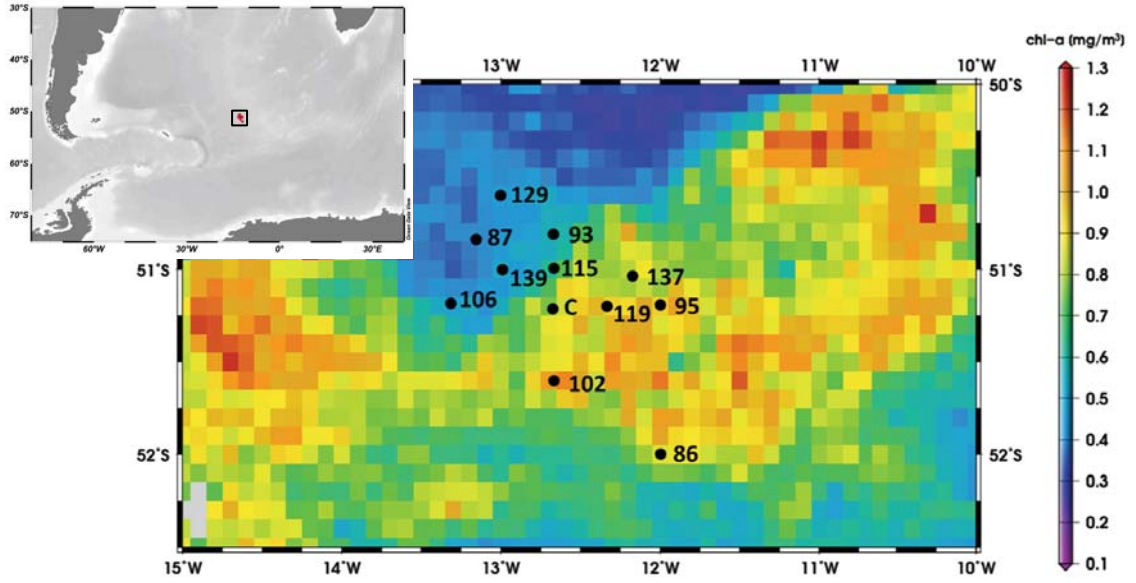

Figure 3.1: Study area and sampled stations during the ANT-XXVIII/3 cruise for ^{234}Th, POC and PON analyses. C represents the central station, which was occupied seven times: C91, C98, C99, C114, C128, C136, C140. See Table 3.1 for further details regarding sampling dates. The satellite plot represents the mean Chl-a concentration from the OC-CCI Chl-a product version-2 during the sampling period (29 January to 17 February 2012).

3.2.2 Total ^{238}U and ^{234}Th

Total ^{234}Th activities were determined from 11-13 depths down to 500-750 m at 14 stations, with the highest resolution in the upper 200 m of the water column. Three seawater profiles were taken at the central station on 3, 12 and 17 February (C91, C128, C140, respectively). Th-234 activities were determined following the methods described in Chapter 2 (see Section 2.1.1). The activity of ^{238}U was derived from salinity using the relationship given by *Owens et al.* [2011]. All data of total ^{238}U and ^{234}Th activities are available at *http://dx.doi.org/10.1594/PANGAEA.848823*.

3.2.3 ^{234}Th, POC and PON in particles

Sinking particles were collected using two surface-tethered sediment traps deployed for one to three days at depths of 100-120 m and 300-320 m (Table 3.2). The ST were attached to a drifting array equipped with two sets of four collection cylinders as described in Chapter 2 (see Section 2.2). The ST were deployed a total of eleven times, including seven deployments at the central station (C91, C98, C99, C114, C128, C136, C140) between 3 and 17 February. One of the cylinders for biogeochemical analyses was used: (i) one half was filtered through a pre-combusted QMA filter to analyse ^{234}Th, POC and PON on the same filter as recommended by *Buesseler et al.* [2006]; and (ii) the other half split was filtered using a pre-combusted GF/F filter to analyse POC and PON. The total POC and PON fluxes collected with the ST were determined as the average of the fluxes obtained from samples (i) and (ii). Additionally, four in situ pumps (ISP) were deployed at 100, 150,

300 and 400 m at two stations (C91 and 139, Table 3.2) to collect particles using 53-µm pore-size nylon-mesh screens. Particles were subsequently rinsed with filtered seawater and re-filtered through a pre-combusted QMA filter to analyse ^{234}Th, POC and PON. The activity of ^{234}Th and POC and PON concentrations were determined as described in Chapter 2 (see Section 2.2). The POC and PON concentrations were corrected for blanks (1.38 and 0.20 µmol, respectively), which on average represented about 2% of the POC and PON measurements.

Table 3.1: Location and date of the stations sampled during the ANT-XXVIII/3 cruise for ^{234}Th, POC and PON analyses. C indicates the central station.

Station	Longitude (°W)	Latitude (°S)	Date (2012)
86	12.00	52.00	29-30 Jan.
87	13.16	50.84	2-3 Feb.
93	12.67	50.81	4 Feb.
95	12.00	51.19	5 Feb.
102	12.67	51.60	7 Feb.
106	13.31	51.18	7 Feb.
115	12.67	50.99	9 Feb.
119	12.33	51.20	10 Feb.
129	13.00	50.60	13 Feb.
137	12.17	51.04	14-15 Feb.
139	12.99	51.00	15-16 Feb.
C91	12.67	51.21	3-5 Feb.
C98	12.67	51.21	5-6 Feb.
C99	12.67	51.21	6-8 Feb.
C114	12.67	51.21	8-11 Feb.
C128	12.67	51.21	12-13 Feb.
C136	12.67	51.21	14-15 Feb.
C140	12.67	51.21	16-17 Feb.

3.2.4 Pigments in sediment traps

One fifth of a ST cylinder dedicated to biogeochemical analyses was used to analyse pigments after picking off swimmers. Diluted ST samples were filtered through GF/F filters, under low-vacuum pressure (below 20 kPa). Filtered samples were then immediately shock-frozen in liquid nitrogen and stored at -80°C until further analyses at the Alfred Wegener Institute. Pigments were analysed based on the high-performance liquid chromatography (HPLC) method of *Barlow et al.* [1997] as detailed in *Cheah et al.* [2017]. The samples were measured using a Waters 600 (Waters, USA) controller combined with a Waters 2998 photodiode array detector, and a Water 717plus auto-sampler. Hundred microliter of canthaxanthin was added to each sample as an internal standard. Pigments were identified and quantified using the EMPOWER software provided by Waters. Three pigment-based phytoplankton size classes (micro-, nano-, and picophytoplankton) were estimated following the method of *Uitz et al.* [2009], which has been tested for the Southern Ocean.

Microphytoplankton corresponded to phytoplankton with size >20 µm, nanophytoplankton between 2 and 20 µm, and picophytoplankton between 0.2 and 2 µm.

Table 3.2: Sampling of particles using sediment traps and in situ pumps: location, depth, date, duration of the deployment (sediment traps) and filtered volume (in situ pumps).

Station	Deployment sediment traps			Deployment in situ pumps		
	Depth (m)	Date (2012)	Duration (h)	Depth (m)	Date (2012)	Volume (L)
86	100, 300	29 Jan.	23			
87	100, 300	2 Feb.	20			
137	120, 320	14 Feb.	15			
139	120, 320	15 Feb.	19	100, 150, 300, 400	16 Feb.	250-900
C91	100, 300	3 Feb.	53	100, 150, 300, 400	3 Feb.	450-1200
C98	100, 300	5 Feb.	18			
C99	100, 300	6 Feb.	50			
C114	100, 300	8 Feb.	72			
C128	120, 320	12 Feb.	29			
C136	120, 320	14 Feb.	22			
C140	120, 320	16 Feb.	18			

3.2.5 Chl-a and POC in the water column

Seawater samples for Chl-a (Chl-a_{SW}) and POC determination were obtained from Niskin bottles attached to a conductivity-temperature-depth (CTD) rosette from five to six depths in the upper 100 m at 33 stations. For Chl-a_{SW} analysis, samples were filtered onto GF/F filters at a pressure below 20 kPa. The filters were immediately transferred to centrifuge tubes with 10 mL 90% acetone and 1 cm^3 of glass beads. The tubes were sealed and stored at -20°C for at least 30 minutes. Chl-a was extracted by placing the centrifuge tubes in a grinder for three minutes followed by centrifugation at 0°C. The supernatant was poured in quartz tubes and measured for Chl-a content in a Turner 10-AU fluorometer, which was calibrated at the beginning and at the end of the expedition. Chl-a content was calculated using the equation given in *Knap et al.* [1996] using average parameter values from both calibrations. For POC analysis, samples were filtered onto pre-combusted GF/F filters at pressure not exceeding 20 kPa. Filters were immediately transferred to pre-combusted glass Petri dishes and dried overnight at 50°C. Filters were stored at -20°C until analysis at the home laboratory using an EuroVector Elemental Analyser. The samples were corrected for POC blanks and the uncertainty of the POC measurements was 1.9% based on three reference standards.

3.2.6 Satellite Chl-a concentration

Satellite Chl-a concentration was taken from the merged daily OC-CCI Chl-a data (ESACCI-OC-L3S product, ~4 km, version-2) [*http://www.oceancolour.org/*] and averaged over the time period of the sampling. The OC-CCI data product combines the Medium Resolution Imaging Spectrometer (MERIS) on the Envisat satellite, the Moderate Resolution Imaging Spectrometer (MODIS) on the Aqua satellite and the Sea-viewing Wide Field-of-view Sensor (SeaWiFS) on the OrbView-2 satellite to one Chl-a product. This data product improves coverage of satellite Chl-a data in polar regions by a factor of 2 to 3 as compared to using the products of one single sensor. More details on the processing steps can be found in the product user guide [*OC-CCI*, 2015].

3.3 Results

3.3.1 Study area

Detailed hydrographic information can be found in *Strass et al.* [2017]. The study area was placed between the APF and the SPF within the ACC and around a central station located at 51.21°S 12.67°W. The main water masses identified were: Winter Water (WW, minimum potential temperature, θ_{min} = 1.1-1.9°C, 100-200 m), Upper Circumpolar Deep Water (UCDW, θ_{max} = 2.1-2.4°C, 400-500 m) and Antarctic Bottom Water (AABW, θ_{min} ~-0.2°C). The mixed layer depth (MLD) varied from 24 to 98 m (average: 67 ± 18 m, n = 73) [*Strass et al.*, 2017]. At the central station the structure of the upper water column varied over time: (i) the MLD ranged from ~75 to 100 m, and some profiles did not show a homogeneous surface layer; (ii) the location of the WW θ_{min} fluctuated several tens of meters above and below 150 m; (iii) many profiles showed temperature inversions below the θ_{min} depth and fluctuations of salinity and density within the depth range 200-300 m during the second half of the sampling period. Moreover, at the central station currents flowing to the NE were intensified over time, with speeds averaging from 2 to 10 cm s^{-1} for the top 500 m [*Strass et al.*, 2017].

Satellite-derived Chl-a concentrations during the sampling period were, on average, lower than 1.5 mg m^{-3} (Figure 3.1), whereas at the peak of the bloom, during the first half of January, the Chl-a concentrations were ~3 mg m^{-3} [*Hoppe et al.*, 2017]. The euphotic zone depth ranged between 36 and 66 m (average: 45 ± 7 m, n = 40) [*Cheah et al.*, 2017]. Nutrient concentrations and deficits are described in *Hoppe et al.* [2017]. On average, macronutrient concentrations within the euphotic zone were ~21 mmol NO_3 m^{-3}, ~1.4 mmol PO_4 m^{-3} and ~6.6 mmol $Si(OH)_4$ m^{-3}. High iron concentrations that allowed the development of the massive bloom likely reached the study site via advection through the ACC (L.M. Laglera pers. comm.). Concentrations of dissolved iron

(<0.2 µm) were on average 0.12 ± 0.03 nM within the top 100 m of the water column [*Hoppe et al.*, 2017], suggesting that dissolved iron was already depleted by phytoplankton activity during our sampling.

3.3.2 ^{234}Th activity profiles and fluxes

The vertical profiles of ^{238}U and ^{234}Th activity in the water column are shown in Figure 3.2. Significant deficits of ^{234}Th with respect to ^{238}U were present in surface waters down to 100-170 m at all stations, with ^{234}Th/^{238}U ratios averaging 0.67 ± 0.11 throughout the upper 100 m. In most cases, the base of these deficits matched well with the base of the primary production zone (PPZ, Figure 3.2), defined as the depth at which fluorescence reaches 10% of its maximum value [*Owens*, 2013]. The PPZ extended, on average, down to 117 ± 12 m, and the NPP at 100 m (deepest depth for NPP determination) ranged from 0.09 to 0.44 mmol C m^{-3} d^{-1}, confirming that primary production was occurring at least until 100 m (C. Hoppe pers. comm.). Below the PPZ, significant excesses of ^{234}Th (^{234}Th/^{238}U ratio >1.1) were detected at stations C91 and 106 at one single depth (500 m). Significant ^{234}Th deficits (^{234}Th/^{238}U ratio <0.9) below the PPZ were also found at single depths at stations 93, C128, 137 and 139 (150, 750, 500 and 400 m, respectively). The central station showed a greater ^{234}Th deficit along the top 100 m during the second and third visits (C128 and C140: (90 ± 6) ·10^3 and (86 ± 6) ·10^3 dpm m^{-2}, respectively) compared to the first sampling (C91: (71 ± 6) ·10^3 dpm m^{-2}).

Th-234 fluxes (F_{Th}, in dpm m^{-2} d^{-1}) are attributed to scavenging of ^{234}Th onto particles sinking out of surface waters. Here, these fluxes were estimated using two methods: (i) from seawater samples ($F_{Th,SW}$), and (ii) directly from sediment traps ($F_{Th,ST}$). The $F_{Th,SW}$ were calculated using a steady-state (SS) model, neglecting advective and diffusive fluxes [*Buesseler et al.*, 1992]:

$$F_{Th} = \lambda (A_U - A_{Th}) \quad (3.1),$$

where λ is the decay constant of ^{234}Th (0.029 d^{-1}) and (A_U - A_{Th}) is the integrated ^{234}Th deficit in the upper water column (dpm m^{-2}). We obtained the integrated ^{234}Th deficit with rectangular integration for two different horizon depths (100 and 300 m), allowing comparison with the ^{234}Th fluxes obtained directly from ST (Table 3.3).

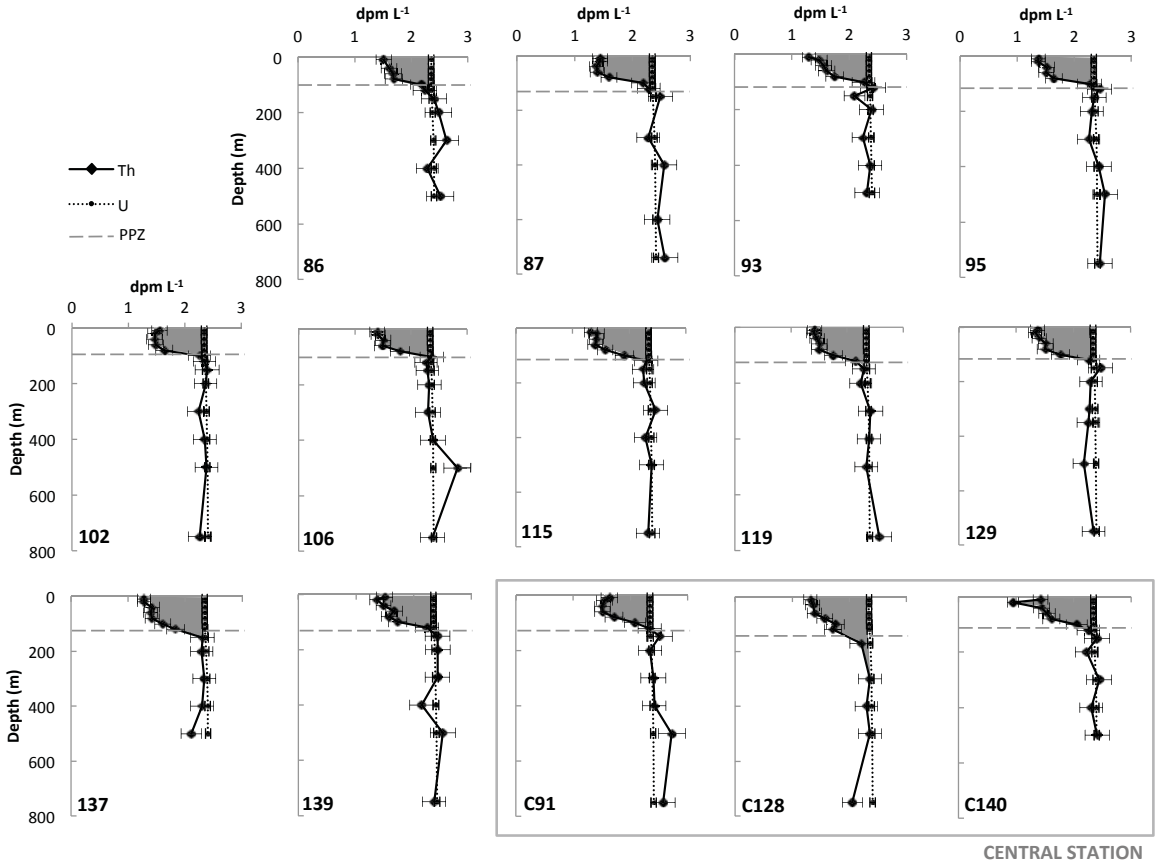

Figure 3.2: Vertical activity profiles for ^{234}Th (black diamonds) and ^{238}U (dotted line) from 10 to 500-750 m depth. Grey shaded area indicates surface ^{234}Th deficits with respect to ^{238}U. U-238 was derived from salinity [*Owens et al.*, 2011]. Primary production zone (PPZ, dashed grey line) is defined as the depth at which fluorescence reaches 10% of its maximum value [*Owens*, 2013].

Additionally, since the central station was sampled several times and the activity of ^{234}Th may have changed over time as a consequence of the sinking of the phytoplankton bloom, ^{234}Th fluxes were also calculated using a non-steady state (NSS) model at 100 and 300 m (Table 3.4). This model assumes that the same water masses are sampled at all visits and ignores advective and diffusive fluxes of ^{234}Th [*Savoye et al.*, 2006]:

$$F_{Th} = \lambda \left[\frac{A_U\left(1-e^{-\lambda \Delta t}\right)+A_{Th1}e^{-\lambda \Delta t}-A_{Th2}}{1-e^{-\lambda \Delta t}} \right] \quad (3.2),$$

where A_U is the activity of ^{238}U, Δt is the time interval between two visits of a single station and A_{Th1} and A_{Th2} are the activities of ^{234}Th at the first and second visits, respectively.

Table 3.3: ^{234}Th export fluxes derived from seawater ($F_{Th,SW}$) assuming steady-state conditions, together with the fluxes derived directly from the sediment traps ($F_{Th,ST}$) at different depths.

Station	Depth (m)	$F_{Th,SW}$ (dpm m^{-2} d^{-1})	$F_{Th,ST}$ (dpm m^{-2} d^{-1})
86	100	1960 ± 210	1700 ± 140
	300	1490 ± 710	970 ± 80
87	100	2360 ± 170	4000 ± 320
	300	2350 ± 710	1990 ± 170
93	100	2080 ± 180	
	300	2530 ± 630	
95	100	2220 ± 180	
	300	2510 ± 620	
102	100	2150 ± 180	
	300	2360 ± 640	
106	100	2090 ± 190	
	300	2440 ± 660	
115	100	2480 ± 170	
	300	2860 ± 470	
119	100	2440 ± 170	
	300	3020 ± 640	
129	100	2520 ± 170	
	300	2910 ± 520	
137	120	3100 ± 180	1090 ± 100
	300-320	3620 ± 620	620 ± 60
139	120	2510 ± 200	2440 ± 200
	150	2540 ± 260	
	300-320	2340 ± 660	1870 ± 160
	400	2660 ± 900	
C91	100	2050 ± 180	1470 ± 120
	150	2070 ± 270	
	300	1980 ± 660	900 ± 70
	400	1910 ± 910	
C98	100		1430 ± 120
	300		790 ± 70
C99	100		1370 ± 110
	300		960 ± 80
C114	100		1200 ± 100
	300		590 ± 50
C128	120	2950 ± 200	1050 ± 90
	300-320	3870 ± 700	920 ± 80
C140	120	2600 ± 210	1450 ± 130
	300-320	2800 ± 650	1220 ± 110

$F_{Th,SW}$ and $F_{Th,ST}$ estimates at 100 and 300 m are presented in Table 3.3 and Table 3.4 and Figure 3.3. Though some traps were placed 20 m deeper than the seawater sampling, we will still use 100 and 300 m to refer to 100 or 120 m and 300 or 320 m, respectively.

The SS estimates of $F_{Th,SW}$ at 100 m were relatively homogeneous over the entire study area and not significantly different from those at the base of the ^{234}Th deficit (~120 m, Wilcoxon test, $p > 0.05$), ranging from 1960 ± 210 to 3100 ± 180 dpm m^{-2} d^{-1} (average: 2390 ± 340 dpm m^{-2} d^{-1}, n = 14). Fluxes at 300 m had greater uncertainties than those at 100 m, and ranged from 1490 ± 710 to 3870 ± 700 dpm m^{-2} d^{-1} (average: 2650 ± 610 dpm m^{-2} d^{-1}, n = 14). The $F_{Th,SW}$ over the study area showed no significant differences between 100 and 300 m (t-test, $p > 0.05$) (Figure 3.3). Focusing on the central station, $F_{Th,SW}$ increased from C91 to C128 at both 100 and 300 m depth, reaching ~3000 and 4000 dpm m^{-2} d^{-1}, respectively. The $F_{Th,SW}$ at station C140 were not significantly different from those at station C128 (Table 3.3). According to the NSS model, the $F_{Th,SW}$ decreased substantially from C91-C128 to C128-C140, especially at 300 m (Table 3.4).

Table 3.4: ^{234}Th export fluxes derived from seawater ($F_{Th,SW}$) at 100 and 300 m at the central station assuming non-steady state conditions. t_2-t_1 is the time interval between two occupations of the central station.

Stations	t_2-t_1 (days)	Depth (m)	$F_{Th,SW}$ (dpm m^{-2} d^{-1})
C91-C128	10	100	4290 ± 880
		300	9600 ± 3400
C128-C140	4	100	1600 ± 2000
		300	-5500 ± 7600

$F_{Th,ST}$ at 100 m ranged from 1050 ± 90 to 4000 ± 320 dpm m^{-2} d^{-1} (average: 1720 ± 890 dpm m^{-2} d^{-1}, n = 10) (Table 3.3). A flux reduction of about 40% between 100 to 300 m was found at most stations, except at C128 and C140, where no significant differences were observed. At the central station, $F_{Th,ST}$ at 100 m were relatively constant from C91 to C140, with an average of 1330 ± 170 dpm m^{-2} d^{-1} (n = 6). $F_{Th,ST}$ at 300 m were also similar during the entire sampling time, averaging 900 ± 200 dpm m^{-2} d^{-1} (n = 6).

Globally, the ^{234}Th fluxes estimated using the SS approach and ST were comparable at 100 m (Wilcoxon test, $p > 0.05$; $F_{Th,SW}/F_{Th,ST}$ = 1.7 ± 0.9, n = 7), whereas at 300 m the $F_{Th,SW}$ were higher than the $F_{Th,ST}$ estimates by an average factor of 2.6 ± 1.7 (n = 7).

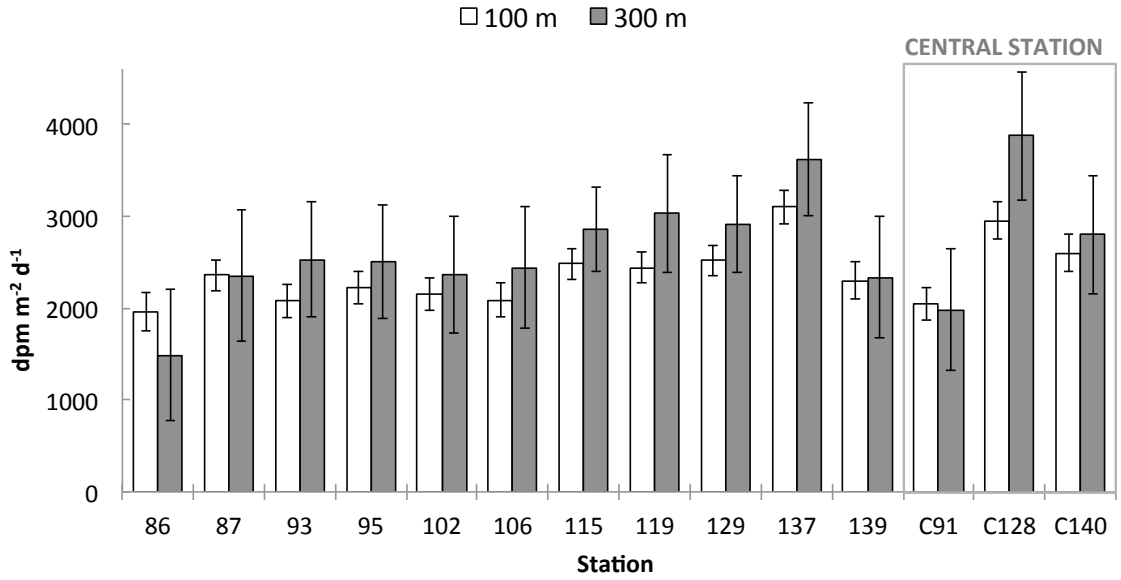

Figure 3.3: ^{234}Th export fluxes derived from seawater at 100 m (in white) and 300 m (in grey) assuming steady-state conditions. The negligence of horizontal advection would lead to an error on these estimates of 580 ± 440 dpm m^{-2} d^{-1} at 100 m and 1500 ± 1700 dpm m^{-2} d^{-1} at 300 m (i.e. ~25% and ~50%, respectively, see Section 3.3.2.1 for details).

3.3.2.1 Impact of physical transport processes on the $F_{Th,SW}$ estimates

Vertical advection needs to be considered in areas of established upwelling, while horizontal advection should be taken into account in ocean margins, where this process likely plays a relevant role [*Savoye et al.*, 2006]. During our survey the vertical advection was presumably negligible, while horizontal advection was significant with mean currents of about 7 cm s^{-1} for the top 100 and 300 m (V. Strass pers. comm.). *Buesseler et al.* [1994] showed that advection is dominant over diffusion in the horizontal transport of ^{234}Th in open waters. Therefore, we focused our attention on the horizontal advection in order to have a first estimate of the importance of the physical transport in the present study or, in other words, to test the accuracy of the ^{234}Th export estimates. This issue was addressed using Equation 1.4 (see Section 1.5.3, Chapter 1) and considering: (i) the mean u and v velocities over the area 50.67-51.67°S and 11.92-13.50°W for the top 100 and 300 m: u = 5.6 cm s^{-1}, v = 4.3 cm s^{-1} and u = 5.7 cm s^{-1}, v = 3.9 cm s^{-1}, respectively (V. Strass pers. comm.); (ii) the ^{234}Th activity gradients for the top 100 and 300 m (excluding station 86): $\frac{\partial A_{Th}}{\partial x}$ = (6.3 ± 7.9) ·10^{-2} dpm m^{-3}, $\frac{\partial A_{Th}}{\partial y}$ = (7.4 ± 6.1) ·10^{-2} dpm m^{-3} and $\frac{\partial A_{Th}}{\partial x}$ = (2.4 ± 3.0) ·10^{-1} dpm m^{-3}, $\frac{\partial A_{Th}}{\partial y}$ = (0.9 ± 2.2) ·10^{-1} dpm m^{-3}, respectively. In this way, the negligence of horizontal advection would lead to an error on the $F_{Th,SW}$ estimates of 580 ± 440 dpm m^{-2} d^{-1} at 100 m and 1500 ± 1700 dpm m^{-2} d^{-1} at 300 m. Thus, the physical processes would have a smaller impact on the $F_{Th,SW}$ estimates at 100 m (~25%) than at 300 m (~50%) at the investigated stations due to the smaller spatial variability of ^{234}Th activities in the upper 100 m.

Additionally, we have tested the influence of vertical diffusivity on ^{234}Th export using an intermediate K_z value of 10^{-4} m^2 s^{-1} at 100 m [*Strass et al.*, 2017], obtaining a maximum contribution of this process of 30 to 180 dpm m^{-2} d^{-1}. Thus, the contribution of the vertical diffusivity to the $F_{Th,SW}$ estimates at 100 m must have been very small, generally lower than the uncertainties associated with the estimates. It was not possible to reproduce this exercise at 300 m due to the low ^{234}Th resolution around that depth.

3.3.2.2 SS vs. NSS models at the central station

At the central station we determined the ^{234}Th export with both the SS and NSS models. However, changes in the upper water column properties occurred during the sampling period, especially evident when station C128 was occupied (see Section 3.3.1) [*Strass et al.*, 2017], indicating that different water masses with particular scavenging histories were likely sampled. Furthermore, we have quantified an appreciable impact of advection on the $F_{Th,SW}$ estimates, especially at 300 m (see Section 3.3.2.1). This has led us to discard the use of the NSS approach since it can produce substantial errors when spatial variability is misinterpreted as temporal variability, improving ^{234}Th export estimates only if sampling is conducted in a Lagrangian framework [*Resplandy et al.*, 2012]. Additionally, the results obtained from the NSS model (Table 3.4) are not consistent with the results from the ST, which tend to be more constant. Thus, we consider that the SS model gives the best estimate of ^{234}Th export in this study.

3.3.3 POC/^{234}Th and PON/^{234}Th ratios in particles

POC/^{234}Th and PON/^{234}Th (C/Th and N/Th) ratios in particles from ST (C/Th_{ST} and N/Th_{ST}) and in particles >53 µm collected using ISP (C/Th_{ISP} and N/Th_{ISP}), usually considered to be sinking particles [e.g. *Buesseler et al.*, 2006], are presented in Table 3.5.

C/Th_{ST} and N/Th_{ST} ratios at 100 m averaged 14 ± 3 and 1.7 ± 0.4 µmol dpm^{-1} (n = 10), respectively, and were about 30% lower at 300 m depth (10 ± 3 and 1.1 ± 0.3 µmol dpm^{-1}, n = 9, respectively). C/Th_{ISP} and N/Th_{ISP} ratios also decreased with depth between 100-150 and 300-400 m by about 60%. At the central station, C/Th_{ST} and N/Th_{ST} ratios at 100 m decreased by 30% from the beginning until the end of the study, but no significant change was observed at 300 m.

ST and ISP ratios (C/Th and N/Th) were in reasonable agreement (within a factor of 1.4), except at station 139 at 100 m depth, where the ISP ratios were about three to four times higher than the ST ratios. The molar C/N ratio was 8 ± 1 for ST ratios (n = 19) and 7 ± 1 for ISP ratios (n = 8).

3.3.4 POC and PON fluxes

We used three methods to estimate POC and PON fluxes (F_C and F_N, respectively) (Table 3.5): (i) measured directly with the ST (ST method: $F_{C,ST}$ and $F_{N,ST}$), (ii) combining the $F_{Th,SW}$ and the ST ratios (SWST method: $F_{C,SWST}$ and $F_{N,SWST}$), and (iii) combining the $F_{Th,SW}$ and the ISP ratios (SWISP method: $F_{C,SWISP}$ and $F_{N,SWISP}$). For (ii) and (iii) we used the SS estimates of F_{Th} and the C/Th (or N/Th) ratios in sinking particles, as:

$$F_C = F_{Th}(C/Th) \quad (3.3).$$

The average $F_{C,ST}$ and $F_{N,ST}$ at 100 m were 19 ± 9 and 2 ± 1 mmol m^{-2} d^{-1} (n = 11), respectively, with maximums at station 87. $F_{C,ST}$ and $F_{N,ST}$ at 300 m averaged 9 ± 3 and 1.0 ± 0.3 mmol m^{-2} d^{-1} (n = 11), respectively, about 60% less than the fluxes at 100 m except at stations C128, C136 and C140. During the occupation of the central station, $F_{C,ST}$ and $F_{N,ST}$ at 100 m decreased by 25% over the study period, while they increased by 30% and 50%, respectively, at 300 m.

$F_{C,SWST}$ and $F_{N,SWST}$ at 100 m averaged 30 ± 10 and 4 ± 1 mmol m^{-2} d^{-1} (n = 7), respectively. Fluxes at 300 m averaged 20 ± 10 and 2 ± 1 mmol m^{-2} d^{-1} (n = 6), respectively, about 40% less than the fluxes at 100 m except at stations C128 and C140. $F_{C,SWST}$ and $F_{N,SWST}$ estimates at the central station showed changes <5% with time at 100 m, whereas the fluxes at 300 m were more variable, with a maximum $F_{C,SWST}$ of 50 ± 10 mmol C m^{-2} d^{-1} at C128.

The SWISP method was used at the two stations where ISP were deployed. $F_{C,SWISP}$ and $F_{N,SWISP}$ at station 139 were higher than at C91 by a factor of about 2, at both 100-150 m and 300-400 m. Fluxes at 300 m were lower than those at 100 m by 40% (C91) and 70% (139).

Overall, the F_C and F_N estimated by using SW samples ($F_{C,SWST}$, $F_{N,SWST}$ and $F_{C,SWISP}$, $F_{N,SWISP}$) were greater than those measured with ST by a factor of 2.0 ± 1.0 and 2.3 ± 1.3 (n = 17), respectively, at 100 m, and 2.4 ± 1.0 and 2.5 ± 1.0 (n = 17), respectively, at 300 m.

Table 3.5: POC/^{234}Th and PON/^{234}Th (C/Th and N/Th) ratios in particles collected using sediment traps (ST) and in situ pumps (ISP, particles >53 µm), and POC and PON export fluxes (F_C and F_N) estimated using the ST, SWST and SWISP methods at different depths (see text for further details).

Station	Depth (m)	C/Th (µmol dpm^{-1}) ST	C/Th (µmol dpm^{-1}) ISP (> 53 µm)	N/Th (µmol dpm^{-1}) ST	N/Th (µmol dpm^{-1}) ISP (> 53 µm)	F_C (mmol m^{-2} d^{-1}) ST	F_C (mmol m^{-2} d^{-1}) SWST	F_C (mmol m^{-2} d^{-1}) SWISP	F_N (mmol m^{-2} d^{-1}) ST	F_N (mmol m^{-2} d^{-1}) SWST	F_N (mmol m^{-2} d^{-1}) SWISP
86	100	10.8 ± 0.9		1.4 ± 0.1		16	21 ± 3		2.0	2.6 ± 0.4	
	300	8.3 ± 0.7		0.85 ± 0.07		7.3	12 ± 6		0.74	1.3 ± 0.6	
87	100	13 ± 1		1.5 ± 0.1		44	31 ± 3		5.1	3.6 ± 0.4	
	300	10.3 ± 0.9		1.05 ± 0.09		16	24 ± 8		1.7	2.5 ± 0.8	
137	120	17 ± 2		2.2 ± 0.2		15	54 ± 6		1.8	6.7 ± 0.7	
	320					*6.3					
139	100-120	10.6 ± 0.9	29 ± 2	1.2 ± 0.1	5.2 ± 0.4	23	26 ± 3	67 ± 8	2.5	2.9 ± 0.3	12 ± 1
	150		20 ± 2		2.8 ± 0.3			52 ± 7			7 ± 1
	300-320	7.1 ± 0.6	9.9 ± 0.9	0.89 ± 0.07	1.1 ± 0.1	11	17 ± 5	23 ± 7	1.3	2.1 ± 0.6	2.6 ± 0.8
	400		9.0 ± 0.8		1.3 ± 0.1			24 ± 8			3 ± 1
C91	100	16 ± 1	13 ± 1	1.9 ± 0.2	2.1 ± 0.2	17	33 ± 4	26 ± 3	2.0	4.0 ± 0.5	4.2 ± 0.5
	150		12 ± 1		1.7 ± 0.1			25 ± 4			3.5 ± 0.5
	300	7.9 ± 0.6	7.6 ± 0.6	0.90 ± 0.07	1.3 ± 0.1	6.5	16 ± 5	15 ± 5	0.74	1.8 ± 0.6	2.5 ± 0.9
	400		4.3 ± 0.3		0.73 ± 0.06			8 ± 4			1.4 ± 0.7
C98	100	19 ± 2		2.4 ± 0.2		25			3.1		
	300	17 ± 2		1.8 ± 0.2		12			1.2		
C99	100	15 ± 1		1.8 ± 0.1		16			2.0		
	300	9.1 ± 0.8		1.06 ± 0.09		7.5			0.88		
C114	100	14 ± 1		1.9 ± 0.2		16			2.3		
	300	9.8 ± 0.8		1.3 ± 0.1		5.8			0.77		
C128	120	11 ± 1		1.6 ± 0.1		13	34 ± 4		1.7	4.6 ± 0.5	
	320	12 ± 1		1.1 ± 0.1		11	50 ± 10		1.0	4.3 ± 0.9	
C136	120					11					
	320					6.3					
C140	120	11 ± 1		1.3 ± 0.1		13	28 ± 3		1.6	3.5 ± 0.4	
	320	8.6 ± 0.8		1.1 ± 0.1		8.6	24 ± 6		1.1	3.0 ± 0.8	

*Calculated from the filter used for POC analysis. The filter used for ^{234}Th and POC analyses has not been considered because it was likely contaminated with organic carbon, presenting an unusually high C/N molar ratio (14) compared with the overall sample average (8 ± 1).

3.3.5 Chl-a and POC in the water column

The Chl-a_{SW} inventories down to 100 m were, in most instances, higher than 100 mg m^{-2} (Figure 3.4A), with highest inventories (>180 mg m^{-2}) at the SE quadrant of the study site, while stations 87 and 139, located to the NW, presented the lowest values (~50 mg m^{-2}). At the central station the Chl-a_{SW} inventories ranged from 130 to 200 mg m^{-2}, decreasing by about 30% from the beginning until the end of sampling, with fluctuations over time. The POC inventories down to 100 m ranged from $10 \cdot 10^3$ to $26 \cdot 10^3$ mg m^{-2}, showing a strong positive correlation with Chl-a_{SW} ($p < 0.001$; Pearson correlation coefficient, $r = 0.84$, $n = 20$; Figure 3.4A).

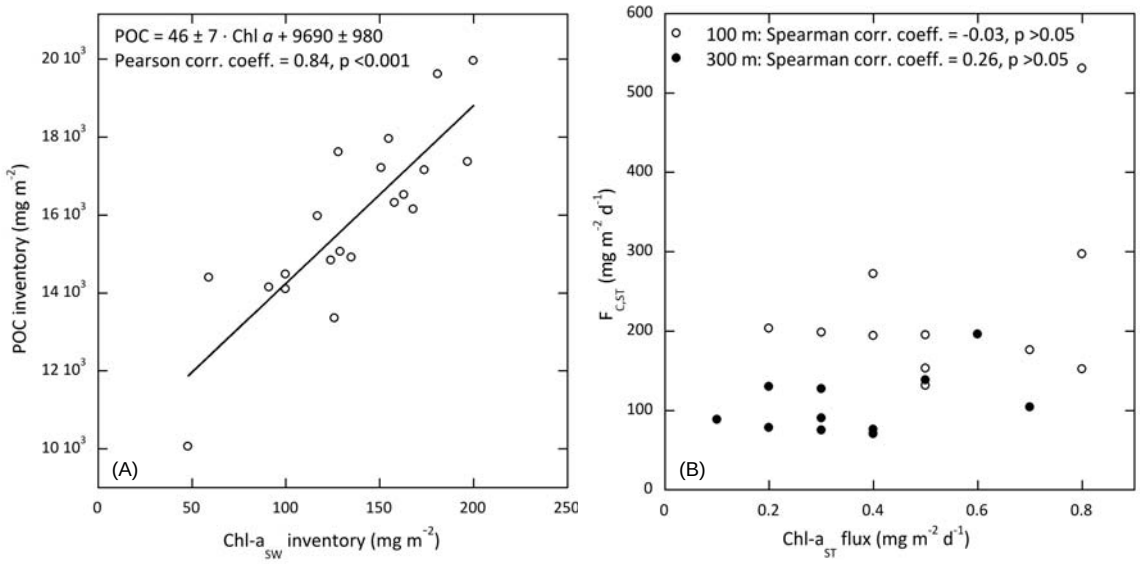

Figure 3.4: POC vs. Chl-a: (A) inventories in the upper 100 m of the water column and (B) fluxes measured with sediment traps at 100 m (in white) and 300 m (in black).

3.3.6 Pigments and POC in sediment traps

In contrast to the water column, there was no significant correlation between the fluxes of Chl-a measured with ST (Chl-a_{ST}) and $F_{C,ST}$, neither at 100 m ($p > 0.05$; Spearman correlation coefficient, $\rho = -0.03$, $n = 11$) nor 300 m ($p > 0.05$; $\rho = 0.26$, $n = 11$) (Figure 3.4B). Both Chl-a_{ST} fluxes and $F_{C,ST}$ decreased with depth (except Chl-a_{ST} flux at station C114), although this decrease was stronger for POC at most stations (Figure 3.5A, Table 3.5).

Maximum Chl-a_{ST} flux was recorded at station C98 (0.79 mg m^{-2} d^{-1} at 100 m), whereas minimum Chl-a_{ST} flux was observed at station 86 (0.11 mg m^{-2} d^{-1} at 300 m). Fluxes of total pheopigments (TPheo, i.e. sum of pheophytin-a, pyropheophytin-a, pheophorbide-a, and pyropheophorbide-a pigments) were generally higher at 100 m than at 300 m except at stations C91 and C114 (Figure 3.5A). Maximum TPheo fluxes were recorded at station 87 (2.67 and 1.27 mg m^{-2} d^{-1} at 100 and 300 m, respectively). Ratios of TPheo/Chl-a_{ST} were generally higher at 100 m than at 300 m except at station C91. TPheo/Chl-a_{ST} ratios above one were recorded at most of the investigated stations except at 137, 139, C98, C136 and C140 (Figure 3.5A). Among the marker pigments, fluxes of fucoxanthin were much higher than other pigments (Figure 3.5B) and the phytoplankton size classification showed that more than 80% of the phytoplankton were microphytoplankton (Figure 3.5C).

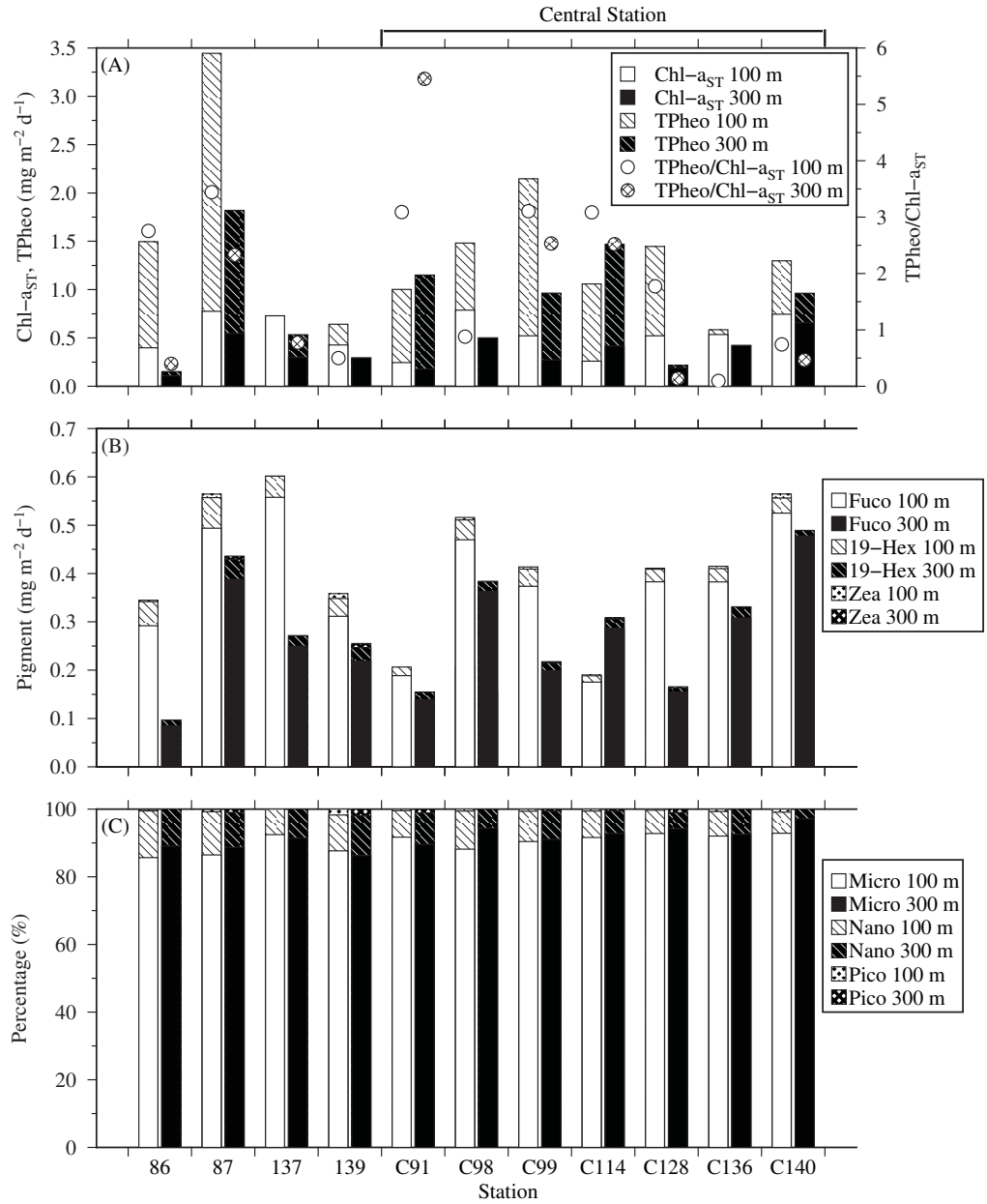

Figure 3.5: Pigment composition of sediment trap samples at 100 and 300 m. (A) Chl-a$_{ST}$ fluxes, total pheopigment (TPheo) fluxes, and ratios of total pheopigment to Chl-a$_{ST}$ fluxes (TPheo/Chl-a$_{ST}$); (B) fucoxanthin (Fuco), 19-hexanoyloxyfucoxanthin (19-Hex), and zeaxanthin (Zea) fluxes; (C) percentage of phytoplankton size classes: microphytoplankton (Micro), nanophytoplankton (Nano) and picophytoplankton (Pico).

3.4 Discussion

3.4.1 ^{234}Th fluxes

3.4.1.1 Seawater approach vs. sediment traps

In this study, the ^{234}Th fluxes were estimated using the seawater approach and sediment traps. The SW approach integrates about five weeks before sampling (^{234}Th mean life = 35 days), while ST provide information at the sampling time. In general, as shown in Section 3.3.2, the ^{234}Th fluxes based on these techniques were not significantly different at 100 m. This agreement indicates a sustained export rate in the weeks prior to and during the sampling period, suggesting export fluxes at steady state.

At 300 m the $F_{Th,ST}$ were about three times lower than the $F_{Th,SW}$. A review by *Buesseler et al.* [2007] suggested that ^{234}Th-bearing particles were under-trapped by a factor of about 2 and suggested some processes that could be sources of trap error, such as under-collection of slow settling particles by hydrodynamic bias, particle solubilization within the trap before sample processing, and swimmer-related artefacts. *Haskell et al.* [2013] reported that ST collected about ≤20% of the $F_{Th,SW}$ in two consecutive years and proposed that the main cause of this mismatch was the under-trapping of small, ^{234}Th-enriched slow sinking particles. Additionally, the active transport of surface-derived particles to hundreds of meters down via zooplankton migration [e.g. *Angel*, 1989] is another factor that may lead to underestimation of the particle export based on ST. Here, we tried to minimize the sources of error by using two surface floats and 12 buoyancy balls as wave breakers, while the cylinders of the ST were gimbal mounted. In addition, samples were processed within 24 hours after collection to decrease the impact of solubilization and zooplankton swimmers on material, which were picked under a binocular microscope.

Buesseler et al. [2007] also suggested that the mismatch between the SW approach and ST could be related to the use of inaccurate assumptions in the ^{234}Th model. The exclusion of physical processes in our study could introduce a significant error on the $F_{Th,SW}$ estimates at 300 m (~50%, see Section 3.3.2.1). Besides, in a late stage of a bloom, the SS assumption may lead to an overestimation of the $F_{Th,SW}$ if higher export occurred before sampling (within the ^{234}Th time scale). However, similar $F_{Th,SW}$ were found over the entire study area at both 100 and 300 m (Figure 3.3), irrespectively of phytoplankton biomass (see Section 3.3.5). This indicates that ^{234}Th fluxes probably did not change significantly during the weeks before our arrival and, therefore, the SS model gives reasonable estimates of ^{234}Th export flux.

3.4.1.2 Results and comparison with other studies

On average, ^{234}Th fluxes at 100 and 300 m were 2100 ± 700 and 2000 ± 1000 dpm m^{-2} d^{-1}, respectively. Hence, the fluxes were high and quite similar over the entire study area, despite the differences observed in Chl-a$_{SW}$ inventories (see Section 3.3.5) and production rates [*Hoppe et al.*, 2017]. However, satellite images show widespread high Chl-a concentrations in January 2012 (data not shown). Thus, stations with low phytoplankton biomass and production rates (e.g. stations 139 and C136) but high F_{Th} evidenced a temporal decoupling between production and export. *Buesseler et al.* [2003, 2001a], *Rutgers van der Loeff et al.* [2011] and *Henson et al.* [2015] showed that export lags production by up to one to two months in the Southern Ocean, which is a time frame compatible with the present study.

The F_{Th} estimates at 100 m are within the range of values for blooms during their peak and/or decline occurring in the Southern Ocean, either in land-remote areas [*Rutgers van der Loeff et al.*, 1997] or near islands [*Morris et al.*, 2007; *Savoye et al.*, 2008]. In contrast, our estimates are higher than the F_{Th} of ≤1000 dpm m^{-2} d^{-1} reported during the onset of a bloom by *Planchon et al.* [2015], and during the artificial iron fertilization experiments SOIREE [*Charette and Buesseler*, 2000], EisenEx [*Rutgers van der Loeff and Vöge*, 2001] and LOHAFEX [*Martin et al.*, 2013]. However, the SOFeX-South experiment revealed an increase of particle fluxes after fertilization, which resulted in F_{Th} of ~1800 dpm m^{-2} d^{-1} at the MLD [*Buesseler et al.*, 2004, 2005]. The variability within the plankton community structure and different sampling time strategies among these experiments most likely played a crucial role in the variety of results obtained [*Buesseler et al.*, 2004; *Boyd et al.*, 2007].

A release of ^{234}Th from sinking particles, either via remineralization or disaggregation, was evidenced by a 40% decrease of the $F_{Th,ST}$ between 100 and 300 m at the majority of the stations. However, the seawater approach did not show excesses of ^{234}Th in the depth range 100-300 m at any station. As a result, ^{234}Th flux attenuation from 100 to 300 m estimated using the two methods was different at three out of seven stations, taking into account the substantial uncertainties of the $F_{Th,SW}$ estimates at 300 m (16-48%, Table 3.3). The potential impact of advection on the $F_{Th,SW}$ estimates at 300 m (see Section 3.3.2.1) together with a low resolution of the seawater sampling between 100 and 300 m (2-3 samples) likely explain most of the disagreement between the ST and SW approaches on this issue. Remineralization and/or particle break-up was also indicated in previous studies in the Southern Ocean [*Usbeck et al.*, 2002; *Savoye et al.*, 2004; *Buesseler et al.*, 2005; *Rutgers van der Loeff et al.*, 2011; *Planchon et al.*, 2013]. In this study, $F_{Th,ST}$ were attenuated between 100 and 300 m at the first four visits of the central station, but not at stations C128 and C140 (Table 3.3), indicating that attenuation of $F_{Th,ST}$ in this depth range became negligible at the end of

the sampling period. This observation is similar to one of the major findings of the SOFeX-South experiment: the attenuation of F_{Th} with depth disappeared as the bloom progressed [*Buesseler et al.*, 2005]. This was attributed to changes in the nature of the sinking particles (less labile or more rapidly sinking) and/or less efficient biological and physical processes responsible for particle break-up and consumption below the bloom.

3.4.2 POC/^{234}Th and PON/^{234}Th ratios in particles

C/Th and N/Th ratios were >10 µmol C dpm^{-1} (average: 15 ± 5 µmol C dpm^{-1}) and >1 µmol N dpm^{-1} (average: 2 ± 1 µmol N dpm^{-1}), respectively, in all samples collected either with ST or ISP at 100 m. Overall, these values were higher than those reported by most studies conducted in the Southern Ocean [*Rutgers van der Loeff et al.*, 1997, 2011, *Buesseler et al.*, 2001b, 2005; *Coppola et al.*, 2005; *Morris et al.*, 2007; *Savoye et al.*, 2008; *Jacquet et al.*, 2011; *Martin et al.*, 2013; *Planchon et al.*, 2013], but similar to others [*Cochran et al.*, 2000; *Rutgers van der Loeff et al.*, 2002; *Smetacek et al.*, 2012; *Puigcorbé et al.*, 2017]. Multiple factors may have played a role in shaping the C/Th and N/Th ratios, such as particle source, sinking velocity, Th speciation and remineralization of C, N and ^{234}Th associated with sinking particles [*Buesseler et al.*, 2006]. *Buesseler* [1998] and *Buesseler et al.* [2006] hypothesized that high C/Th ratios encountered in productive regimes and high latitude areas may be related to the dominance of sinking of large cells, such as diatoms. This was explained by the fact that diatoms have a high volume relative to surface area (V:SA), and hence high C/Th ratios because C varies as a function of volume, whereas Th adsorption varies as a function of surface area. In this study, the dominance of fucoxanthin, a marker pigment for diatoms, and microphytoplankton in trap material (Figure 3.5B and Figure 3.5C) revealed that diatoms were the major phytoplankton group contributing to vertical fluxes. Additionally, according to microscopic analyses (C. Klaas pers. comm.), the needle-shaped *Pseudo-nitzschia lineola* and the large centric diatom *Dactyliosolen antarcticus* dominated the bloom, with significant contributions from *Fragilariopsis kerguelensis* as well as other *Pseudo-nitzschia*, *Rhizosolenia* and *Chaetoceros* species. Thus, diatoms with a high V:SA, including *Dactyliosolen antarcticus* and *Chaetoceros* spp. played a relevant role in the bloom, which could be responsible for the high ratios observed.

C/Th and N/Th ratios at 300 m were, on average, about 30% lower than at 100 m. The reduction of C/Th ratios with depth is commonly observed [*Buesseler et al.*, 2006]. It is likely due to the production of ^{234}Th in the entire water column leading to additional adsorption of ^{234}Th onto particles at depth, which compensates its decay, and a preferential remineralization of POC with respect to ^{234}Th [*Rutgers van der Loeff et al.*, 2002]. The same reasons would apply for PON.

The C/N ratios averaged 8 ± 1 and 7 ± 1 for ST and ISP samples, respectively, and were within the range of values previously reported for bloom events [*Morris et al.*, 2007; *Savoye et al.*, 2008; *Martin et al.*, 2013], with a diverse composition of the dominant particle type, i.e. diatoms [*Salter et al.,* 2007] or faecal material [*Ebersbach and Trull*, 2008; *Ebersbach et al.*, 2014].

3.4.3 POC and PON fluxes at 100 m

POC and PON export fluxes at 100 m averaged 26 ± 15 mmol C m^{-2} d^{-1} (range: 11-67 mmol C m^{-2} d^{-1}) and 4 ± 2 mmol N m^{-2} d^{-1} (range: 1.6-12 mmol N m^{-2} d^{-1}, Table 3.5), respectively. The F_C are high in relation to the average fluxes compiled by *Le Moigne et al.* [2013b] and *Maiti et al.* [2013]. *Le Moigne et al.* [2013b] reported an average F_C of 9 ± 13 mmol C m^{-2} d^{-1} (range: <0-125 mmol C m^{-2} d^{-1}, n = 726) for the global ocean, and 13 ± 14 mmol C m^{-2} d^{-1} (range: 0-91 mmol C m^{-2} d^{-1}, n = 196) for the Southern Ocean. *Maiti et al.* [2013] reported a range of F_C from 1 to 50 mmol C m^{-2} d^{-1} for the Southern Ocean, averaging 11 ± 8 mmol C m^{-2} d^{-1} (n = 140).

Considering other natural blooms observed in the Southern Ocean, our estimates of F_C are comparable to those reported in KEOPS (average: 23 ± 4 mmol C m^{-2} d^{-1}) [*Savoye et al.*, 2008], the JGOFS Southern Ocean expedition (range: 20-39 mmol C m^{-2} d^{-1}) [*Rutgers van der Loeff et al.,* 1997], and the CROZEX project (average: 14 ± 4 mmol C m^{-2} d^{-1}) [*Morris et al.,* 2007]. The estimates of F_N are also similar to the results from KEOPS and CROZEX [*Morris et al.*, 2007; *Savoye et al.*, 2008]. In contrast, the F_C are higher than those reported in KEOPS II (average: 7 ± 2 mmol C m^{-2} d^{-1}) [*Planchon et al.,* 2015] for a bloom during its growing stage. On the other hand, the F_C determined during SOIREE [*Charette and Buesseler*, 2000], SOFeX-South [*Buesseler et al.*, 2005] and LOHAFEX [*Martin et al.*, 2013] were clearly lower (average ≤8 mmol C m^{-2} d^{-1}) than in this study. In the case of LOHAFEX, it was explained by silica limitation that prevented diatom growth. The low F_C measured during SOIREE and SOFeX-South were likely due to a limited sampling period. However, the artificially-induced bloom during EIFEX [*Smetacek et al.*, 2012] led to an extraordinarily high F_C (~80 mmol C m^{-2} d^{-1}) with a high export efficiency. Thus, the high export fluxes found in our study are comparable to other studies of the later stages of natural and iron-fertilized blooms in the Southern Ocean that were not silica limited.

3.4.4 Export efficiency

The export efficiency is a useful parameter to illustrate the strength of the biological pump, even though production and export operate at distinct time scales [*Buesseler and Boyd*, 2009]. It should also be noted the temporal mismatch between the measurements of production and export: 24 hours incubation for NPP [*Hoppe et al.*, 2017], 15-72 hours deployment for ST and several weeks of

integration for the SW approach. We assessed the export efficiency by dividing the F_C at 100 m, either from the SW methods or ST, by the NPP integrated down to 100 m [*Hoppe et al.*, 2017].

Table 3.6: Export and transfer efficiencies using the POC export estimated from the ST, SWST and SWISP methods (see text for further details).

Station	Export efficiency (%)			Transfer efficiency (%)		
	ST	SWST	SWISP	ST	SWST	SWISP
86	7.5	10 ± 1		45	60 ± 30	
87				37	80 ± 30	
137	13	47 ± 5		43		
139	34	40 ± 5	100 ± 10	47	60 ± 20	30 ± 10
C91	7.2	14 ± 2	11 ± 1	38	50 ± 20	60 ± 20
C98				47		
C99				46		
C114	8.1			35		
C128	9.2	24 ± 3		84	140 ± 30	
C136	12			58		
C140	7.6	17 ± 2		68	90 ± 20	

The export efficiency within the bloom averaged 23 ± 24% (range: 7-100%; Table 3.6, Figure 3.6A), taking into account all the techniques used to estimate the export of POC (ST, SWST, SWISP). The export efficiency was around 10% according to the ST, which is common in the open ocean [*Buesseler*, 1998], whereas it was around 25% considering the SWST method. Besides these differences, the export efficiency was always ≤50% for the ST and SWST methods, contrasting with export efficiencies >50% reported during blooms at high latitudes, mostly characterized by large diatoms [*Buesseler*, 1998; *Smetacek et al.*, 2012] and a combination of *Phaeocystis* and diatoms [*Buesseler et al.*, 2003; *Poulton et al.*, 2007]. Other Southern Ocean studies [*Buesseler et al.*, 2005; *Planchon et al.*, 2015] have also reported export efficiencies of ~10% during not yet declining diatom blooms, where low POC export fluxes were measured (7-8 mmol C m^{-2} d^{-1}). In contrast, during our study the bloom was declining, which led to high downward fluxes. We propose that this relatively low strength of the biological pump was likely related to an active recycling of carbon and nutrients in surface waters. Only for one station (139), which evidenced a temporal decoupling between production and export (lowest Chl-a_{SW} inventories and NPP rates), the export efficiency was >30% according to all techniques. Indeed, we found an inverse relationship between export efficiency and NPP ($p < 0.05$; ST method: $\rho = -0.95$, $n = 8$; SWST method: $\rho = -0.89$, $n = 6$) supporting recent observations [*Maiti et al.*, 2013; *Cavan et al.*, 2015; *Laurenceau-Cornec et al.*, 2015]. This relationship could be explained by a combination of temporal decoupling between primary production and export [*Henson et al.*, 2015; *Puigcorbé et al.*, 2017], and other processes such as zooplankton grazing [*Cavan et al.*, 2015], bacterial activity and recycling efficiency [*Maiti et al.*, 2013].

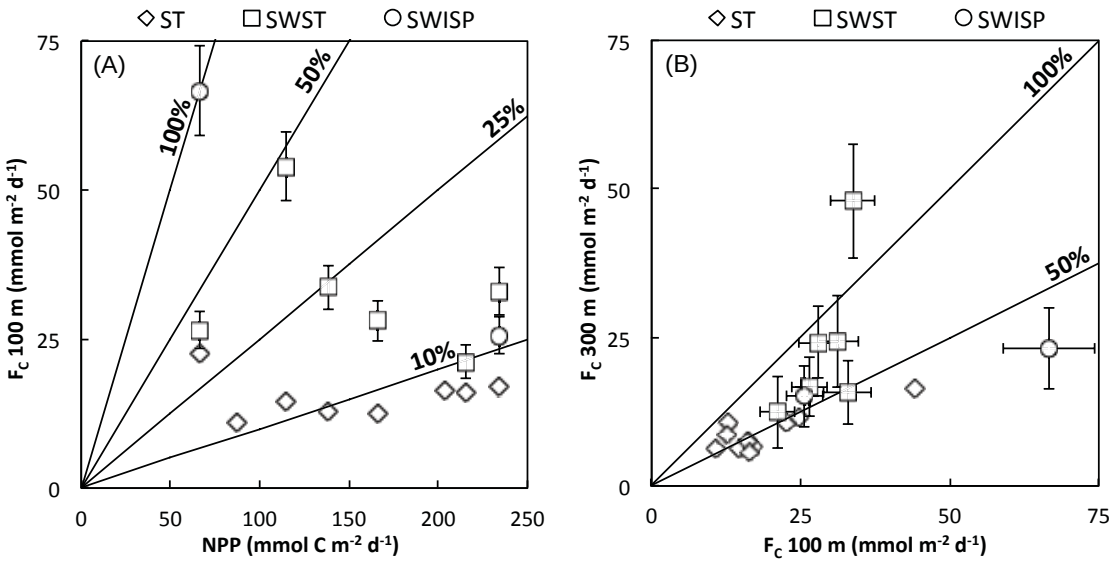

Figure 3.6: (A) POC export fluxes (F_C) at 100 m vs. integrated net primary production (NPP) at 100 m, and (B) POC export fluxes at 300 m vs. POC export fluxes at 100 m. Solid lines indicate the export and transfer efficiencies in (A) and (B), respectively. POC export fluxes were estimated using three methods: ST (diamonds), SWST (squares) and SWISP (circles, see text for further details).

3.4.5 Transfer efficiency

The upper 300 m of the water column is where intense biological and physical processes transform the size distribution of particles and thus modify the flux of particles to the mesopelagic layer [*Guidi et al.*, 2009]. To account for the change of the F_C magnitude within the upper twilight zone, we estimated the transfer efficiency by dividing the F_C at 300 m by those at 100 m.

The transfer efficiency averaged 59 ± 26% (range: 35->100%; Table 3.6, Figure 3.6B) with a general discrepancy among techniques <30%. Most of the transfer efficiencies were higher than the estimates presented by (i) *Schlitzer* [2002]: 40% for the same depth range using an inverse model based on observations of temperature, salinity and nutrient concentrations; and (ii) *Guidi et al.* [2009]: <42% when microphytoplankton dominated the phytoplankton community based on a world-ocean analysis. *Guidi et al.* [2009] showed that maximum values of F_C at 400 m were associated with a dominance of microphytoplankton in the euphotic zone, although the flux experienced a sharp decrease from 100 to 300 m. In our study, the transfer efficiency at the central station was lower during the first four visits (C91-C114: 42 ± 6%) than during the last three (C128-C140: 70 ± 10%) according to the ST results (Table 3.6). This change coincided with a decrease of the TPheo/Chl-a_{ST} ratio in the trap material from the first group of stations to the second: from 2.5 ± 1.1 to 0.9 ± 0.8 at 100 m and from 3.5 ± 1.7 to 0.3 ± 0.2 at 300 m (Figure 3.5A). Pheopigments are degraded Chl-a products that are associated with grazing activity and phytoplankton senescence [*Wright et al.*, 2010]. Thus, this observation indicates that when the

transfer efficiency was higher, the organic material being exported was fresher. Indeed, there is a negative relationship between TPheo/Chl-a_{ST} ratios at 100 m and the transfer efficiency of POC from 100 to 300 m derived from ST ($p < 0.01$; $\rho = -0.77$, $n = 10$). This correlation highlights the relevance of the particle composition sinking out from the ocean surface in shaping the efficiency of the biological pump. *Buesseler and Boyd* [2009] pointed out that very high transfer efficiencies are attributed to direct sinking of algae with low flux attenuation. Here, more than 60% of the Chl-a_{ST} and fucoxanthin fluxes at 100 m reached 300 m (Figure 3.5A and Figure 3.5B), which highlights the contribution of diatoms to vertical fluxes in the study area. In particular, the direct sinking of diatoms might be the main explanation for the high transfer efficiencies at stations C136 and C140, since at these locations the high fucoxanthin fluxes at 100 m (>0.4 mg m^{-2} d^{-1}) showed a decrease of only ~10-20% at 300 m, and the TPheo/Chl-a_{ST} ratios were <1 (Figure 3.5A and Figure 3.5B). Indeed, a study by *Cedhagen et al.* [2014] from the same cruise showed that abyssal benthic foraminifera at ~4000 m were feeding on fresh phytodetritus. This indicates that at least part of the phytoplankton was rapidly transported to the seafloor.

The lack of relationship between Chl-a_{ST} and $F_{C,ST}$ at both 100 and 300 m depth (Figure 3.4B), however, indicated that reprocessed material or dead phytoplankton also contributed significantly to the export fluxes at most stations. The high fluxes of pheopigments (>0.6 mg m^{-2} d^{-1}) together with TPheo/Chl-a_{ST} ratios >1 (Figure 3.5A) at stations 87, C91, C99 and C114 at 100 and 300 m may be associated with grazing activity and, hence, indicate the contribution of faecal pellets to sinking fluxes. Preliminary results confirmed a significant abundance of faecal pellets in trap material during our survey [*Iversen and Klaas*, 2013]. Salp faecal pellets made up less than 1% of the POC fluxes at 100 and 300 m, but high amounts of faecal pellets from crustaceans were observed in the gel traps (analyses underway) [*Iversen et al.*, 2017]. Specifically, at station C114 the TPheo, Chl-a_{ST} and fucoxanthin fluxes increased from 100 to 300 m (Figure 3.5A and Figure 3.5B), which may have been due to zooplankton consumption of diatoms in the euphotic zone and release of faecal pellets between 100 and 300 m. Indeed, fresh faecal pellets were observed in abyssal sediments of the study area at the end of the sampling period, showing the transport of fast-settling faecal pellets to the seafloor [*Emil Ruff et al.*, 2014]. Therefore, production of faecal pellets and zooplankton vertical migration might have modulated the transfer efficiency in this study. Similar conclusions have been reached by *Buesseler and Boyd* [2009] and *Cavan et al.* [2015].

3.5 Conclusions

We measured downward fluxes of POC and PON during the decline of a vast diatom bloom in a land-remote area of the Atlantic sector of the Southern Ocean. Our main conclusions are:

1) The simultaneous use of sediment traps and the $^{234}Th/^{238}U$ proxy evidenced that ^{234}Th export rates at 100 m were high and constant in the weeks prior to and during the survey.

2) Stations distributed over an area of 8000 km^2 showed similar vertical export fluxes in spite of the heterogeneity in phytoplankton standing stocks and productivity, indicating a decoupling between production and export.

3) The diatom bloom led to high POC export fluxes at 100 m (26 ± 15 mmol C m^{-2} d^{-1}), although the export efficiencies were generally low (<20%) in comparison to other diatom blooms occurred at high latitudes. An active recycling of carbon and nutrients in surface waters was likely the reason for the low export efficiencies.

4) In contrast to the low export efficiencies at 100 m depth, the transfer efficiency of POC between 100 and 300 m was high during the entire study period (~60%), partly driven by the sinking of fresh diatoms. Faecal pellets and the active transport of POC linked to zooplankton vertical migration may have also contributed significantly to vertical fluxes. If we are to understand the efficiency of the biological pump in the Southern Ocean, these processes should be further investigated in the future.

Chapter 4

Carbon export fluxes and export efficiency in the central Arctic during the record sea-ice minimum in 2012: a joint $^{234}Th/^{238}U$ and $^{210}Po/^{210}Pb$ study

This chapter has been published as:
Roca-Martí, M., Puigcorbé, V., Rutgers van der Loeff, M., Katlein, C., Fernández-Méndez, M., Peeken, I., Masqué, P (2016). Carbon export fluxes and export efficiency in the central Arctic during the record sea-ice minimum in 2012: a joint $^{234}Th/^{238}U$ and $^{210}Po/^{210}Pb$ study. *Journal of Geophysical Research: Oceans*, 121, 5030-5049. doi: 10.1002/2016JC011816

4.1 Aim

The Arctic sea-ice extent reached a record minimum in September 2012, amounting to less than half of its 1979-2000 baseline [*Overland and Wang*, 2013]. Sea-ice decline increases the absorption of solar energy in the Arctic Ocean, affecting primary production and the plankton community. How this will modulate the sinking of particulate organic carbon (POC) from the ocean surface remains a key question. Our present understanding is that the downward fluxes of POC from the Arctic surface are highly variable, being very low in the central Arctic (<3 mmol C m^{-2} d^{-1}) as a consequence of low primary production [*Cai et al.*, 2010]. However, in summer 2012, a widespread deposition of ice algal biomass on the seafloor (>3000 m, median estimate of 750 mmol C m^{-2}) was observed in the Eurasian Basin associated with rapid ice melt [*Boetius et al.*, 2013].

In this study, we aim to estimate the magnitude of the POC fluxes at the bottom of the euphotic zone and within the upper mesopelagic layer in the central Arctic during the record sea-ice minimum in 2012, as well as identify mechanisms that control particle export by means of the disequilibrium between $^{234}Th/^{238}U$ and $^{210}Po/^{210}Pb$ in seawater. The use of both pairs may shed light on the apparent mismatch between the low ^{234}Th-based export production estimates [*Cai et al.*, 2010] and the benthic observations of massive sea-ice algae deposits [*Boetius et al.*, 2013] in the central Arctic. It might also give a hint of the trend that POC fluxes may follow as the sea ice continues to decline. To this purpose we:

1) Quantify the POC export fluxes at the bottom of the euphotic zone, 50, 100 and 150 m on short-term and seasonal scales by using the $^{234}Th/^{238}U$ and $^{210}Po/^{210}Pb$ pairs.

2) Identify potential relationships between sea-ice conditions, phytoplankton community and particle export.

3) Assess the export efficiency combining the export estimates at the bottom of the euphotic zone with daily, weekly and annual net primary production (NPP) estimates.

4.2 Methods

4.2.1 Study area

The sampling was performed from 11 August to 28 September 2012 during the ARK-XXVII/3 expedition in the Eurasian Basin of the central Arctic (2 August to 8 October, 2012; R/V Polarstern) [*Boetius*, 2013]. The survey coincided with a new record low of sea-ice cover since the beginning of satellite imagery in 1978 [*Parkinson and Comiso*, 2013]. The specific locations and dates of the sea-ice stations are given in Figure 4.1 and Table 4.1.

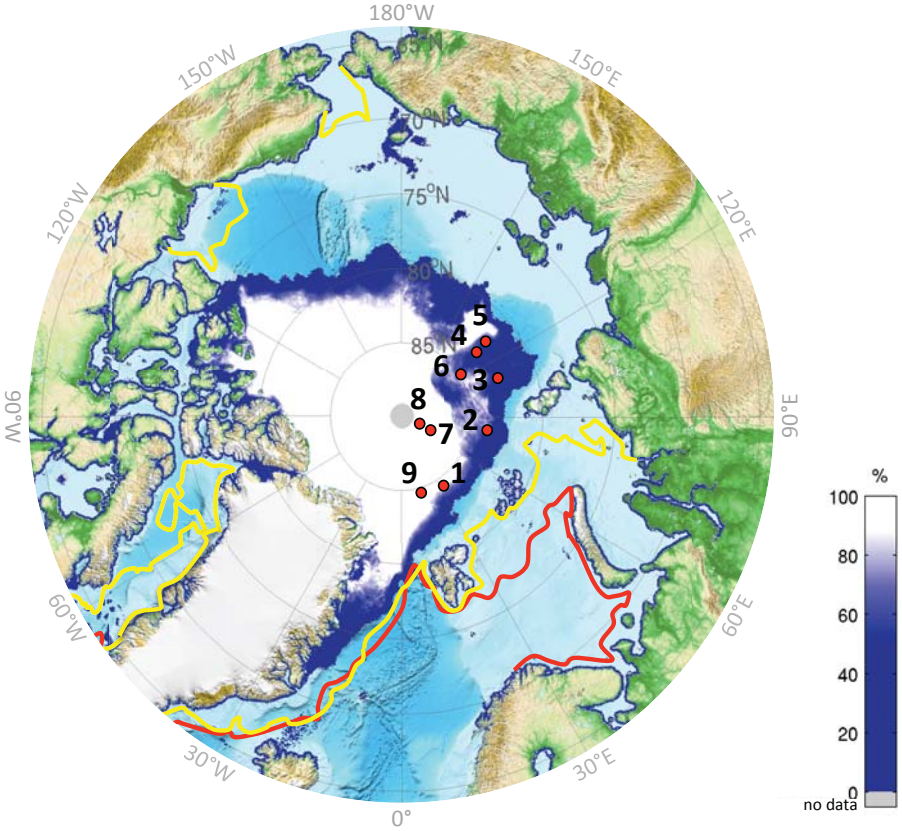

Figure 4.1: Location of sea-ice stations sampled during the IceArc cruise (ARK-XXVII/3, August-September 2012) (red dots). Average sea-ice concentration in September 2012. Contour lines represent the sea-ice extent in February (red) and July (yellow) 2012. Sea-ice concentration data were obtained from *http://www.meereisportal.de/* [*Spreen et al.*, 2008].

4.2.2 Total $^{234}Th/^{238}U$ and $^{210}Po/^{210}Pb$

Total ^{234}Th, ^{210}Pb and ^{210}Po activities were determined from 12-depth vertical profiles from 10 to 400 m, with higher resolution in the upper 150 m of the water column. Total ^{234}Th activities were determined at nine stations following the methods described in Chapter 2 (see Section 2.1.1). The parent ^{238}U activity was derived from salinity using the relationship given by *Owens et al.* [2011].

Total ^{210}Pb and ^{210}Po activities were determined at seven stations using the cobalt-ammonium pyrrolidine dithiocarbamate (Co-APDC) co-precipitation technique as described in Chapter 2 (see Section 2.1.2). All data of total ^{238}U, ^{234}Th, ^{210}Pb and ^{210}Po activities are available at *http://doi.pangaea.de/10.1594/PANGAEA.858790*.

4.2.3 Particulate fraction

Large (>53 µm) particles for analyses of ^{234}Th, ^{210}Pb, ^{210}Po, POC and particulate organic nitrogen (PON) were collected using four in situ pumps (ISP) at 25, 50, 100 and 150 m at each station. Particles were retained using 53-µm pore-size nylon-mesh screens and rinsed with filtered seawater. The samples were subdivided into two aliquots: one was filtered through pre-combusted QMA filters to analyse ^{234}Th, POC and PON on the same filter, and the other aliquot was filtered through QMA filters to analyse ^{210}Pb and ^{210}Po. The activity of ^{234}Th, ^{210}Pb and ^{210}Po and the concentrations of POC and PON were measured as described in Chapter 2 (see Section 2.2). The POC and PON results were corrected for blanks (1.7 ± 0.1 and 0.35 ± 0.06 µmol, respectively), representing on average 5 and 8% of the POC and PON measurements, respectively. All data of particulate ^{234}Th, ^{210}Pb, ^{210}Po, and organic carbon and nitrogen concentrations are available at *http://doi.pangaea.de/10.1594/PANGAEA.858790*.

4.2.4 Pigments

One litre of seawater samples were taken from Niskin bottles attached to a conductivity-temperature-depth (CTD) rosette from three to four depths in the upper 30 m at eight stations. The samples were immediately filtered on GF/F filters, frozen in liquid nitrogen, and stored at -80°C until further analyses by high-performance liquid chromatography (HPLC) at the home laboratory. The samples were measured using a Waters 600 controller equipped with an auto-sampler (717 plus), a photodiode array detector (2996), a fluorescence detector (2475) and the EMPOWER software. Fifty microliter of internal standard (canthaxanthin) and 1.5 mL acetone were added to each filter vial and then homogenized for 20 seconds in a Precellys tissue homogenizer. After centrifugation the supernatant liquids were filtered through 0.2 µm PTFE filters (Rotilabo) and placed in Eppendorf cups. Aliquots of 100 µL were transferred to the auto-sampler (4°C), premixed with 1 M ammonium acetate solution in a 1:1 volume ratio just prior to analysis, and injected onto the HPLC-system. Pigments were analysed by reverse-phase HPLC using a VARIAN Microsorb-MV3 C8 column (4.6 x 100 mm) and HPLC-grade solvents (Merck). Solvent A consisted of 70% methanol and 30% 1 M ammonium acetate, and solvent B contained 100% methanol. The gradient was modified after *Barlow et al.* [1997]. Eluted pigments were detected by absorbance (440 nm) and fluorescence (Ex: 410 nm, Em: >600 nm). Pigments were identified by comparing their

retention times with those of pure standards. Additional confirmation for each pigment was done by comparing the sample spectra with online diode array absorbance spectra between 390 and 750 nm stored in the library. Pigment concentrations were quantified based on peak areas of external standards, which were spectrophotometrically calibrated using extinction coefficients published by *Bidigare* [1991] and *Jeffrey et al.* [1997]. The taxonomic structure of the phytoplankton groups (diatoms, dinoflagellates_1, dinoflagellates_2, haptophytes_3, haptophytes_4, cryptophytes, prasinophytes_1, prasinophytes_2, pelagophytes and chlorophytes) was calculated from marker pigment ratios using the CHEMTAX program [*Mackey et al.*, 1996]. Pigment ratios were constrained as suggested by *Higgins et al.* [2011] based on molecular analyses of 18S rDNA [*Kilias et al.*, 2013] and microscopic examination of representative samples. Phytoplankton size classes (micro-, nano-, and picophytoplankton) were estimated according to *Uitz et al.* [2006] and *Hirata et al.* [2011], summarized by *Taylor et al.* [2011]. Microphytoplankton corresponded to phytoplankton with size between 20 and 200 µm, nanophytoplankton between 2 and 20 µm and picophytoplankton <2 µm. The phytoplankton classifications by group and size are expressed as percentage of total chlorophyll *a* (Chl-a) biomass.

4.2.5 Primary production

In situ NPP was measured at eight stations using the ^{14}C uptake method [*Steemann Nielsen*, 1952], with minor modifications as described in *Fernández-Méndez et al.* [2015]. Seawater, melted sea-ice cores and melt-pond samples (one 200 mL sample per environment and station) were spiked with 0.1 µCi mL^{-1} of ^{14}C labelled sodium bicarbonate (Moravek Biochemicals, USA) and incubated for 12 hours at -1.3°C under different scalar irradiances (0–420 µmol photons m^{-2} s^{-1}). Depth-integrated in situ rates were calculated for each environment as a function of the available photosynthetically active radiation (PAR) using the photosynthetic parameters obtained in the photosynthesis vs. irradiance curves. Water column production was integrated over the euphotic zone (1% of incoming PAR) and sea-ice algae production over the length of the ice cores retrieved.

At the same stations we calculated the integrated amount of NPP that potentially occurred one and two weeks before sampling using the Central Arctic Ocean Primary Productivity (CAOPP) model [*Fernández-Méndez et al.*, 2015]. This model calculates NPP from incident light and sea-ice conditions based on different remote-sensing datasets on the basis of photosynthesis vs. irradiance curves measured during the cruise. NPP was calculated for each day during the 14 days prior to sampling, summed up to integrate values for the one- and two-week period before sampling, and divided by 7 and 14 days, respectively, to obtain average daily rates for these two periods.

Annual new NPP was calculated from the nitrate drawdown in the mixed layer since previous winter at nine stations, as described in *Fernández-Méndez et al.* [2015]. The annual total inorganic nitrogen uptake was then transformed to carbon units using the Redfield ratio 106C:16N [*Smith et al.*, 1997; *Codispoti et al.*, 2013], giving annual new NPP estimates for sea ice and water column during the Arctic productive season. To calculate an average daily rate we assumed a productive season of 120 days [*Gradinger et al.*, 1999]. Although most of the new NPP occurs before late summer, we note that these estimates may be underestimated, especially for the first stations sampled in August. This method assumes that lateral input of nitrate from rivers or shelves is negligible, which should be the case of the present study (>81°N) due to its consumption in Arctic shelf waters [*Le Fouest et al.*, 2013]. Further, this method does not take into consideration nitrification and upward flux of nitrate, which are assumed to have a relatively small contribution to the nitrate concentrations in the mixed layer in comparison with the biological uptake.

4.3 Results

4.3.1 Study area

Sea-ice conditions, phytoplankton community and primary production rates in the study area are described below and summarized in Table 4.1.

4.3.1.1 Hydrography and sea-ice conditions

Stations were located over the deep Arctic (>3000 m) in the Nansen (stations 1-3 and 9) and Amundsen Basins (stations 4-8, Figure 4.1). The sea-ice conditions encountered during the expedition are described in *Katlein et al.* [2014]. Stations located north of 87°N (stations 7 and 8) had multi-year ice, 1.6-1.8 m thick, while the rest consisted of degraded first-year ice of 0.7-1.3 m. The sea-ice concentration varied from 50 to 80% at stations 1-6, but it was 100% at those stations visited in mid-late September (stations 7-9, Table 4.1). The coverage of melt ponds ranged from 10 to 50% [*Boetius et al.*, 2013]. The euphotic zone was on average 25 m deep and was nutrient-depleted by phytoplankton consumption: (i) silicate-depleted at stations 1-3; (ii) nitrate-depleted at stations 4 and 5; and (iii) silicate, nitrate and phosphate-depleted at stations 6-9 [*Fernández-Méndez et al.*, 2015]. The mixed layer was on average 22 m thick and was defined by the depth where density increased from its surface value to 20% of the difference between 100 m and the surface [*Shaw et al.*, 2009] using the CTD profiles obtained during the cruise (doi:10.1594/PANGAEA.802904). The winter mixed layer depth was found at around 55 m [*Fernández-Méndez et al.*, 2015] above the lower halocline (salinity range: 33.5-34.5) [*Rudels*, 2009], which reached depths down to 115 m. The potential temperature maximum indicative of the Atlantic Water core was found between 180 and

290 m. The Arctic intermediate waters as well as deep and bottom waters were present below the warm Atlantic layer.

Table 4.1: Location and date of the stations sampled during the ARK-XXVII/3 cruise together with information on hydrography and sea-ice conditions, Chl-a inventory at 30 m depth, phytoplankton classifications by size and group, and NPP estimates (see text for further details).

Station	1	2	3	4	5	6	7	8	9
Polarstern station #	PS80/ 224	PS80/ 237	PS80/ 255	PS80/ 277	PS80/ 323	PS80/ 335	PS80/ 349	PS80/ 360	PS80/ 384
Longitude (°E)	31.19	75.99	110.11	129.83	131.12	123.47	60.97	57.07	17.59
Latitude (°N)	84.03	83.92	83.08	82.89	81.93	85.17	87.93	88.80	84.37
Date (2012)	9-11 Aug.	14-16 Aug.	20-22 Aug.	25-26 Aug.	4-5 Sept.	7-9 Sept.	18-19 Sept.	22-23 Sept.	28-29 Sept.
Euphotic zone depth (m)[a]	24	29	30	29	33	29	15	7	27
Mixed layer depth (m)	16	20	18	22	20	25	29	30	22
Sea-ice thickness (m)[a,b]	1.0	1.3	0.9	0.9	0.8	0.7	1.6	1.8	1.2
Sea ice-concentration (%)[a,b]	80	80	70	80	60	50	100	100	100
Chl-a inventory (mg m^{-2})	4.8	22.8	8.9	7.0	8.9	11.2	6.1	3.3	2.5
Phytoplankton size (% Chl-a biomass)									
Micro-	36	29	38	54	36	14	34	nd	39
Nano-	22	0	2	13	4	28	44	nd	32
Pico-	42	71	60	33	60	58	22	nd	29
Phytoplankton group (% Chl-a biomass)									
Diatoms	19	5	4	44	27	3	23	nd	22
Dinoflagellates_1	0	0	8	2	0	0	0	nd	0
Dinoflagellates_2	8	0	9	0	2	11	1	nd	12
Haptophytes_3	21	0	0	4	0	26	61	nd	19
Haptophytes_4	0	0	8	5	3	3	2	nd	4
Cryptophytes	0	0	1	18	10	0	0	nd	0
Prasinophytes_1	51	33	8	26	27	35	12	nd	22
Prasinophytes_2	0	61	61	0	28	0	0	nd	0
Pelagophytes	0	0	1	1	3	0	0	nd	21
Chlorophytes	0	0	0	0	0	21	1	nd	0
NPP estimates (mmol C m^{-2} d^{-1})									
In situ	3.3	2.7	1.3	0.5	5.0	2.3	0.2	0.1	nd
One week	2.3	2.3	2.2	3.5	1.8	1.9	0.6	0.5	nd
Two weeks	2.4	2.5	2.2	3.3	2.2	2.3	0.8	0.6	nd
Annual	3.3	4.8	2.1	2.9	5.6	3.2	11.9	9.9	7.9

nd = no available data. $^{234}Th/^{238}U$, $^{210}Po/^{210}Pb$ and sediment traps [*Lalande et al.*, 2014] were used to estimate POC export fluxes at all the stations, except at stations 5 and 9 for $^{210}Po/^{210}Pb$. [a] Data from *Fernández-Méndez et al.* [2015]. [b] Data from *Katlein et al.* [2014].

4.3.1.2 Biology

The Chl-a inventories in the upper 30 m of the water column were on average 8.4 ± 6.1 mg m^{-2}, with a maximum at station 2 (22.8 mg m^{-2}) and a minimum at station 9 (2.5 mg m^{-2}). The phytoplankton community was picophytoplankton dominated at many stations (1, 2, 3, 5 and 6), accounting for ~40-70% of the total Chl-a biomass. At those stations prasinophytes were the most relevant group with a relative biomass of up to 95%. Large cells dominated the community at station 4 with a significant contribution from diatoms (44%), while nanophytoplankton prevailed at station 7 with a dominance of haptophytes (63%). Finally, station 9 had a similar biomass distribution between size classes (Table 4.1).

The integrated in situ NPP rates in the euphotic zone, sea ice and melt ponds ranged from 0.1 mmol C m^{-2} d^{-1} at the northernmost station (8), to 5.0 mmol C m^{-2} d^{-1} at the southernmost station (5). In situ NPP was highest at the picophytoplankton-dominated stations (>1.3 mmol C m^{-2} d^{-1}). The daily NPP estimates during one and two weeks prior to sampling were higher than the in situ estimates by a factor of 2 to 7 at stations 3, 4, 7 and 8, while they were a factor of 3 lower at station 5. These estimates were comparable at stations 1, 2 and 6. The annual new primary production estimates compared well with the in situ, one- and two-week daily estimates from stations 1 to 6. However, north of 87°N (stations 7 and 8) the annual estimates were higher than the average of the other estimates by a factor >20 (~10-12 mmol C m^{-2} d^{-1}, Table 4.1).

4.3.2 Total $^{234}Th/^{238}U$ and $^{210}Po/^{210}Pb$

4.3.2.1 Seawater profiles

The profiles of the total activities of ^{238}U and ^{234}Th, and ^{210}Pb and ^{210}Po are illustrated in Figure 4.2.

The specific activities of each radionuclide ranged from 2.04 ± 0.05 to 2.44 ± 0.05 dpm L^{-1} for ^{238}U, 1.54 ± 0.06 to 2.59 ± 0.13 dpm L^{-1} for ^{234}Th, 0.84 ± 0.09 to 7.3 ± 0.4 dpm 100L^{-1} for ^{210}Pb, and 0.7 ± 0.3 to 5.4 ± 0.5 dpm 100L^{-1} for ^{210}Po. Within the upper 25 m of the water column, significant deficits of ^{234}Th (i.e. $^{234}Th/^{238}U$ <0.9, given uncertainties) were observed at stations 1, 5 and 6, while significant deficits of ^{210}Po (i.e. $^{210}Po/^{210}Pb$ <0.8, given uncertainties) were detected at all the stations. Below 25 m depth, deficits of ^{234}Th were detected at one single depth at stations 5 and 9 (at 100 and 150 m, respectively), but deficits of ^{210}Po were found at every station usually at several depths (30-150 m). Excesses of ^{234}Th (i.e. $^{234}Th/^{238}U$ >1.1) were not observed at any profile below 25 m, whereas excesses of ^{210}Po (i.e. $^{210}Po/^{210}Pb$ >1.2) were observed at four stations (1, 2, 4 and 6).

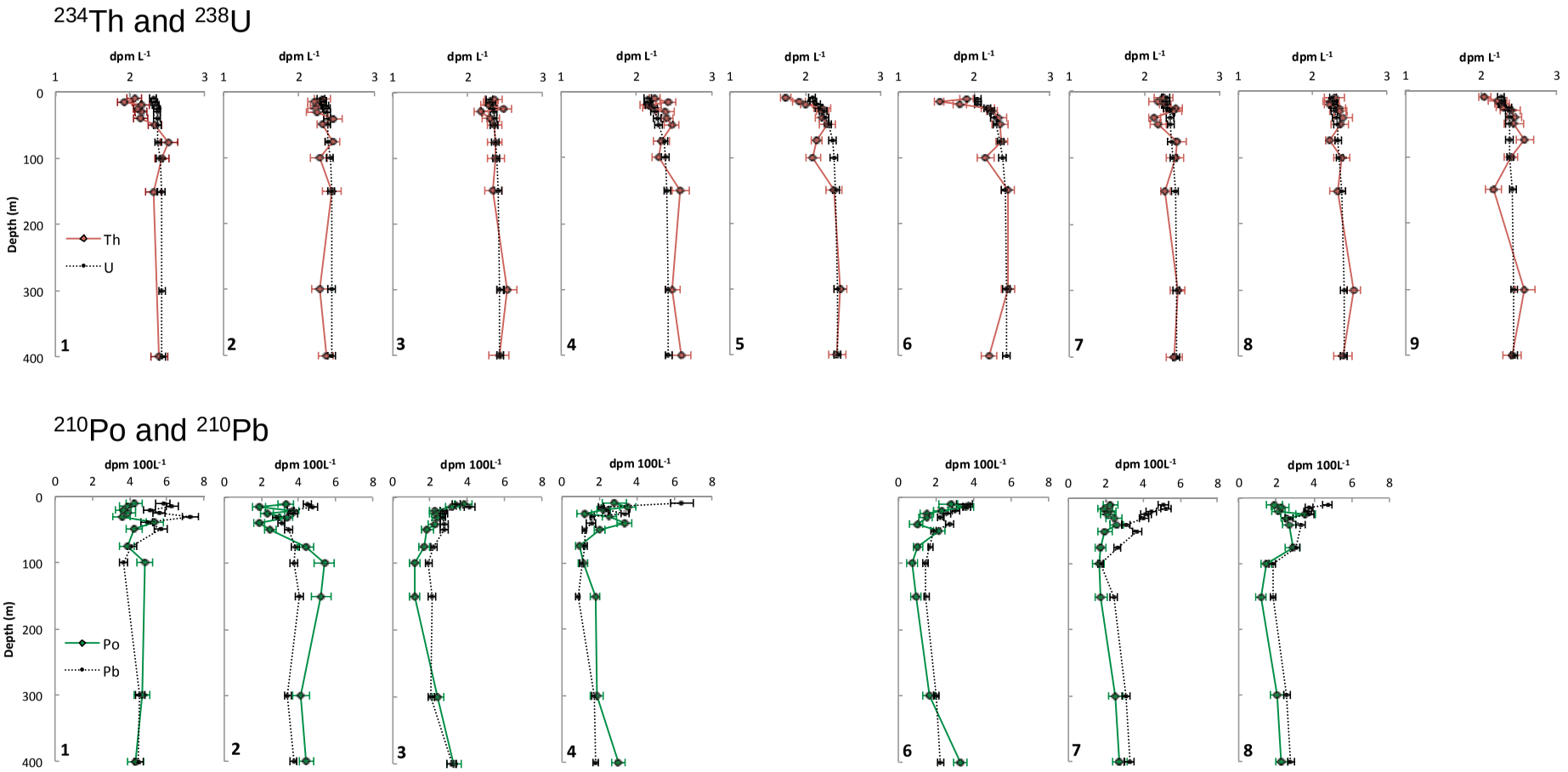

Figure 4.2: Vertical activity profiles for ^{234}Th (red solid line) and ^{238}U (dotted line) (top panels) and for ^{210}Po (green solid line) and ^{210}Pb (dotted line) (bottom panels), from 10 to 400 m depth. U-238 was derived from salinity [*Owens et al.*, 2011].

Station 1 showed deficits of ^{234}Th and ^{210}Po within the upper 50 m: 11500 ± 2100 and 770 ± 120 dpm m^{-2}, respectively. Station 6 also showed deficits of both isotopes, down to 25 m for ^{234}Th (160 ± 40 dpm m^{-2}) and 150 m for ^{210}Po (930 ± 200 dpm m^{-2}). At five stations (2, 3, 4, 7 and 8) ^{234}Th was not significantly depleted in the upper water column. On the contrary, at those stations the integrated ^{210}Po deficits in the upper water column (50-150 m) ranged from 130 ± 150 to 1640 ± 220 dpm m^{-2}. The integrated excesses of ^{210}Po observed at stations 2 (30 and 100-300 m) and 4 (15, 30-50, 150 and 400 m) exceeded the integrated deficits observed in the surface water. Finally, at stations 5 and 9 (only ^{234}Th sampling), ^{234}Th was in equilibrium with ^{238}U throughout the upper 400 m with only a few exceptions.

4.3.2.2 ^{234}Th and ^{210}Po fluxes

The ^{234}Th and ^{210}Po fluxes are attributed to scavenging of ^{234}Th and ^{210}Po onto sinking particles. The fluxes were calculated using a steady-state (SS) model, neglecting advective and diffusive fluxes, following Equation 1.2 (see Section 1.5.3, Chapter 1). The fluxes calculated down to 25, 50, 100 and 150 m are listed in Table 4.2.

The ^{234}Th fluxes were negligible or very low at five out of nine stations (2, 3, 4, 7 and 8). At stations 1, 5 and 6, the ^{234}Th fluxes averaged 175 ± 19 dpm m^{-2} d^{-1} at 25 m, 210 ± 100 dpm m^{-2} d^{-1} at 50 m, 280 ± 140 dpm m^{-2} d^{-1} at 100 m, and 400 ± 200 dpm m^{-2} d^{-1} at 150 m. At station 9 the already low ^{234}Th flux at 25 m (90 ± 40 dpm m^{-2} d^{-1}) became negligible in deeper waters. The ^{210}Po fluxes were significant at all the stations, averaging 1.8 ± 1.1 dpm m^{-2} d^{-1} at 25 m, 2.6 ± 1.5 dpm m^{-2} d^{-1} at 50 m, 3 ± 2 dpm m^{-2} d^{-1} at 100 m and 3 ± 3 dpm m^{-2} d^{-1} at 150 m. The ^{210}Po fluxes did not decrease with depth at the majority of stations (1, 3, 6, 7 and 8), whereas at stations 2 and 4 the fluxes became negligible at 100-150 m.

Table 4.2: ^{234}Th and ^{210}Po export fluxes assuming steady-state conditions at 25, 50, 100 and 150 m.

Station	Depth (m)	^{234}Th fluxes (dpm m^{-2} d^{-1})	^{210}Po fluxes (dpm m^{-2} d^{-1})
1	25	200 ± 50	2.1 ± 0.4
	50	330 ± 60	3.9 ± 0.6
	100	230 ± 130	4.3 ± 1.0
	150	280 ± 190	1.8 ± 1.5
2	25	40 ± 50	1.6 ± 0.3
	50	70 ± 70	2.4 ± 0.4
	100	100 ± 120	1.3 ± 0.9
	150	200 ± 200	-2.2 ± 1.5
3	25	-20 ± 50	0.2 ± 0.3
	50	10 ± 70	0.8 ± 0.4
	100	20 ± 120	2.5 ± 0.7
	150	70 ± 200	4.5 ± 1.0
4	25	-70 ± 40	2.2 ± 0.6
	50	-160 ± 60	1.0 ± 0.7
	100	-160 ± 120	0.8 ± 0.8
	150	-220 ± 180	-0.4 ± 1.0
5	25	170 ± 40	nd
	50	190 ± 60	nd
	100	440 ± 110	nd
	150	660 ± 180	nd
6	25	160 ± 40	0.9 ± 0.3
	50	130 ± 60	2.1 ± 0.4
	100	180 ± 120	3.2 ± 0.7
	150	310 ± 190	4.7 ± 1.0
7	25	20 ± 50	3.4 ± 0.4
	50	90 ± 70	5.0 ± 0.5
	100	90 ± 140	7.2 ± 0.8
	150	160 ± 200	8.2 ± 1.1
8	25	0 ± 60	2.5 ± 0.4
	50	-50 ± 80	3.0 ± 0.5
	100	0 ± 120	3.7 ± 0.9
	150	20 ± 190	4.9 ± 1.1
9	25	90 ± 40	nd
	50	60 ± 70	nd
	100	-110 ± 140	nd
	150	70 ± 190	nd

nd = no available data.

4.3.3 Particulate fraction

Particulate ^{234}Th, ^{210}Pb, ^{210}Po, and organic carbon and nitrogen concentrations in large particles are given in Table 4.3, as well as the ^{210}Po/^{210}Pb and molar C/N ratios.

The mean ^{234}Th activities in particles decreased with depth, ranging from ~1 dpm 100L^{-1} at 25 m to ~0.3 dpm 100L^{-1} at 150 m. Pb-210 activities were on average ~0.06 dpm 100L^{-1} at 25 and 50 m, and ~0.02 dpm 100L^{-1} at 100 and 150 m, while ^{210}Po activities were ~0.04 dpm 100L^{-1} at 25 m

and ~0.02 dpm 100L^{-1} below that depth. The variation between stations was substantial, with deviations from those means of >50% for ^{234}Th, >100% for ^{210}Pb, and >80% for ^{210}Po. Only about 0.3% of the total activity of ^{234}Th in seawater, 1.7% of ^{210}Pb and 1.1% of ^{210}Po was associated with large particles. The maximum particulate activities were found at stations 2 and 3 and the minimum at stations 7 and 8 (negligible in some instances for ^{210}Pb and ^{210}Po). The ^{210}Po/^{210}Pb ratios ranged from 0.2 to 6 (average: 1.2 ± 1.4, n = 18), varying considerably between stations and depths.

The POC and PON concentrations were highest at 25 m, averaging 0.23 ± 0.08 and 0.028 ± 0.011 µmol L^{-1} (n = 8), respectively. Below that depth the concentrations decreased by a factor of 3. The mean C/N ratio was similar at all the investigated depths, averaging 8.8 ± 1.9 (n = 34).

Table 4.3: Particulate ^{234}Th, ^{210}Po, ^{210}Pb, organic carbon and nitrogen concentrations, ^{210}Po/^{210}Pb ratios and molar C/N ratios in particles >53 µm.

Station	Depth (m)	Part. ^{234}Th (dpm 100L^{-1})	Part. ^{210}Po (dpm 100L^{-1})	Part. ^{210}Pb (dpm 100L^{-1})	^{210}Po/^{210}Pb	POC (µmol C L^{-1})	PON (µmol N L^{-1})	C/N (mol:mol)
1	15	0.45 ± 0.03	0.026 ± 0.003	0.0042 ± 0.0012	6 ± 2	0.25	0.038	6.6
	50	nd	nd	nd	nd	nd	nd	nd
	90	0.335 ± 0.019	0.008 ± 0.003	0.0144 ± 0.0018	0.6 ± 0.2	0.074	0.0092	8.1
	190	0.138 ± 0.008	0.011 ± 0.002	0.0057 ± 0.0011	1.8 ± 0.5	0.034	0.0054	6.3
2	25	nd	nd	nd	nd	nd	nd	nd
	50	1.71 ± 0.12	0.032 ± 0.006	0.031 ± 0.003	1.0 ± 0.2	0.23	0.034	6.7
	100	1.86 ± 0.12	0.120 ± 0.011	0.073 ± 0.004	1.6 ± 0.2	0.12	0.020	6.3
	150	0.89 ± 0.06	0.050 ± 0.007	0.055 ± 0.004	0.91 ± 0.14	0.042	0.0068	6.1
3	25	1.63 ± 0.09	0.066 ± 0.010	0.217 ± 0.010	0.30 ± 0.05	0.27	0.033	8.1
	50	1.60 ± 0.11	0.054 ± 0.014	0.221 ± 0.011	0.24 ± 0.07	0.15	0.020	7.8
	100	0.215 ± 0.012	*<0.003*	0.039 ± 0.003	-	0.032	0.0043	7.4
	150	0.51 ± 0.02	0.035 ± 0.006	0.040 ± 0.004	0.9 ± 0.2	0.087	0.010	8.5
4	25	0.55 ± 0.03	0.025 ± 0.003	0.044 ± 0.003	0.57 ± 0.08	0.28	0.029	9.8
	50	0.47 ± 0.03	0.015 ± 0.003	0.031 ± 0.002	0.47 ± 0.12	0.036	0.0056	6.4
	100	0.276 ± 0.010	*<0.003*	0.0152 ± 0.0016	-	0.097	0.014	7.0
	150	0.43 ± 0.02	0.007 ± 0.003	0.023 ± 0.002	0.31 ± 0.15	0.058	0.0078	7.5
5	25	1.50 ± 0.10	nd	nd	nd	0.38	0.047	8.0
	50	0.88 ± 0.06	nd	nd	nd	0.14	0.016	8.5
	100	0.414 ± 0.016	nd	nd	nd	0.097	0.011	9.2
	150	0.58 ± 0.03	nd	nd	nd	0.061	0.0075	8.2
6	25	1.25 ± 0.08	0.077 ± 0.006	0.106 ± 0.005	0.73 ± 0.06	0.15	0.014	11
	50	0.250 ± 0.014	0.006 ± 0.003	0.026 ± 0.002	0.21 ± 0.12	0.025	0.0025	10
	100	0.094 ± 0.005	*<0.003*	0.008 ± 0.002	-	0.015	0.0014	10
	150	0.096 ± 0.009	0.013 ± 0.003	0.0059 ± 0.0016	2.2 ± 0.8	0.012	0.00090	14
7	25	0.42 ± 0.02	0.0126 ± 0.0018	0.0076 ± 0.0014	1.7 ± 0.4	0.23	0.023	10
	50	0.062 ± 0.007	*<0.003*	*<0.003*	-	0.029	0.0028	11
	100	0.061 ± 0.009	*<0.003*	0.0040 ± 0.0018	-	0.088	0.0074	12
	150	0.078 ± 0.006	0.009 ± 0.003	*<0.003*	-	0.036	0.0029	12
8	25	0.51 ± 0.02	0.009 ± 0.003	0.010 ± 0.002	0.9 ± 0.3	0.16	0.020	8.1
	50	0.286 ± 0.016	0.008 ± 0.003	0.026 ± 0.003	0.31 ± 0.13	0.049	0.0051	9.6
	100	0.133 ± 0.014	*<0.003*	0.012 ± 0.003	-	0.080	0.0070	11
	150	0.100 ± 0.008	*<0.003*	0.0040 ± 0.0018	-	0.032	0.0040	8.2
9	25	1.34 ± 0.10	nd	nd	nd	0.15	0.020	7.4
	50	0.64 ± 0.03	nd	nd	nd	0.088	0.0091	9.7
	100	0.229 ± 0.011	nd	nd	nd	0.069	0.0077	9.0
	150	0.18 ± 0.02	nd	nd	nd	0.059	0.0064	9.3

nd = no available data.

Table 4.4 displays the POC/^{234}Th and POC/^{210}Po ratios (C/Th and C/Po) at 25, 50, 100 and 150 m. The average ratios at the different horizon depths ranged from 17 to 40 μmol C dpm^{-1} for C/Th and from 300 to 1100 μmol C dpm^{-1} for C/Po. The ratios did not change significantly with depth (Kruskal-Wallis test, $p > 0.05$).

4.3.4 POC fluxes

The POC fluxes were calculated multiplying the ^{234}Th and ^{210}Po fluxes derived from the SS model by the C/Th and C/Po ratios in large particles, respectively (Table 4.4).

Table 4.4: Particulate C/Th and C/Po ratios and POC fluxes derived from ^{234}Th and ^{210}Po.

Station	Depth (m)	C/Th (μmol C dpm^{-1})	C/Po (μmol C dpm^{-1})	POC fluxes (mmol C m^{-2} d^{-1}) ^{234}Th-derived	^{210}Po-derived
1	15	56 ± 4	970 ± 100	7 ± 2	1.2 ± 0.4
	50	nd	nd	nd	nd
	90	22.1 ± 1.3	900 ± 400	5 ± 3	4 ± 2
	190	25.0 ± 1.5	330 ± 70	10 ± 6	0.1 ± 0.7
2	25	nd	nd	nd	nd
	50	13.2 ± 0.9	700 ± 120	0.9 ± 0.9	1.7 ± 0.4
	100	6.7 ± 0.5	104 ± 9	0.7 ± 0.8	0.13 ± 0.09
	150	4.7 ± 0.3	83 ± 12	0.9 ± 0.9	-0.19 ± 0.13
3	25	16.3 ± 0.9	400 ± 60	-0.4 ± 0.8	0.06 ± 0.14
	50	9.6 ± 0.6	280 ± 80	0.1 ± 0.7	0.23 ± 0.14
	100	14.8 ± 0.8	-	0 ± 2	-
	150	16.9 ± 0.8	250 ± 40	1 ± 3	1.1 ± 0.3
4	25	51 ± 3	1140 ± 140	-4 ± 2	2.5 ± 0.7
	50	7.7 ± 0.4	250 ± 60	-1.2 ± 0.5	0.3 ± 0.2
	100	35.2 ± 1.3	-	-6 ± 4	-
	150	13.6 ± 0.6	800 ± 400	-3 ± 2	-0.3 ± 0.9
5	25	25.1 ± 1.7	nd	4.3 ± 1.0	nd
	50	15.6 ± 1.0	nd	2.9 ± 0.9	nd
	100	23.5 ± 0.9	nd	10 ± 3	nd
	150	10.5 ± 0.5	nd	7 ± 2	nd
6	25	12.2 ± 0.8	197 ± 14	1.9 ± 0.5	0.18 ± 0.07
	50	10.1 ± 0.5	500 ± 200	1.3 ± 0.6	1.0 ± 0.5
	100	15.5 ± 0.8	-	3 ± 2	-
	150	12.7 ± 1.2	90 ± 20	4 ± 2	0.44 ± 0.13
7	25	54 ± 3	1800 ± 300	1 ± 3	6.3 ± 1.1
	50	48 ± 6	-	4 ± 3	-
	100	150 ± 20	-	10 ± 20	-
	150	47 ± 4	390 ± 110	7 ± 9	3.2 ± 1.0
8	25	32.3 ± 1.4	1900 ± 600	0 ± 2	4.8 ± 1.6
	50	17.1 ± 1.0	600 ± 300	-0.9 ± 1.3	1.8 ± 1.3
	100	60 ± 6	-	0 ± 7	-
	150	32 ± 3	-	1 ± 6	-
9	25	11.2 ± 0.8	nd	1.0 ± 0.5	nd
	50	13.7 ± 0.8	nd	0.9 ± 0.9	nd
	100	30.2 ± 1.4	nd	-3 ± 4	nd
	150	32 ± 4	nd	2 ± 6	nd

nd = no available data.

The ^{234}Th-derived POC fluxes ranged from negligible to 10 mmol C m^{-2} d^{-1} and averaged 1.3 to 4 mmol C m^{-2} d^{-1} at 25, 50, 100 and 150 m. The ^{210}Po-derived POC fluxes ranged from negligible to 6.3 mmol C m^{-2} d^{-1} and averaged 0.8 to 3 mmol C m^{-2} d^{-1} at the same depths. The POC fluxes estimated using the two proxies were not significantly different considering all depths together, or each depth individually (Wilcoxon test, $p > 0.05$).

4.4 Discussion

In this study we have used two pairs of radionuclides, ^{234}Th/^{238}U and ^{210}Po/^{210}Pb, as tools to estimate POC fluxes in the Eurasian Basin of the Arctic Ocean in summer 2012. Deficits of ^{234}Th and ^{210}Po are attributed to particle export, while the excesses of these radionuclides evidence their release from sinking particles by means of remineralization or particle disaggregation into the suspended pool. Their simultaneous application allows integrating a temporal scale over a span of weeks (^{234}Th mean life = 35 days) to months (^{210}Po mean life = 200 days).

4.4.1 ^{234}Th/^{238}U

4.4.1.1 ^{234}Th export fluxes

Th-234 export fluxes were calculated using a SS model because the stations were not reoccupied during the expedition. Yet, in a review study *Savoye et al.* [2006] did not find significant differences between the SS and non-steady state (NSS) models at low flux rates (<800 dpm m^{-2} d^{-1}), which is the case of the present work.

Significant ^{234}Th fluxes within the upper 150 m of the water column were obtained at stations 1, 5 and 6, and at specific depths at some other stations (Table 4.2). The ^{234}Th fluxes ranged from negligible to 660 dpm m^{-2} d^{-1}, averaging 120 ± 140 dpm m^{-2} d^{-1} (n = 36). Our results are one order of magnitude lower than the ^{234}Th flux average reported by *Le Moigne et al.* [2013b] for the world's oceans (1200 ± 900 dpm m^{-2} d^{-1}, 75-210 m, n = 421). Previous research conducted in the central Arctic, mainly during summer, has also revealed low export fluxes escaping from the ocean surface (Figure 4.3). *Cai et al.* [2010] reported an average of 90 ± 300 dpm m^{-2} d^{-1} (n = 26) in the most extensive study of ^{234}Th over the central basins to date, and *Moran et al.* [1997] and *Gustafsson and Andersson* [2012] reported similar flux averages of 190 ± 140 dpm m^{-2} d^{-1} (n = 7) and 130 ± 100 dpm m^{-2} d^{-1} (n = 3), respectively. *Le Moigne et al.* [2015] reported ^{234}Th fluxes of 140 ± 210 dpm m^{-2} d^{-1} in the ice-covered Fram Strait, which is also in line with our results. Nevertheless, other studies have reported high ^{234}Th export fluxes (>2000 dpm m^{-2} d^{-1}) at specific locations in the Canada Basin [*Ma et al.*, 2005], although they are more typical of the shelf environment (Figure 4.3)

[e.g. *Coppola et al.*, 2002; *Lepore et al.*, 2007]. Overall, the ^{234}Th flux data presented here and the limited data available to date illustrate the central Arctic basins as deserts in terms of particle export during summer.

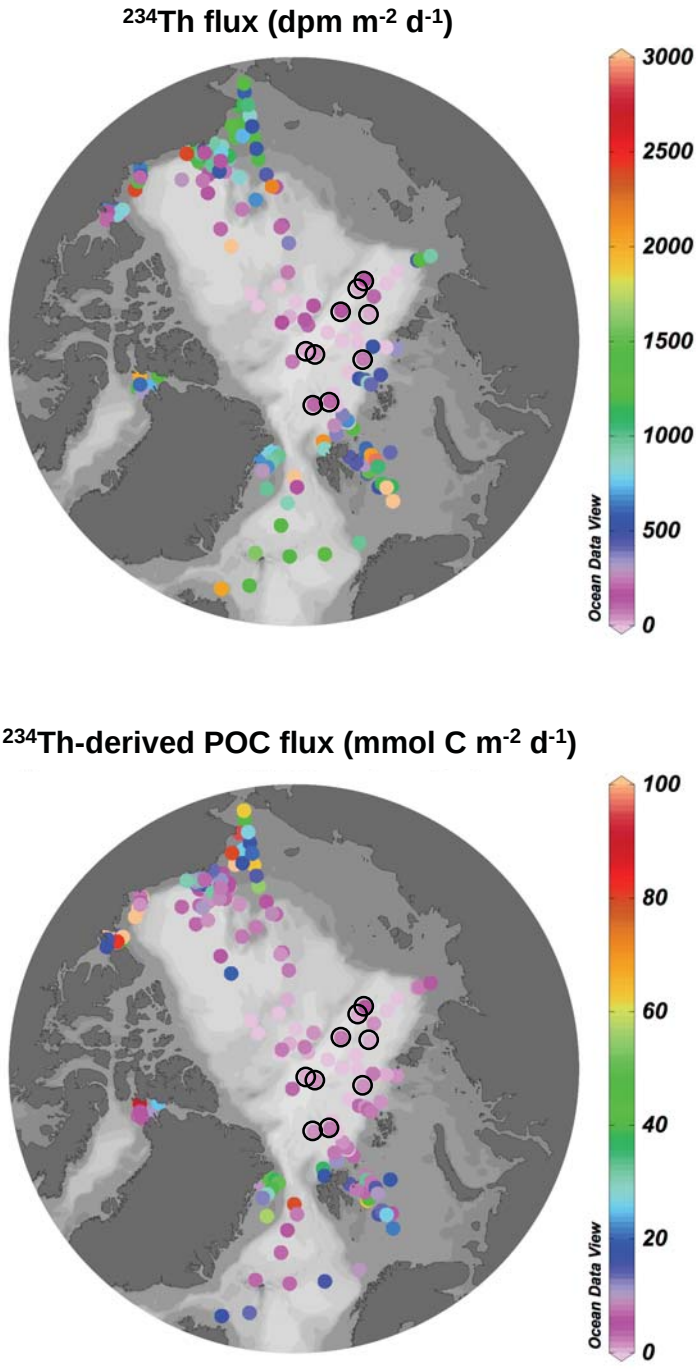

Figure 4.3: Compilation of ^{234}Th flux data (top) and ^{234}Th-derived POC flux data (bottom) from the Arctic Ocean (236 stations) [*Cochran et al.*, 1995b; *Moran et al.*, 1997, 2005; *Moran and Smith*, 2000; *Amiel et al.*, 2002; *Coppola et al.*, 2002; *Baskaran et al.*, 2003; *Chen et al.*, 2003; *Ma et al.*, 2005; *Trimble and Baskaran*, 2005; *Lepore et al.*, 2007; *Lalande et al.*, 2007b, 2008; *Amiel and Cochran*, 2008; *Yu et al.*, 2010, 2012; *Cai et al.*, 2010; *Gustafsson and Andersson*, 2012; *Le Moigne et al.*, 2015; this study]. Black circles indicate the results obtained in this study. The depth horizon taken to calculate the POC export fluxes ranges from 25 to 200 m.

4.4.1.2 ^{234}Th-derived POC export fluxes

The mean ^{234}Th-derived POC export fluxes measured in the upper 150 m were 3 ± 3 mmol C m^{-2} d^{-1} (n = 34), with a maximum of 10 mmol C m^{-2} d^{-1} (Table 4.4). At the bottom of the euphotic zone (~25 m) the fluxes ranged from negligible to 7 mmol C m^{-2} d^{-1} (average: 2 ± 2 mmol C m^{-2} d^{-1}, n = 8). These results are in very good agreement with the POC fluxes measured with cylindrical sediment traps (HydroBios, Germany) deployed under the ice during periods of 24-53 hours from station 1 to 9 [*Lalande et al.*, 2014]. The sediment trap results ranged from 0.4 to 9 mmol C m^{-2} d^{-1} (average: 3 ± 3 mmol C m^{-2} d^{-1}, n = 9). The in situ NPP rates showed positive correlations with ^{234}Th fluxes at 25 m ($p < 0.05$; Spearman correlation coefficient, $\rho = 0.83$, n = 8), ^{234}Th-derived POC fluxes at 25 m ($p < 0.05$; $\rho = 0.78$, n = 7) and sediment trap-derived POC fluxes at 25 m ($p < 0.05$; $\rho = 0.83$, n = 8), which indicates enhanced particle fluxes with increasing NPP. Our results also compare well with previous literature values from sediment traps deployed at 150-175 m north of the Laptev Sea continental margin in August-September during the years 1995-1996 and 2005-2006 (~0.5-2.5 mmol C m^{-2} d^{-1}) [*Fahl and Nöthig*, 2007; *Lalande et al.*, 2009b] and ^{234}Th-derived POC fluxes in the central Arctic (Figure 4.3). *Cai et al.* [2010] documented very low POC export fluxes (average: 0.2 ± 1.0 mmol C m^{-2} d^{-1}, n = 26) across the deep Arctic, suggesting that they were a consequence of low biological productivity. Our low POC export flux estimates are in good agreement with the low NPP observed in the present study within the ^{234}Th time window (in situ, one- and two-week estimates; ≤5 mmol C m^{-2} d^{-1}; Table 4.1).

4.4.1.3 Relationships with phytoplankton community

We did not find any significant relationship between the ^{234}Th data (particulate ^{234}Th activity, ^{234}Th fluxes and ^{234}Th-derived POC fluxes) and the phytoplankton size structure at the sampling time, although two correlations were obtained with regards to the phytoplankton composition. The relative biomass of prasinophytes_1 was positively correlated with ^{234}Th fluxes ($p < 0.05$; $\rho = 0.75$, n = 8) and ^{234}Th-derived POC fluxes ($p < 0.05$; $\rho = 0.77$, n = 7) at 25 m. This suggests that prasinophytes_1 would have contributed significantly to vertical export fluxes during the late summer in 2012 when picophytoplankton, and particularly prasinophytes, were the predominant group in terms of biomass (Prasinophytes_1 and 2, Table 4.1). Prasinophytes are green algae that can be usually found in the eukaryotic picophytoplankon fraction. A molecular study by *Metfies et al.* [2016] corroborates the biomass dominance of picophytoplankton in the upper water column during our expedition and identifies the prasinophyte *Micromonas* spp. as its major constituent. Our finding is in line with recent observations that reveal that small cells are important contributors to POC export fluxes in diverse oceanic regimes [e.g. *Richardson and Jackson*, 2007; *Lomas and Moran*, 2011; *Durkin et al.*, 2015; *Mackinson et al.*, 2015; *Puigcorbé et al.*, 2015]. Prasinophytes, including

Micromonas spp., are common in the central Arctic [*Booth and Horner*, 1997; *Sherr et al.*, 2003; *Zhang et al.*, 2015], and are considered to be among the most abundant photosynthetic cells in pan-Arctic waters [*Lovejoy et al.*, 2007]. Genetic analyses in trap samples revealed that prasinophytes contributed to downward fluxes in the Sargasso Sea [*Amacher et al.*, 2013], but to our knowledge, this has not been observed before in Arctic waters. It is relevant to note that neither genetic nor pigment techniques inform about whether they sink as single cells or as part of other export pathways.

The pathways by which picophytoplankton cells can be removed from the ocean surface are fundamentally: (i) zooplankton grazing and subsequent incorporation into faecal pellets [*Waite et al.*, 2000; *Wilson and Steinberg*, 2010]; (ii) adhesion into mucous nets formed by gelatinous zooplankton, such as pteropods, and later settling [*Noji et al.*, 1997]; and (iii) inclusion into marine snow via particle aggregation, which is enhanced by transparent exopolymer particles [*Passow*, 2002]. Passive sinking of faecal pellets could be a significant pathway for particle export in the central Arctic, where zooplankton exert a strong grazing pressure on algae preventing their biomass accumulation and sedimentation [*Olli et al.*, 2007]. Indeed, the copepod food demand during our cruise was estimated to be similar to the in situ NPP rates [*David et al.*, 2015], leaving a small fraction of algae available for direct export. Yet, *Lalande et al.* [2014] estimated that only up to 7.5% of the POC collected by traps at 25 m consisted of faecal pellets. Trap samples also consisted of marine snow, debris, appendicularian houses, animal body parts and very sticky material, even though their relative importance in POC content was not quantified (C. Lalande, pers. comm.). Copepods clearly dominated the zooplankton community with regards to abundance, whereas pteropods, ctenophores and appendicularians, which are prone to produce mucous, represented less than 3-5% of the total zooplankton abundance either beneath the ice [*David et al.*, 2015] or within the upper 50 m [*Ehrlich*, 2015]. However, ctenophores and appendicularians dominated the under-ice zooplankton biomass at some stations, which could have contributed notably to the export of mucous (C. David, pers. comm.). Moreover, sea-ice algal aggregates of the centric diatom *Melosira arctica* and pennate diatoms were observed at all the stations [*Fernández-Méndez et al.*, 2014]. They reached abundances of up to 16 ind m^{-2} and extraordinary sizes (mean diameter of 2.1-4.1 cm), although they showed a highly patchy distribution [*Katlein et al.*, 2014]. The aggregates were associated with mucous matrices that increased their stickiness and, at the same time, their predisposition to aggregation [*Fernández-Méndez et al.*, 2014]. Indeed, *Melosira arctica* was intercepted using sediment traps deployed at 25 m at some stations [*Lalande et al.*, 2014], confirming that it was part of the sinking pool. Taken all together, sea-ice algal aggregates and zooplankton-derived material might have acted as carriers of picophytoplankton cells from the ocean surface to depth (Figure 4.4B).

4.4.2 ^{210}Po/^{210}Pb

4.4.2.1 ^{210}Po and ^{210}Pb activities

Po-210 activities were lower than those of ^{210}Pb at every station in the upper 50-150 m, indicating export driven by sinking particles, while excesses of ^{210}Po were observed at several depths throughout the upper 400 m at stations 2 and 4, suggesting remineralization or particle disaggregation (Figure 4.2). At stations 2 and 4 the integrated excess surpassed the integrated deficit at 150 m and below, which can be explained by (i) a previous substantial export event that occurred at the study sites, and/or (ii) advection of waters that were enriched in ^{210}Po as a consequence of a previous export event [*Stewart et al.,* 2007a]. Thus, the assumption of SS and/or neglecting the advective term would have added uncertainty to our flux estimates of ^{210}Po. We note that the ^{210}Po flux estimates are subject to be affected by NSS conditions or advection transport processes to a larger extent than the ^{234}Th flux estimates due to the longer half-life of ^{210}Po.

Very few studies have investigated the distribution of ^{210}Pb and/or ^{210}Po in the Arctic water column [*Moore and Smith*, 1986; *Cochran et al.*, 1995a; *Smith and Ellis*, 1995; *Roberts et al.*, 1997; *Smith et al.*, 2003; *Lepore et al.*, 2009a; *Chen et al.*, 2012]. The ^{210}Pb and ^{210}Po activities presented here are comparable to the wide activity range reported by those studies, including shelf and basin areas.

In the Arctic, sea ice intercepts and accumulates atmospheric fluxes of chemical species, such as ^{210}Pb, during its transit through the ocean [*Masqué et al.*, 2007; *Cámara-Mor et al.*, 2011] and, therefore, sea-ice melting may increase ^{210}Pb activities in surface waters where that occurs [*Roberts et al.*, 1997; *Masqué et al.,* 2007; *Chen et al.*, 2012]. One might wonder whether sea-ice melting may significantly impact the ^{210}Pb and ^{210}Po activities in seawater and, thus, affect the use of the ^{210}Po proxy. Data on ^{210}Pb and ^{210}Po activities in entire sea-ice cores collected during the same expedition (results not shown) show that the ^{210}Po/^{210}Pb ratios were ≤0.5, indicating ^{210}Pb enrichment in sea ice, and consistent with the dominance of first-year ice [*Masqué et al.,* 2007]. Given the inventories of both isotopes in sea-ice cores, even with complete melting of sea ice, the ^{210}Po/^{210}Pb ratio in the upper 25 m of the water column would have not changed or would have decreased as much as 10%. Since this change is relatively small, we are confident that the principal cause of the ^{210}Po deficit in the upper water column was its preferential removal via particle scavenging with respect to ^{210}Pb.

4.4.2.2 ^{210}Po export fluxes

The ^{210}Po export fluxes in the upper 150 m ranged from negligible to 8.2 dpm m^{-2} d^{-1}, averaging 3 ± 2 dpm m^{-2} d^{-1} (n = 28, Table 4.2). The fluxes obtained in this study are very low in comparison to other studies conducted in other regions of the world ocean [*Shimmield et al.*, 1995; *Kim and Church*, 2001; *Friedrich and Rutgers van der Loeff*, 2002; *Murray et al.*, 2005; *Stewart et al.*, 2007a; *Buesseler et al.*, 2008b; *Verdeny et al.*, 2008; *Le Moigne et al.*, 2013a], which reported fluxes from 5 to >100 dpm m^{-2} d^{-1}. However, ^{210}Po fluxes were significant at every station and at most of the investigated depths, in contrast to ^{234}Th fluxes, which were only measurable throughout the upper 150 m at three stations (Table 4.2). Given the half-lives of both tracers, ^{210}Po would track particle export for the entire productive season, whereas ^{234}Th distribution misses events that occurred more than one month before sampling. Thus, the more common ^{210}Po depletion than that of ^{234}Th in the upper water column suggests that the magnitude of the particle export fluxes was more important before July/August 2012 than in the weeks prior to and during the sampling (Figure 4.4).

Boetius et al. [2013] revealed the presence of vast deposits of sea-ice algal aggregates on the seafloor at the majority of stations, which would have been exported from the ocean surface earlier in the season, particularly before June at stations 4-6 as suggested by the large body size and fecundity of the deep-sea holothurians that fed on the algae (Figure 1.10). The aggregates were mainly composed of *Melosira arctica* [*Boetius et al.*, 2013] that can form long strands hanging from the ice bottom, sometimes up to 6 meters long [*Melnikov and Bondarchuk*, 1987], allowing a rapid sinking throughout the water column once detached. *Boetius et al.* [2013] estimated that algae covered up to 10% of the seafloor by means of high-resolution pictures, accounting for a median of 750 mmol C m^{-2} (± 50%). This POC inventory of algae was obtained by applying a cell volume to carbon ratio (0.15 pg C µm^{3}) and a fixed thickness of the algal cover (1 cm). This supports the ^{210}Po evidence that the peak of export in the study area occurred in early summer and sheds light on the composition of a major part of the sinking pool (Figure 4.4A). It was estimated that diatoms were responsible for at least 45% of the total primary production in 2012 [*Boetius et al.*, 2013], indicating that the phytoplankton community varied over the productive season, since diatoms did not contribute much to the Chl-a biomass during our cruise (~20%, Table 4.1), when surface waters were silicate-depleted in most of the study area. Previous studies with sediment traps also revealed that highest fluxes in the central Arctic occur mainly in June-August when ice algae appear to be significant contributors to the export fluxes [*Fahl and Nöthig*, 2007; *Lalande et al.*, 2009a].

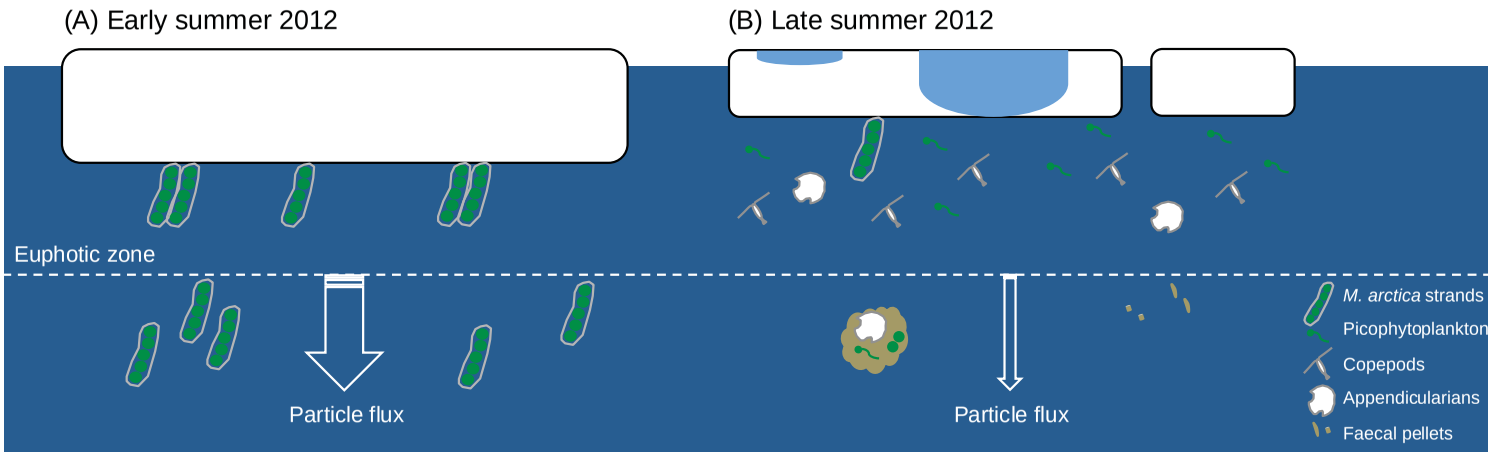

Figure 4.4: Scheme of the magnitude and composition of the particle fluxes in the central Arctic during the early (A) and late summer (B) in 2012 based on results from the present study and others [*Boetius et al.*, 2013*; Lalande et al.*, 2014*; David et al.*, 2015*; Fernández-Méndez et al.*, 2015] (see Sections 4.4.1 and 4.4.2 for further details). Symbols are not drawn to scale.

4.4.2.3 Relationships with sea-ice conditions

There were significant relationships between the sea-ice conditions and the ^{210}Po-derived fluxes. Sea-ice concentration was positively correlated with both ^{210}Po fluxes ($p < 0.01$; $\rho = 0.92$, $n = 7$) and ^{210}Po-derived POC fluxes ($p < 0.05$; $\rho = 0.91$, $n = 6$) at 25 m. Indeed, the stations located north of 87°N and covered by multi-year ice (stations 7 and 8) showed the most substantial depletion of ^{210}Po within the upper 400 m (Figure 4.2) and the highest annual NPP rates (Table 4.1) and seafloor algal coverage [*Boetius et al.*, 2013]. This suggests that primary production and particle export were more important under heavy sea-ice conditions than under partially ice-covered stations and first-year ice, also suggesting that ^{210}Po tracked, to some extent, the massive algal export that occurred earlier in 2012. On the contrary, at stations with heavy sea-ice conditions we found the minimum in situ NPP rates (Table 4.1) and ^{234}Th in equilibrium with ^{238}U throughout the upper water column (Figure 4.2), indicating low or negligible primary production and particle export fluxes during the late summer.

The results presented here, combined with those from *Boetius et al.* [2013], show that the central Arctic underwent significant changes during the productive season in terms of primary production, phytoplankton composition and export fluxes during the record low of sea ice in 2012. This has implications for the use of ^{210}Po as a tracer: the depth distribution of total ^{210}Po activity likely changed with time (NSS conditions) and the sinking material collected during the survey probably did not cause the observed ^{210}Po depletion in the upper water column. Actually, ^{210}Po activities in large particles collected at the time of sampling were inversely correlated with ^{210}Po export fluxes at 25 m ($p < 0.05$; $\rho = -0.89$, $n = 6$). The SS model would tend to smooth out episodic export events that took place earlier in the season, and hence underestimate the mean ^{210}Po fluxes and ^{210}Po-derived POC fluxes on a seasonal scale. On the other hand, we measured C/Po ratios in particles that fall in the upper range of previous values [see review by *Verdeny et al.*, 2009]. *Stewart et al.* [2007a] showed that C/Po ratios varied according to the sinking material composition as follows: degraded material > fresh phytoplankton > faecal pellets. In some instances we also found particulate ^{210}Po/^{210}Pb ratios below one (Table 4.3), which is inconsistent with the ^{210}Po deficiency observed in surface waters. Particle types that may potentially explain low ^{210}Po/^{210}Pb ratios could be: those remineralized by chemical and biological processes [*Stewart et al.*, 2007b]; faecal material [*Stewart et al.*, 2005; *Rodriguez y Baena et al.*, 2007]; picoplankton aggregates [*Stewart et al.*, 2010]; substrates rich in transparent exopolymer particles [*Quigley et al.*, 2002]; and sea-ice drafted material incorporated over the shelves, such as sea-ice sediments (SIS), and enriched in ^{210}Pb via atmospheric input (^{210}Po/^{210}Pb ratios in SIS collected during the expedition were ≤1, results not shown). If the sinking pool responsible for ^{210}Po scavenging had different C/Po ratios with respect

to that collected at the sampling time, the ^{210}Po-derived POC fluxes obtained in this study would not be fully representative of the fluxes that occurred in the productive season in 2012.

4.4.3 Export efficiency

The export efficiency has been estimated by dividing the POC export fluxes derived from ^{234}Th and ^{210}Po at 25 m (i.e. ~bottom of the euphotic zone) by different estimates of NPP that encompass daily, weekly and annual time scales (Table 4.5).

Table 4.5: Export efficiency according to the ^{234}Th and ^{210}Po proxies estimated using different estimates of daily NPP (in situ, one and two weeks before sampling and annual new primary production; see text for further details).

Station	Export efficiency (%)			
	In situ	One week	Two weeks	Annual
Th proxy				
1[a]	>100	>100	>100	>100
2[b]	*30 ± 40*	*40 ± 40*	*30 ± 40*	*20 ± 20*
3	0	0	0	0
4	0	0	0	0
5	90 ± 20	>100	>100	77 ± 18
6	80 ± 20	100 ± 30	80 ± 20	60 ± 17
7	*>100*	*>100*	*>100*	*10 ± 20*
8	0	0	0	0
9	nd	nd	nd	13 ± 6
Po proxy				
1[a]	37 ± 12	53 ± 17	50 ± 16	37 ± 12
2[b]	64 ± 16	74 ± 19	67 ± 17	36 ± 9
3	*5 ± 11*	*3 ± 6*	*3 ± 6*	*3 ± 7*
4	>100	70 ± 20	80 ± 20	90 ± 30
5	nd	nd	nd	nd
6	8 ± 3	9 ± 4	8 ± 3	6 ± 2
7	>100	>100	>100	53 ± 9
8	>100	>100	>100	48 ± 16
9	nd	nd	nd	nd

nd = no available data. The values in italics have relative uncertainties ≥100%. [a] POC fluxes were measured at 15 m instead of 25 m. [b] POC fluxes were measured at 50 m instead of 25 m.

Considering the in situ NPP rates, the export efficiencies varied widely over the study site, from 0 to >100%, averaging 50 ± 50% (n = 8) and 60 ± 40% (n = 7) for the ^{234}Th and ^{210}Po proxies, respectively. The export efficiencies calculated using the fluxes measured with sediment traps [*Lalande et al.*, 2014] were >100% at six out of eight stations. Export efficiencies over 100% suggest that primary production that occurred earlier in the season contributed to the export fluxes measured (i.e. temporal decoupling between production and export). In order to cover longer time scales of NPP, we have also used estimates that integrate one and two weeks before sampling and the entire productive season (see Section 4.3.1.2). The increase in daily NPP observed between the

in situ and the weekly estimates at stations 3, 4, 7 and 8, only changed significantly the export efficiency at station 4 (^{210}Po proxy), obtaining estimates of ~70% (Table 4.5). Export efficiencies over 100% were still observed in several instances, indicating that the lag between production and export was longer than two weeks. On the contrary, the export efficiencies decreased by about 40% applying the annual NPP estimates (^{234}Th: 30 ± 40%, n = 9; ^{210}Po: 40 ± 30%, n = 7) and were mostly below 100%, except for ^{234}Th at station 1. In contrast to ^{234}Th, ^{210}Po fluxes and ^{210}Po-derived POC fluxes at 25 m showed a positive correlation with the integrated deficits of nitrate found in the upper water column [*Fernández-Méndez et al.*, 2015] ($p < 0.05$; $\rho = 0.83$, n = 6), which are used to estimate the annual new NPP rates [e.g. *Codispoti et al.*, 2013]. This confirms that the ^{210}Po proxy covered the productive season better than ^{234}Th, and suggests that consumption of nitrate resulted in the increase in export production. Thus, the ^{210}Po-derived POC fluxes and annual NPP estimates can be useful to assess the seasonal strength of the biological pump, allowing to overcome the temporal decoupling between production and export, which is especially long in Arctic waters according to a global biogeochemical model presented by *Henson et al.* [2015].

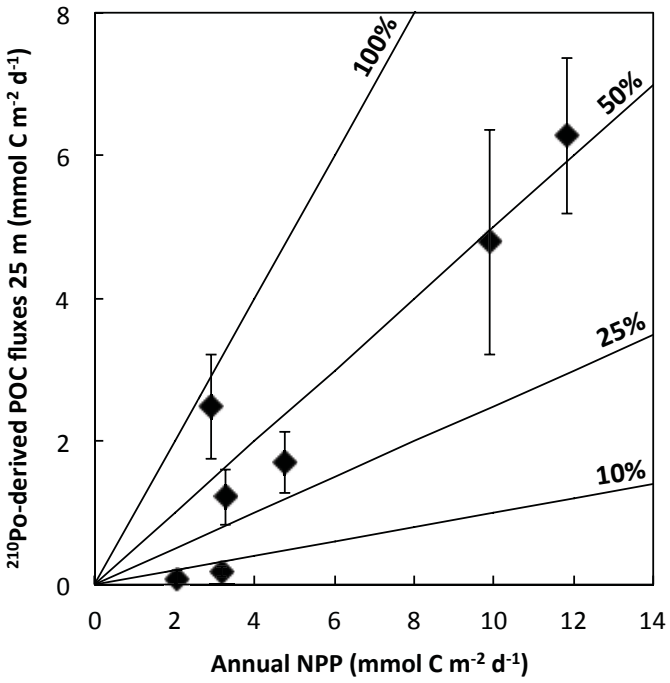

Figure 4.5: ^{210}Po-derived POC export fluxes at 25 m vs. annual new primary production reported in *Fernández-Méndez et al.* [2015]. Solid lines indicate the export efficiency.

The export efficiencies based on the annual NPP and the ^{210}Po-derived POC fluxes are illustrated in Figure 4.5. Only two locations showed export efficiencies <10% (stations 3 and 6, Table 4.5), which are those typically found in the world's oceans [*Buesseler*, 1998]. In this line, *Cai et al.* [2010] reported export efficiencies <6% in the central Arctic using historical measurements of primary production. In contrast, export efficiencies >30% (average: 50 ± 20%, n = 5) were found at the

other stations, which are in good agreement with those reported by *Gustafsson and Andersson* [2012] in the Eurasian Basin (average: 34 ± 8%, n = 3) and *Chen et al.* [2003] in the Canada Basin (26%, n = 1) applying ^{234}Th-derived POC fluxes and in situ NPP rates. Our estimates are also similar to the ^{234}Th-derived export efficiencies of ~30-40% reported for Chukchi shelf, slope and basin stations in summer [*Moran et al.*, 2005; *Lepore et al.*, 2007]. Although only a limited set of observations of export efficiency is available in the central Arctic, overall they point to high export efficiencies as also indicated by *Henson et al.* [2015]. The assessment of the export efficiency in the central Arctic deserves more attention to better understand its role as an export regime in a climate change framework. Observations of strong aggregation and rapid algal falls in the central Arctic [*Boetius et al.*, 2013; *Katlein et al.*, 2014] suggest an export system that works differently than in most of the world's oceans.

4.5 Conclusions

We have used concurrently the ^{234}Th/^{238}U and ^{210}Po/^{210}Pb proxies to estimate POC fluxes in the central Arctic during the record sea-ice minimum in 2012. The main findings of the present work are:

1) Th-234 reveals that POC fluxes at the bottom of the euphotic zone were very low (2 ± 2 mmol C m^{-2} d^{-1}) in August/September, which is in good agreement with results obtained using sediment traps (3 ± 3 mmol C m^{-2} d^{-1}) deployed at the same locations [*Lalande et al.,* 2014]. The positive relationships found between prasinophytes_1 and ^{234}Th and ^{234}Th-derived POC fluxes suggest that picophytoplankton contributed significantly to downward fluxes in late summer.

2) In contrast to ^{234}Th, the upper water column was depleted in ^{210}Po over the entire study area, indicating that particle export fluxes were higher before July/August than in the weeks prior to and during the survey.

3) The positive relationships obtained between sea-ice concentration and ^{210}Po and ^{210}Po-derived POC fluxes show that particle sinking was greater under heavy sea-ice conditions than under partially ice-covered areas. Further, the strongest ^{210}Po deficits in the water column coincided with the highest seafloor coverage of algae reported by *Boetius et al.* [2013], suggesting that ^{210}Po tracked, to some extent, the massive algal export that occurred earlier in the season.

4) Although the POC fluxes were low, a great fraction of primary production (>30%) was exported at the base of the euphotic zone in most of the study area, according to ^{210}Po-derived POC fluxes and annual NPP estimates. Seasonal estimates of primary production and export would be very helpful in characterizing the role of the Arctic biological pump in the context of climate change.

We encourage future studies applying radionuclide proxies to consider NSS conditions and follow the trend of C/Th and C/Po ratios with time to better constrain the POC fluxes in the Arctic. Further, the simultaneous use of sediment traps would allow the determination of the particle flux composition, which has been pointed out as a crucial factor shaping the biological pump efficiency [e.g. *Mackinson et al.*, 2015; *Puigcorbé et al.*, 2015; *Roca-Martí et al.*, 2016].

Chapter 5

Distribution of ^{210}Pb and ^{210}Po in the Arctic water column during the 2007 sea-ice minimum: particle export in the ice-covered basins

Roca-Martí, M., Puigcorbé, V., Friedrich, J., Rutgers van der Loeff, M., Rabe, B., Korhonen, M., Cámara-Mor, P., Garcia-Orellana, J., Masqué, P. Distribution of ^{210}Po and ^{210}Pb in the Arctic water column during the 2007 sea-ice minimum: particle export in the ice-covered basins.
Submitted to *Deep Sea Research Part I: Oceanographic Research Papers.*

5.1 Aim

Further in situ research is needed to understand the impacts of climate change on biogeochemical cycles in the Arctic Ocean, including the transport of particles to depth and its implications for carbon export. Here, we analyse the distribution of ^{210}Pb and ^{210}Po in the water column of the Barents, Kara and Laptev Seas and the Nansen, Amundsen and Makarov Basins during the 2007 sea-ice minimum. The naturally occurring pair ^{210}Po/^{210}Pb is commonly used as a proxy for particle (and carbon) export, but their application in the Arctic is limited [*Moore and Smith*, 1986; *Smith and Ellis*, 1995; *Smith et al.*, 2003; *Roca-Martí et al.*, 2016]. The objective is to investigate the processes governing the dynamics of particles and the particle export in the Arctic Ocean based on the largest dataset of ^{210}Pb and ^{210}Po in this ocean to date. Pb-210 and ^{210}Po data are discussed together with information on physical and biological characteristics of the study area, seasonal primary production and the export production derived from other tracers (^{234}Th).

5.2 Methods

5.2.1 Study area

Seawater samples were collected during the ARK-XXII/2 expedition (R/V Polarstern) that took place from 28 July to 7 October in 2007 along the shelves of the Barents, Kara and Laptev Seas and the Nansen, Amundsen and Makarov Basins [*Schauer*, 2008]. Stations have been classified into three categories according to the water depth (Table 5.1): shelf (<350 m), slope (350-1050 m) and basin (>1050 m), similarly to *Cai et al.* [2010]. The study area has been divided into five sections (S1-S5, see Figure 5.1): S1 and S2 extend from the Barents Sea to the interior Nansen Basin, S3 from the Kara shelf edge to the Amundsen Basin, S4 from the Lomonosov Ridge to the Alpha and Mendeleev Ridges, and S5 from the Laptev Sea towards the central Arctic over the Gakkel Ridge.

5.2.2 ^{210}Pb and ^{210}Po

Pb-210 and ^{210}Po activities were measured in the dissolved (<1 µm) and particulate fractions in the upper ~500 m of the water column, while only total activities were determined for deeper samples. Surface seawater was sampled at 50 stations using the ship seawater intake (10 m). Vertical profiles were collected at 17 stations using Niskin bottles attached to a conductivity-temperature-depth (CTD) rosette sampler. The sample volumes were about 20 L (dissolved and total) and 40 to 160 L (particulate). The procedure for the determination of ^{210}Pb and ^{210}Po activities in the total/dissolved and particulate fractions is described in Chapter 2 (see Section 2.1.2 and 2.2, respectively). The complete ^{210}Pb and ^{210}Po dataset is available at PANGAEA [*Friedrich*, 2011].

Table 5.1: Location, date and water depth of the stations sampled for ^{210}Pb and ^{210}Po analyses during the ARK-XXII/2 expedition. Stations have been classified into sections (S1-S5) and areas (shelf/slope/basin, see text for further details).

Section	Station	Longitude (°E)	Latitude (°N)	Date (2007)	Water depth (m)	Area
S1	236	33.98	77.50	31 Jul.	196	Shelf
	237	33.97	79.00	31 Jul.	272	Shelf
	239	34.00	80.99	1 Aug.	224	Shelf
	249	33.98	82.00	2 Aug.	2281	Basin
	255	33.89	82.52	4 Aug.	3135	Basin
	257	34.05	83.50	5 Aug.	3958	Basin
	258	34.00	84.00	6 Aug.	4055	Basin
	260	36.08	84.51	8 Aug.	4054	Basin
S2	261	60.92	84.64	11 Aug.	3846	Basin
	263	60.96	84.17	11 Aug.	3713	Basin
	264	60.43	83.65	12 Aug.	3512	Basin
	266	61.81	83.12	14 Aug.	3011	Basin
	268	60.81	82.81	14 Aug.	1609	Basin
	271	60.80	82.50	15 Aug.	327	Shelf
	272	61.99	82.25	15 Aug.	231	Shelf
	274	67.10	82.52	16 Aug.	1176	Basin
	276	68.95	82.09	17 Aug.	680	Slope
S3	279	86.23	81.24	19 Aug.	336	Shelf
	285	86.34	82.14	20 Aug.	724	Slope
	290	86.44	82.58	21 Aug.	2071	Basin
	295	86.30	83.27	22 Aug.	3357	Basin
	299	89.06	84.05	23 Aug.	3694	Basin
	301	89.76	84.56	24 Aug.	3758	Basin
	303	90.23	85.25	25 Aug.	3985	Basin
	306	91.18	85.92	26 Aug.	4019	Basin
	309	104.98	87.04	28 Aug.	4449	Basin
	312	120.15	88.12	29 Aug.	3009	Basin
S4	320	150.33	88.41	31 Aug.	1952	Basin
	328	-170.33	87.82	2 Sept.	3992	Basin
	333	-146.39	87.03	4 Sept.	3285	Basin
	338	-134.96	85.69	6 Sept.	1570	Basin
	342	-138.30	84.50	7 Sept.	2289	Basin
	349	-164.55	85.07	9 Sept.	1996	Basin
	352	177.54	86.64	10 Sept.	4005	Basin
	358	151.96	86.51	11 Sept.	1459	Basin
	363	134.92	86.47	13 Sept.	3991	Basin
S5	371	102.73	84.66	16 Sept.	4271	Basin
	377	115.55	83.41	18 Sept.	4301	Basin
	379	117.85	82.86	18 Sept.	4413	Basin
	382	120.72	81.36	19 Sept.	5343	Basin
	383	122.21	80.66	19 Sept.	3902	Basin
	384	123.46	80.00	20 Sept.	3653	Basin
	385	124.36	79.35	20 Sept.	3525	Basin
	387	124.61	78.64	21 Sept.	2865	Basin
	391	124.24	78.13	21 Sept.	2435	Basin
	400	123.42	77.37	22 Sept.	1049	Slope
	404	122.87	76.90	23 Sept.	94	Shelf
	407	122.13	76.18	23 Sept.	75	Shelf
	409	121.77	75.71	23 Sept.	65	Shelf
	411	121.36	75.20	24 Sept.	48	Shelf

5.2.3 CTD observations and nutrients

Profiles of temperature and salinity in the water column were obtained using a CTD system with a Carousel Water Sampler (Sea-Bird Electronics Inc., USA). Salinity was calibrated using discrete samples from the rosette, and processed with an on-board salinometer. Discrete nutrient water samples from the rosette were processed using a Technicon TRAACS 800 continuous flow auto-analyser and standards previously prepared on land. Details of the measurements and processing are described in *Schauer* [2008]. The data are published in *Laan et al.* [2008], *Wisotzki and Bakker* [2008] and *Schauer and Wisotzki* [2010].

5.2.4 Annual new primary production

Net primary production (NPP) during the productive season after the Arctic winter (from April to sampling time) was calculated by using the winter mixed layer depth (WMLD) and the seasonal nutrient uptake following *Rudels et al.* [1996] and *Korhonen et al.* [2013]. The method uses data interpolation by *Reiniger and Ross* [1968] and is described in detail in *Boetius et al.* [2013] and *Fernández-Méndez et al.* [2015]. Briefly, the nutrient uptake since the previous winter was estimated by the difference between the nutrient concentration profiles in late summer (August-September) and the nutrient concentrations at the WMLD. The annual total inorganic nitrogen (nitrite + nitrate), phosphate and silicate uptake was then converted to carbon units using the Redfield-Brzezinski ratio 106C:16N:15Si:1P [*Redfield et al.*, 1963; *Brzezinski*, 1985]. The elemental stoichiometry 106C:16N was confirmed for the central Arctic by analysis of suspended particulate organic matter collected during several research programmes (n = 255) [*Frigstad et al.*, 2014]. Since this method assumes that lateral input of nutrients from rivers and shelves is negligible, we have estimated annual new NPP only at those stations located in the basins.

5.3 Results and discussion

First, physical and biological characteristics of the study area, including hydrography, sea-ice conditions, nutrient regime and annual new NPP estimates, are described (see Section 5.3.1). Second, the activities of both radionuclides and the ^{210}Po/^{210}Pb ratios in surface waters and vertical profiles are discussed in relation to the water masses, Chl-a concentration and light transmission, and compared to literature data (see Section 5.3.2). Last, the total ^{210}Po deficits are discussed in parallel with the annual new NPP estimates and the origin of freshwater in the upper water column [*Bauch et al.*, 2011], and compared to ^{234}Th-derived export estimates [*Cai et al.*, 2010] (see Section 5.3.3).

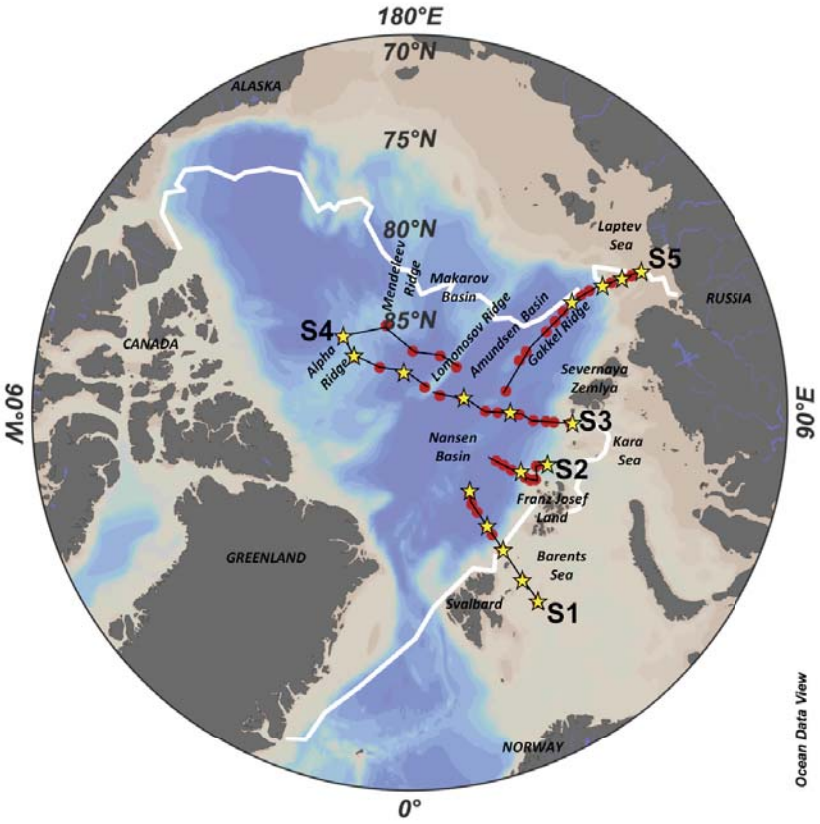

Figure 5.1: Location of the stations sampled for surface waters (red dots) and vertical profiles (yellow stars) during the ARK-XXII/2 cruise (July-October 2007). The study area is divided into five sections: S1, stations 236-260; S2, stations 261-276; S3, stations 279-312; S4, stations 320-363; S5, stations 371-411. The contour white line represents the minimum sea-ice extent in September 2007 [*http://www.meereisportal.de/*].

5.3.1 Study area

5.3.1.1 Hydrography and sea-ice conditions

The temperature and salinity profiles reflected the highly stratified central Arctic environment (Figure 5.2A and Figure 5.2B). The water masses can be identified after *Rudels* [2009] and *Korhonen et al.* [2013]. The core of the Atlantic Water (AW) was observed at salinities above ~34.5 and temperatures above 0°C (Figure 5.2C and Figure 5.2D). The deeper waters were found at lower temperatures, whereas the lower ("cold") halocline (LHC) was located around a change in the vertical temperature gradient, between near-freezing temperatures and 0°C, with salinities just above 34.0. At lower salinities, the upper halocline (UHC) was most distinct in the Makarov Basin (stations 320-358), where Pacific Water (PW) was present (Figure 5.2D). In this region, the polar mixed layer (PML), which lies between the depth of winter mixing ("temperature minimum") and the surface, could not reach into the LHC (salinities >34.0). Low near-surface salinity, the presence of PW, and resulting stratification limited the depth of the PML here. In most of the Nansen Basin, the PML reached salinities higher than 34.0, as much of the LHC is formed in this basin.

Temperatures above 0°C and salinities lower than 34.0 in central Arctic waters around the basins boundaries represent the influence of waters originating on the shelves ("shelf waters", Figure 5.2C and Figure 5.2D).

The mixed layer depth (MLD) was defined by the depth where density increased from its surface value to 20% of the difference between 100 m and the surface [*Shaw et al.*, 2009]. For the seawater profiles included in this study, the mixed layer was on average 18 ± 4 m thick, varying from 12 to 26 m (n = 17). The WMLD was found at 60 ± 20 m (n = 12), the UHC between 60 ± 5 m and 120 ± 30 m (n = 4), and the LHC between 80 ± 40 m and 130 ± 60 m (n = 12).

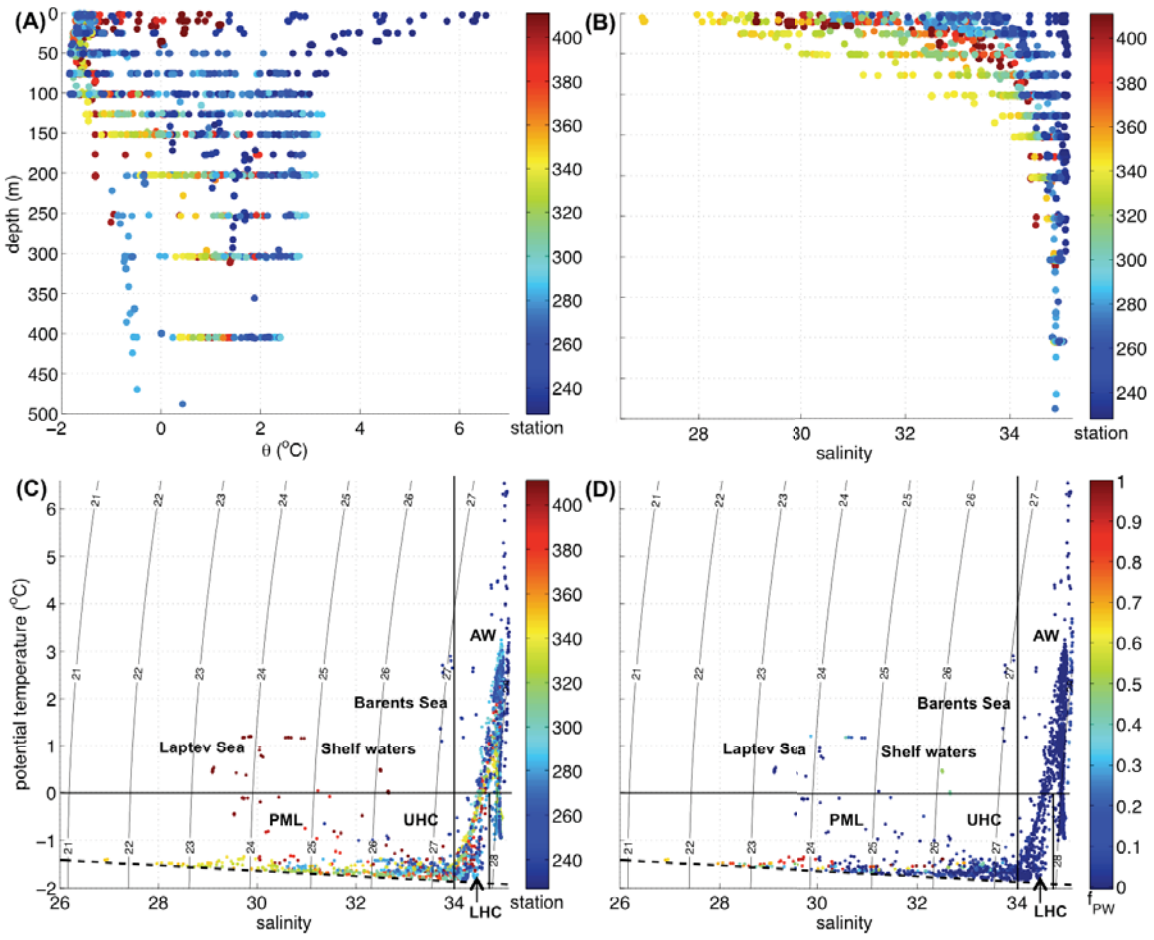

Figure 5.2: Potential temperature (A) and salinity (B) profiles in the upper 500 m, and T-S diagrams (C, D) from the ARK-XXII/2 cruise. The colour bars indicate the number of station (A, B, C) and the fraction of Pacific Water (PW, D). Water masses are shown in the T-S diagrams: polar mixed layer (PML), upper halocline (UHC), lower halocline (LHC), and Atlantic Water (AW).

The sea-ice conditions encountered during the expedition are described in *Schauer et al.* [2008] and *Cámara-Mor et al.* [2011] based on routine visual observations recorded from the R/V Polarstern's bridge and satellite images, respectively. Ice-covered waters were first found northeast of Svalbard.

The average sea-ice concentration along the cruise track was between 70 and 80%, with low concentrations along the St. Anna and the Voronin Troughs (north of the Kara Sea) and the section from the central Arctic to the Laptev Sea (S5) sampled in September. In section S5, sea-ice concentration was around 30% and open water was commonly found towards the south. About 20 to 40% of the ice was covered with melt ponds [*Kramer and Kiko*, 2011], and the ice consisted primarily of first-year ice with a mean thickness of 1.3 m [*Haas et al.*, 2008].

Table 5.2: Nitrite + nitrate, phosphate and silicate drawdown above the winter mixed layer depth (WMLD) and annual new primary production estimated using the Redfield-Brzezinski ratio (106C:16N:15Si:1P).

		Nutrient deficits (mmol m^{-2})			Annual new NPP (g C m^{-2} yr^{-1})		
Station	WMLD (m)	Nitrite+nitrate	Phosphate	Silicate	Nitrite+nitrate	Phosphate	Silicate
255	38	86	5	52	6.8	6.4	4.4
260[a]	81	88	5	17	7.0	6.2	1.5
266	22	26	2	11	2.0	2.0	0.9
301	60	120	7	15	9.8	9.3	1.3
309	59	130	8	59	10	11	5.0
328	54	190	16	210	15	21	18
338	60	210	13	310	17	17	27
342	67	350	30	590	28	38	50
385[a]	50	88	6	10	7.0	7.6	0.9

[a] Different casts were taken for nutrient deficits and WMLD determination.

5.3.1.2 Nutrients and annual new primary production

In general, the concentration of nutrients in the mixed layer was low, suggesting phytoplankton consumption earlier in the season. Here, nutrient depletion is defined as concentrations of nitrate <1 µmol L^{-1}, phosphate <0.2 µmol L^{-1}, and silicate <1.5 µmol L^{-1} [*Fernández-Méndez et al.*, 2015]. The study area was depleted in nitrate with the exception of the Nansen Basin and the Kara shelf edge. The shelves from the Barents, Kara and Laptev Seas were silicate and phosphate-depleted, while the stations located over the Gakkel Ridge were depleted in phosphate.

The annual new NPP estimates in the Nansen, Amundsen and Makarov Basins are presented in Table 5.2. The nitrogen consumed above the WMLD during the productive season was on average 90 ± 40 mmol m^{-2} in the Eurasian sector (n = 6), whereas it was 250 ± 90 mmol m^{-2} in the Canadian sector (n = 3). Annual nitrogen-derived NPP estimates were similar across the Nansen and Amundsen Basins with an average of 7 ± 3 g C m^{-2} yr^{-1}, although it was about four times lower north of Franz Josef Land (station 266). In the Makarov Basin, annual new NPP was always higher than in the Eurasian Basin, averaging 20 ± 7 g C m^{-2} yr^{-1}. Phosphate-derived estimates were similar to those derived from nitrogen at most of the stations (<6% difference), although differences between estimates of 11 to 37% were obtained at stations 260, 328 and 342. Considering all the nitrogen- and phosphate-derived estimates, the annual new NPP was on average 12 g C m^{-2} yr^{-1},

which is similar to other reported estimates of about 9 g C m^{-2} yr^{-1} including values from the Nansen, Amundsen, Makarov and Canada Basins during years 2011 and 2012 [*Ulfsbo et al.*, 2014; *Fernández-Méndez et al.*, 2015]. *Ulfsbo et al.* [2014] also found higher estimates in the Makarov Basin, particularly over the Mendeleev Ridge, when compared to the other basins. Silicate-derived NPP estimates were on average 2.3 ± 1.9 g C m^{-2} yr^{-1} in the Eurasian sector, whereas they averaged 32 ± 17 g C m^{-2} yr^{-1} in the Makarov Basin. Comparison between silicate-derived NPP with the other two estimates gives an indication of the contribution of diatoms to new production. Diatom production varied widely across the study area amounting to 10 to 70% of annual new NPP in the Eurasian sector and about 100% in the Makarov Basin. This suggests that diatom production had a pivotal role in the Canadian sector of the study area during the productive season in 2007.

5.3.2 ^{210}Pb and ^{210}Po

The activities of ^{210}Pb and ^{210}Po and the ^{210}Po/^{210}Pb ratios in the Arctic water column in summer 2007 are presented in Table A1 (Appendix).

5.3.2.1 Surface waters

The MLD was mostly confined to the upper 20 m of the water column (see Section 5.3.1.1) including 10 m depth, which is taken as representative of the surface waters.

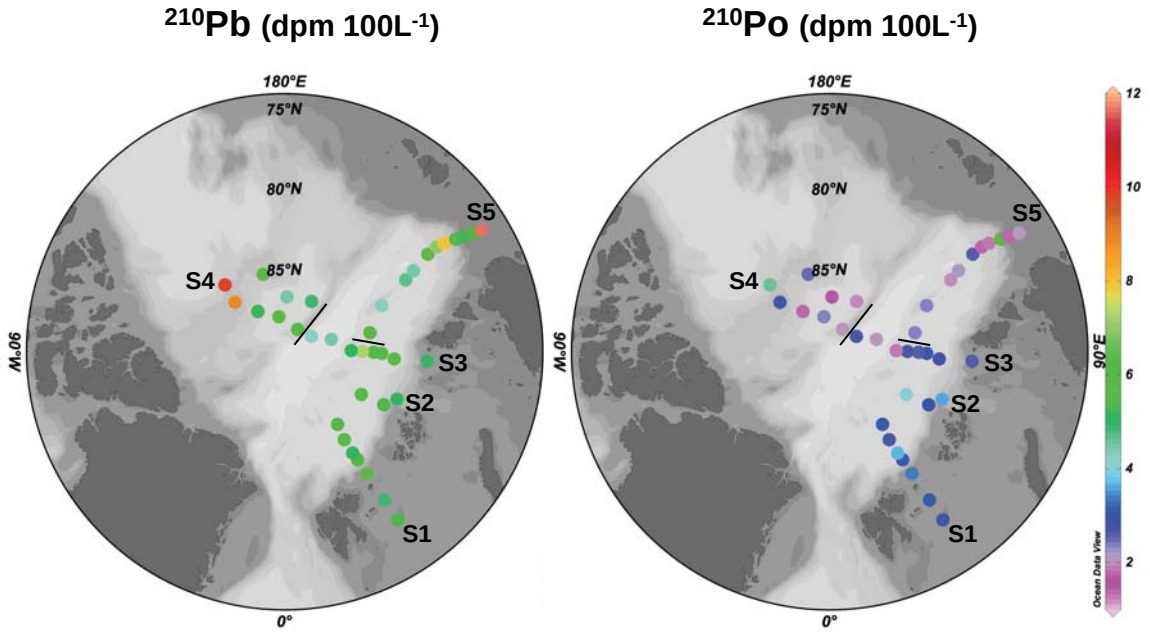

Figure 5.3: Total ^{210}Pb and ^{210}Po activities in surface waters (10 m) along five sections (S1, stations 236-260; S2, stations 261-276; S3, stations 279-312; S4, stations 320-363; S5, stations 371-411).

Total activities of ^{210}Pb and ^{210}Po in surface waters were on average 5.8 ± 1.5 dpm 100L^{-1} (n = 37) and 2.6 ± 0.9 dpm 100L^{-1} (n = 36), respectively. Two-fold higher activities of ^{210}Pb and ^{210}Po (10.1 ± 1.4 and 5.3 ± 1.0 dpm 100L^{-1}, respectively) were found on the shelf/slope of the Laptev Sea and at the Alpha Ridge (Figure 5.3). The dissolved and total activities of both radionuclides presented similar patterns since the dissolved fractions accounted, on average, for >80% of the total activities. Particulate activities were on average 0.9 ± 0.8 dpm 100L^{-1} for ^{210}Pb (n = 37) and 0.4 ± 0.3 dpm 100L^{-1} for ^{210}Po (n = 36) and contributed >25% to total activities at several shelf and basin locations, mainly from the Laptev section (S5, Figure 5.4). This high contribution of particulate ^{210}Pb and ^{210}Po coincided, in part, with the highest Chl-a concentrations measured in surface waters during the cruise (0.5-1.1 mg m^{-3} at stations 239, 266, 279 and 407) [*Cai et al.*, 2010], and, generally, with low light transmission values (indicative of particle concentration) observed with the transmissometer installed on the CTD [*Schauer and Wisotzki*, 2010]. Indeed, light transmission was negatively correlated with the fraction of particulate ^{210}Pb ($p < 0.001$; Spearman correlation coefficient, $\rho = -0.59$, n = 29) and ^{210}Po ($p = 0.01$; $\rho = -0.48$, n = 28) at 10 m depth (not shown).

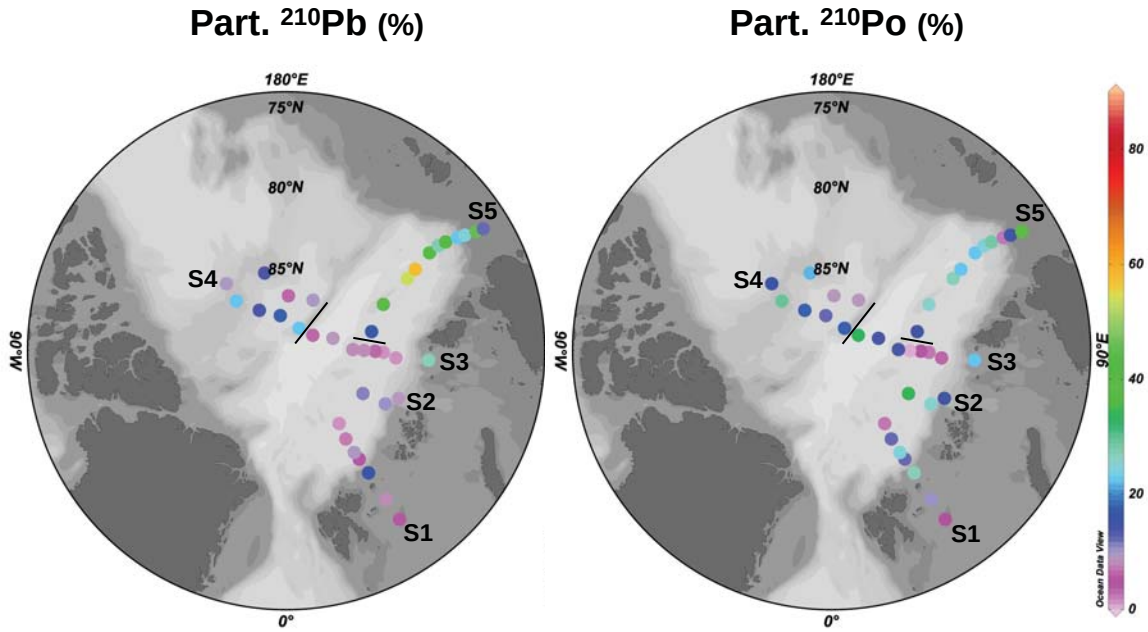

Figure 5.4: Relative contribution of particulate ^{210}Pb and ^{210}Po to total activities in surface waters (10 m) along five sections (S1, stations 236-260; S2, stations 261-276; S3, stations 279-312; S4, stations 320-363; S5, stations 371-411).

Total ^{210}Po/^{210}Pb ratios in surface waters were lower than 0.90 throughout the entire study area, except at one specific location (station 400), indicating a clear deficiency of ^{210}Po in Arctic surface waters (0.46 ± 0.19, n = 36; Figure 5.5). Substantial deficits of ^{210}Po were observed in the Canadian sector, with total ^{210}Po/^{210}Pb ratios ranging from 0.30 to 0.46. Total ^{210}Po/^{210}Pb ratios below 0.50 were also commonly found in the Nansen Basin and over the Gakkel Ridge. Indeed, the most substantial ^{210}Po deficiency was observed at stations 387 and 391 (0.25 ± 0.04 and 0.23 ± 0.04, respectively). Particulate ^{210}Po/^{210}Pb ratios ranged from 0.18 to 3.7, being higher than one in one-third of the stations, mainly from the Nansen Basin (Figure 5.5).

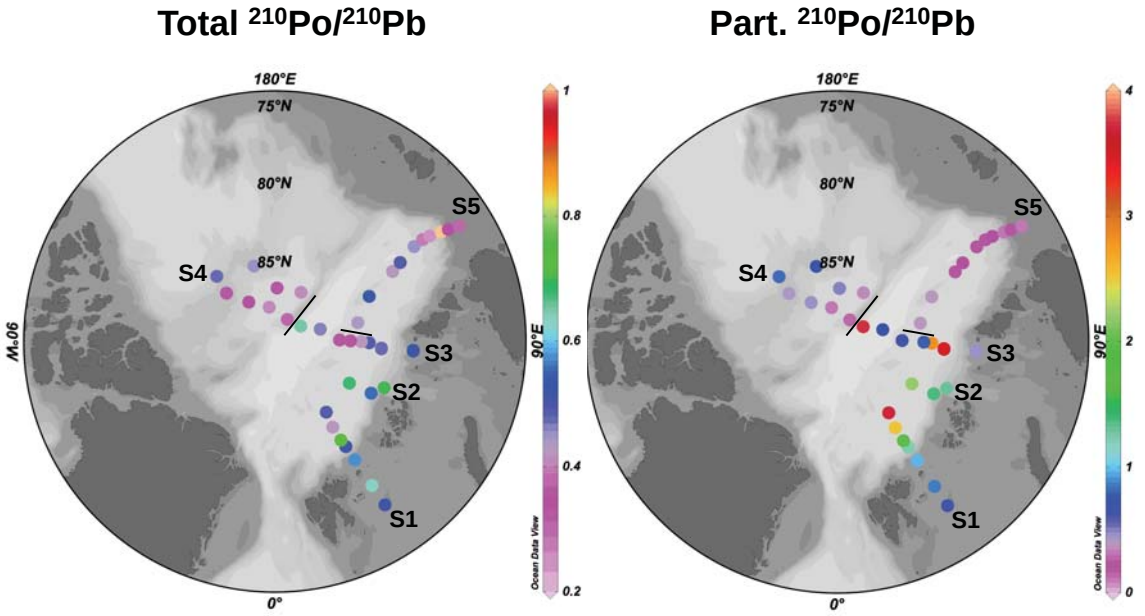

Figure 5.5: Total and particulate ^{210}Po/^{210}Pb ratios in surface waters (10 m) along five sections (S1, stations 236-260; S2, stations 261-276; S3, stations 279-312; S4, stations 320-363; S5, stations 371-411). Notice the different colour scales.

5.3.2.2 Vertical profiles

Vertical profiles were taken down to 25 to 320 m (shelf), 650 to 1015 m (slope), and 1000 to 4365 m (basin). Total activities of ^{210}Pb and ^{210}Po and the relative contribution of particulate to total activities for the upper 500 m of the water column are illustrated in Figure 5.6. Box plots of the total ^{210}Pb and ^{210}Po activities in the mixed layer, upper and lower haloclines and intermediate and deep waters are shown in Figure 5.7.

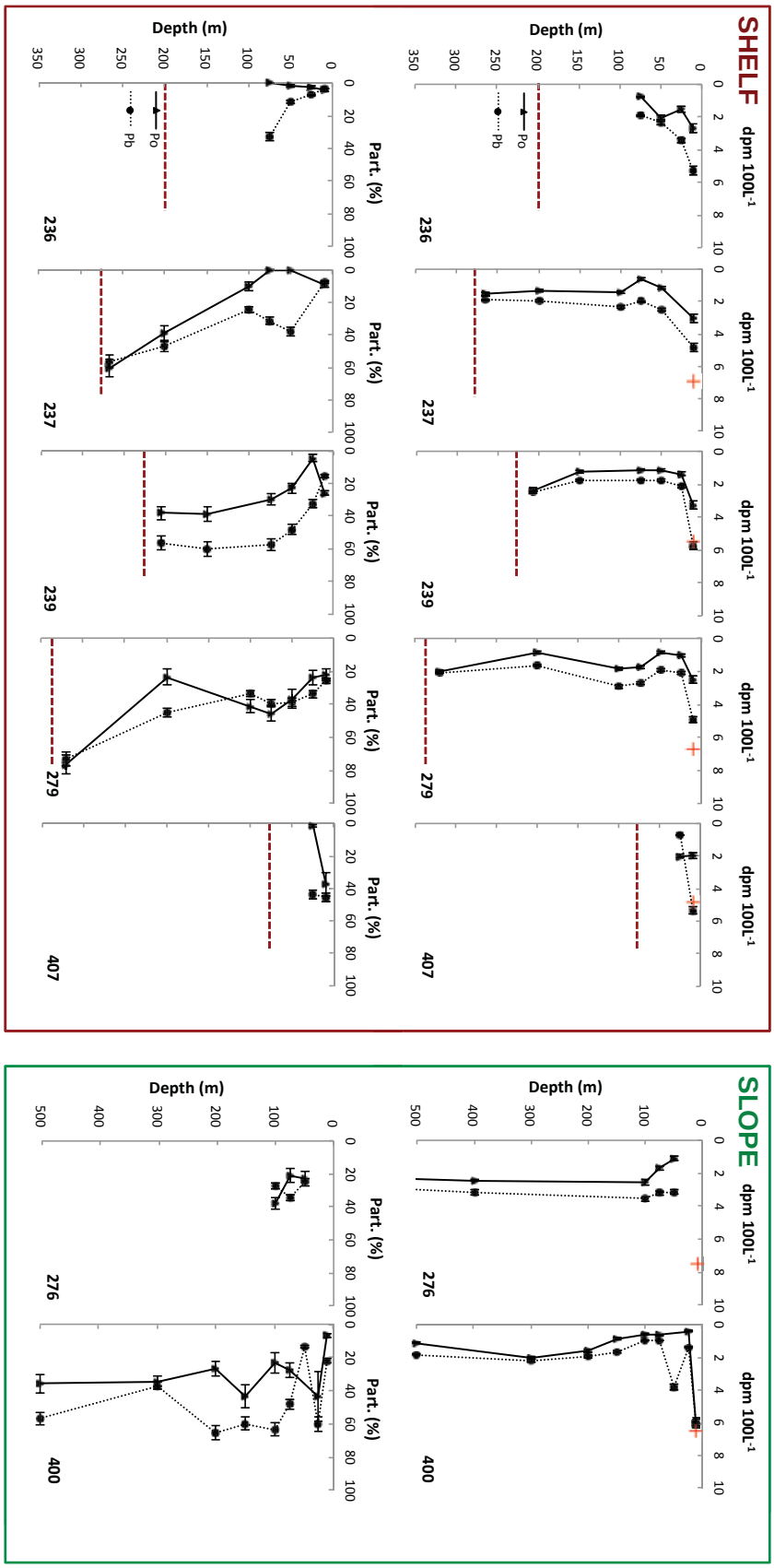
SHELF
SLOPE
dpm 100L-1
Depth (m)
Part. (%)
Po
Pb
236
237
239
279
407
276
400

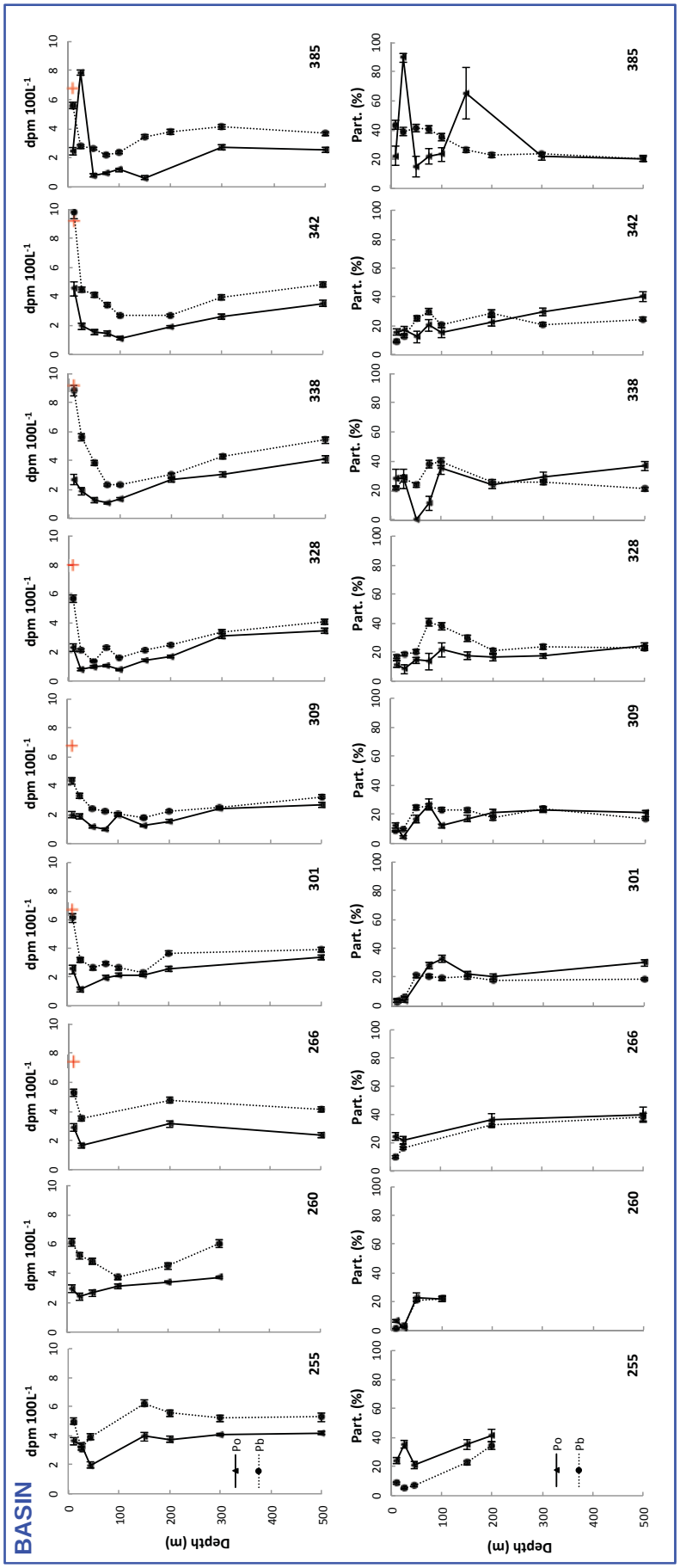

Figure 5.6: Vertical activity profiles for total ^{210}Po (solid line) and ^{210}Pb (dotted line) and relative contribution of the particulate activities of both radionuclides for the upper 500 m of the water column (ARK-XXII/2 cruise) in the shelf (<350 m), slope (350-1050 m) and basin (>1050 m) environments. The red cross indicates the total activity of ^{226}Ra in surface waters [*Rutgers van der Loeff et al.*, 2012]. Notice the different scale on the y-axis between the shelf and the slope/basin profiles. The horizontal dashed line in the shelf panel indicates the bottom depth.

In the mixed layer, total ^{210}Pb and ^{210}Po activities were on average 5.8 ± 1.5 and 2.9 ± 1.1 dpm 100L^{-1} (n = 17), respectively. These activities decreased steeply by a factor of 2 at the first depth sampled below the MLD, except at some stations for ^{210}Po (255, 385 and 407, Figure 5.6). Considering the entire water column, the average ^{210}Pb and ^{210}Po activities found below the MLD (3.5 ± 1.7 dpm 100L^{-1} for ^{210}Pb, n = 123; and 2.6 ± 1.7 dpm 100L^{-1} for ^{210}Po, n = 120), show that the mixed layer was enriched in ^{210}Pb with respect to underlying waters. The ocean mixed layer usually presents higher activities of ^{210}Pb with respect to its parent, ^{226}Ra, due to the atmospheric deposition of ^{210}Pb produced from the decay of ^{222}Rn, representing the major input of ^{210}Pb into the ocean surface [*Nozaki et al.*, 1980; *Rutgers van der Loeff and Geibert*, 2008]. In the Arctic, a fraction of the atmospheric fluxes are intercepted by the sea-ice cover, accumulated during its transit through the ocean and released when and where melting occurs [*Roberts et al.*, 1997; *Masqué et al.*, 2007; *Cámara-Mor et al.*, 2011; *Chen et al.*, 2012]. Considering the surface ^{226}Ra measured during the same expedition (range: 3.3 to 9.5 dpm 100L^{-1}) [*Rutgers van der Loeff et al.*, 2012], we found ^{210}Pb/^{226}Ra ratios >1.0 at several stations (Table A1, Appendix, and Figure 5.6). These stations were located near the ice edge (239, 407 and 409), and under the sea-ice cover in the Nansen Basin (303) and at the Alpha Ridge (342). Significant amounts of melt water (2-8%) [*Bauch et al.*, 2011] were found in the surface waters of these stations. Indeed, there was a positive relationship between the fraction of sea-ice melt water [*Bauch et al.*, 2011] and ^{210}Pb/^{226}Ra ratios considering all the stations with data available ($p < 0.01$; ρ = 0.63-0.67 for the two approaches used by *Bauch et al.* [2011], n = 20-22; not shown). This shows a significant role of sea-ice melting in enhancing ^{210}Pb activities in surface waters through the release of accumulated ^{210}Pb in sea ice and/or the direct input of atmospheric ^{210}Pb. We cannot quantify the effect of sea-ice melting in driving the enrichment of ^{210}Pb in surface waters without considering the concentration of ^{210}Pb in sea ice and its removal by scavenging once released into the ocean. In the case of ^{210}Po, its atmospheric flux to the ocean surface usually accounts for only about 10-20% of that of ^{210}Pb [*Lambert et al.*, 1982]. However, in the Arctic, any inputs of ^{210}Po to the ocean surface due to sea-ice melting would lead to greater ^{210}Po/^{210}Pb ratios resulting from the ingrowth of ^{210}Po from ^{210}Pb decay in sea ice [*Masqué et al.*, 2007]. Then, a preferential removal of ^{210}Po over ^{210}Pb by particle export in surface waters [*Nozaki et al.*, 1997] may explain the similar ^{210}Po activities observed in the mixed layer and the underlying water column.

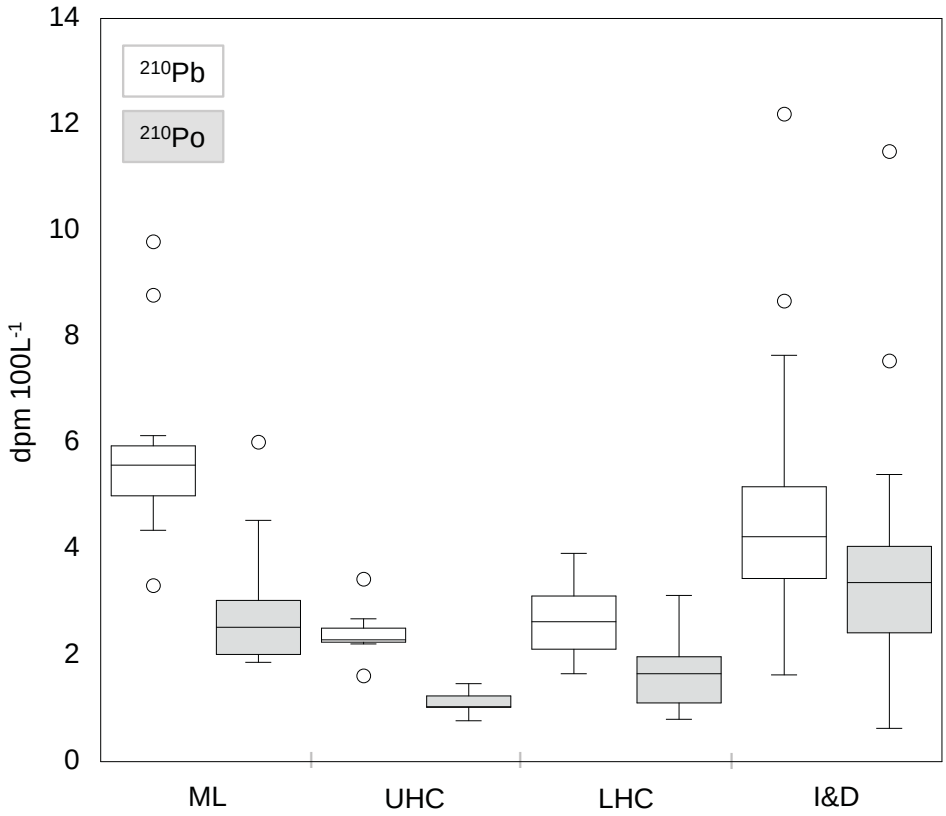

Figure 5.7: Box plots for total ^{210}Pb and ^{210}Po activities in the mixed layer (ML: surface to MLD), upper halocline (UHC), lower halocline (LHC) and intermediate and deep waters (I&D). The bottom and top of the boxes mark the 25th and 75th percentiles, respectively, and the middle line represents the median (50th percentile). The lines extending from the bottom and top of the boxes mark the minimum and maximum values. Outliers are displayed as empty circles. ML n = 17; UHC n = 7; LHC n = 17; I&D n = 64 (^{210}Po) or 65 (^{210}Pb).

In the upper halocline (stations 309, 328, 338, 342), total ^{210}Pb and ^{210}Po activities were on average 2.4 ± 0.6 and 1.1 ± 0.2 dpm 100L^{-1} (n = 7), respectively, similarly to the lower halocline, where the activities averaged 2.7 ± 0.7 and 1.6 ± 0.7 dpm 100L^{-1} (n = 17), respectively. These values are low in comparison with overlying and intermediate/deep waters (Figure 5.7). Low total activities of ^{210}Pb and ^{210}Po in the upper halocline were firstly reported for the CESAR site (85.83°N, 108.83°W) located over the Alpha Ridge [*Moore and Smith*, 1986], and later for the Makarov and Canada Basins for both ^{210}Pb and ^{210}Po [*Smith et al.*, 2003] or ^{210}Pb alone [*Lepore et al.*, 2009a; *Hu et al.*, 2014]. This observation was explained by particle scavenging of ^{210}Pb and ^{210}Po at the sediment-water interface over the Chukchi and Beaufort shelves, where the upper halocline is formed, and subsequent advective transport into the interior Arctic [e.g. *Rutgers van der Loeff et al.*, 2012]. The lower halocline, in contrast to the upper halocline, is a common feature in the Arctic Ocean, with origin in the Barents Sea or the Nansen Basin [*Rudels*, 2009]. *Smith et al.* [2003] reported lower ^{210}Pb activities in lower halocline waters formed in the Barents Sea compared to those formed by haline convection in the Nansen Basin. This difference was ascribed to enhanced

particle scavenging on the productive and particle-rich Barents Sea, with respect to the Nansen Basin, and removal during boundary current transport into the central Arctic. In summer 2007, ^{210}Pb activities in the lower halocline were higher in sections S1 and S2 (3.5 ± 0.3 dpm 100L^{-1}, n = 5) than in sections S3, S4 and S5 (2.3 ± 0.5 dpm 100L^{-1}, n = 12) by a factor of 1.5 (Wilcoxon test, p <0.01). Temperature and salinity profiles indicate a potential shelf influence in the lower halocline from station 300 onwards (sections S3-S5). Yet, this cannot be confirmed without data from previous years because the advective time scales of the lower halocline may be a few years from its interaction with the shelves until it reaches the central Arctic. In particular, high polynya activity took place in the Laptev Sea in April 2007 with a high influence of brine-enriched waters in the surface regime that was detected out of the shelf [*Bauch et al.*, 2010]. This could have weakened stratification and enhanced winter convection into the range of the lower halocline. Indeed, a winter mixed layer deeper than 100 m was found on the continental slope at station 400 and surroundings, suggesting an influence from the Laptev shelf. These observations suggest that the lower halocline in sections S3-S5 had been more affected by shelf processes than in sections S1-S2, where the halocline is generally not influenced by the Barents Sea. Thus, enhanced particle scavenging during formation and/or transport of the lower halocline to the Makarov and eastern Eurasian Basins would explain the lower activities of ^{210}Pb observed.

For comparison with literature, inventories of ^{210}Pb and ^{210}Po were calculated at 25 m, which covers the mixed layer (at least two depths considered), and at 200 m, which comprises surface and subsurface waters, including, if present, the upper and lower haloclines (at least five depths considered). Total inventories in the upper 25 m were on average 1300 ± 300 dpm m^{-2} for ^{210}Pb and 700 ± 200 dpm m^{-2} for ^{210}Po (n = 14), which are in very good agreement with those obtained in the Eurasian Basin in summer 2012 (1100 ± 200 and 710 ± 160 dpm m^{-2}, respectively, n = 7) [*Roca-Martí et al.*, 2016]. Total inventories in the upper 200 m were on average 5900 ± 1800 dpm m^{-2} for ^{210}Pb and 3400 ± 1200 dpm m^{-2} for ^{210}Po (n = 12), which are comparable to those previously reported at a similar depth resolution in the Eurasian and Canada Basins, and at the CESAR site (5200 ± 2000 and 4500 ± 2600 dpm m^{-2}, respectively, n = 9; Wilcoxon test, p >0.05) [*Moore and Smith*, 1986; *Smith et al.*, 2003; *Roca-Martí et al.*, 2016].

In intermediate and deep waters, total activities of ^{210}Pb and ^{210}Po recovered to 4.3 ± 1.7 dpm 100L^{-1} (n = 65) and 3.4 ± 1.6 dpm 100L^{-1} (n = 64), respectively, with values up to 12 dpm 100L^{-1} for both radionuclides at 3900 m at station 328. These activities, in the case of ^{210}Pb, were generally lower than those found in the mixed layer, but, in the case of ^{210}Po, they were generally higher than in overlying waters (Figure 5.7). Good agreement is found with the activities obtained at the CESAR site of 4.1 ± 0.5 dpm 100L^{-1} for ^{210}Pb and 3.6 ± 0.9 dpm 100L^{-1} for ^{210}Po (n = 3, depth range: 800-1200 m) [*Moore and Smith*, 1986]. The activities obtained in this study are

also comparable to those from the Eurasian Basin (3.0 ± 1.0 dpm 100L^{-1} for ^{210}Pb and 2.9 ± 0.9 dpm 100L^{-1} for ^{210}Po, n = 14, depth range: 300-400 m) [*Roca-Martí et al.*, 2016], but are twice as high as those from the Arctic Ocean Section [*Aagaard et al.*, 1996] that went from the Chukchi Sea to the Fram Strait (2.4 ± 0.8 dpm 100L^{-1} for ^{210}Pb and 1.5 ± 0.7 dpm 100L^{-1} for ^{210}Po, n = 17, depth range: 300-4200 m) [*Smith et al.*, 2003].

Particulate activities were, on average, 0.8 ± 0.3 dpm 100L^{-1} for ^{210}Pb and 0.4 ± 0.2 dpm 100L^{-1} for ^{210}Po (n = 26) in the upper and lower haloclines, similar to those in surface waters (see Section 5.3.2.1), and 1.0 ± 0.3 dpm 100L^{-1} for ^{210}Pb (n = 29) and 0.8 ± 0.4 dpm 100L^{-1} for ^{210}Po (n = 28) in intermediate and deep waters. Generally, the relative contribution of the particulate fraction to total activities was higher on the shelves and near the shelf break (less than 250 km away, stations 255, 266, 276, 385 and 400) than in the interior Arctic.

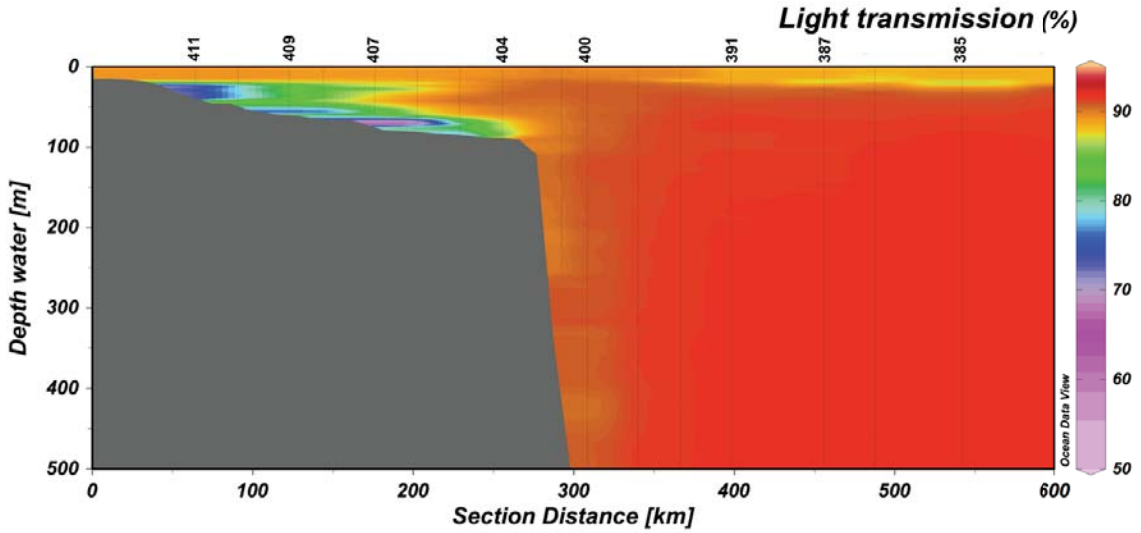

Figure 5.8: Light transmission in the upper 500 m of the water column of the Laptev section (S5) from station 385 to 411 [*Schauer and Wisotzki*, 2010].

Considering the entire water column, the particulate fraction of ^{210}Pb and ^{210}Po was especially high along section S5 (Figure 5.6), representing on average 35% of the total activities. This is consistent with pronounced low light transmission in the water column of the Laptev Sea, with the lowest values measured at the bottom, as well as in the upper ~30 m over the Gakkel Ridge (Figure 5.8). Moreover, the maximum Chl-a inventory was found on the Laptev shelf (60 mg m^{-2} at station 407, Figure 5.9). Sediment and nutrient discharge from the Lena River influences strongly the shallow Laptev Sea. As such, input of riverine sediments and in situ primary production would explain, in part, the scavenging of ^{210}Pb and ^{210}Po in this area. Further, resuspension of sediments most likely explain the very high fractions of particulate ^{210}Pb and ^{210}Po near the bottom of the Laptev shelf (up to 90%). The high fractions of particulate ^{210}Pb and ^{210}Po on the Laptev slope and at the Gakkel

Ridge suggest offshelf transport of particles. In particular, a very high activity of particulate ^{210}Po was found at 25 m at the Gakkel Ridge (station 385, 7.08 ± 0.15 dpm 100L^{-1}) that amounted to 90% of its total activity. Shelf particles are exported into the basins by two main pathways: (i) sea-ice transport of sediments entrained during freezing, especially in the Laptev Sea, one of the main producers of sea ice, where its formation occurs in close interaction with bottom sediments [*Eicken et al.*, 1997]; and (ii) resuspension of shelf bottom particles and lateral transport by thermohaline convection of dense water resulting from ice formation, eddies, storm events or other turbulent processes [e.g. *Forest et al.*, 2007; *O'Brien et al.*, 2013]. Indeed, high ^{228}Ra activities and a great fraction of river water in the upper waters of this section indicate the influence of shelf waters [*Roeske et al.*, 2012; *Rutgers van der Loeff et al.*, 2012].

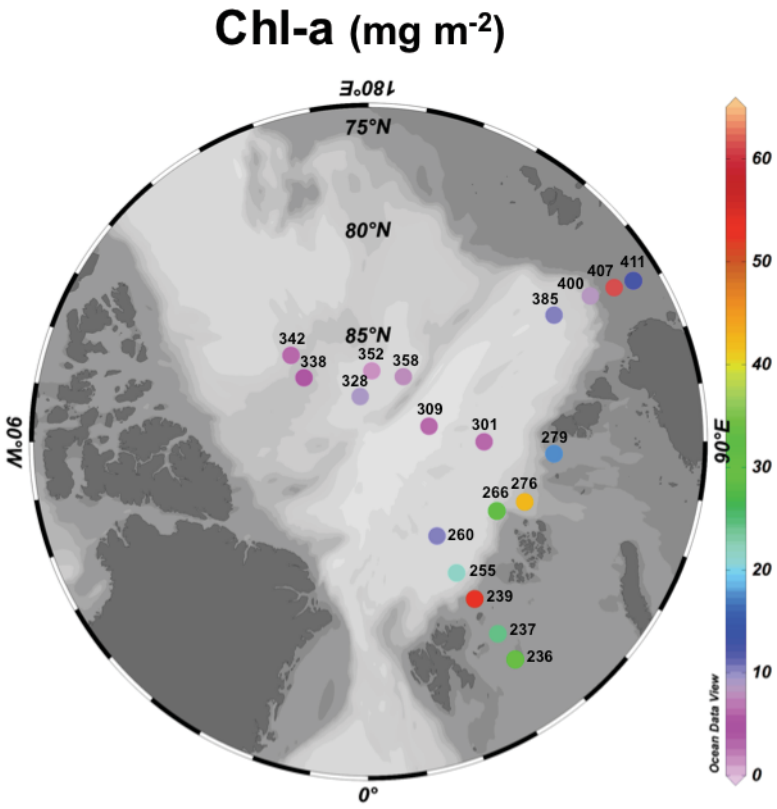

Figure 5.9: Chl-a inventory in the upper 75 to 100 m of the water column, except for stations 407 and 411 from the shallow Laptev shelf (upper 50 and 40 m, respectively) [*Cai et al.*, 2010].

In the water column of the Barents and Kara Seas, the particulate fraction of ^{210}Pb and ^{210}Po was also significant (>25%, stations 237, 239 and 279, Figure 5.6), coinciding with relatively high Chl-a inventories (50 mg m^{-2} at station 239, Figure 5.9). Particulate fractions of ^{210}Pb and ^{210}Po were greater near the bottom of the continental shelves (40-80%) compared to the overlying water column at stations 237 and 279 (Figure 5.6), in agreement with decreases in light transmission (not shown). As in the Laptev Sea, this likely results from scavenging by resuspended sediments.

In the Nansen, Amundsen and Makarov Basins, the particulate fraction of both radionuclides was on average ~20%, with values of ~25 to 30% at locations north of the Barents and Kara Seas (stations 255 and 266). At these stations light transmission in the upper 100 m was relatively low in comparison to further offshore stations, and the Chl-a inventory at station 266 was relatively high (30 mg m^{-2}, Figure 5.9). Therefore, offshelf transport of particles and biological production may explain these relatively high fractions of particulate ^{210}Pb and ^{210}Po.

Significant deficits of ^{210}Po (i.e. total ^{210}Po/^{210}Pb ratio <0.90, considering uncertainties) were observed throughout most of the water column in the study area. The most substantial deficits of ^{210}Po (total ^{210}Po/^{210}Pb ratios ≤0.50) were found in surface and subsurface waters spanning depths from 10 to 200 m, covering the mixed layer and the halocline. Total ^{210}Po/^{210}Pb ratios averaged 0.50 ± 0.23 in the mixed layer (n = 17), 0.46 ± 0.14 in the upper halocline (n = 7) and 0.60 ± 0.29 in the lower halocline (n = 17). We find good agreement between the mean total ^{210}Po/^{210}Pb ratio in the upper 25 m in summer 2007 (0.54 ± 0.21, n = 14) and that measured in the Eurasian Basin in summer 2012 (0.66 ± 0.19, n = 7) [*Roca-Martí et al.*, 2016]. Total ^{210}Po/^{210}Pb ratios of 0.50 to 0.60 correspond to a ^{210}Po residence time of 7 to 10 months based on a steady-state balance and the assumption of negligible atmospheric flux of ^{210}Po [*Nozaki et al.*, 1998]. The estimated residence time compares well with results obtained for the mixed layer in the Atlantic, Pacific and Indian Oceans [*Shannon et al.*, 1970; *Bacon et al.*, 1976; *Nozaki et al.*, 1976; *Cochran et al.*, 1983]. The mean total ^{210}Po/^{210}Pb ratio in the upper 200 m (0.58 ± 0.26, n = 12) was very similar to that found in the upper 25 m, and to that reported in the upper 200 m for the Canada Basin in summer 1994 (0.54 ± 0.13, n = 1) [*Smith et al.*, 2003]. However, it was lower than that found in summer 2012 (0.89 ± 0.58, n = 7) [*Roca-Martí et al.*, 2016] and at the CESAR site in spring 1983 (0.96 ± 0.04, n = 1) [*Moore and Smith*, 1986]. Po-210 deficits in the upper water column are usually attributed to biological particle production and subsequent scavenging and export, which will be discussed in Section 5.3.3.

Apart from the ^{210}Po deficits found in the upper ocean, they were also detected in the mesopelagic and bathypelagic zones. Total ^{210}Po/^{210}Pb ratios averaged 0.78 ± 0.49 in intermediate and deep waters (n = 64), where equilibrium between both radionuclides was only approached in one-third of the instances (ratio >0.90, Table A1, Appendix). A deficiency of ^{210}Po in the ocean interior has been observed before [e.g. *Bacon et al.*, 1976; *Kim*, 2001; *Chung and Wu*, 2005; *Church et al.*, 2012], but it remains unknown whether this feature is related to an artefact of sampling, a methodological bias or due to a missing sink of ^{210}Po in deep waters, such as accumulation in the food web [*Kim*, 2001; *Chung and Wu*, 2005; *Rutgers van der Loeff and Geibert*, 2008; *Church et al.*, 2012; *Hong et al.*, 2013]. Previously reported studies of ^{210}Pb and ^{210}Po in the Arctic used the cobalt APDC co-precipitation technique instead of using iron hydroxides as in the present study. Mean total ^{210}Po/^{210}Pb ratios

were near equilibrium in the Eurasian Basin (1.04 ± 0.48, n = 14, depth range: 300-400 m) [*Roca-Martí et al.*, 2016] and at the CESAR site (0.87 ± 0.24, n = 3, depth range: 800-1200 m) [*Moore and Smith*, 1986], but were significantly far from equilibrium during the Arctic Ocean Section (0.61 ± 0.35, n = 17, depth range: 300-4200 m) [*Smith et al.*, 2003]. While this study cannot elucidate the reasons for these deficits, the interpretation of the ^{210}Po/^{210}Pb pair at depth remains uncertain until further investigations are made.

Particulate ^{210}Po/^{210}Pb ratios averaged 0.50 ± 0.50 in the mixed layer (n = 17), 0.30 ± 0.18 in the upper halocline (n = 7), 0.52 ± 0.34 in the lower halocline (n = 19), and 0.79 ± 0.47 in intermediate waters down to 500 m (n = 28). These ratios fell below one in most cases, likewise for surface stations (see Section 5.3.2.1), except for one-tenth of the samples that showed ^{210}Po enrichment (i.e. particulate ^{210}Po/^{210}Pb ratio >1.10, up to 4-8 at 10-25 m). This fact seems to be inconsistent with the removal of ^{210}Po by particle export as shown by the widespread deficiency of ^{210}Po in the upper ocean (see Section 5.3.3). As such, we believe that the investigated particles were not representative of the export, either because the sampling device used, in this case Niskin bottles, did not effectively sample the sinking particles, or because the sinking particles in late summer were not responsible for the ^{210}Po deficiency. Significant contributions of different particle types could help explain the particulate ^{210}Po/^{210}Pb ratios <1 observed in the Arctic water column, including sea-ice drafted particles enriched in ^{210}Pb via atmospheric input (^{210}Po/^{210}Pb ratios <1 in sea-ice sediments) [*Roca-Martí et al.*, 2016], material remineralized by chemical and biological processes [*Stewart et al.*, 2007b], faecal pellets [*Stewart et al.*, 2005; *Rodriguez y Baena et al.*, 2007], picoplankton aggregates [*Stewart et al.*, 2010] and substrates rich in transparent exopolymer particles [*Quigley et al.*, 2002]. This could be investigated by particle composition analyses together with the concurrent application of the ^{210}Po/^{210}Pb pair and sediment traps, which, to our knowledge, has not been done in the Arctic.

5.3.3 Particle export in the Arctic as revealed by ^{210}Po deficits

In summer 2007, *Cai et al.* [2010] found ^{234}Th deficits in the upper 100 m over the Arctic shelves in association with enhanced Chl-a concentrations, indicating that in situ production and export of biogenic particles were the main mechanism for ^{234}Th removal. Nevertheless, we did not observe significant correlations between Chl-a concentrations and ^{210}Po deficits. This may not be surprising given that Chl-a concentration is a snapshot of the sampling time (i.e. late summer), whereas ^{210}Po integrates a time scale of several months (^{210}Po mean life = 200 days), covering, in this case, from the onset of the growing season (i.e. as early as March) [*Wassmann and Reigstad*, 2011]. Satellite images of the ice-free area in the Barents Sea revealed five-fold higher Chl-a concentrations in May/June, with respect to those in July/August in 2007, showing that the sampling was conducted

in a post-bloom situation [*Klunder et al.*, 2012]. Indeed, the concentrations of nutrients in the mixed layer were low during the expedition (see Section 5.3.1.2).

We note that ^{210}Po deficits were not restricted to the shelf environment, being also pronounced in the central Arctic (Figure 5.5 and Figure 5.6). The basins are characterized by low primary production due to stratified, oligotrophic and ice-covered conditions [*Hill et al.*, 2013], and low export, as reported by *Cai et al.* [2010] using ^{234}Th. This apparent discrepancy between ^{234}Th and ^{210}Po may be explained by significant export fluxes that occurred more than one month before sampling. This would be recorded by ^{210}Po but missed by ^{234}Th. Indeed, *Rutgers van der Loeff et al.* [2012] argued that the ^{234}Th-based scavenging rate could not explain the distribution of ^{228}Th in the central Arctic in summer 2007 due to seasonal variations in scavenging and the different half-lives of ^{234}Th and ^{228}Th. We can explore this hypothesis by comparing the deficits of ^{210}Po with the estimates of annual new NPP.

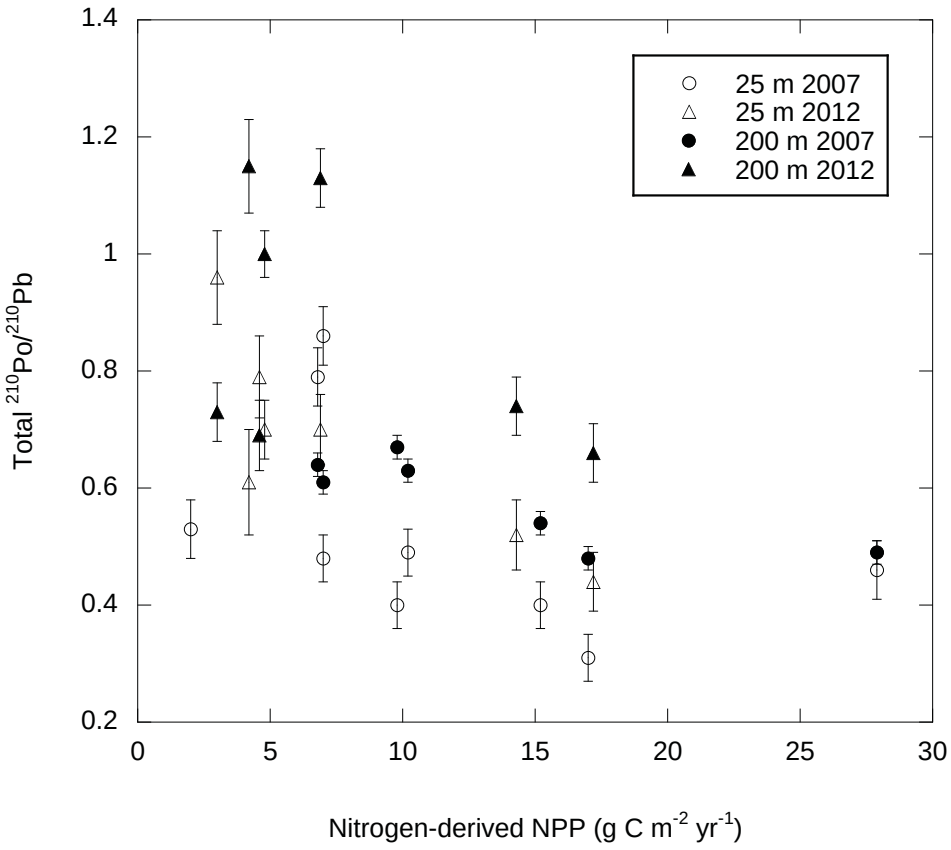

Figure 5.10: Total ^{210}Po/^{210}Pb ratios in the upper 25 m (white) and 200 m (black) vs. nitrogen-derived new primary production in summer 2007 (circles, this study) and 2012 (triangles, *Roca-Martí et al.* [2016]).

Although the number of data points is small, we find a negative relationship between the new NPP estimates based on nitrogen consumption and total ^{210}Po/^{210}Pb ratios in the upper 25 and 200 m of the basin stations ($p < 0.05$; 25 m: $\rho = -0.72$, $n = 9$; 200 m: $\rho = -0.79$, $n = 7$; Figure 5.10).

This suggests that greater deficits of ^{210}Po in the upper Arctic were related to higher in situ new production and subsequent export of biogenic material to depth. This would be analogous to the situation reported for the central Arctic in summer 2012 [*Roca-Martí et al.*, 2016]. Indeed, if we combine the results from both studies, the significance of the observed relationship increases ($p < 0.01$; 25 m: $\rho = -0.73$, $n = 16$; 200 m: $\rho = -0.68$, $n = 14$; Figure 5.10).

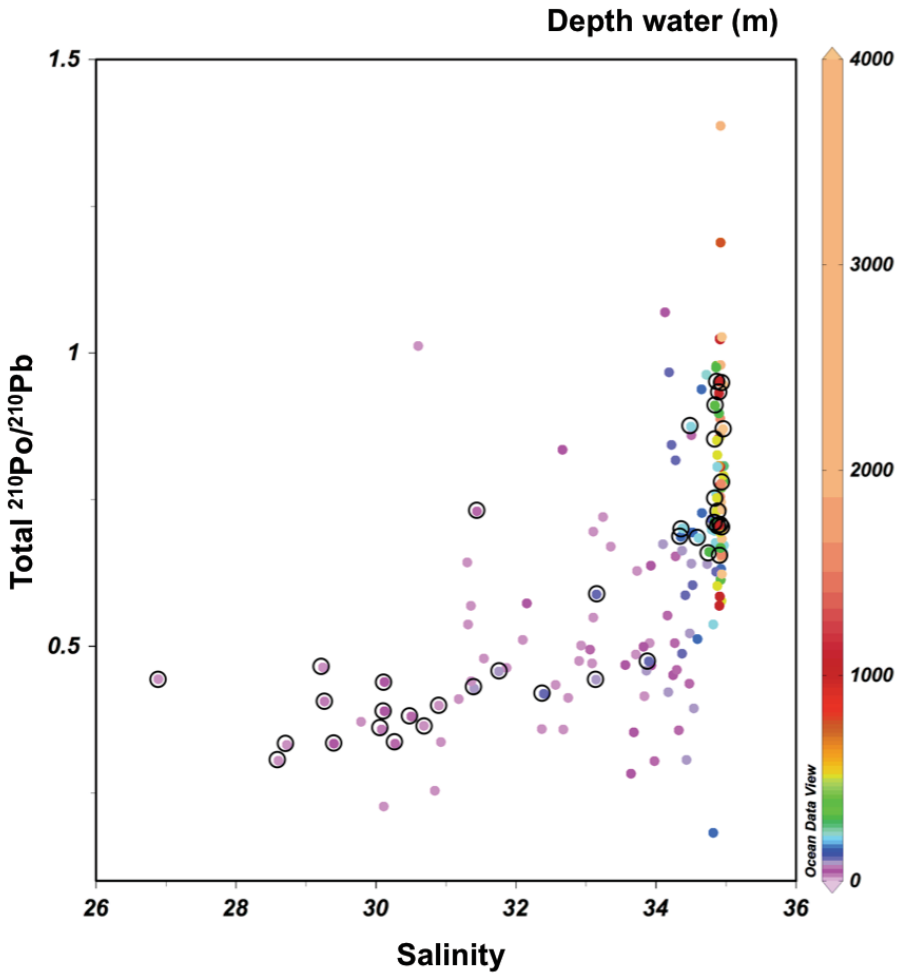

Figure 5.11: Total ^{210}Po/^{210}Pb ratios vs. salinity in the entire study area. The colour bar indicates the sampled depth and the black circles the data points from the Makarov Basin (stations 320-358). Two samples with ratios >1.5 have been excluded from the plot.

Total ^{210}Po/^{210}Pb ratios were lower for waters in the salinity range from about 27 to 34, covering the mixed layer and the upper halocline (basically confined in the Canadian sector), than for higher salinities and, hence, deeper waters (Figure 5.11). This was particularly the case in the Makarov Basin, where the ratios were generally <0.50 for waters extending down to the upper halocline. These waters were influenced by freshwater inputs from river runoff and local precipitation (jointly referred to as river water) [see details in *Bauch et al.*, 2011], net sea-ice melting, and by waters of Pacific origin [*Bauch et al.*, 2011; *Roeske et al.*, 2012; *Rutgers van der Loeff et al.*, 2012]. Melt water was

measured over the Alpha Ridge (stations 338 and 342), amounting to 1 to 2% of surface waters [*Bauch et al.*, 2011; *Rutgers van der Loeff et al.*, 2012]. *Roca-Martí et al.* [2016] have recently shown that a complete melting of sea ice in the central Arctic would change the total ^{210}Po/^{210}Pb ratios by less than 10% in surface waters. Therefore, the substantial deficits of ^{210}Po observed would not be explained by the input of melt water depleted in ^{210}Po with respect to ^{210}Pb. Moreover, the upper 100 m of stations 328, 338 and 342 were composed of 5 to 15% of river water and a great fraction of Pacific water (up to >80%) [*Bauch et al.*, 2011]. Seawater with salinities of ~30 to 32 (part of the PML) found in the central Arctic, especially near the Lomonosov Ridge (stations 320 and 328), originated from the bottom of the Laptev Sea [*Bauch et al.*, 2011], whereas waters with salinities of 32.5 to 33.3 (part of the UHC) found over the Alpha and Mendeleev Ridges came from the Chukchi Sea [*Roeske et al.*, 2012]. These waters from the Laptev and Chukchi Seas carried river water and Pacific-derived water, respectively, and were transported to the central Arctic by the Transpolar Drift. Thus, a hypothesis would be that the substantial deficiency of ^{210}Po observed in the upper water column of the Makarov Basin was created as a consequence of biological activity and particle export that occurred in the shelf regime. The transit time of shelf waters must be shorter than three months to explain the ^{210}Po deficits measured in the upper water column of the Alpha Ridge (^{210}Po/^{210}Pb ratios of ~0.4), considering the most substantial deficits occurred near the continental margin (~0.2, station 391). This hypothesis can be rejected because it was estimated that the shelf waters encountered at the surface of the Makarov Basin and the Lomonosov Ridge in summer 2007 travelled for at least two years [*Bauch et al.*, 2011; *Rutgers van der Loeff et al.*, 2012]. During the productive season in 2007, the average annual new NPP in the Makarov Basin was higher than in the Eurasian Basin by a factor of 3, with diatoms dominating the phytoplankton community (see Section 5.3.1.2). Consistent with this, *Middag et al.* [2009] measured minimum concentrations of Al in the upper 300 m of the Makarov Basin, which were related to biological uptake favoured by silica inputs from the UHC. Particularly, at stations 338 and 342 nitrate was depleted from the surface to 50 m depth. The mixed layer depth at these stations decreased from 60-67 m in winter to 20-26 m at the sampling time and, therefore, the uptake of nitrate had to take place early in the productive season when the seasonal mixed layer was deep enough. This would most likely have occurred before July, since from May surface warming and ice melt establish stratification and, thus, limit the mixing of nutrients within the winter mixed layer [*Kawaguchi et al.*, 2012; *Korhonen et al.*, 2013]. Therefore, the ^{210}Po deficiency found in the Makarov Basin likely originated in situ by means of enhanced new NPP and subsequent export. Over the Alpha Ridge, in particular, this might have been related to ice-algae export resulting from sea-ice melt, as observed in the Eurasian Basin in 2012 [*Boetius et al.*, 2013].

The major deficits of ^{210}Po in the upper 75 m of the Barents Sea and the Nansen Basin were found in cold and relatively low salinity waters (total ^{210}Po/^{210}Pb ratios ≤0.50 at stations 236, 237, 249, 257, 260 in section S1). Most of this section had a significant fraction of melt water in the upper 50 to 100 m (~2%) [*Bauch et al.*, 2011]. Substantial depletions of ^{234}Th, ^{226}Ra, Ba and dissolved Fe were concurrent with the ice edge (81-82°N), together with particularly high phytoplankton biomass, suggesting the occurrence of an ice-edge bloom [*Cai et al.*, 2010; *Klunder et al.*, 2012; *Roeske et al.*, 2012; *Rutgers van der Loeff et al.*, 2012]. As observed for ^{210}Po, ^{234}Th was depleted in the upper 100 m south of the ice edge [*Cai et al.*, 2010], where Chl-a levels were found to be very high two months prior to the sampling (~5 mg m^{-3}) [*Klunder et al.,* 2012]. In the nutrient-rich Barents Sea, the association between freshwater from sea-ice melting and ^{210}Po deficits may be explained by enhanced primary production when melting occurs. This would improve light conditions for phytoplankton growth and subsequent particle settling, in accordance with previous studies of particle fluxes conducted in the area [*Coppola et al.*, 2002; *Wassmann et al.*, 2004; *Lalande et al.*, 2008; *Wiedmann et al.*, 2014].

In section S5, river water had a great presence in the entire water column of the Laptev shelf and in the upper 25 m offshore [*Bauch et al.*, 2011]. The inflow of waters from the Lena River supplies significant amounts of nutrients to the Laptev Sea [e.g. *Le Fouest et al.*, 2013], which may have nourished the high phytoplankton biomass observed on the shelf [*Cai et al.*, 2010]. Moreover, a great reduction of the sea-ice cover was observed in the Laptev sector in summer 2007, and melt water in surface waters was detected from the shelf to station 385 [*Bauch et al.*, 2011]. This sea-ice decline extended the growing season by 50 to 80 days and boosted primary production [*Arrigo et al.*, 2008a]. The maximum inventory of Chl-a was measured at station 407 (Figure 5.9), where a substantial deficit of ^{210}Po was found in surface waters overlying an excess at 25 m (total ^{210}Po/^{210}Pb ratios of 0.37 and 2.79, respectively). This suggests export driven by biogenic particles in surface waters and remineralization or particle disaggregation below, in agreement with the conclusions drawn from Ba, ^{226}Ra and dissolved Fe in the Laptev Sea [*Klunder et al.*, 2012; *Roeske et al.*, 2012; *Rutgers van der Loeff et al.*, 2012]. The ^{210}Po deficits found north of the Laptev Sea (stations 371-400) could be related to biogenic fluxes that occurred prior to sampling, as they are significant in this area from June to August [*Fahl and Nöthig*, 2007; *Lalande et al.*, 2009b]. Indeed, sediment traps deployed on the Laptev slope revealed about two-fold higher annual POC export in 2006-2007 relative to 2005-2006 [*Lalande et al.*, 2009a]. This was mainly attributed to an increase in POC export during and following ice melt in 2007, with maximum fluxes in July. Resuspension of bottom sediments and offshelf transport may be another process contributing to the preferential removal of ^{210}Po in the water column. Since ^{210}Po is preferentially scavenged by organic compounds rather than by inorganic particles with respect to ^{210}Pb [*Yang et al.*, 2015], these processes could have played a role if the particles involved were rich in organic matter.

5.4 Conclusions

The main conclusions drawn from the distribution of ^{210}Pb and ^{210}Po in the water column of the Arctic Ocean during the sea-ice minimum in 2007 are:

1) Phytoplankton biomass, resuspension of shelf sediments, and offshelf transport of particles are mechanisms that modulate the particulate fraction of ^{210}Pb and ^{210}Po in the Arctic.

2) Activities of total ^{210}Pb and ^{210}Po were minimum in the upper and lower haloclines. In the upper halocline (Makarov Basin), this is ascribed to particle scavenging in the shelf environment, where this water mass is formed, and subsequent transport of the signal to the central Arctic. In the lower halocline, these low activities are attributed to particle scavenging during formation and/or transport of the water mass to the central Arctic, especially in the Makarov and eastern Eurasian Basins.

3) Widespread deficits of ^{210}Po were observed all over the Arctic, both on the shelves and in the basins. In the shelf areas of the Barents and Laptev Seas, the ^{210}Po deficits were related to elevated phytoplankton biomass. These deficits were usually associated with sea-ice melt water and riverine water inputs, which may improve light and/or nutrient conditions for photosynthesis. In the basins, seasonal estimates of new primary production were negatively correlated to total ^{210}Po/^{210}Pb ratios in the upper 200 m of the water column, suggesting that in situ production and subsequent export also control the removal of ^{210}Po in this environment. This, in combination with ^{234}Th data [*Cai et al.*, 2010], indicates that particle export fluxes in the Arctic basins would have been, in contrast to late summer, significant before July/August 2007. The ^{210}Po deficits were most substantial (total ^{210}Po/^{210}Pb ratios <0.50) in the mixed layer and the upper halocline of the Makarov Basin, where annual new NPP was found to be particularly high and dominated by diatoms.

4) We frequently found deficits of ^{210}Po in intermediate and deep waters, as well as particulate ^{210}Po/^{210}Pb ratios below one, although the reasons are not clear. Simultaneous use of the ^{210}Po/^{210}Pb proxy and sediment traps, together with analyses of particle composition, and further investigation of the impact of food-web processes on ^{210}Po fractionation, will be helpful to better understand the biogeochemical behaviour of these radionuclides.

Pb-210 and ^{210}Po combined with other tracers, including ^{234}Th, can be very useful to track particle export with different time horizons in the Arctic Ocean, where changing environmental conditions can potentially enhance primary production if accompanied by inputs of nutrients to the surface, impacting the export regime in the ocean as we know it today.

Chapter 6

Conclusions and future perspectives

6.1 General conclusions

The overall objective of this PhD dissertation was to evaluate the particle export and the strength and efficiency of the biological pump in the upper water column of both polar oceans. To this purpose, the two pairs of radionuclides $^{234}Th/^{238}U$ and $^{210}Po/^{210}Pb$ have been used in combination with other techniques that provide complementary information on environmental conditions and particle fluxes. This objective is addressed by means of three studies (see Chapters 3-5) that encompass a variety of spatial and temporal scales. First, a local study in the Atlantic sector of the Southern Ocean was performed to quantify the export flux of particulate organic carbon (POC) during the decline of a vast diatom bloom (see Chapter 3). Second, the export of POC in the upper Arctic Ocean was investigated under the ice-covered Eurasian Basin in the late summer of 2012, providing integrated information of the productive season (see Chapter 4). Last, particle dynamics and particle export in the water column of the Arctic Ocean were studied by analysing the distribution of ^{210}Pb and ^{210}Po on a pan-Arctic scale (see Chapter 5). The contributions of each of these studies are summarized below.

- **Decline of a vast diatom bloom in the Southern Ocean**

Downward fluxes of POC were measured during the decline of a vast diatom bloom in open waters of the Atlantic sector of the Southern Ocean (around 51°S 13°W). Th-234 was used as a particle tracer in combination with free-drifting sediment traps. The export of ^{234}Th at 100 m estimated from both techniques was in good agreement (~2100 dpm m^{-2} d^{-1}), showing a high export at steady state in the weeks prior to and during the sampling period. The study site (~8000 km^2) presented similar vertical fluxes irrespectively of differences in phytoplankton standing stocks and productivity, indicating a decoupling between production and export. The POC fluxes at 100 m were high, averaging 26 ± 15 mmol C m^{-2} d^{-1}, which are comparable to other studies of the later stages of natural and iron-fertilized blooms in the Southern Ocean that were not silica limited. However, the export efficiency of the bloom was generally low: only <20% of the daily net primary production (NPP) reached 100 m, presumably due to an active recycling of carbon and nutrients in surface waters. Moreover, an inverse relationship between export efficiency and NPP was found, supporting recent findings [*Maiti et al.*, 2013; *Cavan et al.*, 2015, 2017; *Laurenceau-Cornec et al.*, 2015; *Le Moigne et al.*, 2016]. In contrast, the transfer efficiency of POC measured between 100 and 300 m was high (~60%). Pigment analyses in sediment trap material indicated that direct sinking of diatoms was likely responsible for the limited attenuation of the POC flux within the upper mesopelagic zone. Indeed, benthic foraminifera collected at ~4000 m below the bloom were feeding on fresh phytodetritus, indicating a rapid transport of phytoplankton to the seafloor [*Cedhagen et al.*, 2014]. Yet, the lack of relationship between fluxes of chlorophyll *a* (Chl-a) and POC

at 100 and 300 m, showed that particles other than fresh phytoplankton contributed significantly to carbon export. Substantial fluxes of pheopigments in the upper mesopelagic zone, together with observations of fresh faecal pellets in abyssal sediments in the study site [*Emil Ruff et al.*, 2014], suggest that faecal material and transport of POC linked to zooplankton vertical migration played a significant role in shaping the efficiency of the biological pump.

- **POC export in the central Arctic**

Carbon export fluxes in the ice-covered Arctic Ocean were assessed for the first time by the joint application of the $^{234}Th/^{238}U$ and $^{210}Po/^{210}Pb$ pairs during the record sea-ice minimum in 2012. The $^{234}Th/^{238}U$ proxy revealed that POC fluxes at the base of the euphotic zone were very low (2 ± 2 mmol C m^{-2} d^{-1}) in the late summer of 2012 in agreement with low values of NPP and the results from sediment traps [*Lalande et al.*, 2014]. Relationships obtained between ^{234}Th fluxes and ^{234}Th-derived POC fluxes with the phytoplankton community suggest that prasinophytes contributed significantly to the downward fluxes, likely via incorporation into sea-ice algal aggregates and zooplankton-derived material. The widespread depletion of ^{210}Po in the upper water column of the study area, unlike ^{234}Th, indicated that particle export fluxes were higher before July/August than later in the season. At the time of sampling, *Fernández-Méndez et al.* [2014] and *Katlein et al.* [2014] found sea-ice algal aggregates, composed of diatoms, under the sea ice at all the stations. Moreover, *Boetius et al.* [2013] revealed large deposits of diatom aggregates on the seafloor at most of the study area associated with rapid ice melting. Po-210 fluxes and ^{210}Po-derived POC fluxes correlated positively with sea-ice concentration. Indeed, the stations covered with multi-year ice showed the most substantial depletion of ^{210}Po together with the highest annual new NPP rates and seafloor coverage of algae [*Boetius et al.*, 2013]. This shows that primary production and particle sinking were more important under heavy sea-ice conditions than under partially ice-covered regions and suggests that ^{210}Po tracked, to some extent, the massive algal export that occurred earlier in the season. A great fraction of the annual new NPP (>30%) was exported from the euphotic zone in most of the study area during summer 2012, indicating a high export efficiency of the biological pump in the central Arctic.

- **Pan-Arctic study of ^{210}Pb and ^{210}Po**

The distribution of the naturally occurring pair $^{210}Po/^{210}Pb$ was investigated in the water column of the Barents, Kara and Laptev Seas and the Nansen, Amundsen and Makarov Basins during the 2007 sea-ice minimum. This is the largest dataset of ^{210}Pb and ^{210}Po in the Arctic Ocean to date. The particulate fractions of both radionuclides were generally higher (>25%) on the shelves and near the shelf break, in association with relatively high phytoplankton biomass, resuspension of sediments and offshelf transport of particles, especially in the Laptev sector. Minimum activities of

total ^{210}Pb and ^{210}Po were found in the upper and lower haloclines, which are attributed to particle scavenging over the shelves, boundary current transport and transfer of the signal to the central Arctic. Widespread and substantial deficits of ^{210}Po (>50% with respect to ^{210}Pb) were detected from surface waters to 200 m on the shelves, but also in the basins. On the shelves, the deficits of ^{210}Po were usually related to elevated phytoplankton biomass, and water from sea-ice melt and rivers, which could improve light and/or nutrient conditions for photosynthesis. In the basins, annual new NPP correlated with the deficits of ^{210}Po in the upper 200 m of the water column, indicating that in situ production and subsequent export of biogenic material are the mechanisms that control the removal of ^{210}Po. The ^{210}Po deficiency was particularly pronounced in the Makarov Basin. In this basin, the annual new NPP was dominated by diatoms and was higher than in the Eurasian Basin by a factor of 3. Yet, during the same expedition ^{234}Th-derived export estimates were found to be very low in the basins [*Cai et al.*, 2010]. Given the shorter time scale of ^{234}Th compared to that of ^{210}Po, this observation suggests that export fluxes in the central Arctic were significant before July/August in contrast to later in the season in August/September.

The results obtained from this work stress the importance of the concurrent application of more than one technique to estimate POC export and the inclusion of ecologically relevant parameters when studying particle export. The use of the ^{234}Th/^{238}U and ^{210}Po/^{210}Pb pairs provides particle export information on time scales of weeks to months, respectively, which allow identifying changes during the polar summer, and, at the same time, can be applied at high spatial resolution. The simultaneous use of radionuclides and sediment traps, or other devices that allow the investigation of the nature of the export, offers a more complete picture of the biological pump beyond the quantification of POC sinking rates.

In the decline of the Southern Ocean bloom (see Chapter 3), pigment analyses in trapped material and benthic observations [*Cedhagen et al.*, 2014] revealed that diatoms were responsible for high POC export fluxes over an area of several thousands of square kilometres. This is consistent with the general view that diatoms are the main phytoplankton group contributing to organic export in the Southern Ocean [*Falkowski et al.*, 1998; *Smetacek*, 1999]. However, a number of studies suggest that a great fraction of primary production by diatoms is exported from the euphotic zone but this fraction undergoes increased remineralization in the mesopelagic realm compared to picophytoplankton [e.g. *Buesseler*, 1998; *Guidi et al.*, 2015], in contrast to the results obtained here. The reasons for this variability underlines the necessity to gain knowledge of the impact of the phytoplankton species composition, food-web dynamics and environmental conditions on determining where carbon attenuation occurs, which determines the time scale of carbon removal from the atmosphere [*Passow and Carlson*, 2012].

In the central Arctic, the combination of the results from both radionuclide pairs during the last two sea-ice minimums in 2007 and 2012 (see Chapters 4 and 5) shows that particle export is significant in spring/early summer rather than later in the season, when icebreakers usually explore the area due to improved conditions for navigation. Seasonal primary production estimates, together with information provided by under-ice and benthic observations (Figure 1.10) [*Boetius et al.*, 2013; *Fernández-Méndez et al.*, 2014; *Katlein et al.*, 2014], illustrate that diatoms locally have a significant role in new and export production in the central Arctic. This suggests that under-ice production and export in the Arctic basins, which is indeed ignored by satellite-derived estimates, could be significantly greater than is currently thought, arising questions such as: what is the extension and magnitude of the under-ice fluxes in terms of carbon export and sequestration? How the nature of these fluxes depends on the overlying sea-ice cover? These research questions urgently need further investigations, especially in the likely scenario of a summer ice-free Arctic in the next thirty-three years [*IPCC*, 2013].

6.2 Future perspectives

The disequilibrium between ^{234}Th and ^{238}U and ^{210}Po and ^{210}Pb has proven to be valuable to evaluate the export of POC in the modern ocean [*Verdeny et al.*, 2009]. During the last decades great advances have been achieved with regard to analytical methods and the study of their biogeochemical behaviour, although there is still much room for improvement [*Santschi et al.*, 2006; *Fowler*, 2011]. Besides this, many questions regarding the fraction of production that can be exported from the euphotic zone, how efficiently it can be transferred to greater depths and the conditions for that to happen remain unanswered. Some aspects that may be addressed in the future in order to overcome methodological limitations and better understand the biological pump in the polar oceans have been pointed out in Chapters 3-5 and are summarized hereafter.

- **The ^{210}Po/^{210}Pb pair**

The ^{210}Po/^{210}Pb pair has been far less studied than the ^{234}Th/^{238}U pair and, as a consequence, our knowledge of the biogeochemical behaviour of ^{210}Pb and ^{210}Po is smaller. Furthermore, both ^{210}Pb and ^{210}Po are particle reactive, which makes the interpretation of ^{210}Po-derived data more complex than those derived from ^{234}Th. Further research should examine the speciation of ^{210}Pb and ^{210}Po in seawater, their affinity for different particle types and the mechanisms of adsorption and, in the case of ^{210}Po, biological uptake. The observation of substantial disequilibrium of ^{210}Po in the deep ocean deserves, in particular, further attention. One might wonder whether deep ^{210}Po deficits reflect the settling of particles to the deep ocean, or they are totally or partly associated with other processes or methodological issues. In the Arctic in 2007 (see Chapter 5), the magnitude of these

deficits was substantial throughout the mesopelagic and bathypelagic zones (mean ^{210}Po/^{210}Pb ratio of 0.80), indicating that they do not solely correspond to particle export. Indeed, although in 2012 ^{210}Pb and ^{210}Po sampling was not conducted throughout the entire water column (see Chapter 4), ^{210}Pb and ^{210}Po at 300-400 m depth were found to be near equilibrium, in contrast to the results obtained in 2007. *Kim* [2001] suggested that deep ^{210}Po deficits in the oligotrophic ocean could be explained by bacteria uptake of ^{210}Po and its transfer to higher trophic levels, which are usually missed by sampling techniques. *Church et al.* [2012] pointed out that there is a potential analytical issue for different extraction of the Po spike and the in situ ^{210}Po isotope during the co-precipitation phase. Therefore, the impact of food-web processes on ^{210}Po fractionation, as well as testing the extraction efficiency of Po isotopes using different co-precipitation techniques may help to elucidate the reasons behind this disequilibrium. The simultaneous use of the ^{210}Po approach in the water column and sediment traps deployed at different depths down to the bathypelagic zone would also allow clarifying to what extent ^{210}Po removal by deep particle export is important. All of this would improve significantly the interpretation of the distribution of ^{210}Pb and ^{210}Po in the water column and the application of this pair as a proxy for export of POC (or other elements and compounds of interest).

- **C/Th(Po) ratios and time-series measurements**

The determination of representative POC/^{234}Th and POC/^{210}Po (C/Th(Po)) ratios of the particle pool that creates the ^{234}Th and ^{210}Po deficits in the overlying water column is essential to obtain accurate POC export estimates. The use of devices that allow the capture of setting particles, separated from suspended matter, is recommended over filtering seawater and making a size-based assumption of the particles that sink. The measurement of C/Th(Po) ratios in material collected during a time window comparable to the mean lives of ^{234}Th and ^{210}Po (e.g. by using sediment traps or moorings) could also improve the accuracy of the POC export estimates. This would have been very helpful in the central Arctic in 2012 (see Chapter 4), since the composition of the sinking-particle pool changed significantly over the productive season and, hence, the C/Po ratios measured in the late summer may have not been representative of the particles that contributed to most of the ^{210}Po removal. Therefore, the study of the change of C/Th(Po) ratios in relation to the ecosystem structure and their seasonal evolution during the polar summer would be very relevant for future studies. Time-series measurements of seawater profiles would also allow applying a non-steady state model to test the validity of the most commonly applied scavenging model.

- **Remineralization**

Excess ^{234}Th and ^{210}Po below the mixed layer can be used to calculate rates of remineralization, which is a key factor in shaping the efficiency of the biological pump. Increased depth-sampling resolution of ^{234}Th and ^{210}Po in the upper mesopelagic zone, where most of the POC flux attenuation generally occurs [*Schlitzer,* 2002], in a similar fashion than the resolution applied in the upper ocean to characterize well the deficits, would increase the chances to identify excess activity of ^{234}Th and ^{210}Po. However, this excess may be dispersed over such a wide depth interval that it is too small to differentiate from the background activity of ^{234}Th or ^{210}Po [*Waples et al.,* 2006]. Therefore, the combined use of the ^{234}Th and ^{210}Po proxies with other techniques could provide more insights into the attenuation of sinking particle fluxes below the mixed layer. This includes the use of sediment traps at different depth horizons within the mesopelagic zone [e.g. *Marsay et al.*, 2015] and the assessment of particulate biogenic barium stocks in the mesopelagic as a proxy for remineralization of organic matter [e.g. *Planchon et al.*, 2013].

- **Biological pump in the polar oceans**

Many unknowns still exist about the contribution of the biological pump to the export and sequestration of carbon in the polar oceans, especially in the current context of accelerated environmental changes. As an illustration, in the Southern Ocean, the inverse correlation found between export efficiency and primary production [e.g. *Maiti et al.*, 2013] has profound implications for the validity of satellite-based export models, which typically predict increasing export efficiency with primary production. The reasons for this relationship are unclear, but the plankton community structure and the zooplankton and microbial activity in surface waters are believed to play an essential role [*Cavan et al.*, 2015, 2017; *Laurenceau-Cornec et al.*, 2015; *Le Moigne et al.*, 2016]. To shed light on this issue it will be necessary to further investigate how these components regulate the attenuation of the POC flux coupled with sufficiently long time scales to overcome the temporal mismatch between primary production and export. In the Arctic Ocean, it is suggested that ~30% of the ice-covered waters present, in recent years, favourable light conditions to support the occurrence of under-ice blooms around July as a consequence of sea-ice thinning [*Horvat et al.*, 2017]. One of the major challenges will be to define the extension and magnitude of these blooms, how the continued sea-ice retreat will affect primary production and the diverse components of the biological pump, and, ultimately, the implications for carbon export. Interdisciplinary efforts will be indispensable to clarify these questions, among others, and gain a comprehensive understanding of the biological pump and the processes involved.

Lagrangian studies and the coordinate use of multiple approaches, including sediment traps, biogeochemical and radionuclide budgets and autonomous vehicles can be a very powerful tool to characterize the spatial and temporal variability of the biological pump [*Honjo et al.*, 2014; *Findlay et al.*, 2015a; *Siegel et al.*, 2016]. Region-specific food-web dynamics could then be incorporated into satellite-based export estimates [*Boyd*, 2015; *Stukel et al.*, 2015; *Britten and Primeau*, 2016; *Le Moigne et al.*, 2016], which would help to predict the future role of the ocean as a carbon sink.

References

Aagaard, K. et al. (1996), U.S., Canadian researchers explore Arctic Ocean, *Eos, Trans. Am. Geophys. Union*, *77*(22), 209–213, doi:10.1029/96EO00141.

Amacher, J., S. Neuer, and M. Lomas (2013), DNA-based molecular fingerprinting of eukaryotic protists and cyanobacteria contributing to sinking particle flux at the Bermuda Atlantic time-series study, *Deep Sea Res. Part II Top. Stud. Oceanogr.*, *93*, 71–83, doi:10.1016/j.dsr2.2013.01.001.

Amiel, D., and J. K. Cochran (2008), Terrestrial and marine POC fluxes derived from ^{234}Th distributions and δ^{13}C measurements on the Mackenzie Shelf, *J. Geophys. Res.*, *113*(C3), C03S06, doi:10.1029/2007JC004260.

Amiel, D., J. K. Cochran, and D. J. Hirschberg (2002), ^{234}Th/^{238}U disequilibrium as an indicator of the seasonal export flux of particulate organic carbon in the North Water, *Deep Sea Res. Part II Top. Stud. Oceanogr.*, *49*(22–23), 5191–5209, doi:10.1016/S0967-0645(02)00185-6.

Anderson, L. G., and R. W. Macdonald (2015), Observing the Arctic Ocean carbon cycle in a changing environment, *Polar Res.*, *34*(26891), doi:10.3402/polar.v34.26891.

Anderson, L. G., P. S. Andersson, G. Björk, E. Peter Jones, S. Jutterström, and I. Wåhlström (2013), Source and formation of the upper halocline of the Arctic Ocean, *J. Geophys. Res. Ocean.*, *118*(1), 410–421, doi:10.1029/2012JC008291.

Anderson, T. R., and K. W. Tang (2010), Carbon cycling and POC turnover in the mesopelagic zone of the ocean: Insights from a simple model, *Deep Sea Res. Part II Top. Stud. Oceanogr.*, *57*(16), 1581–1592, doi: 10.1016/j.dsr2.2010.02.024.

Angel, M. V (1989), *Does mesopelagic biology affect the vertical flux? In: Productivity of the ocean: Present and past*, edited by W. H. Berger, V. S. Smetacek, and G. Wefer, John Wiley and Sons, New York.

Anisimov, O. A., D. G. Vaughan, T. V. Callaghan, C. Furgal, H. Marchant, T. D. Prowse, H. Vilhjálmsson, and J. E. Walsh (2007), *Polar regions (Arctic and Antarctic). Climate change 2007: Impacts, adaptation and vulnerability. Contribution of working group II to the fourth assessment report of the Intergovernmental Panel on Climate Change*, edited by M. L. Parry, O. F. Canziani, J. P. Palutikof, P. J. van der Linden, and C. E. Hanson, Cambridge University Press, Cambridge.

Ardyna, M., M. Babin, M. Gosselin, E. Devred, L. Rainville, and J.-É. Tremblay (2014), Recent Arctic Ocean sea ice loss triggers novel fall phytoplankton blooms, *Geophys. Res. Lett.*, *41*(17), 6207–6212, doi:10.1002/2014GL061047.

Armstrong, R. A., C. Lee, J. I. Hedges, S. Honjo, and S. G. Wakeham (2002), A new, mechanistic model for organic carbon fluxes in the ocean based on the quantitative association of POC with ballast minerals, *Deep Sea Res. Part II Top. Stud. Oceanogr.*, *49*(1–3), 219–236, doi:10.1016/S0967-0645(01)00101-1.

Arrigo, K. R. (2014), Sea Ice Ecosystems, *Ann. Rev. Mar. Sci.*, *6*, 439–467, doi:10.1146/annurev-marine-010213-135103.

Arrigo, K. R., and G. L. van Dijken (2015), Continued increases in Arctic Ocean primary production, *Prog. Oceanogr.*, *136*, 60–70, doi:10.1016/j.pocean.2015.05.002.

Arrigo, K. R., and D. N. Thomas (2004), Large scale importance of sea ice biology in the Southern Ocean, *Antarct. Sci.*, *16*(4), 471–486, doi:10.1017/S0954102004002263.

Arrigo, K. R., G. van Dijken, and S. Pabi (2008a), Impact of a shrinking Arctic ice cover on marine primary production, *Geophys. Res. Lett.*, *35*(19), L19603.

Arrigo, K. R., G. L. van Dijken, and S. Bushinsky (2008b), Primary production in the Southern Ocean, 1997–2006, *J. Geophys. Res.*, *113*, C08004, doi:10.1029/2007JC004551.

Arrigo, K. R. et al. (2012), Massive phytoplankton blooms under Arctic sea ice, *Science*, *336*(6087), 1408, doi:10.1126/science.1215065.

Asper, V. L. (1987), Measuring the flux and sinking speed of marine snow aggregates, *Deep Sea Res. Part A. Oceanogr. Res. Pap.*, *34*(1), 1–17, doi:10.1016/0198-0149(87)90117-8.

Assmy, P., K. Lochte, and V. Smetacek (2009), Plankton productivity and the role of iron in the Southern Ocean, in *Biological studies in polar oceans - Exploration of life in icy waters*, edited by G. Hempel and I. Hempel, pp. 227–235, Wirtschaftsverlag NW, Bremerhaven.

Assmy, P. et al. (2013), Thick-shelled, grazer-protected diatoms decouple ocean carbon and silicon cycles in the iron-limited Antarctic Circumpolar Current, *Proc. Natl. Acad. Sci. U. S. A.*, *110*(51), 20633–20638, doi:10.1073/pnas.1309345110.

de Baar, H. J. W., A. G. J. Buma, R. F. Nolting, G. C. Cadée, G. Jacques, and P. J. Tréguer (1990), On iron limitation of the Southern Ocean: Experimental observations in the Weddell and Scotia Seas, *Mar. Ecol. Prog. Ser.*, *65*, 105–122.

de Baar, H. J. W. et al. (2005), Synthesis of iron fertilization experiments: From the Iron Age in the Age of Enlightenment, *J. Geophys. Res.*, *110*(C09S16), 1–24, doi:10.1029/2004JC002601.

Bach, L. T., T. Boxhammer, A. Larsen, N. Hildebrandt, K. G. Schulz, and U. Riebesell (2016), Influence of plankton community structure on the sinking velocity of marine aggregates, *Global Biogeochem. Cycles*, *30*, 21 pp., doi:10.1002/2016GB005372.

Bacon, M. P., and M. M. Rutgers van der Loeff (1989), Removal of thorium-234 by scavenging in the bottom nepheloid layer of the ocean, *Earth Planet. Sci. Lett.*, *92*(2), 157–164, doi:10.1016/0012-821X(89)90043-5.

Bacon, M. P., D. W. Spencer, and P. G. Brewer (1976), ^{210}Pb/^{226}Ra and ^{210}Po/^{210}Pb disequilibria in seawater and suspended particulate matter, *Earth Planet. Sci. Lett.*, *32*(2), 277–296, doi:10.1016/0012-821X(76)90068-6.

Bacon, M. P., R. A. Belastock, M. Tecotzky, K. K. Turekian, and D. W. Spencer (1988), Lead-210 and polonium-210 in ocean water profiles of the continental shelf and slope south of New England, *Cont. Shelf Res.*, *8*(5–7), 841–853, doi:10.1016/0278-4343(88)90079-9.

Barber, D. G. et al. (2012), Consequences of change and variability in sea ice on marine ecosystem and biogeochemical processes during the 2007–2008 Canadian International Polar Year program, *Clim. Change*, *115*(1), 135–159, doi:10.1007/s10584-012-0482-9.

Barlow, R. G., D. G. Cummings, and S. W. Gibb (1997), Improved resolution of mono- and divinyl chlorophylls *a* and *b* and zeaxanthin and lutein in phytoplankton extracts using reverse phase C-8 HPLC, *Mar. Ecol. Prog. Ser.*, *161*, 303–307, doi:10.3354/meps161303.

Baskaran, M., P. W. Swarzenski, and D. Porcelli (2003), Role of colloidal material in the removal of ^{234}Th in the Canada basin of the Arctic Ocean, *Deep Sea Res. Part I Oceanogr. Res. Pap.*, *50*(10–11), 1353–1373, doi:10.1016/S0967-0637(03)00140-7.

Bates, N. R., and J. T. Mathis (2009), The Arctic Ocean marine carbon cycle: evaluation of air-sea CO_2 exchanges, ocean acidification impacts and potential feedbacks, *Biogeosciences*, *6*(11), 2433–2459, doi:10.5194/bg-6-2433-2009.

Bathmann, U. V., R. Scharek, C. Klaas, C. D. Dubischar, and V. Smetacek (1997), Spring development of phytoplankton biomass and composition in major water masses of the Atlantic sector of the Southern Ocean, *Deep Sea Res. Part II Top. Stud. Oceanogr.*, *44*(1–2), 51–67, doi:10.1016/S0967-0645(96)00063-X.

Bauch, D., J. Hölemann, S. Willmes, M. Gröger, A. Novikhin, A. Nikulina, H. Kassens, and L. Timokhov (2010), Changes in distribution of brine waters on the Laptev Sea shelf in 2007, *J. Geophys. Res.*, *115*(C11), C11008, doi:10.1029/2010JC006249.

Bauch, D., M. Rutgers van der Loeff, N. Andersen, S. Torres-Valdes, K. Bakker, and E. P. Abrahamsen (2011), Origin of freshwater and polynya water in the Arctic Ocean halocline in summer 2007, *Prog. Oceanogr.*, *91*(4), 482–495, doi:10.1016/j.pocean.2011.07.017.

Bauerfeind, E., C. Garrity, M. Krumbholz, R. O. Ramseier, and M. Voβ (1997), Seasonal variability of sediment trap collections in the Northeast Water Polynya. Part 2. Biochemical and microscopic composition of sedimenting matter, *J. Mar. Syst.*, *10*(1–4), 371–389, doi:10.1016/S0924-7963(96)00069-3.

Belcher, A., M. Iversen, C. Manno, S. A. Henson, G. A. Tarling, and R. Sanders (2016), The role of particle associated microbes in remineralization of fecal pellets in the upper mesopelagic of the Scotia Sea, Antarctica, *Limnol. Oceanogr.*, *61*(3), 1049–1064, doi:10.1002/lno.10269.

Benitez-Nelson, C. R., and W. S. Moore (2006), Future applications of ^{234}Th in aquatic ecosystems, *Mar. Chem.*, *100*, 163–165, doi:10.1016/j.marchem.2005.10.010.

Benitez-Nelson, C. R., K. O. Buesseler, M. Rutgers van der Loeff, J. Andrews, L. Ball, G. Crossin, and M. A. Charette (2001), Testing a new small-volume technique for determining ^{234}Th in seawater, *J. Radioanal. Nucl. Chem.*, *248*(3), 795–799, doi:10.1023/A:1010621618652.

Bhat, S. G., S. Krishnaswamy, D. Lal, Rama, and W. S. Moore (1968), ^{234}Th/^{238}U ratios in the ocean, *Earth Planet. Sci. Lett.*, *5*, 483–491, doi:10.1016/S0012-821X(68)80083-4.

Bhatt, U. S. et al. (2014), Implications of Arctic sea ice decline for the Earth system, *Annu. Rev. Environ. Resour.*, *39*(1), 57–89, doi:10.1146/annurev-environ-122012-094357.

Bidigare, R. R. (1991), Analysis of algal chlorophylls and carotenoids, in *Marine particles: Analysis and characterization*, edited by D. C. Hurd and D. W. Spencer, pp. 119–123, American Geophysical Union, Washington, D. C.

Blain, S. et al. (2007), Effect of natural iron fertilization on carbon sequestration in the Southern Ocean, *Nature*, *446*(7139), 1070–1074, doi:10.1038/nature05700.

Bluhm, B. A., K. N. Kosobokova, and E. C. Carmack (2015), A tale of two basins: An integrated physical and biological perspective of the deep Arctic Ocean, *Prog. Oceanogr.*, *139*, 89–121, doi:10.1016/j.pocean.2015.07.011.

Boetius, A. (2013), *The expedition of the research vessel "Polarstern" to the Arctic in 2012 (ARK-XXVII/3). Reports on polar and marine research 663*, Bremerhaven.

Boetius, A. et al. (2013), Export of algal biomass from the melting Arctic sea ice, *Science*, *339*(6126), 1430–1432, doi:10.1126/science.1231346.

Booth, B. C., and R. A. Horner (1997), Microalgae on the Arctic Ocean Section, 1994: species abundance and biomass, *Deep Sea Res. Part II Top. Stud. Oceanogr.*, *44*(8), 1607–1622, doi:10.1016/S0967-0645(97)00057-X.

Borges Mendes, C. R., V. M. Tavano, T. S. Dotto, R. Kerr, M. S. de Souza, C. A. Eiras Garcia, and E. R. Secchi (2017), New insights on the dominance of cryptophytes in Antarctic coastal waters: A case study in Gerlache Strait, *Deep Sea Res. Part II Top. Stud. Oceanogr.*, doi:10.1016/j.dsr2.2017.02.010.

Bowie, A. R., D. Lannuzel, T. A. Remenyi, T. Wagener, P. J. Lam, P. W. Boyd, C. Guieu, A. T. Townsend, and T. W. Trull (2009), Biogeochemical iron budgets of the Southern Ocean south of Australia: Decoupling of iron and nutrient cycles in the subantarctic zone by the summertime supply, *Global Biogeochem. Cycles*, *23*(4), GB4034, doi:10.1029/2009GB003500.

Boyd, P. W. (2015), Toward quantifying the response of the oceans' biological pump to climate change, *Front. Mar. Sci.*, *2*, 77, doi:10.3389/fmars.2015.00077.

Boyd, P. W., and P. P. Newton (1999), Does planktonic community structure determine downward particulate organic carbon flux in different oceanic provinces?, *Deep Sea Res. Part I Oceanogr. Res. Pap.*, *46*(1), 63–91, doi:10.1016/S0967-0637(98)00066-1.

Boyd, P. W., and T. W. Trull (2007), Understanding the export of biogenic particles in oceanic waters: Is there consensus?, *Prog. Oceanogr.*, *72*(4), 276–312, doi:10.1016/j.pocean.2006.10.007.

Boyd, P. W. et al. (2000), A mesoscale phytoplankton bloom in the polar Southern Ocean stimulated by iron fertilization, *Nature*, *407*(6805), 695–702, doi:10.1038/35037500.

Boyd, P. W. et al. (2007), Mesoscale iron enrichment experiments 1993-2005: synthesis and future directions, *Science*, *315*(5812), 612–617, doi:10.1126/science.1131669.

Boyd, P. W., A. McDonnell, J. Valdez, D. LeFevre, and M. P. Gall (2015), RESPIRE: An in situ particle interceptor to conduct particle remineralization and microbial dynamics studies in the oceans' Twilight Zone, *Limnol. Oceanogr. Methods*, *13*(9), 494–508, doi:10.1002/lom3.10043.

Bring, A., I. Fedorova, Y. Dibike, L. Hinzman, J. Mård, S. H. Mernild, T. Prowse, O. Semenova, S. L. Stuefer, and M.-K. Woo (2016), Arctic terrestrial hydrology: A synthesis of processes, regional effects, and research challenges, *J. Geophys. Res. Biogeosciences*, *121*(3), 621–649, doi:10.1002/2015JG003131.

Britten, G. L., and F. W. Primeau (2016), Biome-specific scaling of ocean productivity, temperature, and carbon export efficiency, *Geophys. Res. Lett.*, *43*(10), 5210–5216, doi:10.1002/2016GL068778.

Brzezinski, M. A. (1985), The Si:C:N ratio of marine diatoms: interspecific variability and the effect of some environmental variables, *J. Phycol.*, *21*(3), 347–357, doi:10.1111/j.0022-3646.1985.00347.x.

Buesseler, K. O. (1998), The decoupling of production and particulate export in the surface ocean, *Global Biogeochem. Cycles*, *12*(2), 297–310, doi:10.1029/97GB03366.

Buesseler, K. O., and P. Boyd (2009), Shedding light on processes that control particle export and flux attenuation in the twilight zone of the open ocean, *Limnol. Oceanogr.*, *54*(4), 1210–1232, doi:10.4319/lo.2009.54.4.1210.

Buesseler, K. O., M. P. Bacon, J. K. Cochran, and H. D. Livingston (1992), Carbon and nitrogen export during the JGOFS North Atlantic Bloom experiment estimated from ^{234}Th:^{238}U disequilibria, *Deep Sea Res. Part A. Oceanogr. Res. Pap.*, *39*(7–8), 1115–1137, doi:10.1016/0198-0149(92)90060-7.

Buesseler, K. O., A. F. Michaels, D. A. Siegel, and A. H. Knap (1994), A three dimensional time-dependent approach to calibrating sediment trap fluxes, *Global Biogeochem. Cycles*, *8*(2), 179–193, doi:10.1029/94GB00207.

Buesseler, K. O., C. Benitez-Nelson, M. M. Rutgers van der Loeff, J. Andrews, L. Ball, G. Crossin, and M. A. Charette (2001a), An intercomparison of small- and large-volume techniques for thorium-234 in seawater, *Mar. Chem.*, *74*(1), 15–28, doi:10.1016/S0304-4203(00)00092-X.

Buesseler, K. O., L. Ball, J. Andrews, J. K. Cochran, D. J. Hirschberg, M. P. Bacon, A. Fleer, and M. Brzezinski (2001b), Upper ocean export of particulate organic carbon and biogenic silica in the Southern Ocean along 170°W, *Deep Sea Res. Part II Top. Stud. Oceanogr.*, *48*(19–20), 4275–4297, doi:10.1016/S0967-0645(01)00089-3.

Buesseler, K. O., R. T. Barber, M. L. Dickson, M. R. Hiscock, J. K. Moore, and R. Sambrotto (2003), The effect of marginal ice-edge dynamics on production and export in the Southern Ocean along 170 degrees W, *Deep Sea Res. Part II Top. Stud. Oceanogr.*, *50*(3–4), 579–603, doi:10.1016/S0967-0645(02)00585-4.

Buesseler, K. O., J. E. Andrews, S. M. Pike, and M. A. Charette (2004), The effects of iron fertilization on carbon sequestration in the Southern Ocean, *Science*, *304*, 414–417, doi:10.1126/science.1086895.

Buesseler, K. O., J. E. Andrews, S. M. Pike, M. A. Charette, L. E. Goldson, M. A. Brzezinski, and V. P. Lance (2005), Particle export during the Southern Ocean Iron Experiment (SOFeX), *Limnol. Oceanogr.*, *50*(1), 311–327, doi:10.4319/lo.2005.50.1.0311.

Buesseler, K. O. et al. (2006), An assessment of particulate organic carbon to thorium-234 ratios in the ocean and their impact on the application of ^{234}Th as a POC flux proxy, *Mar. Chem.*, *100*(3–4), 213–233, doi:10.1016/j.marchem.2005.10.013.

Buesseler, K. O. et al. (2007), An assessment of the use of sediment traps for estimating upper ocean particle fluxes, *J. Mar. Res.*, *65*(3), 345–416.

Buesseler, K. O. et al. (2008a), Ocean iron fertilization - moving forward in a sea of uncertainty, *Science*, *319*(5860), 162, doi:10.1126/science.1154305.

Buesseler, K. O., C. Lamborg, P. Cai, R. Escoube, R. Johnson, S. Pike, P. Masqué, D. McGillicuddy, and E. Verdeny (2008b), Particle fluxes associated with mesoscale eddies in the Sargasso Sea, *Deep Sea Res. Part II Top. Stud. Oceanogr.*, *55*(10–13), 1426–1444, doi:10.1016/j.dsr2.2008.02.007.

Burd, A., A. Buchan, M. J. Church, M. R. Landry, A. M. P. McDonnell, U. Passow, D. K. Steinberg, and H. M. Benway (2016), Towards a transformative understanding of the ocean's biological pump: Priorities for future research - Report on the NSF Biology of the Biological Pump Workshop, 67 pp., doi:10.1575/1912/8263.

Burd, A. B., and G. A. Jackson (2009), Particle aggregation, *Ann. Rev. Mar. Sci.*, *1*, 65–90, doi:10.1146/annurev.marine.010908.163904.

Burd, A. B. et al. (2010), Assessing the apparent imbalance between geochemical and biochemical indicators of meso- and bathypelagic biological activity: What the @$#! is wrong with present calculations of carbon budgets?, *Deep Sea Res. Part II Top. Stud. Oceanogr.*, *57*(16), 1557–1571, doi:10.1016/j.dsr2.2010.02.022.

Cai, P., M. M. Rutgers van der Loeff, I. Stimac, E.-M. Nöthig, K. Lepore, and S. B. Moran (2010), Low export flux of particulate organic carbon in the central Arctic Ocean as revealed by ^{234}Th:^{238}U disequilibrium, *J. Geophys. Res.*, *115*, C10037, doi:10.1029/2009JC005595.

Cámara-Mor, P., P. Masqué, J. Garcia-Orellana, S. Kern, J. K. Cochran, and C. Hanfland (2011), Interception of atmospheric fluxes by Arctic sea ice: Evidence from cosmogenic ^{7}Be, *J. Geophys. Res. Ocean.*, *116*, C12041, doi:10.1029/2010JC006847.

Carmack, E., and D. C. Chapman (2003), Wind-driven shelf/basin exchange on an Arctic shelf: The joint roles of ice cover extent and shelf-break bathymetry, *Geophys. Res. Lett.*, *30*(14), doi:10.1029/2003GL017526.

Carmack, E., and F. McLaughlin (2011), Towards recognition of physical and geochemical change in Subarctic and Arctic Seas, *Prog. Oceanogr.*, *90*(1), 90–104, doi:10.1016/j.pocean.2011.02.007.

Carmack, E., and P. Wassmann (2006), Food webs and physical–biological coupling on pan-Arctic shelves: Unifying concepts and comprehensive perspectives, *Prog. Oceanogr.*, *71*(2–4), 446–477, doi:10.1016/j.pocean.2006.10.004.

Carmack, E., D. Barber, J. Christensen, R. Macdonald, B. Rudels, and E. Sakshaug (2006), Climate variability and physical forcing of the food webs and the carbon budget on panarctic shelves, *Prog. Oceanogr.*, *71*(2), 145–181, doi:10.1016/j.pocean.2006.10.005.

Carmack, E., P. Winsor, and W. Williams (2015), The contiguous panarctic Riverine Coastal Domain: A unifying concept, *Prog. Oceanogr.*, *139*, 13–23, doi:10.1016/j.pocean.2015.07.014.

Carmack, E. C. et al. (2016), Freshwater and its role in the Arctic Marine System: Sources, disposition, storage, export, and physical and biogeochemical consequences in the Arctic and global oceans, *J. Geophys. Res. Biogeosciences*, *121*(3), 675–717, doi:10.1002/2015JG003140.

Cavan, E. L., F. A. C. Le Moigne, A. J. Poulton, G. A. Tarling, P. Ward, C. J. Daniels, G. Fragoso, and R. Sanders (2015), Attenuation of particulate organic carbon flux in the Scotia Sea, Southern Ocean, is controlled by zooplankton fecal pellets, *Geophys. Res. Lett.*, *42*, 821–830, doi:10.1002/2014GL062744.

Cavan, E. L., S. A. Henson, A. Belcher, and R. Sanders (2017), Role of zooplankton in determining the efficiency of the biological carbon pump, *Biogeosciences*, *14*, 177–186, doi:10.5194/bg-14-177-2017.

Ceballos-Romero, E., F. A. C. Le Moigne, S. Henson, C. M. Marsay, R. J. Sanders, R. García-Tenorio, and M. Villa-Alfageme (2016), Influence of bloom dynamics on Particle Export Efficiency in the North Atlantic: a comparative study of radioanalytical techniques and sediment traps, *Mar. Chem.*, *186*, 198–210, doi:10.1016/j.marchem.2016.10.001.

Cedhagen, T., W. Cheah, A. Bracher, and F. Lejzerowicz (2014), Algal pigments in Southern Ocean abyssal foraminiferans indicate pelagobenthic coupling, *Deep Sea Res. Part II Top. Stud. Oceanogr.*, *108*, 27–32, doi:10.1016/j.dsr2.2014.07.017.

Charette, M. A., and K. O. Buesseler (2000), Does iron fertilization lead to rapid carbon export in the Southern Ocean?, *Geochemistry, Geophys. Geosystems*, *1*(10), 1–7, doi:10.1029/2000GC000069.

Cheah, W., M. A. Soppa, S. Wiegmann, S. Ossebaar, L. M. Laglera, V. H. Strass, J. Santos-Echeandía, M. Hoppema, D. Wolf-Gladrow, and A. Bracher (2017), Importance of deep-mixing and silicic acid in regulating phytoplankton biomass and community in the iron-limited Antarctic Polar Front region in summer, *Deep Sea Res. Part II Top. Stud. Oceanogr.*, *138*, 74–85, doi:10.1016/j.dsr2.2016.05.019.

Chen, J. H., R. Lawrence Edwards, and G. J. Wasserburg (1986), ^{238}U, ^{234}U and ^{232}Th in seawater, *Earth Planet. Sci. Lett.*, *80*, 241–251.

Chen, M., Y. Huang, P. Cai, and L. Guo (2003), Particulate organic carbon export fluxes in the Canada Basin and Bering Sea as derived from ^{234}Th/^{238}U disequilibria, *ARCTIC*, *56*(1), 32–44, doi:10.14430/arctic600.

Chen, M., Q. Ma, L. Guo, Y. Qiu, Y. Li, and W. Yang (2012), Importance of lateral transport processes to ^{210}Pb budget in the eastern Chukchi Sea during summer 2003, *Deep Sea Res. Part II Top. Stud. Oceanogr.*, *81–84*, 53–62, doi:10.1016/j.dsr2.2012.03.011.

Cherrier, J., W. C. Burnett, and P. A. LaRock (1995), Uptake of polonium and sulfur by bacteria, *Geomicrobiol. J.*, *13*(2), 103–115, doi:10.1080/01490459509378009.

Choppin, G. R., and P. J. Wong (1998), The chemistry of actinide behavior in marine systems, *Aquat. Geochemistry*, *4*(1), 77–101, doi:10.1023/A:1009679303073.

Chung, Y. (1987), ^{210}Pb in the western Indian Ocean: distribution, disequilibrium, and partitioning between dissolved and particulate phases, *Earth Planet. Sci. Lett.*, *85*(1–3), 28–40, doi:10.1016/0012-821X(87)90018-5.

Chung, Y., and T. Wu (2005), Large ^{210}Po deficiency in the northern South China Sea, *Cont. Shelf Res.*, *25*(10), 1209–1224, doi:10.1016/j.csr.2004.12.016.

Church, T. et al. (2012), Intercalibration studies of ^{210}Po and ^{210}Pb in dissolved and particulate seawater samples, *Limnol. Oceanogr. Methods*, *10*, 776–789, doi: 10.4319/lom.2012.10.776.

Church, T. M., and M. M. Sarin (2008), U- and Th-series nuclides in the atmosphere: Supply, exchange, scavenging, and applications to aquatic processes, in *U-Th series nuclides in aquatic systems*, edited by S. Krishnaswami and J. K. Cochran, pp. 11–47, Elsevier Science.

Coale, K. H., and K. W. Bruland (1985), ^{234}Th:^{238}U disequilibria within the California Current, *Limnol. Oceanogr.*, *30*(1), 22–33, doi:10.4319/lo.1985.30.1.0022.

Coale, K. H., and K. W. Bruland (1987), Oceanic stratified euphotic zone as elucidated by ^{234}Th:^{238}U disequilibria, *Limnol. Oceanogr.*, *32*(1), 189–200, doi:10.4319/lo.1987.32.1.0189.

Coale, K. H. et al. (2004), Southern Ocean iron enrichment experiment: carbon cycling in high- and low-Si waters, *Science*, *304*(5669), 408–14, doi:10.1126/science.1089778.

Cochran, J. K., and P. Masqué (2003), Short-lived U/Th series radionuclides in the ocean: Tracers for scavenging rates, export fluxes and particle dynamics, *Rev. Mineral. Geochemistry*, *52*(1), 461–492, doi:10.2113/0520461.

Cochran, J. K., M. P. Bacon, S. Krishnaswami, and K. K. Turekian (1983), ^{210}Po and ^{210}Pb distributions in the central and eastern Indian Ocean, *Earth Planet. Sci. Lett.*, *65*(2), 433–452, doi:10.1016/0012-821X(83)90180-2.

Cochran, J. K., T. McKibbin-Vaughan, M. M. Dornblaser, D. Hirschberg, H. D. Livingston, and K. O. Buesseler (1990), ^{210}Pb scavenging in the North Atlantic and North Pacific Oceans, *Earth Planet. Sci. Lett.*, *97*(3–4), 332–352, doi:10.1016/0012-821X(90)90050-8.

Cochran, J. K., D. J. Hirschberg, H. D. Livingston, K. O. Buesseler, and R. M. Key (1995a), Natural and anthropogenic radionuclide distributions in the Nansen Basin, Arctic Ocean: Scavenging rates and circulation timescales, *Deep Sea Res. Part II Top. Stud. Oceanogr.*, *42*(6), 1495–1517, doi:10.1016/0967-0645(95)00051-8.

Cochran, J. K., C. Barnes, D. Achman, and D. J. Hirschberg (1995b), Thorium-234/Uranium-238 disequilibrium as an indicator of scavenging rates and particulate organic carbon fluxes in the Northeast Water Polynya, Greenland, *J. Geophys. Res.*, *100*(C3), 4399–4410, doi:10.1029/94JC01954.

Cochran, J. K., K. O. Buesseler, M. P. Bacon, H. W. Wang, D. J. Hirschberg, L. Ball, J. Andrews, G. Crossin, and A. Fleer (2000), Short-lived thorium isotopes (Th-234, Th-228) as indicators of POC export and particle cycling in the Ross Sea, Southern Ocean, *Deep Sea Res. Part II Top. Stud. Oceanogr.*, *47*(15–16), 3451–3490, doi:10.1016/S0967-0645(00)00075-8.

Codispoti, L. A., V. Kelly, A. Thessen, P. Matrai, S. Suttles, V. Hill, M. Steele, and B. Light (2013), Synthesis of primary production in the Arctic Ocean: III. Nitrate and phosphate based estimates of net community production, *Prog. Oceanogr.*, *110*, 126–150, doi:10.1016/j.pocean.2012.11.006.

Comiso, J. C., C. L. Parkinson, R. Gersten, and L. Stock (2008), Accelerated decline in the Arctic sea ice cover, *Geophys. Res. Lett.*, *35*(1), L01703, doi:10.1029/2007GL031972.

Coppola, L., M. Roy-Barman, P. Wassmann, S. Mulsow, and C. Jeandel (2002), Calibration of sediment traps and particulate organic carbon export using ^{234}Th in the Barents Sea, *Mar. Chem.*, *80*(1), 11–26, doi:10.1016/S0304-4203(02)00071-3.

Coppola, L., M. Roy-Barman, S. Mulsow, P. Povinec, and C. Jeandel (2005), Low particulate organic carbon export in the frontal zone of the Southern Ocean (Indian sector) revealed by ^{234}Th, *Deep Sea Res. Part I Oceanogr. Res. Pap.*, *52*(1), 51–68, doi:10.1016/j.dsr.2004.07.020.

Cota, G. F., and R. E. . Smith (1991), Ecology of bottom ice algae: II. Dynamics, distributions and productivity, *J. Mar. Syst.*, *2*(3–4), 279–295, doi:10.1016/0924-7963(91)90037-U.

Dai, A., and K. E. Trenberth (2002), Estimates of Freshwater Discharge from Continents: Latitudinal and Seasonal Variations, *J. Hydrometeorol.*, *3*(6), 660–687, doi:10.1175/1525-7541(2002)003<0660:EOFDFC>2.0.CO;2.

David, C., B. Lange, B. Rabe, and H. Flores (2015), Community structure of under-ice fauna in the Eurasian central Arctic Ocean in relation to environmental properties of sea-ice habitats, *Mar. Ecol. Prog. Ser.*, *522*, 15–32, doi: 10.3354/meps11156.

Death, R., J. L. Wadham, F. Monteiro, A. M. Le Brocq, M. Tranter, A. Ridgwell, S. Dutkiewicz, and R. Raiswell (2014), Antarctic ice sheet fertilises the Southern Ocean, *Biogeosciences*, *11*, 2635–2644, doi:10.5194/bg-11-2635-2014.

Doney, S. C. et al. (2012), Climate change impacts on marine ecosystems, *Ann. Rev. Mar. Sci.*, *4*, 11–37, doi:10.1146/annurev-marine-041911-111611.

Downs, J. (1989), Export of production in oceanic systems: information from phaeopigment, carbon and nitrogen analyses, PhD thesis, University of Washington, Seattle.

Ducklow, H., D. K. Steinberg, and K. O. Buesseler (2001), Upper ocean carbon export and the biological pump, *Oceanography*, *14*(4), 50–58.

Dugdale, R. C., and J. J. Goering (1967), Uptake of new and regenerated forms of nitrogen in primary productivity, *Limnol. Oceanogr.*, *12*(2), 196–206, doi:10.4319/lo.1967.12.2.0196.

Dunne, J. P., R. A. Armstrong, A. Gnanadesikan, and J. L. Sarmiento (2005), Empirical and mechanistic models for the particle export ratio, *Global Biogeochem. Cycles*, *19*(4), GB4026, doi:10.1029/2004GB002390.

Durkin, C. A., M. L. Estapa, and K. O. Buesseler (2015), Observations of carbon export by small sinking particles in the upper mesopelagic, *Mar. Chem.*, *175*, 72–81, doi:10.1016/j.marchem.2015.02.011.

Ebersbach, F., and T. W. Trull (2008), Sinking particle properties from polyacrylamide gels during the KErguelen Ocean and Plateau compared Study (KEOPS): Zooplankton control of carbon export in an area of persistent natural iron inputs in the Southern Ocean, *Limnol. Oceanogr.*, *53*(1), 212–224, doi:10.4319/lo.2008.53.1.0212.

Ebersbach, F., T. W. Trull, D. M. Davies, and S. G. Bray (2011), Controls on mesopelagic particle fluxes in the Sub-Antarctic and Polar Frontal Zones in the Southern Ocean south of Australia in summer - Perspectives from free-drifting sediment traps, *Deep Sea Res. Part II Top. Stud. Oceanogr.*, *58*(21–22), 2260–2276, doi:10.1016/j.dsr2.2011.05.025.

Ebersbach, F., P. Assmy, P. Martin, I. Schulz, S. Wolzenburg, and E.-M. Nöthig (2014), Particle flux characterisation and sedimentation patterns of protistan plankton during the iron fertilisation experiment LOHAFEX in the Southern Ocean, *Deep Sea Res. Part I Oceanogr. Res. Pap.*, *89*, 94–103, doi:10.1016/j.dsr.2014.04.007.

Ehrlich, J. (2015), Diversity and distribution of high-Arctic zooplankton in the Eurasian Basin in late summer 2012, Master thesis, University of Hamburg, Alfred Wegener Institute.

Eicken, H., E. Reimnitz, V. Alexandrov, T. Martin, H. Kassens, and T. Viehoff (1997), Sea-ice processes in the Laptev Sea and their importance for sediment export, *Cont. Shelf Res.*, *17*(2), 205–233, doi:10.1016/S0278-4343(96)00024-6.

Ellingsen, I. H., P. Dalpadado, D. Slagstad, and H. Loeng (2008), Impact of climatic change on the biological production in the Barents Sea, *Clim. Change*, *87*(1–2), 155–175, doi:10.1007/s10584-007-9369-6.

Emil Ruff, S., D. Probandt, A.-C. Zinkann, M. H. Iversen, C. Klaas, N. Krombholz, D. Wolf-Gladrow, R. Amann, and K. Knittel (2014), Indications for algae-degrading benthic microbial communities in deep-sea sediments along the Antarctic Polar Front, *Deep Sea Res. Part II Top. Stud. Oceanogr.*, *108*, 6–16, doi:10.1016/j.dsr2.2014.05.011.

Eppley, R. (1989), New production: history, methods, problems, in *Productivity of the ocean: Present and past*, edited by W. Berger, V. Smetacek, and G. Wefer, pp. 85–97, John Wiley and Sons, New York.

Eppley, R., and B. Peterson (1979), Particulate organic matter flux and planktonic new production in the deep ocean, *Nature*, *282*, 677–680, doi:10.1038/282677a0.

Fahl, K., and E.-M. Nöthig (2007), Lithogenic and biogenic particle fluxes on the Lomonosov Ridge (central Arctic Ocean) and their relevance for sediment accumulation: Vertical vs. lateral transport, *Deep Sea Res. Part I Oceanogr. Res. Pap.*, *54*(8), 1256–1272, doi:10.1016/j.dsr.2007.04.014.

Falk-Petersen, S., P. Mayzaud, G. Kattner, and J. R. Sargent (2009), Lipids and life strategy of Arctic *Calanus*, *Mar. Biol. Res.*, *5*(1), 18–39, doi:10.1080/17451000802512267.

Falkowski, P. G., R. T. Barber, and V. Smetacek (1998), Biogeochemical controls and feedbacks on ocean primary production, *Science*, *281*(5374), 200–206, doi:10.1126/science.281.5374.200.

Fernández-Méndez, M., F. Wenzhöfer, I. Peeken, H. L. Sørensen, R. N. Glud, and A. Boetius (2014), Composition, buoyancy regulation and fate of ice algal aggregates in the Central Arctic Ocean, *PLoS One*, *9*(9), e107452, doi:10.1371/journal.pone.0107452.

Fernández-Méndez, M., C. Katlein, B. Rabe, M. Nicolaus, I. Peeken, K. Bakker, H. Flores, and A. Boetius (2015), Photosynthetic production in the central Arctic Ocean during the record sea-ice minimum in 2012, *Biogeosciences*, *12*(11), 3525–3549, doi:10.5194/bg-12-3525-2015.

Findlay, H., F. Cottier, N. Morata, R. Hindshaw, A. Nikolopoulos, M. Ardyna, C. März, B. Queguiner, M. Roca-Martí, and S. Bourgois (2015a), *Arctic oceanography - oceanography: Atmosphere-ocean exchange, biogeochemistry* & *physics*, Arctic in Rapid Transition, Brest.

Findlay, H. S. et al. (2015b), Responses in Arctic marine carbon cycle processes: Conceptual scenarios and implications for ecosystem function, *Polar Res.*, *34*(1), 24252, doi:10.3402/polar.v34.24252.

Fisher, N. S., K. A. Burns, R. D. Cherry, and M. Heyraud (1983), Accumulation and cellular distribution of ^{241}Am, ^{210}Po and ^{210}Pb in two marine algae, *Mar. Ecol. Prog. Ser.*, *11*(3), 233–237.

Fitzwater, S. E., K. S. Johnson, R. M. Gordon, K. H. Coale, and W. O. Smith (2000), Trace metal concentrations in the Ross Sea and their relationship with nutrients and phytoplankton growth, *Deep Sea Res. Part II Top. Stud. Oceanogr.*, *47*(15), 3159–3179, doi:10.1016/S0967-0645(00)00063-1.

Fleer, A. P., and M. P. Bacon (1984), Determination of ^{210}Pb and ^{210}Po in seawater and marine particulate matter, *Nucl. Instruments Methods Phys. Res.*, *223*(2–3), 243–249, doi:10.1016/0167-5087(84)90655-0.

Flores, H. et al. (2012), Impact of climate change on Antarctic krill, *Mar. Ecol. Prog. Ser.*, *458*, 1–19, doi:10.3354/meps09831.

Flynn, W. W. (1968), The determination of low levels of polonium-210 in environmental materials, *Anal. Chim. Acta*, *43*(2), 221–227, doi: 10.1016/S0003-2670(00)89210-7.

Forest, A., M. Sampei, H. Hattori, R. Makabe, H. Sasaki, M. Fukuchi, P. Wassmann, and L. Fortier (2007), Particulate organic carbon fluxes on the slope of the Mackenzie Shelf (Beaufort Sea): Physical and biological forcing of shelf-basin exchanges, *J. Mar. Syst.*, *68*(1), 39–54, doi:10.1016/j.jmarsys.2006.10.008.

Forest, A. et al. (2011), Biogenic carbon flows through the planktonic food web of the Amundsen Gulf (Arctic Ocean): A synthesis of field measurements and inverse modeling analyses, *Prog. Oceanogr.*, *91*(4), 410–436, doi:10.1016/j.pocean.2011.05.002.

Fortier, M., L. Fortier, C. Michiel, and L. Legendre (2002), Climatic and biological forcing of the vertical flux of biogenic particles under seasonal Arctic sea ice, *Mar. Ecol. Prog. Ser.*, *225*, 1–16, doi:10.3354/meps225001.

Le Fouest, V., M. Babin, and J.-É. Tremblay (2013), The fate of riverine nutrients on Arctic shelves, *Biogeosciences*, *10*, 3661– 3677, doi:10.5194/bg-10-3661-2013.

Fowler, S. W. (2011), ^{210}Po in the marine environment with emphasis on its behaviour within the biosphere, *J. Environ. Radioact.*, *102*(5), 448–461, doi:10.1016/j.jenvrad.2010.10.008.

Fowler, S. W., and G. A. Knauer (1986), Role of large particles in the transport of elements and organic compounds through the oceanic water column, *Prog. Oceanogr.*, *16*(3), 147–194, doi:10.1016/0079-6611(86)90032-7.

Frankignoulle, M., C. Canon, and J.-P. Gattuso (1994), Marine calcification as a source of carbon dioxide: Positive feedback of increasing atmospheric CO_2, *Limnol. Oceanogr.*, *39*(2), 458–462, doi:10.4319/lo.1994.39.2.0458.

Friedrich, J. (2011), Polonium-210 and Lead-210 activities measured on 17 water bottle profiles and 50 surface water samples during POLARSTERN cruise ARK-XXII/2, *Alfred Wegener Institute, Helmholtz Cent. Polar Mar. Res. Bremerhaven*, doi:10.1594/PANGAEA.763937.

Friedrich, J., and M. M. Rutgers van der Loeff (2002), A two-tracer (^{210}Po–^{234}Th) approach to distinguish organic carbon and biogenic silica export flux in the Antarctic Circumpolar Current, *Deep Sea Res. Part I Oceanogr. Res. Pap.*, *49*(1), 101–120, doi:10.1016/S0967-0637(01)00045-0.

Frigstad, H., T. Andersen, R. G. J. Bellerby, A. Silyakova, and D. O. Hessen (2014), Variation in the seston C:N ratio of the Arctic Ocean and pan-Arctic shelves, *J. Mar. Syst.*, *129*, 214–223, doi:10.1016/j.jmarsys.2013.06.004.

Geibert, W., M. M. Rutgers van der Loeff, R. Usbeck, R. Gersonde, G. Kuhn, and J. Seeberg-Elverfeldt (2005), Quantifying the opal belt in the Atlantic and southeast Pacific sector of the Southern Ocean by means of ^{230}Th normalization, *Global Biogeochem. Cycles*, *19*(4), GB4001, doi:10.1029/2005GB002465.

Gervais, F., U. Riebesell, and M. Y. Gorbunov (2002), Changes in primary productivity and chlorophyll a in response to iron fertilization in the Southern Polar Frontal Zone, *Limnol. Oceanogr.*, *47*(5), 1324–1335, doi:10.4319/lo.2002.47.5.1324.

Giering, S. L. C. et al. (2014), Reconciliation of the carbon budget in the ocean's twilight zone, *Nature*, *507*, 480–483, doi:10.1038/nature13123.

Gille, S. T. (2002), Warming of the Southern Ocean since the 1950s, *Science*, *295*(5558), 1275–1277, doi:10.1126/science.1065863.

Gille, S. T. (2008), Decadal-scale temperature trends in the Southern Hemisphere ocean, *J. Clim.*, *21*, 4749–4765, doi:10.1175/2008JCLI2131.1.

Gosselin, M., M. Levasseur, P. A. Wheeler, R. A. Horner, and B. C. Booth (1997), New measurements of phytoplankton and ice algal production in the Arctic Ocean, *Deep Sea Res. Part II Top. Stud. Oceanogr.*, *44*(8), 1623–1644, doi:10.1016/S0967-0645(97)00054-4.

Gradinger, R., C. Friedrich, and M. Spindler (1999), Abundance, biomass and composition of the sea ice biota of the Greenland Sea pack ice, *Deep Sea Res. Part II Top. Stud. Oceanogr.*, *46*(6–7), 1457–1472, doi:10.1016/S0967-0645(99)00030-2.

Grebmeier, J. M. (2012), Shifting patterns of life in the Pacific Arctic and sub-Arctic seas, *Ann. Rev. Mar. Sci.*, *4*, 63–78, doi:10.1146/annurev-marine-120710-100926.

Grebmeier, J. M., L. W. Cooper, H. M. Feder, and B. I. Sirenko (2006), Ecosystem dynamics of the Pacific-influenced Northern Bering and Chukchi Seas in the Amerasian Arctic, *Prog. Oceanogr.*, *71*(2), 331–361, doi:10.1016/j.pocean.2006.10.001.

Grenfell, T. C., B. Light, and D. K. Perovich (2006), Spectral transmission and implications for the partitioning of shortwave radiation in arctic sea ice, *Ann. Glaciol.*, *44*(1), 1–6, doi:10.3189/172756406781811763.

Gruber, N., and J. L. Sarmiento (2002), Large scale biochemical-physical interactions in elemental cycles, in *The sea: biological-physical interactions in the oceans*, edited by A. Robinson, J. McCarthy, and B. Rothschild, pp. 337–399, John Wiley and Sons, New York.

Gruber, N. et al. (2009), Oceanic sources, sinks, and transport of atmospheric CO_2, *Global Biogeochem. Cycles*, *23*(1), GB1005, doi:10.1029/2008GB003349.

Guidi, L., L. Stemmann, G. A. Jackson, F. Ibanez, H. Claustre, L. Legendre, M. Picheral, and G. Gorsky (2009), Effects of phytoplankton community on production, size and export of large aggregates: A world-ocean analysis, *Limnol. Oceanogr.*, *54*(6), 1951–1963, doi:10.4319/lo.2009.54.6.1951.

Guidi, L., L. Legendre, G. Reygondeau, J. Uitz, L. Stemmann, and S. A. Henson (2015), A new look at ocean carbon remineralization for estimating deepwater sequestration, *Global Biogeochem. Cycles*, *29*(7), 1044–1059, doi:10.1002/2014GB005063.

Gustafsson, Ö., and P. S. Andersson (2012), ^{234}Th-derived surface export fluxes of POC from the Northern Barents Sea and the Eurasian sector of the Central Arctic Ocean, *Deep Sea Res. Part I Oceanogr. Res. Pap.*, *68*, 1–11, doi:10.1016/j.dsr.2012.05.014.

Gustafsson, Ö., P. Andersson, P. Roos, Z. Kukulska, D. Broman, U. Larsson, S. Hajdu, and J. Ingri (2004), Evaluation of the collection efficiency of upper ocean sub-photic-layer sediment traps: a 24-month in situ calibration in the open Baltic Sea using ^{234}Th, *Limnol. Oceanogr. Methods*, *2*, 62–74, doi:10.4319/lom.2004.2.62.

Haas, C., A. Pfaffling, S. Hendricks, L. Rabenstein, J.-L. Etienne, and I. Rigor (2008), Reduced ice thickness in Arctic Transpolar Drift favors rapid ice retreat, *Geophys. Res. Lett.*, *35*, L17501, doi:10.1029/2008GL034457.

Haine, T. W. N. et al. (2015), Arctic freshwater export: Status, mechanisms, and prospects, *Glob. Planet. Change*, *125*, 13–35, doi:10.1016/j.gloplacha.2014.11.013.

Hansell, D. A., C. A. Carlson, D. J. Repeta, and R. Schlitzer (2009), Dissolved organic matter in the ocean: a controversy stimulates new insights, *Oceanography*, *22*(4), 202–211, doi:10.5670/oceanog.2009.109.

Hansen, A. N., and A. W. Visser (2016), Carbon export by vertically migrating zooplankton: an optimal behavior model, *Limnol. Oceanogr.*, *61*(2), 701–710, doi:10.1002/lno.10249.

Harada, N. (2016), Review: Potential catastrophic reduction of sea ice in the western Arctic Ocean: Its impact on biogeochemical cycles and marine ecosystems, *Glob. Planet. Change*, *136*, 1–17, doi:10.1016/j.gloplacha.2015.11.005.

Haskell, W. Z., W. M. Berelson, D. E. Hammond, and D. G. Capone (2013), Particle sinking dynamics and POC fluxes in the Eastern Tropical South Pacific based on ^{234}Th budgets and sediment trap deployments, *Deep Sea Res. Part I Oceanogr. Res. Pap.*, *81*, 1–13, doi:10.1016/j.dsr.2013.07.001.

Hauck, J., C. Völker, T. Wang, M. Hoppema, M. Losch, and D. A. Wolf-Gladrow (2013), Seasonally different carbon flux changes in the Southern Ocean in response to the southern annular mode, *Global Biogeochem. Cycles*, *27*(4), 1236–1245, doi:10.1002/2013GB004600.

Henson, S. A., R. Sanders, E. Madsen, P. J. Morris, F. Le Moigne, and G. D. Quartly (2011), A reduced estimate of the strength of the ocean's biological carbon pump, *Geophys. Res. Lett.*, *38*(4), L04606, doi:10.1029/2011GL046735.

Henson, S. A., R. Sanders, and E. Madsen (2012), Global patterns in efficiency of particulate organic carbon export and transfer to the deep ocean, *Global Biogeochem. Cycles*, *26*(1), GB1028, doi:10.1029/2011GB004099.

Henson, S. A., A. Yool, and R. Sanders (2015), Variability in efficiency of particulate organic carbon export: A model study, *Global Biogeochem. Cycles*, *29*(1), 33–45, doi:10.1002/2014GB004965.

Higgins, H. W., S. W. Wright, and L. Schlüter (2011), Quantitative interpretation of chemotaxonomic pigment data, in *Phytoplankton pigments. Characterization, chemotaxonomy and applications in oceanography*, edited by S. Roy, C. Llewellyn, E. S. Egeland, and G. Johnsen, pp. 257–313, Cambridge University Press, Cambridge.

Hill, V. J., P. A. Matrai, E. Olson, S. Suttles, M. Steele, L. A. Codispoti, and R. C. Zimmerman (2013), Synthesis of integrated primary production in the Arctic Ocean: II. In situ and remotely sensed estimates, *Prog. Oceanogr.*, *110*, 107–125, doi:10.1016/j.pocean.2012.11.005.

Hirata, T. et al. (2011), Synoptic relationships between surface Chlorophyll-*a* and diagnostic pigments specific to phytoplankton functional types, *Biogeosciences*, *8*(2), 311–327, doi:10.5194/bg-8-311-2011.

Hoffmann, L., I. Peeken, K. Lochte, P. Assmy, and M. Veldhuis (2006), Different reactions of Southern Ocean phytoplankton size classes to iron fertilization, *Limnol. Oceanogr.*, *51*(3), 1217–1229, doi:10.4319/lo.2006.51.3.1217.

Holmes, R. M. et al. (2012), Seasonal and annual fluxes of nutrients and organic matter from large rivers to the Arctic Ocean and surrounding seas, *Estuaries and Coasts*, *35*(2), 369–382, doi:10.1007/s12237-011-9386-6.

Hong, G. H., M. Baskaran, T. M. Church, and M. Conte (2013), Scavenging, cycling and removal fluxes of ^{210}Po and ^{210}Pb at the Bermuda time-series study site, *Deep Sea Res. Part II Top. Stud. Oceanogr.*, *93*, 108–118, doi:10.1016/j.dsr2.2013.01.005.

Honjo, S., S. J. Manganini, R. A. Krishfield, and R. Francois (2008), Particulate organic carbon fluxes to the ocean interior and factors controlling the biological pump: A synthesis of global sediment trap programs since 1983, *Prog. Oceanogr.*, *76*(3), 217–285, doi:10.1016/j.pocean.2007.11.003.

Honjo, S., R. A. Krishfield, T. I. Eglinton, S. J. Manganini, J. N. Kemp, K. Doherty, J. Hwang, T. K. McKee, and T. Takizawa (2010), Biological pump processes in the cryopelagic and hemipelagic Arctic Ocean: Canada Basin and Chukchi Rise, *Prog. Oceanogr.*, *85*(3–4), 137–170, doi:10.1016/j.pocean.2010.02.009.

Honjo, S. et al. (2014), Understanding the role of the biological pump in the global carbon cycle: an imperative for ocean science, *Oceanography*, *27*(3), 10–16, doi:10.5670/oceanog.2014.78.

Hoppe, C. J. M. et al. (2017), Controls of primary production in two phytoplankton blooms in the Antarctic Circumpolar Current, *Deep Sea Res. Part II Top. Stud. Oceanogr.*, *138*(63–73), doi:10.1016/j.dsr2.2015.10.005.

Horvat, C., D. R. Jones, S. Iams, D. Schroeder, D. Flocco, and D. Feltham (2017), The frequency and extent of sub-ice phytoplankton blooms in the Arctic Ocean, *Sci. Adv.*, *3*(3), e1601191, doi:10.1126/sciadv.1601191.

Hu, W., M. Chen, W. Yang, R. Zhang, Y. Qiu, and M. Zheng (2014), Low ^{210}Pb in the upper thermocline in the Canadian Basin: scavenge process over the Chukchi Sea, *Acta Oceanol. Sin.*, *33*(6), 28–39, doi:10.1007/s13131-014-0486-6.

Hunt, G. L. et al. (2016), Advection in polar and sub-polar environments: Impacts on high latitude marine ecosystems, *Prog. Oceanogr.*, *149*, 40–81, doi:10.1016/j.pocean.2016.10.004.

IPCC (2013), *Climate change 2013: the physical science basis. Contribution of working group I to the fifth assessment report of the Intergovernmental Panel on Climate Change*, edited by T. F. Stocker, D. Qin, G.-K. Plattner, M. Tignor, S. K. Allen, J. Boschung, A. Nauels, Y. Xia, V. Bex, and P. M. Midgley, Cambridge University Press, Cambridge and New York.

Iversen, M. H., and C. Klaas (2013), Controls on the vertical fluxes of the Southern Ocean, in *The expedition of the research vessel "Polarstern" to the Antarctic in 2012 (ANT-XXVIII/3)*, pp. 70–74, Bremerhaven.

Iversen, M. H., and H. Ploug (2013), Temperature effects on carbon-specific respiration rate and sinking velocity of diatom aggregates – potential implications for deep ocean export processes, *Biogeosciences*, *10*(6), 4073–4085, doi:10.5194/bg-10-4073-2013.

Iversen, M. H., and M. L. Robert (2015), Ballasting effects of smectite on aggregate formation and export from a natural plankton community, *Mar. Chem.*, *175*, 18–27, doi:10.1016/j.marchem.2015.04.009.

Iversen, M. H., N. Nowald, H. Ploug, G. A. Jackson, and G. Fischer (2010), High resolution profiles of vertical particulate organic matter export off Cape Blanc, Mauritania: Degradation processes and ballasting effects, *Deep Sea Res. Part I Oceanogr. Res. Pap.*, *57*(6), 771–784, doi:10.1016/j.dsr.2010.03.007.

Iversen, M. H., E. A. Pakhomov, B. P. V. Hunt, H. van der Jagt, D. Wolf-Gladrow, and C. Klaas (2017), Sinkers or floaters? Contribution from salp pellets to the export flux during a large bloom event in the Southern Ocean, *Deep Sea Res. Part II Top. Stud. Oceanogr.*, *138*, 116–125, doi:10.1016/j.dsr2.2016.12.004.

Jackson, G. A., D. M. Checkley, and M. Dagg (2015), Settling of particles in the upper 100 m of the ocean detected with autonomous profiling floats off California, *Deep Sea Res. Part I Oceanogr. Res. Pap.*, *99*, 75–86, doi:10.1016/j.dsr.2015.02.001.

Jacquet, S. H. M., P. J. Lam, T. Trull, and F. Dehairs (2011), Carbon export production in the subantarctic zone and polar front zone south of Tasmania, *Deep Sea Res. Part II Top. Stud. Oceanogr.*, *58*(21–22), 2277–2292, doi:10.1016/j.dsr2.2011.05.035.

Jannasch, H. W., O. C. Zafiriou, and J. W. Farrington (1980), A sequencing sediment trap for time-series studies of fragile particles, *Limnol. Oceanogr.*, *25*(5), 939–943, doi:10.4319/lo.1980.25.5.0939.

Jeffrey, S. W., R. F. C. Mantoura, and T. Bjørnland (1997), Data for the identification of 47 key phytoplankton pigments, in *Phytoplankton pigments in oceanography: guidelines to modern methods*, edited by S. W. Jeffrey, R. F. C. Mantoura, and S. W. Wright, pp. 449–559, Cambridge University Press, Paris.

Jenkins, W. J., and D. W. R. Wallace (1992), Tracer based inferences of new primary production in the sea, in *Primary productivity and biogeochemical cycles in the sea*, pp. 299–316, Springer US, Boston, MA.

Juul-Pedersen, T., T. Nielsen, C. Michel, E. Friis Møller, P. Tiselius, P. Thor, M. Olesen, E. Selander, and S. Gooding (2006), Sedimentation following the spring bloom in Disko Bay, West Greenland, with special emphasis on the role of copepods, *Mar. Ecol. Prog. Ser.*, *314*, 239–255, doi:10.3354/meps314239.

Juul-Pedersen, T., C. Michel, M. Gosselin, and L. Seuthe (2008), Seasonal changes in the sinking export of particulate material under first-year sea ice on the Mackenzie Shelf (western Canadian Arctic), *Mar. Ecol. Prog. Ser.*, *353*, 13–25, doi:10.3354/meps07165.

Katlein, C., M. Fernández-Méndez, F. Wenzhöfer, and M. Nicolaus (2014), Distribution of algal aggregates under summer sea ice in the Central Arctic, *Polar Biol.*, *38*(5), 719–731, doi:10.1007/s00300-014-1634-3.

Kawaguchi, Y., J. K. Hutchings, T. Kikuchi, J. H. Morison, and R. A. Krishfield (2012), Anomalous sea-ice reduction in the Eurasian Basin of the Arctic Ocean during summer 2010, *Polar Sci.*, *6*(1), 39–53, doi:10.1016/j.polar.2011.11.003.

Kilias, E., C. Wolf, E.-M. Nöthig, I. Peeken, and K. Metfies (2013), Protist distribution in the Western Fram Strait in summer 2010 based on 454-pyrosequencing of 18S rDNA, *J. Phycol.*, *49*(5), 996–1010, doi:10.1111/jpy.12109.

Kim, G. (2001), Large deficiency of polonium in the oligotrophic ocean's interior, *Earth Planet. Sci. Lett.*, *192*(1), 15–21, doi:10.1016/S0012-821X(01)00431-9.

Kim, G., and T. M. Church (2001), Seasonal biogeochemical fluxes of ^{234}Th and ^{210}Po in the Upper Sargasso Sea: Influence from atmospheric iron deposition, *Global Biogeochem. Cycles*, *15*(3), 651–661, doi:10.1029/2000GB001313.

Kiørboe, T. (2001), Formation and fate of marine snow: small-scale processes with large-scale implications, *Sci. Mar.*, *65*, 57–71, doi:10.3989/scimar.2001.65s257.

Kirchman, D. L., X. A. G. Morán, and H. Ducklow (2009), Microbial growth in the polar oceans - role of temperature and potential impact of climate change, *Nat. Rev. Microbiol.*, *7*(6), 451–459, doi:10.1038/nrmicro2115.

Klaas, C., and D. E. Archer (2002), Association of sinking organic matter with various types of mineral ballast in the deep sea: Implications for the rain ratio, *Global Biogeochem. Cycles*, *16*(4), 1116, doi:10.1029/2001GB001765.

Klunder, M. B., D. Bauch, P. Laan, H. J. W. de Baar, S. van Heuven, and S. Ober (2012), Dissolved iron in the Arctic shelf seas and surface waters of the central Arctic Ocean: Impact of Arctic river water and ice-melt, *J. Geophys. Res. Ocean.*, *117*, C01027, doi:10.1029/2011JC007133.

Knap, A., A. Michaels, A. Close, H. Ducklow, and A. Dickson (1996), *Protocols for the Joint Global Ocean Flux Study (JGOFS) core measurements. JGOFS Report Nr. 19*.

Korhonen, M., B. Rudels, M. Marnela, A. Wisotzki, and J. Zhao (2013), Time and space variability of freshwater content, heat content and seasonal ice melt in the Arctic Ocean from 1991 to 2011, *Ocean Sci.*, *9*(6), 1015–1055, doi:10.5194/os-9-1015-2013.

Kosobokova, K., and H.-J. Hirche (2009), Biomass of zooplankton in the eastern Arctic Ocean – A base line study, *Prog. Oceanogr.*, *82*(4), 265–280, doi:10.1016/j.pocean.2009.07.006.

Kramer, M., and R. Kiko (2011), Brackish meltponds on Arctic sea ice - a new habitat for marine metazoans, *Polar Biol.*, *34*(4), 603–608, doi:10.1007/s00300-010-0911-z.

Krishnaswami, S., and J. K. Cochran (2008), Introduction, in *U-Th series nuclides in aquatic systems*, edited by S. Krishnaswami and J. K. Cochran, pp. 1–10, Elsevier Science.

Kritzberg, E. S., C. M. Duarte, and P. Wassmann (2010), Changes in Arctic marine bacterial carbon metabolism in response to increasing temperature, *Polar Biol.*, *33*(12), 1673–1682, doi:10.1007/s00300-010-0799-7.

Ku, T.-L., and S. Luo (2008), Ocean circulation/mixing studies with decay-series isotopes, in *U-Th series nuclides in aquatic systems*, edited by S. Krishnaswami and J. K. Cochran, pp. 307–344, Elsevier Science.

Kwok, R., G. F. Cunningham, M. Wensnahan, I. Rigor, H. J. Zwally, and D. Yi (2009), Thinning and volume loss of the Arctic Ocean sea ice cover: 2003–2008, *J. Geophys. Res.*, *114*(C7), C07005, doi:10.1029/2009JC005312.

Laan, P., S. Ober, L. Boom, and K. Bakker (2008), Hydrochemistry measured on water bottle samples during POLARSTERN cruise ARK-XXII/2 (SPACE), *R. Netherlands Inst. Sea Res. Texel*, doi:10.1594/PANGAEA.708642.

De La Rocha, C. L., and U. Passow (2007), Factors influencing the sinking of POC and the efficiency of the biological carbon pump, *Deep Sea Res. Part II Top. Stud. Oceanogr.*, *54*(5), 639–658, doi:10.1016/j.dsr2.2007.01.004.

Lalande, C., J. M. Grebmeier, P. Wassmann, L. W. Cooper, M. V. Flint, and V. M. Sergeeva (2007a), Export fluxes of biogenic matter in the presence and absence of seasonal sea ice cover in the Chukchi Sea, *Cont. Shelf Res.*, *27*(15), 2051–2065, doi:10.1016/j.csr.2007.05.005.

Lalande, C., K. Lepore, L. W. Cooper, J. M. Grebmeier, and S. B. Moran (2007b), Export fluxes of particulate organic carbon in the Chukchi Sea: A comparative study using $^{234}Th/^{238}U$ disequilibria and drifting sediment traps, *Mar. Chem.*, *103*(1–2), 185–196, doi:10.1016/j.marchem.2006.07.004.

Lalande, C., S. B. Moran, P. Wassmann, J. M. Grebmeier, and L. W. Cooper (2008), ^{234}Th-derived particulate organic carbon fluxes in the northern Barents Sea with comparison to drifting sediment trap fluxes, *J. Mar. Syst.*, *73*(1–2), 103–113, doi:10.1016/j.jmarsys.2007.09.004.

Lalande, C., S. Bélanger, and L. Fortier (2009a), Impact of a decreasing sea ice cover on the vertical export of particulate organic carbon in the northern Laptev Sea, Siberian Arctic Ocean, *Geophys. Res. Lett.*, *36*(21), L21604, doi:10.1029/2009GL040570.

Lalande, C., A. Forest, D. G. Barber, Y. Gratton, and L. Fortier (2009b), Variability in the annual cycle of vertical particulate organic carbon export on Arctic shelves: Contrasting the Laptev Sea, Northern Baffin Bay and the Beaufort Sea, *Cont. Shelf Res.*, *29*(17), 2157–2165, doi:10.1016/j.csr.2009.08.009.

Lalande, C., E.-M. Nöthig, R. Somavilla, E. Bauerfeind, V. Shevchenko, and Y. Okolodkov (2014), Variability in under-ice export fluxes of biogenic matter in the Arctic Ocean, *Global Biogeochem. Cycles*, *28*(5), 571–583, doi:10.1002/2013GB004735.

Lam, P. J., and J. K. B. Bishop (2007), High biomass, low export regimes in the Southern Ocean, *Deep Sea Res. Part II Top. Stud. Oceanogr.*, *54*(5–7), 601–638, doi:10.1016/j.dsr2.2007.01.013.

Lam, P. J., S. C. Doney, and J. K. B. Bishop (2011), The dynamic ocean biological pump: Insights from a global compilation of particulate organic carbon, $CaCO_3$, and opal concentration profiles from the mesopelagic, *Global Biogeochem. Cycles*, *25*(3), GB3009, doi:10.1029/2010GB003868.

Lambert, G., G. Polian, J. Sanak, B. Ardouin, A. Buisson, A. Jegou, and J. . Le Roulley (1982), Cycle du radon et de ses descendants: application à l'étude des échanges troposphère-stratosphère, *Ann. Géophysique*, *38*, 497–531.

Lampitt, R. S., B. Boorman, L. Brown, M. Lucas, I. Salter, R. Sanders, K. Saw, S. Seeyave, S. J. Thomalla, and R. Turnewitsch (2008), Particle export from the euphotic zone: Estimates using a novel drifting sediment trap, ^{234}Th and new production, *Deep Sea Res. Part I Oceanogr. Res. Pap.*, *55*(11), 1484–1502, doi:10.1016/j.dsr.2008.07.002.

Lannuzel, D., V. Schoemann, J. de Jong, J.-L. Tison, and L. Chou (2007), Distribution and biogeochemical behaviour of iron in the East Antarctic sea ice, *Mar. Chem.*, *106*, 18–32, doi:10.1016/j.marchem.2006.06.010.

Larock, P., J.-H. Hyun, S. Boutelle, W. C. Burnett, and C. D. Hull (1996), Bacterial mobilization of polonium, *Geochim. Cosmochim. Acta*, *60*(22), 4321–4328, doi:10.1016/S0016-7037(96)00255-4.

Laufkötter, C. et al. (2016), Projected decreases in future marine export production: the role of the carbon flux through the upper ocean ecosystem, *Biogeosciences*, *13*, 4023–4047, doi:10.5194/bg-13-4023-2016.

Laurenceau-Cornec, E. C. et al. (2015), The relative importance of phytoplankton aggregates and zooplankton fecal pellets to carbon export: insights from free-drifting sediment trap deployments in naturally iron-fertilised waters near the Kerguelen Plateau, *Biogeosciences*, *12*, 1007–1027, doi:10.5194/bg-12-1007-2015.

Laws, E. A., E. D'Sa, and P. Naik (2011), Simple equations to estimate ratios of new or export production to total production from satellite-derived estimates of sea surface temperature and primary production, *Limnol. Oceanogr. Methods*, *9*(12), 593–601, doi:10.4319/lom.2011.9.593.

Laxon, S. W. et al. (2013), CryoSat-2 estimates of Arctic sea ice thickness and volume, *Geophys. Res. Lett.*, *40*(4), 732–737, doi:10.1002/grl.50193.

Lee, S. H., D. Stockwell, and T. E. Whitledge (2010), Uptake rates of dissolved inorganic carbon and nitrogen by under-ice phytoplankton in the Canada Basin in summer 2005, *Polar Biol.*, *33*(8), 1027–1036, doi:10.1007/s00300-010-0781-4.

Lefèvre, N., and A. J. Watson (1999), Modeling the geochemical cycle of iron in the oceans and its impact on atmospheric CO_2 concentrations, *Global Biogeochem. Cycles*, *13*(3), 727–736, doi:10.1029/1999GB900034.

Lepore, K. et al. (2007), Seasonal and interannual changes in particulate organic carbon export and deposition in the Chukchi Sea, *J. Geophys. Res.*, *112*, C10024, doi:10.1029/2006JC003555.

Lepore, K., S. B. Moran, and J. N. Smith (2009a), ^{210}Pb as a tracer of shelf–basin transport and sediment focusing in the Chukchi Sea, *Deep Sea Res. Part II Top. Stud. Oceanogr.*, *56*(17), 1305–1315, doi:10.1016/j.dsr2.2008.10.021.

Lepore, K., S. B. Moran, A. B. Burd, G. A. Jackson, J. N. Smith, R. P. Kelly, H. Kaberi, S. Stavrakakis, and G. Assimakopoulou (2009b), Sediment trap and in-situ pump size-fractionated POC/^{234}Th ratios in the Mediterranean Sea and Northwest Atlantic: Implications for POC export, *Deep Sea Res. Part I Oceanogr. Res. Pap.*, *56*(4), 599–613, doi:10.1016/j.dsr.2008.11.004.

Leu, E., J. E. Søreide, D. O. Hessen, S. Falk-Petersen, and J. Berge (2011), Consequences of changing sea-ice cover for primary and secondary producers in the European Arctic shelf seas: Timing, quantity, and quality, *Prog. Oceanogr.*, *90*(1–4), doi:10.1016/j.pocean.2011.02.004.

Leu, E., C. J. Mundy, P. Assmy, K. Campbell, T. M. Gabrielsen, M. Gosselin, T. Juul-Pedersen, and R. Gradinger (2015), Arctic spring awakening – Steering principles behind the phenology of vernal ice algal blooms, *Prog. Oceanogr.*, *139*, 151–170, doi:10.1016/j.pocean.2015.07.012.

Li, W. K. W., F. A. McLaughlin, C. Lovejoy, and E. C. Carmack (2009), Smallest algae thrive as the Arctic Ocean freshens., *Science*, *326*(5952), 539, doi:10.1126/science.1179798.

Liu, Z., J. K. Cochran, C. Lee, B. Gasser, J. C. Miquel, and S. G. Wakeham (2009), Further investigations on why POC concentrations differ in samples collected by Niskin bottle and in situ pump, *Deep Sea Res. Part II Top. Stud. Oceanogr.*, *56*(18), 1558–1567, doi:10.1016/j.dsr2.2008.12.019.

Lomas, M. W., and S. B. Moran (2011), Evidence for aggregation and export of cyanobacteria and nano-eukaryotes from the Sargasso Sea euphotic zone, *Biogeosciences*, *8*(1), 203–216, doi:10.5194/bg-8-203-2011.

Longhurst, A. R. (2007), Ecological geography of the sea, in *Chapter 12 – The Southern Ocean*, pp. 443–475, Elsevier.

Löscher, B. M., H. J. W. De Baar, J. T. M. De Jong, C. Veth, and F. Dehairs (1997), The distribution of Fe in the Antarctic Circumpolar Current, *Deep Sea Res. Part II Top. Stud. Oceanogr.*, *44*(1), 143–187, doi:10.1016/S0967-0645(96)00101-4.

Lovejoy, C., W. F. Vincent, S. Bonilla, S. Roy, M.-J. Martineau, R. Terrado, M. Potvin, R. Massana, and C. Pedrós-Alió (2007), Distribution, phylogeny, and growth of cold-adapted picoprasinophytes in Arctic seas, *J. Phycol.*, *43*(1), 78–89, doi:10.1111/j.1529-8817.2006.00310.x.

Lutz, M., R. Dunbar, and K. Caldeira (2002), Regional variability in the vertical flux of particulate organic carbon in the ocean interior, *Global Biogeochem. Cycles*, *16*(3), 1037, doi:10.1029/2000GB001383.

Ma, Q., M. Chen, Y. Qiu, and Y. Li (2005), Regional estimates of POC export flux derived from thorium-234 in the western Arctic Ocean, *Acta Oceanol. Sin.*, *24*(6), 97–108.

Mackey, M., D. Mackey, H. Higgins, and S. Wright (1996), CHEMTAX - a program for estimating class abundances from chemical markers: application to HPLC measurements of phytoplankton, *Mar. Ecol. Ser.*, *144*, 265–283, doi:10.3354/meps144265.

Mackinson, B. L., S. B. Moran, M. W. Lomas, G. Stewart, and R. P. Kelly (2015), Estimates of micro-, nano-, and picoplankton contributions to particle export in the northeast Pacific, *Biogeosciences*, *12*(11), 3429–3446, doi:10.5194/bg-12-3429-2015.

Maiti, K. et al. (2012), Intercalibration studies of short-lived thorium-234 in the water column and marine particles, *Limnol. Oceanogr. Methods*, *10*(9), 631–644, doi:10.4319/lom.2012.10.631.

Maiti, K., M. A. Charette, K. O. Buesseler, and M. Kahru (2013), An inverse relationship between production and export efficiency in the Southern Ocean, *Geophys. Res. Lett.*, *40*(8), 1557–1561, doi:10.1002/grl.50219.

Maiti, K., S. Bosu, E. J. D'Sa, P. L. Adhikari, M. Sutor, and K. Longnecker (2016), Export fluxes in northern Gulf of Mexico - Comparative evaluation of direct, indirect and satellite-based estimates, *Mar. Chem.*, *184*, 60–77, doi:10.1016/j.marchem.2016.06.001.

Maksym, T., S. E. Stammerjohn, S. Ackley, and R. Massom (2012), Antarctic sea ice - A polar opposite?, *Oceanography*, *25*(3), 140–151, doi:10.5670/oceanog.2012.88.

Marsay, C. M., R. J. Sanders, S. A. Henson, K. Pabortsava, E. P. Achterberg, and R. S. Lampitt (2015), Attenuation of sinking particulate organic carbon flux through the mesopelagic ocean, *Proc. Natl. Acad. Sci. U. S. A.*, *112*(4), 1089–1094, doi:10.1073/pnas.1415311112.

Marshall, J., and K. Speer (2012), Closure of the meridional overturning circulation through Southern Ocean upwelling, *Nat. Geosci.*, *5*, 171–180, doi:10.1038/NGEO1391.

Martin, J. H. (1990), Glacial-interglacial CO_2 change: The Iron Hypothesis, *Paleoceanography*, *5*(1), 1–13, doi:10.1029/PA005i001p00001.

Martin, J. H., S. E. Fitzwater, and R. M. Gordon (1990), Iron deficiency limits phytoplankton growth in Antarctic waters, *Global Biogeochem. Cycles*, *4*(1), 5–12, doi:10.1029/GB004i001p00005.

Martin, P. et al. (2013), Iron fertilization enhanced net community production but not downward particle flux during the Southern Ocean iron fertilization experiment LOHAFEX, *Global Biogeochem. Cycles*, *27*(3), 871–881, doi:10.1002/gbc.20077.

Masqué, P., J. A. Sanchez-Cabeza, J. M. Bruach, E. Palacios, and M. Canals (2002), Balance and residence times of ^{210}Pb and ^{210}Po in surface waters of the northwestern Mediterranean Sea, *Cont. Shelf Res.*, *22*(15), 2127–2146, doi:10.1016/S0278-4343(02)00074-2.

Masqué, P., J. K. Cochran, D. J. Hirschberg, D. Dethleff, D. Hebbeln, A. Winkler, and S. Pfirman (2007), Radionuclides in Arctic sea ice: Tracers of sources, fates and ice transit time scales, *Deep Sea Res. Part I Oceanogr. Res. Pap.*, *54*(8), 1289–1310, doi:10.1016/j.dsr.2007.04.016.

Matrai, P. A., E. Olson, S. Suttles, V. Hill, L. A. Codispoti, B. Light, and M. Steele (2013), Synthesis of primary production in the Arctic Ocean: I. Surface waters, 1954–2007, *Prog. Oceanogr.*, *110*, 93–106, doi:10.1016/j.pocean.2012.11.004.

Mayor, D. J., R. Sanders, S. L. C. Giering, and T. R. Anderson (2014), Microbial gardening in the ocean's twilight zone: Detritivorous metazoans benefit from fragmenting, rather than ingesting, sinking detritus: Fragmentation of refractory detritus by zooplankton beneath the euphotic zone stimulates the harvestable productio, *Bioessays*, *36*(12), 1132–1137, doi:10.1002/bies.201400100.

McDonnell, A. M. P., P. W. Boyd, and K. O. Buesseler (2015), Effects of sinking velocities and microbial respiration rates on the attenuation of particulate carbon fluxes through the mesopelagic zone, *Global Biogeochem. Cycles*, *29*(2), 175–193, doi:10.1002/2014GB004935.

McLaughlin, F. A., and E. C. Carmack (2010), Deepening of the nutricline and chlorophyll maximum in the Canada Basin interior, 2003-2009, *Geophys. Res. Lett.*, *37*(24), L24602, doi:10.1029/2010GL045459.

Meier, W. N. (2016), Losing Arctic sea ice: observations of the recent decline and the long-term context, in *Sea Ice*, pp. 290–303, John Wiley & Sons, Ltd, Chichester, UK.

Melnikov, I. A., and L. L. Bondarchuk (1987), Ecology of mass accumulations of colonial diatom algae under drifting Arctic ice, *Oceanology*, *27*(2), 233–236, doi:10.1594/PANGAEA.756627.

Metfies, K., W.-J. von Appen, E. Kilias, A. Nicolaus, and E.-M. Nöthig (2016), Biogeography and photosynthetic biomass of Arctic marine pico-eukaroytes during summer of the record sea ice minimum 2012, *PLoS One*, *11*(2), e0148512, doi:10.1371/journal.pone.0148512.

Middag, R., H. J. W. de Baar, P. Laan, and K. Bakker (2009), Dissolved aluminium and the silicon cycle in the Arctic Ocean, *Mar. Chem.*, *115*(3), 176–195, doi:10.1016/j.marchem.2009.08.002.

Mikaloff Fletcher, S. E. et al. (2006), Inverse estimates of anthropogenic CO_2 uptake, transport, and storage by the ocean, *Global Biogeochem. Cycles*, *20*(2), GB2002, doi:10.1029/2005GB002530.

Le Moigne, F. A. C., M. Villa-Alfageme, R. J. Sanders, C. Marsay, S. Henson, and R. García-Tenorio (2013a), Export of organic carbon and biominerals derived from ^{234}Th and ^{210}Po at the Porcupine Abyssal Plain, *Deep Sea Res. Part I Oceanogr. Res. Pap.*, *72*, 88–101, doi:10.1016/j.dsr.2012.10.010.

Le Moigne, F. A. C., S. A. Henson, R. J. Sanders, and E. Madsen (2013b), Global database of surface ocean particulate organic carbon export fluxes diagnosed from the ^{234}Th technique, *Earth Syst. Sci. Data*, *5*(2), 295–304, doi:10.5194/essd-5-295-2013.

Le Moigne, F. A. C., K. Pabortsava, C. L. J. Marcinko, P. Martin, and R. J. Sanders (2014), Where is mineral ballast important for surface export of particulate organic carbon in the ocean?, *Geophys. Res. Lett.*, *41*, 1–9, doi:10.1002/2014GL061678.

Le Moigne, F. A. C. et al. (2015), Carbon export efficiency and phytoplankton community composition in the Atlantic sector of the Arctic Ocean, *J. Geophys. Res. Ocean.*, *120*(6), 3896–3912, doi:10.1002/2015JC010700.

Le Moigne, F. A. C., S. A. Henson, E. Cavan, C. Georges, K. Pabortsava, E. P. Achterberg, E. Ceballos-Romero, M. Zubkov, and R. J. Sanders (2016), What causes the inverse relationship between primary production and export efficiency in the Southern Ocean?, *Geophys. Res. Lett.*, *43*, 4457–4466, doi:10.1002/2016GL068480.

Moline, M. A., H. Claustre, T. K. Frazer, O. Schofield, and M. Vernet (2004), Alteration of the food web along the Antarctic Peninsula in response to a regional warming trend, *Glob. Chang. Biol.*, *10*, 1973–1980, doi:10.1111/j.1365-2486.2004.00825.x.

Møller, E., P. Thor, and T. Nielsen (2003), Production of DOC by *Calanus finmarchicus*, *C. glacialis* and *C. hyperboreus* through sloppy feeding and leakage from fecal pellets, *Mar. Ecol. Prog. Ser.*, *262*, 185–191, doi:10.3354/meps262185.

Montes-Hugo, M., S. C. Doney, H. W. Ducklow, W. Fraser, D. Martinson, S. E. Stammerjohn, and O. Schofield (2009), Recent changes in phytoplankton communities associated with rapid regional climate change along the western Antarctic Peninsula, *Science*, *323*, 1470–1473, doi:10.1126/science.1164533.

Moore, C. M. et al. (2013), Processes and patterns of oceanic nutrient limitation, *Nat. Geosci.*, *6*(9), 701–710, doi:10.1038/ngeo1765.

Moore, J. K., and M. R. Abbott (2000), Phytoplankton chlorophyll distributions and primary production in the Southern Ocean, *J. Geophys. Res.*, *105*(C12), 28709–28722, doi:10.1029/1999JC000043.

Moore, R. M., and J. N. Smith (1986), Disequilibria between ^{226}Ra, ^{210}Pb and ^{210}Po in the Arctic Ocean and the implications for chemical modification of the Pacific water inflow, *Earth Planet. Sci. Lett.*, *77*(3–4), 285–292, doi:10.1016/0012-821X(86)90140-8.

Moran, S. B., and J. N. Smith (2000), ^{234}Th as a tracer of scavenging and particle export in the Beaufort Sea, *Cont. Shelf Res.*, *20*(2), 153–167, doi:10.1016/S0278-4343(99)00065-5.

Moran, S. B., K. M. Ellis, and J. N. Smith (1997), ^{234}Th/^{238}U disequilibrium in the central Arctic Ocean: implications for particulate organic carbon export, *Deep Sea Res. Part II Top. Stud. Oceanogr.*, *44*(8), 1593–1606, doi:10.1016/S0967-0645(97)00049-0.

Moran, S. B. et al. (2005), Seasonal changes in POC export flux in the Chukchi Sea and implications for water column-benthic coupling in Arctic shelves, *Deep Sea Res. Part II Top. Stud. Oceanogr.*, *52*(24–26), 3427–3451, doi:10.1016/j.dsr2.2005.09.011.

Moreau, S., B. Mostajir, S. Bélanger, I. R. Schloss, M. Vancoppenolle, S. Demers, and G. A. Ferreyra (2015), Climate change enhances primary production in the western Antarctic Peninsula, *Glob. Chang. Biol.*, *21*, 2191–2205, doi:10.1111/gcb.12878.

Morris, P. J., R. Sanders, R. Turnewitsch, and S. Thomalla (2007), ^{234}Th-derived particulate organic carbon export from an island-induced phytoplankton bloom in the Southern Ocean, *Deep Sea Res. Part II Top. Stud. Oceanogr.*, *54*(18–20), 2208–2232, doi:10.1016/j.dsr2.2007.06.002.

Mundy, C. J., D. G. Barber, and C. Michel (2005), Variability of snow and ice thermal, physical and optical properties pertinent to sea ice algae biomass during spring, *J. Mar. Syst.*, *58*(3), 107–120, doi:10.1016/j.jmarsys.2005.07.003.

Murray, J. W., B. Paul, J. P. Dunne, and T. Chapin (2005), ^{234}Th, ^{210}Pb, ^{210}Po and stable Pb in the central equatorial Pacific: Tracers for particle cycling, *Deep Sea Res. Part I Oceanogr. Res. Pap.*, *52*(11), 2109–2139, doi:10.1016/j.dsr.2005.06.016.

Nicolaus, M., and C. Katlein (2013), Mapping radiation transfer through sea ice using a remotely operated vehicle (ROV), *Cryosph.*, *7*(3), 763–777, doi:10.5194/tc-7-763-2013.

Nicolaus, M., C. Katlein, J. Maslanik, and S. Hendricks (2012), Changes in Arctic sea ice result in increasing light transmittance and absorption, *Geophys. Res. Lett.*, *39*, L24501, doi:10.1029/2012GL053738.

Nishino, S., T. Kikuchi, M. Yamamoto-Kawai, Y. Kawaguchi, T. Hirawake, and M. Itoh (2011), Enhancement/reduction of biological pump depends on ocean circulation in the sea-ice reduction regions of the Arctic Ocean, *J. Oceanogr.*, *67*(3), 305–314, doi:10.1007/s10872-011-0030-7.

Noji, T. T., U. V. Bathmann, B. von Bodungen, M. Voss, A. Antia, M. Krumbholz, B. Klein, I. Peeken, C. I.-M. Noji, and F. Rey (1997), Clearance of picoplankton-sized particles and formation of rapidly sinking aggregates by the pteropod, *Limacina retroversa*, *J. Plankton Res.*, *19*(7), 863–875, doi:10.1093/plankt/19.7.863.

Not, C., K. Brown, B. Ghaleb, and C. Hillaire-Marcel (2012), Conservative behavior of uranium vs. salinity in Arctic sea ice and brine, *Mar. Chem.*, *130–131*, 33–39, doi:10.1016/j.marchem.2011.12.005.

Notz, D., and J. Stroeve (2016), Observed Arctic sea-ice loss directly follows anthropogenic CO_2 emission, *Science*, *354*(6313), 747–750, doi:10.1126/science.aag2345.

Nozaki, Y. (1986), ^{226}Ra-^{222}Rn-^{210}Pb systematics in seawater near the bottom of the ocean, *Earth Planet. Sci. Lett.*, *80*(1–2), 36–40, doi:10.1016/0012-821X(86)90017-8.

Nozaki, Y., J. Thomson, and K. K. Turekian (1976), The distribution of ^{210}Pb and ^{210}Po in the surface waters of the Pacific Ocean, *Earth Planet. Sci. Lett.*, *32*(2), 304–312, doi:10.1016/0012-821X(76)90070-4.

Nozaki, Y., K. K. Turekian, and K. Von Damm (1980), ^{210}Pb in GEOSECS water profiles from the North Pacific, *Earth Planet. Sci. Lett.*, *49*(2), 393–400, doi:10.1016/0012-821X(80)90081-3.

Nozaki, Y., J. Zhang, and A. Takeda (1997), ^{210}Pb and ^{210}Po in the equatorial Pacific and the Bering Sea: the effects of biological productivity and boundary scavenging, *Deep Sea Res. Part II Top. Stud. Oceanogr.*, *44*(9–10), 2203–2220, doi:10.1016/S0967-0645(97)00024-6.

Nozaki, Y., F. Dobashi, Y. Kato, and Y. Yamamoto (1998), Distribution of Ra isotopes and the ^{210}Pb and ^{210}Po balance in surface seawaters of the mid Northern Hemisphere, *Deep Sea Res. Part I Oceanogr. Res. Pap.*, *45*(8), 1263–1284, doi:10.1016/S0967-0637(98)00016-8.

O'Brien, M. C., H. Melling, T. F. Pedersen, and R. W. Macdonald (2013), The role of eddies on particle flux in the Canada Basin of the Arctic Ocean, *Deep Sea Res. Part I Oceanogr. Res. Pap.*, *71*, 1–20, doi:10.1016/j.dsr.2012.10.004.

OC-CCI (2015), *Ocean Color Climate Change Initiative product user guide version 2.*, Ed. By M. Grant, T. Jackson, A. Chuprin, S. Sathyendranath, M. Zühlke, T. Storm, M. Boettcher, N. Fomferra, © Plymouth Marine Laboratory.

Olli, K. et al. (2007), The fate of production in the central Arctic Ocean - top-down regulation by zooplankton expatriates?, *Prog. Oceanogr.*, *72*(1), 84–113, doi:10.1016/j.pocean.2006.08.002.

Orsi, A. H., T. Whitworth, and W. D. Nowlin (1995), On the meridional extent and fronts of the Antarctic Circumpolar Current, *Deep Sea Res. Part I Oceanogr. Res. Pap.*, *42*(5), 641–673, doi:10.1016/0967-0637(95)00021-W.

Orsi, A. H., G. C. Johnson, and J. L. Bullister (1999), Circulation, mixing, and production of Antarctic Bottom Water, *Prog. Oceanogr.*, *43*(1), 55–109, doi:10.1016/S0079-6611(99)00004-X.

Overland, J. E., and M. Wang (2013), When will the summer Arctic be nearly sea ice free?, *Geophys. Res. Lett.*, *40*(10), 2097–2101, doi:10.1002/grl.50316.

Owens, S. A. (2013), Advances in measurements of particle cycling and fluxes in the ocean, PhD thesis, Massachusetts Institute of Technology and Woods Hole Oceanographic Institution, Woods Hole, MA.

Owens, S. A., K. O. Buesseler, and K. W. W. Sims (2011), Re-evaluating the ^{238}U-salinity relationship in seawater: Implications for the ^{238}U-^{234}Th disequilibrium method, *Mar. Chem.*, *127*(1–4), 31–39, doi:10.1016/j.marchem.2011.07.005.

Pabi, S., G. L. van Dijken, and K. R. Arrigo (2008), Primary production in the Arctic Ocean, 1998–2006, *J. Geophys. Res.*, *113*(C8), C08005, doi:10.1029/2007JC004578.

Pakhomov, E. A., P. W. Froneman, and R. Perissinotto (2002), Salp/krill interactions in the Southern Ocean: spatial segregation and implications for the carbon flux, *Deep Sea Res. Part II Top. Stud. Oceanogr.*, *49*(9–10), 1881–1907, doi:10.1016/S0967-0645(02)00017-6.

Parekh, P., S. Dutkiewicz, M. J. Follows, and T. Ito (2006), Atmospheric carbon dioxide in a less dusty world, *Geophys. Res. Lett.*, *33*(3), L03610, doi:10.1029/2005GL025098.

Parkinson, C. L., and J. C. Comiso (2013), On the 2012 record low Arctic sea ice cover: Combined impact of preconditioning and an August storm, *Geophys. Res. Lett.*, *40*(7), 1356–1361, doi:10.1002/grl.50349.

Passow, U. (2002), Transparent exopolymer particles (TEP) in aquatic environments, *Prog. Oceanogr.*, *55*(3–4), 287–333, doi:10.1016/S0079-6611(02)00138-6.

Passow, U., and C. Carlson (2012), The biological pump in a high CO_2 world, *Mar. Ecol. Prog. Ser.*, *470*, 249–271, doi:10.3354/meps09985.

Passow, U., A. L. Alldredge, and B. E. Logan (1994), The role of particulate carbohydrate exudates in the flocculation of diatom blooms, *Deep Sea Res. Part I Oceanogr. Res. Pap.*, *41*(2), 335–357, doi:10.1016/0967-0637(94)90007-8.

Peterson, M. L., S. G. Wakeham, C. Lee, M. A. Askea, and J. C. Miquel (2005), Novel techniques for collection of sinking particles in the ocean and determining their settling rates, *Limnol. Oceanogr. Methods*, *3*(12), 520–532, doi:10.4319/lom.2005.3.520.

Piepenburg, D. (2005), Recent research on Arctic benthos: common notions need to be revised, *Polar Biol.*, *28*(10), 733–755, doi:10.1007/s00300-005-0013-5.

Pike, S., K. Buesseler, J. Andrews, and N. Savoye (2005), Quantification of ^{234}Th recovery in small volume sea water samples by inductively coupled plasma-mass spectrometry, *J. Radioanal. Nucl. Chem.*, *263*(2), 355–360, doi:10.1007/s10967-005-0594-z.

Planchon, F., A.-J. Cavagna, D. Cardinal, L. André, and F. Dehairs (2013), Late summer particulate organic carbon export and twilight zone remineralisation in the Atlantic sector of the Southern Ocean, *Biogeosciences*, *10*(2), 803–820, doi:10.5194/bg-10-803-2013.

Planchon, F., D. Ballas, A.-J. Cavagna, A. R. Bowie, D. Davies, T. Trull, E. C. Laurenceau-Cornec, P. Van Der Merwe, and F. Dehairs (2015), Carbon export in the naturally iron-fertilized Kerguelen area of the Southern Ocean based on the ^{234}Th approach, *Biogeosciences*, *12*, 3831–3848, doi:10.5194/bg-12-3831-2015.

Platt, T., W. G. Harrison, M. R. Lewis, W. K. W. Li, S. Sathyendranath, R. E. Smith, and A. F. Vezina (1989), Biological production of the oceans: the case for a consensus, *Mar. Ecol. Prog. Ser.*, *52*(1), 77–88.

Popova, E. E., A. Yool, A. C. Coward, F. Dupont, C. Deal, S. Elliott, E. Hunke, M. Jin, M. Steele, and J. Zhang (2012), What controls primary production in the Arctic Ocean? Results from an intercomparison of five general circulation models with biogeochemistry, *J. Geophys. Res. Ocean.*, *117*(C8), C00D12, doi:10.1029/2011JC007112.

Poulton, A. J., C. Mark Moore, S. Seeyave, M. I. Lucas, S. Fielding, and P. Ward (2007), Phytoplankton community composition around the Crozet Plateau, with emphasis on diatoms and *Phaeocystis*, *Deep Sea Res. Part II Top. Stud. Oceanogr.*, *54*(18–20), 2085–2105, doi:10.1016/j.dsr2.2007.06.005.

Powell, K. J., P. L. Brown, R. H. Byrne, T. Gajda, G. Hefter, A.-K. Leuz, S. Sjöberg, and H. Wanner (2009), Chemical speciation of environmentally significant metals with inorganic ligands. Part 3: The Pb^{2+} + OH^-, Cl^-, CO_3^{2-}, SO_4^{2-}, and PO_4^{3-} systems (IUPAC Technical Report), *Pure Appl. Chem.*, *81*(12), 2425–2476, doi:10.1351/PAC-REP-09-03-05.

Puigcorbé, V. (2016), Use of ^{234}Th:^{238}U disequilibrium to estimate particulate organic carbon export in the upper ocean, PhD thesis, Universitat Autònoma de Barcelona.

Puigcorbé, V., C. R. Benitez-Nelson, P. Masqué, E. Verdeny, A. E. White, B. N. Popp, F. G. Prahl, and P. J. Lam (2015), Small phytoplankton drive high summertime carbon and nutrient export in the Gulf of California and Eastern Tropical North Pacific, *Global Biogeochem. Cycles*, *29*(8), 1309–1332, doi:10.1002/2015GB005134.

Puigcorbé, V. et al. (2017), Particulate organic carbon export across the Antarctic Circumpolar Current at 10°E: Differences between north and south of the Antarctic Polar Front, *Deep Sea Res. Part II Top. Stud. Oceanogr.*, *138*, 86–101, doi:10.1016/j.dsr2.2016.05.016.

Puigcorbé, V., M. Roca-Martí, P. Masqué, C. Benitez-Nelson, M. Rutgers van der Loeff, A. Bracher, and S. Moreau (in revision), Latitudinal distributions of particulate carbon export across the North Western Atlantic Ocean, *Deep Sea Res. Part I Oceanogr. Res. Pap.*

Purkey, S. G., and G. C. Johnson (2010), Warming of global abyssal and deep Southern Ocean waters between the 1990s and 2000s: Contributions to global heat and sea level rise budgets, *J. Clim.*, *23*, 6336–6351, doi:10.1175/2010JCLI3682.1.

Quéguiner, B. (2013), Iron fertilization and the structure of planktonic communities in high nutrient regions of the Southern Ocean, *Deep Sea Res. Part II Top. Stud. Oceanogr.*, *90*, 43–54, doi:10.1016/j.dsr2.2012.07.024.

Le Quéré, C. et al. (2009), Trends in the sources and sinks of carbon dioxide, *Nat. Geosci.*, *2*(12), 831–836, doi:10.1038/ngeo689.

Quigley, M. S., P. H. Santschi, C.-C. Hung, L. Guo, and B. D. Honeyman (2002), Importance of acid polysaccharides for ^{234}Th complexation to marine organic matter, *Limnol. Oceanogr.*, *47*(2), 367–377, doi:10.4319/lo.2002.47.2.0367.

Rabe, B., M. Karcher, F. Kauker, U. Schauer, J. M. Toole, R. A. Krishfield, S. Pisarev, T. Kikuchi, and J. Su (2014), Arctic Ocean basin liquid freshwater storage trend 1992-2012, *Geophys. Res. Lett.*, *41*(3), 961–968, doi:10.1002/2013GL058121.

Raiswell, R., and D. E. Canfield (2012), The Iron Biogeochemical cycle past and present, edited by L. G. Benning, T. Elliott, E. H. Oelkers, and S. L. S. Stipp, *Geochemical Perspect.*, *1*(1), 220 pp.

Randelhoff, A., and J. D. Guthrie (2016), Regional patterns in current and future export production in the central Arctic Ocean quantified from nitrate fluxes, *Geophys. Res. Lett.*, *43*(16), 8600–8608, doi:10.1002/2016GL070252.

Redfield, A. C., B. H. Ketchum, and F. A. Richards (1963), The influence of organisms on the composition of sea-water, in *The sea: ideas and observations on progress in the study of the seas*, edited by M. N. Hill, pp. 26–77, Wiley Interscience, New York.

Reid, P. C. et al. (2009), Chapter 1 Impacts of the oceans on climate change, *Adv. Mar. Biol.*, *56*, 1–150, doi:10.1016/S0065-2881(09)56001-4.

Reiniger, R. F., and C. K. Ross (1968), A method of interpolation with application to oceanographic data, *Deep Sea Res. Oceanogr. Abstr.*, *15*(2), 185–193, doi:10.1016/0011-7471(68)90040-5.

Renner, A. H. H., S. Gerland, C. Haas, G. Spreen, J. F. Beckers, E. Hansen, M. Nicolaus, and H. Goodwin (2014), Evidence of Arctic sea ice thinning from direct observations, *Geophys. Res. Lett.*, *41*(14), 5029–5036, doi:10.1002/2014GL060369.

Resplandy, L., A. P. Martin, F. Le Moigne, P. Martin, A. Aquilina, L. Mémery, M. Lévy, and R. Sanders (2012), How does dynamical spatial variability impact ^{234}Th-derived estimates of organic export?, *Deep Sea Res. Part I Oceanogr. Res. Pap.*, *68*, 24–45, doi:10.1016/j.dsr.2012.05.015.

Rhein, M. et al. (2013), Observations: Ocean, in *Climate change 2013: the physical science basis. Contribution of working group I to the fifth assessment report of the Intergovernmental Panel on Climate Change*, edited by S. T.F., D. Qin, G.-K. Plattner, M. Tignor, S. K. Allen, J. Boschung, A. Nauels, Y. Xia, V. Bex, and P. M. Midgley, pp. 255–315, Cambridge University Press, Cambridge and New York.

Richardson, T. L., and G. A. Jackson (2007), Small phytoplankton and carbon export from the surface ocean, *Science*, *315*(5813), 838–840, doi:10.1126/science.1133471.

Rigaud, S., V. Puigcorbé, P. Cámara-Mor, N. Casacuberta, M. Roca-Martí, J. Garcia-Orellana, C. R. Benitez-Nelson, P. Masqué, and T. Church (2013), A methods assessment and recommendations for improving calculations and reducing uncertainties in the determination of ^{210}Po and ^{210}Pb activities in seawater, *Limnol. Oceanogr. Methods*, *11*(10), 561–571, doi:10.4319/lom.2013.11.561.

Rignot, E., S. Jacobs, J. Mouginot, and B. Scheuchl (2013), Ice-shelf melting around Antarctica, *Science*, *341*(6143), 266–270, doi:10.1126/science.1235798.

Riley, J. S., R. Sanders, C. Marsay, F. A. C. Le Moigne, E. P. Achterberg, and A. J. Poulton (2012), The relative contribution of fast and slow sinking particles to ocean carbon export, *Global Biogeochem. Cycles*, *26*(1), GB1026, doi:10.1029/2011GB004085.

Rintoul, S. R., C. Hughes, and D. Olbers (2001), The Antarctic Circumpolar Current system, in *Ocean circulation and climate*, vol. 77, edited by G. Siedler, J. Church, and J. Gould, pp. 271–302, Academic Press, New York.

Rintoul, S. R., A. Silvano, B. Pena-Molino, E. van Wijk, M. Rosenberg, J. S. Greenbaum, and D. D. Blankenship (2016), Ocean heat drives rapid basal melt of the Totten Ice Shelf, *Sci. Adv.*, *2*(12), e1601610, doi:10.1126/sciadv.1601610.

Roberts, K. A., J. K. Cochran, and C. Barnes (1997), ^{210}Pb and ^{239,240}Pu in the Northeast Water Polynya, Greenland: particle dynamics and sediment mixing rates, *J. Mar. Syst.*, *10*(1–4), 401–413, doi:10.1016/S0924-7963(96)00061-9.

Roca-Martí, M., V. Puigcorbé, M. M. Rutgers van der Loeff, C. Katlein, M. Fernández-Méndez, I. Peeken, and P. Masqué (2016), Carbon export fluxes and export efficiency in the central Arctic during the record sea-ice minimum in 2012: a joint ^{234}Th/^{238}U and ^{210}Po/^{210}Pb study, *J. Geophys. Res. Ocean.*, *121*, 5030–5049, doi:10.1002/2016JC011816.

Roca-Martí, M., V. Puigcorbé, M. H. Iversen, M. M. Rutgers van der Loeff, C. Klaas, W. Cheah, A. Bracher, and P. Masqué (2017), High particulate organic carbon export during the decline of a vast diatom bloom in the Atlantic sector of the Southern Ocean, *Deep Sea Res. Part II Top. Stud. Oceanogr.*, *138*, 102–115, doi:10.1016/j.dsr2.2015.12.007.

Rodellas, V. (2014), Evaluating submarine groundwater discharge to the Mediterranean Sea by using radium isotopes, PhD thesis, Universitat Autònoma de Barcelona.

Rodriguez y Baena, A. M., S. W. Fowler, and J. C. Miquel (2007), Particulate organic carbon: natural radionuclide ratios in zooplankton and their freshly produced fecal pellets from the NW Mediterranean (MedFlux 2005), *Limnol. Oceanogr.*, *52*(3), 966–974, doi:10.4319/lo.2007.52.3.0966.

Roeske, T., D. Bauch, M. Rutgers van der Loeff, and B. Rabe (2012), Utility of dissolved barium in distinguishing North American from Eurasian runoff in the Arctic Ocean, *Mar. Chem.*, *132–133*, 1–14, doi:10.1016/j.marchem.2012.01.007.

Rudels, B. (2009), Arctic ocean circulation, in *Ocean currents: a derivative of the encyclopedia of ocean sciences*, edited by J. H. Steele, S. A. Thorpe, and K. K. Turekian, pp. 211–225, Academic Press, London.

Rudels, B., L. G. Anderson, and E. P. Jones (1996), Formation and evolution of the surface mixed layer and halocline of the Arctic Ocean, *J. Geophys. Res. Ocean.*, *101*(C4), 8807–8821, doi:10.1029/96JC00143.

Rudels, B., H. J. Friedrich, and D. Quadfasel (1999), The Arctic Circumpolar Boundary Current, *Deep Sea Res. Part II Top. Stud. Oceanogr.*, *46*(6), 1023–1062, doi:10.1016/S0967-0645(99)00015-6.

Rudels, B., E. P. Jones, U. Schauer, and P. Eriksson (2004), Atlantic sources of the Arctic Ocean surface and halocline waters, *Polar Res.*, *23*(2), 181–208, doi:10.1111/j.1751-8369.2004.tb00007.x.

Rudels, B., M. Korhonen, G. Budéus, A. Beszczynska-Möller, U. Schauer, A. Nummelin, D. Quadfasel, and H. Valdimarsson (2012), The East Greenland Current and its impacts on the Nordic Seas: observed trends in the past decade, *ICES J. Mar. Sci.*, *69*(5), 841–851, doi:10.1093/icesjms/fss079.

Russell, J. L., K. W. Dixon, A. Gnanadesikan, R. J. Stouffer, J. R. Toggweiler, J. L. Russell, K. W. Dixon, A. Gnanadesikan, R. J. Stouffer, and J. R. Toggweiler (2006), The Southern Hemisphere westerlies in a warming world: Propping open the door to the deep ocean, *J. Clim.*, *19*(24), 6382–6390, doi:10.1175/JCLI3984.1.

Rutgers van der Loeff, M., P. Cai, I. Stimac, D. Bauch, C. Hanfland, T. Roeske, and S. B. Moran (2012), Shelf-basin exchange times of Arctic surface waters estimated from ^{228}Th/^{228}Ra disequilibrium, *J. Geophys. Res. Ocean.*, *117*, C03024, doi:10.1029/2011JC007478.

Rutgers van der Loeff, M. M., and W. Geibert (2008), U- and Th-series nuclides as tracers of particle dynamics, scavenging and biogeochemical cycles in the oceans, in *U-Th series nuclides in aquatic systems*, edited by S. Krishnaswami and J. K. Cochran, pp. 227–268, Elsevier Science.

Rutgers van der Loeff, M. M., and I. Vöge (2001), *Does Fe fertilisation enhance the export production as measured through the ^{234}Th/^{238}U disequilibrium in surface water? In: The expeditions ANTARKTIS XVIII/1-2 of the research vessel "Polarstern" in 2000. Reports on polar and marine research 400*, edited by V. Smetacek, U. Bathmann, and S. E. D. El Naggar, Bremerhaven.

Rutgers van der Loeff, M. M., J. Friedrich, and U. V. Bathmann (1997), Carbon export during the Spring Bloom at the Antarctic Polar Front, determined with the natural tracer ^{234}Th, *Deep Sea Res. Part II Top. Stud. Oceanogr.*, *44*(1–2), 457–478, doi:10.1016/S0967-0645(96)00067-7.

Rutgers van der Loeff, M. M., K. O. Buesseler, U. Bathmann, I. Hense, and J. Andrews (2002), Comparison of carbon and opal export rates between summer and spring bloom periods in the region of the Antarctic Polar Front, SE Atlantic, *Deep Sea Res. Part II Top. Stud. Oceanogr.*, *49*(18), 3849–3869, doi:10.1016/S0967-0645(02)00114-5.

Rutgers van der Loeff, M. M. et al. (2006), A review of present techniques and methodological advances in analyzing ^{234}Th in aquatic systems, *Mar. Chem.*, *100*(3–4), 190–212, doi:10.1016/j.marchem.2005.10.012.

Rutgers van der Loeff, M. M., P. Cai, I. Stimac, A. Bracher, R. Middag, M. Klunder, and S. Van Heuven (2011), ^{234}Th in surface waters: distribution of particle export flux across the Antarctic Circumpolar Current and in the Weddell Sea during the GEOTRACES expedition ZERO and DRAKE, *Deep Sea Res. Part II Top. Stud. Oceanogr.*, *58*, 2749–2766, doi:10.1016/j.dsr2.2011.02.004.

Sabine, C. L. et al. (2004), The oceanic sink for anthropogenic CO_2, *Science*, *305*(5682), 367–371, doi:10.1126/science.1097403.

Salter, I., R. S. Lampitt, R. Sanders, A. Poulton, A. E. S. Kemp, B. Boorman, K. Saw, and R. Pearce (2007), Estimating carbon, silica and diatom export from a naturally fertilised phytoplankton bloom in the Southern Ocean using PELAGRA: A novel drifting sediment trap, *Deep Sea Res. Part II Top. Stud. Oceanogr.*, *54*(18–20), 2233–2259, doi:10.1016/j.dsr2.2007.06.008.

Salter, I., R. Schiebel, P. Ziveri, A. Movellan, R. Lampitt, and G. A. Wolff (2014), Carbonate counter pump stimulated by natural iron fertilization in the Polar Frontal Zone, *Nat. Geosci.*, *7*, 885–889, doi:10.1038/ngeo2285.

Sampei, M., A. Forest, H. Sasaki, H. Hattori, R. Makabe, M. Fukuchi, and L. Fortier (2009), Attenuation of the vertical flux of copepod fecal pellets under Arctic sea ice: evidence for an active detrital food web in winter, *Polar Biol.*, *32*(2), 225–232, doi:10.1007/s00300-008-0523-z.

Sanders, R. et al. (2014), The Biological Carbon Pump in the North Atlantic, *Prog. Oceanogr.*, *129*, 200–218, doi:10.1016/j.pocean.2014.05.005.

Santschi, P. H., J. W. Murray, M. Baskaran, C. R. Benitez-Nelson, L. D. Guo, C.-C. Hung, C. Lamborg, S. B. Moran, U. Passow, and M. Roy-Barman (2006), Thorium speciation in seawater, *Mar. Chem.*, *100*(3–4), 250–268, doi:10.1016/j.marchem.2005.10.024.

Sarmiento, J. L., T. M. C. Hughes, R. J. Stouffer, and S. Manabe (1998), Simulated response of the ocean carbon cycle to anthropogenic climate warming, *Nature*, *393*(6682), 245–249, doi:10.1038/30455.

Savoye, N., K. O. Buesseler, D. Cardinal, and F. Dehairs (2004), ^{234}Th deficit and excess in the Southern Ocean during spring 2001: Particle export and remineralization, *Geophys. Res. Lett.*, *31*(12), L12301, doi:10.1029/2004GL019744.

Savoye, N., C. Benitez-Nelson, A. B. Burd, J. K. Cochran, M. Charette, K. O. Buesseler, G. A. Jackson, M. Roy-Barman, S. Schmidt, and M. Elskens (2006), ^{234}Th sorption and export models in the water column: A review, *Mar. Chem.*, *100*(3–4), 234–249, doi:10.1016/j.marchem.2005.10.014.

Savoye, N., T. W. Trull, S. H. M. Jacquet, J. Navez, and F. Dehairs (2008), ^{234}Th-based export fluxes during a natural iron fertilization experiment in the Southern Ocean (KEOPS), *Deep Sea Res. Part II Top. Stud. Oceanogr.*, *55*(5–7), 841–855, doi:10.1016/j.dsr2.2007.12.036.

Schauer, U. (2008), *The expedition ARKTIS-XXII/2 of the research vessel "Polarstern" in 2007. Reports on polar and marine research 579*, Bremerhaven.

Schauer, U., and A. Wisotzki (2010), Physical oceanography during POLARSTERN cruise ARK-XXII/2 (SPACE), *Alfred Wegener Institute, Helmholtz Cent. Polar Mar. Res. Bremerhaven*, doi:10.1594/PANGAEA.733418.

Schlitzer, R. (2002), Carbon export fluxes in the Southern Ocean: results from inverse modeling and comparison with satellite-based estimates, *Deep Sea Res. Part II Top. Stud. Oceanogr.*, *49*(9–10), 1623–1644, doi:10.1016/S0967-0645(02)00004-8.

Schofield, O., H. W. Ducklow, D. G. Martinson, M. P. Meredith, M. A. Moline, and W. R. Fraser (2010), How do polar marine ecosystems respond to rapid climate change?, *Science*, *328*, 1520–1523, doi:10.1126/science.1185779.

Schweiger, A., R. Lindsay, J. Zhang, M. Steele, H. Stern, and R. Kwok (2011), Uncertainty in modeled Arctic sea ice volume, *J. Geophys. Res.*, *116*(C8), C00D06, doi:10.1029/2011JC007084.

Serreze, M. C., A. P. Barrett, A. G. Slater, R. A. Woodgate, K. Aagaard, R. B. Lammers, M. Steele, R. Moritz, M. Meredith, and C. M. Lee (2006), The large-scale freshwater cycle of the Arctic, *J. Geophys. Res.*, *111*(C11), C11010, doi:10.1029/2005JC003424.

Shannon, L. V., R. D. Cherry, and M. J. Orren (1970), Polonium-210 and lead-210 in the marine environment, *Geochim. Cosmochim. Acta*, *34*(6), 701–711, doi:10.1016/0016-7037(70)90072-4.

Shaw, W. J., T. P. Stanton, M. G. McPhee, J. H. Morison, and D. G. Martinson (2009), Role of the upper ocean in the energy budget of Arctic sea ice during SHEBA, *J. Geophys. Res.*, *114*(C6), C06012, doi:10.1029/2008JC004991.

Sherr, E. B., B. F. Sherr, P. A. Wheeler, and K. Thompson (2003), Temporal and spatial variation in stocks of autotrophic and heterotrophic microbes in the upper water column of the central Arctic Ocean, *Deep Sea Res. Part I Oceanogr. Res. Pap.*, *50*(5), 557–571, doi:10.1016/S0967-0637(03)00031-1.

Shimmield, G. B., G. D. Ritchie, and T. W. Fileman (1995), The impact of marginal ice zone processes on the distribution of ^{210}Pb, ^{210}Po and ^{234}Th and implications for new production in the Bellingshausen Sea, Antarctica, *Deep Sea Res. Part II Top. Stud. Oceanogr.*, *42*(4–5), 1313–1335, doi:10.1016/0967-0645(95)00071-W.

Siegel, D. A. et al. (2016), Prediction of the export and fate of global ocean net primary production: The EXPORTS Science Plan, *Front. Mar. Sci.*, *3*, 22, doi:10.3389/fmars.2016.00022.

Sigman, D. M., M. P. Hain, and G. H. Haug (2010), The polar ocean and glacial cycles in atmospheric CO_2 concentration, *Nature*, *466*(7302), 47–55, doi:10.1038/nature09149.

Slagstad, D., I. H. Ellingsen, and P. Wassmann (2011), Evaluating primary and secondary production in an Arctic Ocean void of summer sea ice: An experimental simulation approach, *Prog. Oceanogr.*, *90*(1–4), 117–131, doi:10.1016/j.pocean.2011.02.009.

Slagstad, D., P. F. J. Wassmann, and I. Ellingsen (2015), Physical constrains and productivity in the future Arctic Ocean, *Front. Mar. Sci.*, *2*, 85, doi:10.3389/fmars.2015.00085.

Sloyan, B. M., and S. R. Rintoul (2001), The Southern Ocean limb of the global deep overturning circulation, *J. Phys. Oceanogr.*, *31*(1), 143–173, doi:10.1175/1520-0485(2001)031<0143:TSOLOT>2.0.CO;2.

Smetacek, V. (1999), Diatoms and the ocean carbon cycle, *Protist*, *150*(1), 25–32, doi:10.1016/S1434-4610(99)70006-4.

Smetacek, V., and S. W. A. Naqvi (2008), The next generation of iron fertilization experiments in the Southern Ocean, *Philos. Trans. R. Soc. A*, *366*(1882), 3947–3967, doi:10.1098/rsta.2008.0144.

Smetacek, V. et al. (2012), Deep carbon export from a Southern Ocean iron-fertilized diatom bloom, *Nature*, *487*(7407), 313–319, doi:10.1038/nature11229.

Smith, J. N., and K. M. Ellis (1995), Radionuclide tracer profiles at the CESAR Ice Station and Canadian Ice Island in the western Arctic Ocean, *Deep Sea Res. Part II Top. Stud. Oceanogr.*, *42*(6), 1449–1470, doi:10.1016/0967-0645(95)00049-6.

Smith, J. N., S. B. Moran, and R. W. Macdonald (2003), Shelf–basin interactions in the Arctic Ocean based on ^{210}Pb and Ra isotope tracer distributions, *Deep Sea Res. Part I Oceanogr. Res. Pap.*, *50*(3), 397–416, doi:10.1016/S0967-0637(02)00166-8.

Smith, R. E. H., M. Gosselin, and S. Taguchi (1997), The influence of major inorganic nutrients on the growth and physiology of high arctic ice algae, *J. Mar. Syst.*, *11*(1–2), 63–70, doi:10.1016/S0924-7963(96)00028-0.

Smith, W. O., and L. I. Gordon (1997), Hyperproductivity of the Ross Sea (Antarctica) polynya during austral spring, *Geophys. Res. Lett.*, *24*(3), 233–236, doi:10.1029/96GL03926.

Smith, W. O., and D. M. Nelson (1986), Importance of ice edge phytoplankton production in the Southern Ocean, *Bioscience*, *36*(4), 251–257, doi:10.2307/1310215.

Soltwedel, T., N. Jaeckisch, N. Ritter, C. Hasemann, M. Bergmann, and M. Klages (2009), Bathymetric patterns of megafaunal assemblages from the arctic deep-sea observatory HAUSGARTEN, *Deep Sea Res. Part I Oceanogr. Res. Pap.*, *56*(10), 1856–1872, doi:10.1016/j.dsr.2009.05.012.

Søreide, J. E., E. Leu, J. Berge, M. Graeve, and S. Falk-Petersen (2010), Timing of blooms, algal food quality and *Calanus glacialis* reproduction and growth in a changing Arctic, *Glob. Chang. Biol.*, *16*(11), 1–9, doi:10.1111/j.1365-2486.2010.02175.x.

Spreen, G., L. Kaleschke, and G. Heygster (2008), Sea ice remote sensing using AMSR-E 89-GHz channels, *J. Geophys. Res. Ocean.*, *113*(C2), C02S03, doi:10.1029/2005JC003384.

Stammerjohn, S., R. Massom, D. Rind, and D. Martinson (2012), Regions of rapid sea ice change: An inter-hemispheric seasonal comparison, *Geophys. Res. Lett.*, *39*, L06501, doi:10.1029/2012GL050874.

Stammerjohn, S. E., D. G. Martinson, R. C. Smith, and R. A. Iannuzzi (2008), Sea ice in the western Antarctic Peninsula region: Spatio-temporal variability from ecological and climate change perspectives, *Deep Sea Res. Part II Top. Stud. Oceanogr.*, *55*, 2041–2058, doi:10.1016/j.dsr2.2008.04.026.

Stanley, R. H. R., K. O. Buesseler, S. J. Manganini, D. K. Steinberg, and J. R. Valdes (2004), A comparison of major and minor elemental fluxes collected in neutrally buoyant and surface-tethered sediment traps, *Deep Sea Res. Part I Oceanogr. Res. Pap.*, *51*(10), 1387–1395, doi:10.1016/j.dsr.2004.05.010.

Steemann Nielsen, E. (1952), The use of radio-active carbon (C^{14}) for measuring organic production in the sea, *J. Cons. Int. Explor. Mer.*, *18*(2), 117–140, doi:10.1093/icesjms/18.2.117.

Steinberg, D. K., B. A. S. Van Mooy, K. O. Buesseler, P. W. Boyd, T. Kobari, and D. M. Karl (2008), Bacterial vs. zooplankton control of sinking particle flux in the ocean's twilight zone, *Limnol. Oceanogr.*, *53*(4), 1327–1338, doi:10.4319/lo.2008.53.4.1327.

Stemmann, L., and E. Boss (2012), Plankton and particle size and packaging: from determining optical properties to driving the biological pump, *Ann. Rev. Mar. Sci.*, *4*(1), 263–290, doi:10.1146/annurev-marine-120710-100853.

Stewart, G., and N. S. Fisher (2003a), Bioaccumulation of polonium-210 in marine copepods, *Limnol. Oceanogr.*, *48*(5), 2011–2019, doi:10.4319/lo.2003.48.5.2011.

Stewart, G., and N. S. Fisher (2003b), Experimental studies on the accumulation of polonium-210 by marine phytoplankton, *Limnol. Oceanogr.*, *48*(3), 1193–1201, doi:10.4319/lo.2003.48.3.1193.

Stewart, G., S. Fowler, J. L. Teyssié, O. Cotret, J. K. Cochran, and N. S. Fisher (2005), Contrasting transfer of polonium-210 and lead-210 across three trophic levels in marine plankton, *Mar. Ecol. Prog. Ser.*, *290*, 27–33, doi:10.3354/meps290027.

Stewart, G., J. K. Cochran, J. C. Miquel, P. Masqué, J. Szlosek, A. M. Rodriguez y Baena, S. W. Fowler, B. Gasser, and D. J. Hirschberg (2007a), Comparing POC export from $^{234}Th/^{238}U$ and $^{210}Po/^{210}Pb$ disequilibria with estimates from sediment traps in the northwest Mediterranean, *Deep Sea Res. Part I Oceanogr. Res. Pap.*, *54*(9), 1549–1570, doi:10.1016/j.dsr.2007.06.005.

Stewart, G., J. K. Cochran, J. Xue, C. Lee, S. G. Wakeham, R. A. Armstrong, P. Masqué, and J. Carlos Miquel (2007b), Exploring the connection between ^{210}Po and organic matter in the northwestern Mediterranean, *Deep Sea Res. Part I Oceanogr. Res. Pap.*, *54*(3), 415–427, doi:10.1016/j.dsr.2006.12.006.

Stewart, G., S. W. Fowler, and N. S. Fisher (2008), The bioaccumulation of U- and Th-series radionuclides in marine organisms, in *U-Th series nuclides in aquatic systems*, edited by S. Krishnaswami and J. K. Cochran, pp. 269–305, Elsevier Science.

Stewart, G., S. B. Moran, and M. W. Lomas (2010), Seasonal POC fluxes at BATS estimated from ^{210}Po deficits, *Deep Sea Res. Part I Oceanogr. Res. Pap.*, *57*(1), 113–124, doi:10.1016/j.dsr.2009.09.007.

Stewart, G., S. B. Moran, M. W. Lomas, and R. P. Kelly (2011), Direct comparison of ^{210}Po, ^{234}Th and POC particle-size distributions and export fluxes at the Bermuda Atlantic Time-series Study (BATS) site., *J. Environ. Radioact.*, *102*(5), 479–489, doi:10.1016/j.jenvrad.2010.09.011.

Stocker, T. F. et al. (2013), *Technical summary. In: Climate change 2013: the physical science basis. Contribution of working group I to the fifth assessment report of the Intergovernmental Panel on Climate Change*, edited by T. F. Stocker, D. Qin, G.-K. Plattner, M. Tignor, S. K. Allen, J. Boschung, A. Nauels, Y. Xia, V. Bex, and P. M. Midgley, Cambridge University Press, Cambridge and New York.

Strass, V. H., H. Leach, H. Prandke, M. Donnelly, A. U. Bracher, and D. A. Wolf-Gladrow (2017), The physical environmental conditions for biogeochemical differences along the Antarctic Circumpolar Current in the Atlantic Sector during late austral summer 2012, *Deep Sea Res. Part II Top. Stud. Oceanogr.*, *138*, 6–25, doi:10.1016/j.dsr2.2016.05.018.

Stroeve, J. C., M. C. Serreze, M. M. Holland, J. E. Kay, J. Malanik, and A. P. Barrett (2012), The Arctic's rapidly shrinking sea ice cover: a research synthesis, *Clim. Change*, *110*(3), 1005–1027, doi:10.1007/s10584-011-0101-1.

Stukel, M. R., M. Kahru, C. R. Benitez-Nelson, M. Décima, R. Goericke, M. R. Landry, and M. D. Ohman (2015), Using Lagrangian-based process studies to test satellite algorithms of vertical carbon flux in the eastern North Pacific Ocean, *J. Geophys. Res. Ocean.*, *120*(11), 7208–7222, doi:10.1002/2015JC011264.

Takahashi, T. et al. (2002), Global sea-air CO_2 flux based on climatological surface ocean pCO_2, and seasonal biological and temperature effects, *Deep Sea Res. Part II Top. Stud. Oceanogr.*, *49*(9–10), 1601–1622, doi:10.1016/S0967-0645(02)00003-6.

Tamelander, T., M. Reigstad, K. Olli, D. Slagstad, and P. Wassmann (2013), New production regulates export stoichiometry in the ocean., *PLoS One*, *8*(1), e54027, doi:10.1371/journal.pone.0054027.

Taylor, B. B., E. Torrecilla, A. Bernhardt, M. H. Taylor, I. Peeken, R. Röttgers, J. Piera, and A. Bracher (2011), Bio-optical provinces in the eastern Atlantic Ocean and their biogeographical relevance, *Biogeosciences Discuss.*, *8*, 7165–7219, doi:10.5194/bg-8-3609-2011.

Thibault, D., E. J. H. Head, and P. A. Wheeler (1999), Mesozooplankton in the Arctic Ocean in summer, *Deep Sea Res. Part I Oceanogr. Res. Pap.*, *46*(8), 1391–1415, doi:10.1016/S0967-0637(99)00009-6.

Thomson, J., and K. K. Turekian (1976), ^{210}Po and ^{210}Pb distributions in ocean water profiles from the Eastern South Pacific, *Earth Planet. Sci. Lett.*, *32*(2), 297–303, doi:10.1016/0012-821X(76)90069-8.

Torres-Valdés, S., T. Tsubouchi, S. Bacon, A. C. Naveira-Garabato, R. Sanders, F. A. McLaughlin, B. Petrie, G. Kattner, K. Azetsu-Scott, and T. E. Whitledge (2013), Export of nutrients from the Arctic Ocean, *J. Geophys. Res. Ocean.*, *118*(4), 1625–1644, doi:10.1002/jgrc.20063.

Tréguer, P. J., and C. L. De La Rocha (2013), The world ocean silica cycle, *Ann. Rev. Mar. Sci.*, *5*(1), 477–501, doi:10.1146/annurev-marine-121211-172346.

Tremblay, J.-É., and J. Gagnon (2009), The effects of irradiance and nutrient supply on the productivity of Arctic waters: a perspective on climate change, in *Influence of climate change on the changing Arctic and sub-Arctic conditions*, pp. 73–93, Springer Netherlands, Dordrecht.

Tremblay, J.-É., L. G. Anderson, P. Matrai, P. Coupel, S. Bélanger, C. Michel, and M. Reigstad (2015), Global and regional drivers of nutrient supply, primary production and CO_2 drawdown in the changing Arctic Ocean, *Prog. Oceanogr.*, *139*, 171–196, doi:10.1016/j.pocean.2015.08.009.

Trimble, S. M., and M. Baskaran (2005), The role of suspended particulate matter in ^{234}Th scavenging and ^{234}Th-derived export fluxes of POC in the Canada Basin of the Arctic Ocean, *Mar. Chem.*, *96*(1–2), 1–19, doi:10.1016/j.marchem.2004.10.003.

Tschudi, M., J. Stroeve, and J. Stewart (2016), Relating the age of Arctic sea ice to its thickness, as measured during NASA's ICESat and IceBridge campaigns, *Remote Sens.*, *8*(6), 457, doi:10.3390/rs8060457.

Turekian, K. K., Y. Nozaki, and L. K. Benninger (1977), Geochemistry of atmospheric radon and radon products, *Annu. Rev. Earth Planet. Sci.*, *5*(1), 227–255, doi:10.1146/annurev.ea.05.050177.001303.

Turner, J., J. C. Comiso, G. J. Marshall, T. A. Lachlan-Cope, T. Bracegirdle, T. Maksym, M. P. Meredith, Z. Wang, and A. Orr (2009), Non-annular atmospheric circulation change induced by stratospheric ozone depletion and its role in the recent increase of Antarctic sea ice extent, *Geophys. Res. Lett.*, *36*, L08502, doi:10.1029/2009GL037524.

Turner, J. T. (2015), Zooplankton fecal pellets, marine snow, phytodetritus and the ocean's biological pump, *Prog. Oceanogr.*, *130*, 205–248, doi:10.1016/j.pocean.2014.08.005.

Uitz, J., H. Claustre, A. Morel, and S. B. Hooker (2006), Vertical distribution of phytoplankton communities in open ocean: An assessment based on surface chlorophyll, *J. Geophys. Res. Ocean.*, *111*(C8), C08005, doi:10.1029/2005JC003207.

Uitz, J., H. Claustre, F. B. Griffiths, J. Ras, N. Garcia, and V. Sandroni (2009), A phytoplankton class-specific primary production model applied to the Kerguelen Islands region (Southern Ocean), *Deep Sea Res. Part I Oceanogr. Res. Pap.*, *56*(4), 541–560, doi:10.1016/j.dsr.2008.11.006.

Ulfsbo, A., N. Cassar, M. Korhonen, S. van Heuven, M. Hoppema, G. Kattner, and L. G. Anderson (2014), Late summer net community production in the central Arctic Ocean using multiple approaches, *Global Biogeochem. Cycles*, *28*, 1129–1148, doi:10.1002/2014GB004833.

Usbeck, R., M. M. Rutgers van der Loeff, M. Hoppema, and R. Schlitzer (2002), Shallow remineralization in the Weddell Gyre, *Geochemistry Geophys. Geosystems*, *3*(1), 1–18, doi:10.1029/2001GC000182.

Vancoppenolle, M. et al. (2013), Role of sea ice in global biogeochemical cycles: emerging views and challenges, *Quat. Sci. Rev.*, *79*, 207–230, doi:10.1016/j.quascirev.2013.04.011.

Vaquer-Sunyer, R., C. M. Duarte, R. Santiago, P. Wassmann, and M. Reigstad (2010), Experimental evaluation of planktonic respiration response to warming in the European Arctic Sector, *Polar Biol.*, *33*(12), 1661–1671, doi:10.1007/s00300-010-0788-x.

Vaquer-Sunyer, R., C. M. Duarte, A. Regaudie-de-Gioux, J. Holding, L. S. García-Corral, M. Reigstad, and P. Wassmann (2013), Seasonal patterns in Arctic planktonic metabolism (Fram Strait – Svalbard region), *Biogeosciences*, *10*(3), 1451–1469, doi:10.5194/bg-10-1451-2013.

Vaughan, D. G., G. J. Marshall, W. M. Connolley, C. Parkinson, R. Mulvaney, D. A. Hodgson, J. C. King, C. J. Pudsey, and J. Turner (2003), Recent rapid regional climate warming on the Antarctic Peninsula, *Clim. Change*, *60*, 243–274, doi:10.1023/A:1026021217991.

Verdeny, E., P. Masqué, K. Maiti, J. Garcia-Orellana, J. M. Bruach, C. Mahaffey, and C. R. Benitez-Nelson (2008), Particle export within cyclonic Hawaiian lee eddies derived from ^{210}Pb–^{210}Po disequilibrium, *Deep Sea Res. Part II Top. Stud. Oceanogr.*, *55*(10–13), 1461–1472, doi:10.1016/j.dsr2.2008.02.009.

Verdeny, E., P. Masqué, J. Garcia-Orellana, C. Hanfland, J. K. Cochran, and G. Stewart (2009), POC export from ocean surface waters by means of ^{234}Th/^{238}U and ^{210}Po/^{210}Pb disequilibria: A review of the use of two radiotracer pairs, *Deep Sea Res. Part II Top. Stud. Oceanogr.*, *56*(18), 1502–1518, doi:10.1016/j.dsr2.2008.12.018.

Volk, T., and M. I. Hoffert (1985), Ocean carbon pumps: analysis of relative strengths and efficiencies in ocean-driven atmospheric CO_2 changes, in *The carbon cycle and atmospheric CO_2: Natural variations Archean to present*, vol. 32, edited by E. T. Sundquist and W. S. Broecker, pp. 99–110, American Geophysical Union, Washington, D. C.

Waite, A. M., K. A. Safi, J. A. Hall, and S. D. Nodder (2000), Mass sedimentation of picoplankton embedded in organic aggregates, *Limnol. Oceanogr.*, *45*(1), 87–97, doi:10.4319/lo.2000.45.1.0087.

Wang, S., D. Bailey, K. Lindsay, J. K. Moore, and M. Holland (2014), Impact of sea ice on the marine iron cycle and phytoplankton productivity, *Biogeosciences*, *11*(17), 4713–4731, doi:10.5194/bg-11-4713-2014.

Waples, J. T., C. Benitez-Nelson, N. Savoye, M. Rutgers van der Loeff, M. Baskaran, and Ö. Gustafsson (2006), An introduction to the application and future use of ^{234}Th in aquatic systems, *Mar. Chem.*, *100*(3), 166–189, doi:10.1016/j.marchem.2005.10.011.

Wassmann, P. (2011), Arctic marine ecosystems in an era of rapid climate change, *Prog. Oceanogr.*, *90*(1–4), 1–17, doi:10.1016/j.pocean.2011.02.002.

Wassmann, P., and M. Reigstad (2011), Future Arctic Ocean seasonal ice zones and implications for pelagic-benthic coupling, *Oceanography*, *24*(3), 220–231, doi:10.5670/oceanog.2011.74.

Wassmann, P., I. Andreassen, M. Reigstad, and D. Slagstad (1996), Pelagic-benthic coupling in the Nordic Seas: the role of episodic events, *Mar. Ecol.*, *17*(1–3), 447–471, doi:10.1111/j.1439-0485.1996.tb00520.x.

Wassmann, P. et al. (2004), Particulate organic carbon flux to the Arctic ocean sea floor, in *The organic carbon cycle in the Arctic Ocean*, edited by R. Stein and R. W. Macdonald, pp. 101–138, Springer Berlin Heidelberg, Berlin.

Wassmann, P. et al. (2006), Food webs and carbon flux in the Barents Sea, *Prog. Oceanogr.*, *71*(2–4), 232–287, doi:10.1016/j.pocean.2006.10.003.

Wassmann, P., J. Carroll, and R. G. J. Bellerby (2008), Carbon flux and ecosystem feedback in the northern Barents Sea in an era of climate change: An introduction, *Deep Sea Res. Part II Top. Stud. Oceanogr.*, *55*(20), 2143–2153, doi:10.1016/j.dsr2.2008.05.025.

Wassmann, P., C. M. Duarte, S. Agustí, and M. K. Sejr (2011), Footprints of climate change in the Arctic marine ecosystem, *Glob. Chang. Biol.*, *17*(2), 1235–1249, doi:10.1111/j.1365-2486.2010.02311.x.

Wassmann, P. et al. (2015), The contiguous domains of Arctic Ocean advection: Trails of life and death, *Prog. Oceanogr.*, *139*, 42–65, doi:10.1016/j.pocean.2015.06.011.

Watanabe, E. et al. (2014), Enhanced role of eddies in the Arctic marine biological pump, *Nat. Commun.*, *5*(3950), 9 pp., doi:10.1038/ncomms4950.

Watson, A. J., and J. C. Orr (2003), Carbon dioxide fluxes in the global ocean, in *Ocean biogeochemistry: the role of the ocean carbon cycle in global change*, edited by M. J. R. Fasham, pp. 123–143, Springer-Verlag, Berlin.

Wei, C.-L., S.-Y. Lin, D. D.-D. Sheu, W.-C. Chou, M.-C. Yi, P. H. Santschi, and L.-S. Wen (2011), Particle-reactive radionuclides (^{234}Th, ^{210}Pb, ^{210}Po) as tracers for the estimation of export production in the South China Sea, *Biogeosciences*, *8*(12), 3793–3808, doi:10.5194/bg-8-3793-2011.

Wexels Riser, C., M. Reigstad, P. Wassmann, E. Arashkevich, and S. Falk-Petersen (2007), Export or retention? Copepod abundance, faecal pellet production and vertical flux in the marginal ice zone through snap shots from the northern Barents Sea, *Polar Biol.*, *30*(6), 719–730, doi:10.1007/s00300-006-0229-z.

Wiedmann, I., M. Reigstad, A. Sundfjord, and S. Basedow (2014), Potential drivers of sinking particle's size spectra and vertical flux of particulate organic carbon (POC): Turbulence, phytoplankton, and zooplankton, *J. Geophys. Res. Ocean.*, *119*(10), 6900–6917, doi:10.1002/2013JC009754.

Wilson, S., and D. K. Steinberg (2010), Autotrophic picoplankton in mesozooplankton guts: evidence of aggregate feeding in the mesopelagic zone and export of small phytoplankton, *Mar. Ecol. Prog. Ser.*, *412*, 11–27, doi:10.3354/meps08648.

Wilson, S. E., D. K. Steinberg, and K. O. Buesseler (2008), Changes in fecal pellet characteristics with depth as indicators of zooplankton repackaging of particles in the mesopelagic zone of the subtropical and subarctic North Pacific Ocean, *Deep Sea Res. Part II Top. Stud. Oceanogr.*, *55*, 1636–1647, doi:10.1016/j.dsr2.2008.04.019.

Wilson, S. E., H. A. Ruhl, and K. L. Smith Jr. (2013), Zooplankton fecal pellet flux in the abyssal northeast Pacific: A 15 year time-series study, *Limnol. Oceanogr.*, *58*(3), 881–892, doi:10.4319/lo.2013.58.3.0881.

Winton, V. H. L., R. Edwards, B. Delmonte, A. Ellis, P. S. Andersson, A. Bowie, N. A. N. Bertler, P. Neff, and A. Tuohy (2016), Multiple sources of soluble atmospheric iron to Antarctic waters, *Global Biogeochem. Cycles*, *30*, 421–437, doi:10.1002/2015GB005265.

Wisotzki, A., and K. Bakker (2008), Hydrochemistry measured on water bottle samples during POLARSTERN cruise ARK-XXII/2, *Alfred Wegener Institute, Helmholtz Cent. Polar Mar. Res. Bremerhaven*, doi:10.1594/PANGAEA.759286.

Wolf-Gladrow, D. (2013), *The expedition of the research vessel "Polarstern" to the Antarctic in 2012 (ANT-XXVIII/3). Reports on polar and marine research 661*, Bremerhaven.

Worby, A. P., C. A. Geiger, M. J. Paget, M. L. Van Woert, S. F. Ackley, and T. L. DeLiberty (2008), Thickness distribution of Antarctic sea ice, *J. Geophys. Res.*, *113*(C5), C05S92, doi:10.1029/2007JC004254.

Wright, S. W., R. L. van den Enden, I. Pearce, A. T. Davidson, F. J. Scott, and K. J. Westwood (2010), Phytoplankton community structure and stocks in the Southern Ocean (30–80°E) determined by CHEMTAX analysis of HPLC pigment signatures, *Deep Sea Res. Part II Top. Stud. Oceanogr.*, *57*(9–10), 758–778, doi:10.1016/j.dsr2.2009.06.015.

Yang, W., L. Guo, C.-Y. Chuang, P. H. Santschi, D. Schumann, and M. Ayranov (2015), Influence of organic matter on the adsorption of ^{210}Pb, ^{210}Po and ^{7}Be and their fractionation on nanoparticles in seawater, *Earth Planet. Sci. Lett.*, *423*, 193–201, doi:10.1016/j.epsl.2015.05.007.

Yool, A., A. P. Martin, C. Fernández, and D. R. Clark (2007), The significance of nitrification for oceanic new production, *Nature*, *447*(7147), 999–1002, doi:10.1038/nature05885.

Yool, A., E. E. Popova, and A. C. Coward (2015), Future change in ocean productivity: Is the Arctic the new Atlantic?, *J. Geophys. Res. Ocean.*, *120*(12), 7771–7790, doi:10.1002/2015JC011167.

Yu, W., L. Chen, J. Cheng, J. He, M. Yin, and Z. Zeng (2010), ^{234}Th-derived particulate organic carbon export flux in the western Arctic Ocean, *Chinese J. Oceanol. Limnol.*, *28*(6), 1146–1151, doi:10.1007/s00343-010-9933-1.

Yu, W., J. He, Y. Li, W. Lin, and L. Chen (2012), Particulate organic carbon export fluxes and validation of steady state model of ^{234}Th export in the Chukchi Sea, *Deep Sea Res. Part II Top. Stud. Oceanogr.*, *81–84*, 63–71, doi:10.1016/j.dsr2.2012.03.003.

Zeebe, R. E. (2012), History of seawater carbonate chemistry, atmospheric CO_2, and ocean acidification, *Annu. Rev. Earth Planet. Sci.*, *40*(1), 141–165, doi:10.1146/annurev-earth-042711-105521.

Zhang, F., J. He, L. Lin, and H. Jin (2015), Dominance of picophytoplankton in the newly open surface water of the central Arctic Ocean, *Polar Biol.*, *38*(7), 1081–1089, doi:10.1007/s00300-015-1662-7.

Zhang, J., and D. A. Rothrock (2003), Modeling global sea ice with a thickness and enthalpy distribution model in generalized curvilinear coordinates, *Mon. Weather Rev.*, *131*(5), 845–861, doi:10.1175/1520-0493(2003)131<0845:MGSIWA>2.0.CO;2.

Zhang, J., Y. H. Spitz, M. Steele, C. Ashjian, R. Campbell, L. Berline, and P. Matrai (2010), Modeling the impact of declining sea ice on the Arctic marine planktonic ecosystem, *J. Geophys. Res.*, *115*(C10), C10015, doi:10.1029/2009JC005387.

Appendix

Table A1: ^{210}Pb and ^{210}Po activities for the dissolved, particulate and total fractions, particulate and total ^{210}Po/^{210}Pb activity ratios, and ^{210}Pb/^{226}Ra activity ratios along five sections (S1-S5, see Chapter 5 for further details) during the ARK-XXII/2 expedition. [a] The ^{226}Ra data was taken from *Rutgers van der Loeff et al.* [2012].

		Dissolved (dpm 100L^{-1})		Particulate (dpm 100L^{-1})		Total (dpm 100L^{-1})		^{210}Po/^{210}Pb		
Station	Depth (m)	^{210}Pb	^{210}Po	^{210}Pb	^{210}Po	^{210}Pb	^{210}Po	Particulate	Total	^{210}Pb/^{226}Ra
S1										
236	10	5.1 ± 0.3	2.6 ± 0.3	0.185 ± 0.010	0.118 ± 0.011	5.3 ± 0.3	2.7 ± 0.3	0.64 ± 0.07	0.50 ± 0.06	
	25	3.19 ± 0.16	1.51 ± 0.17	0.249 ± 0.014	0.041 ± 0.015	3.43 ± 0.16	1.55 ± 0.17	0.16 ± 0.06	0.45 ± 0.05	
	50	2.09 ± 0.11	2.00 ± 0.13	0.275 ± 0.017	0.034 ± 0.017	2.37 ± 0.11	2.04 ± 0.13	0.12 ± 0.06	0.86 ± 0.07	
	75	1.29 ± 0.07	0.76 ± 0.07	0.63 ± 0.04	*<0.004*	1.93 ± 0.08	0.76 ± 0.07	-	0.39 ± 0.04	
	100	2.27 ± 0.12	1.17 ± 0.12							
	150	1.47 ± 0.07	1.00 ± 0.08							
	186			0.65 ± 0.04	0.12 ± 0.04			0.19 ± 0.06		
237	10	4.5 ± 0.2	2.7 ± 0.3	0.35 ± 0.02	0.30 ± 0.02	4.8 ± 0.2	3.0 ± 0.3	0.84 ± 0.08	0.63 ± 0.06	0.70 ± 0.04
	25			0.53 ± 0.03	0.17 ± 0.03			0.32 ± 0.06		
	50	1.53 ± 0.08	1.14 ± 0.09	0.94 ± 0.05	*<0.004*	2.47 ± 0.10	1.14 ± 0.09	-	0.46 ± 0.04	
	75	1.38 ± 0.07	0.61 ± 0.08	0.63 ± 0.04	*<0.004*	2.01 ± 0.08	0.61 ± 0.08	-	0.31 ± 0.04	
	100	1.73 ± 0.08	1.25 ± 0.09	0.57 ± 0.03	0.15 ± 0.03	2.31 ± 0.09	1.39 ± 0.10	0.25 ± 0.06	0.60 ± 0.05	
	200	1.03 ± 0.05	0.80 ± 0.06	0.91 ± 0.05	0.52 ± 0.06	1.95 ± 0.08	1.32 ± 0.08	0.57 ± 0.07	0.68 ± 0.05	
	265	0.83 ± 0.04	0.60 ± 0.04	1.07 ± 0.06	0.93 ± 0.07	1.90 ± 0.07	1.53 ± 0.08	0.87 ± 0.08	0.81 ± 0.05	
239	10	4.9 ± 0.2	2.4 ± 0.2	0.88 ± 0.06	0.85 ± 0.06	5.7 ± 0.2	3.3 ± 0.2	0.96 ± 0.09	0.57 ± 0.05	1.05 ± 0.04
	25	1.46 ± 0.08	1.32 ± 0.09	0.70 ± 0.04	0.06 ± 0.04	2.16 ± 0.09	1.38 ± 0.10	0.09 ± 0.06	0.64 ± 0.05	
	50	0.91 ± 0.05	0.89 ± 0.06	0.85 ± 0.05	0.26 ± 0.05	1.76 ± 0.07	1.15 ± 0.08	0.31 ± 0.06	0.65 ± 0.05	
	75	0.74 ± 0.04	0.79 ± 0.05	1.01 ± 0.05	0.33 ± 0.05	1.75 ± 0.06	1.12 ± 0.07	0.33 ± 0.06	0.64 ± 0.05	
	100	0.67 ± 0.03	0.60 ± 0.04							
	150	0.69 ± 0.04	0.77 ± 0.05	1.04 ± 0.06	0.49 ± 0.07	1.73 ± 0.07	1.26 ± 0.08	0.47 ± 0.07	0.73 ± 0.06	
	207	1.07 ± 0.06	1.47 ± 0.08	1.39 ± 0.08	0.90 ± 0.09	2.46 ± 0.10	2.37 ± 0.12	0.65 ± 0.07	0.96 ± 0.06	
249	10	5.7 ± 0.3	2.7 ± 0.3	0.280 ± 0.015	0.337 ± 0.019	6.0 ± 0.3	3.0 ± 0.3	1.21 ± 0.09	0.50 ± 0.06	

Station	Depth (m)	Dissolved (dpm 100L^{-1})		Particulate (dpm 100L^{-1})		Total (dpm 100L^{-1})		^{210}Po/^{210}Pb		^{210}Pb/^{226}Ra
		^{210}Pb	^{210}Po	^{210}Pb	^{210}Po	^{210}Pb	^{210}Po	Particulate	Total	
255	10	4.6 ± 0.3	2.7 ± 0.3	0.44 ± 0.02	0.87 ± 0.05	5.0 ± 0.3	3.6 ± 0.3	1.97 ± 0.15	0.72 ± 0.07	
	25	2.97 ± 0.14	2.16 ± 0.15	0.154 ± 0.009	1.19 ± 0.07	3.13 ± 0.14	3.34 ± 0.17	7.7 ± 0.6	1.07 ± 0.07	
	45	3.7 ± 0.2	1.6 ± 0.2	0.280 ± 0.016	0.42 ± 0.02	3.9 ± 0.2	2.0 ± 0.2	1.48 ± 0.12	0.50 ± 0.06	
	75			1.48 ± 0.08	0.98 ± 0.08			0.66 ± 0.07		
	100			1.62 ± 0.09	1.57 ± 0.11			0.97 ± 0.09		
	150	4.8 ± 0.2	2.6 ± 0.3	1.42 ± 0.08	1.39 ± 0.10	6.3 ± 0.3	4.0 ± 0.3	0.98 ± 0.09	0.63 ± 0.05	
	200	3.65 ± 0.18	2.20 ± 0.18	1.93 ± 0.12	1.55 ± 0.13	5.6 ± 0.2	3.8 ± 0.2	0.80 ± 0.09	0.67 ± 0.05	
	300					5.2 ± 0.2	4.09 ± 0.08		0.78 ± 0.04	
	500					5.3 ± 0.3	4.18 ± 0.13		0.79 ± 0.05	
	750					3.73 ± 0.18	4.43 ± 0.11		1.19 ± 0.06	
	1000					4.10 ± 0.18	4.19 ± 0.08		1.02 ± 0.05	
257	10	6.2 ± 0.3	2.3 ± 0.3	0.125 ± 0.007	0.312 ± 0.013	6.3 ± 0.3	2.6 ± 0.3	2.49 ± 0.18	0.42 ± 0.06	0.88 ± 0.05
258	10	6.4 ± 0.4	2.8 ± 0.4							
260	10	6.1 ± 0.3	2.8 ± 0.3	0.055 ± 0.003	0.204 ± 0.009	6.1 ± 0.3	3.0 ± 0.3	3.7 ± 0.3	0.49 ± 0.05	
	25	5.1 ± 0.2	2.4 ± 0.2	0.161 ± 0.009	0.056 ± 0.010	5.2 ± 0.2	2.4 ± 0.2	0.35 ± 0.06	0.47 ± 0.05	
	50	3.8 ± 0.2	2.1 ± 0.2	1.02 ± 0.06	0.62 ± 0.06	4.8 ± 0.2	2.7 ± 0.2	0.60 ± 0.07	0.55 ± 0.05	
	75	2.91 ± 0.13	2.34 ± 0.14							
	100	2.91 ± 0.13	2.44 ± 0.14	0.81 ± 0.05	0.69 ± 0.05	3.72 ± 0.14	3.13 ± 0.15	0.85 ± 0.08	0.84 ± 0.05	
	125	2.72 ± 0.12	2.97 ± 0.14							
	200					4.5 ± 0.2	3.44 ± 0.07		0.76 ± 0.04	
	300					6.1 ± 0.3	3.72 ± 0.08		0.61 ± 0.03	
	750					4.7 ± 0.3	4.51 ± 0.14		0.95 ± 0.06	
	1000					4.8 ± 0.2	4.87 ± 0.10		1.02 ± 0.05	
S2										
261	10	5.3 ± 0.3	2.6 ± 0.3	0.61 ± 0.04	1.32 ± 0.06	5.9 ± 0.3	4.0 ± 0.3	2.17 ± 0.17	0.67 ± 0.06	0.82 ± 0.04
263	10	6.3 ± 0.3	2.7 ± 0.3							
264	10	5.1 ± 0.3	1.9 ± 0.3							

Station	Depth (m)	Dissolved (dpm 100L^{-1}) ^{210}Pb	Dissolved (dpm 100L^{-1}) ^{210}Po	Particulate (dpm 100L^{-1}) ^{210}Pb	Particulate (dpm 100L^{-1}) ^{210}Po	Total (dpm 100L^{-1}) ^{210}Pb	Total (dpm 100L^{-1}) ^{210}Po	^{210}Po/^{210}Pb Particulate	^{210}Po/^{210}Pb Total	^{210}Pb/^{226}Ra
266	10	4.7 ± 0.3	2.2 ± 0.3	0.52 ± 0.03	0.70 ± 0.04	5.3 ± 0.3	2.9 ± 0.3	1.36 ± 0.12	0.55 ± 0.06	0.71 ± 0.04
	25	2.96 ± 0.15	1.30 ± 0.15	0.58 ± 0.03	0.36 ± 0.04	3.53 ± 0.15	1.66 ± 0.16	0.63 ± 0.07	0.47 ± 0.05	
	50	2.62 ± 0.13	1.44 ± 0.14							
	75	2.63 ± 0.13	1.10 ± 0.13							
	100	2.79 ± 0.14	1.53 ± 0.15							
	200	3.21 ± 0.18	2.01 ± 0.19	1.57 ± 0.10	1.14 ± 0.11	4.8 ± 0.2	3.2 ± 0.2	0.73 ± 0.08	0.66 ± 0.05	
	300	2.80 ± 0.15	2.56 ± 0.18							
	500	2.57 ± 0.15	1.44 ± 0.16	1.59 ± 0.10	0.95 ± 0.11	4.15 ± 0.18	2.39 ± 0.19	0.60 ± 0.08	0.58 ± 0.05	
	1000					4.0 ± 0.2	3.08 ± 0.10		0.77 ± 0.05	
	1500					4.0 ± 0.2	3.22 ± 0.11		0.81 ± 0.05	
	2000					3.9 ± 0.2	5.41 ± 0.18		1.39 ± 0.09	
	2500					4.5 ± 0.3	3.39 ± 0.12		0.75 ± 0.05	
	2950					5.3 ± 0.3	3.61 ± 0.12		0.68 ± 0.04	
268	10	5.2 ± 0.3	2.3 ± 0.3							
271	10	5.2 ± 0.3	2.8 ± 0.3							
272	10	4.8 ± 0.3	3.1 ± 0.3							
274	10	4.6 ± 0.2	3.0 ± 0.3	0.39 ± 0.02	0.50 ± 0.03	5.0 ± 0.2	3.5 ± 0.3	1.26 ± 0.11	0.70 ± 0.06	0.69 ± 0.03
276	10	3.8 ± 0.2	2.1 ± 0.2							
	25	2.21 ± 0.12	1.34 ± 0.13							
	50	2.36 ± 0.12	0.86 ± 0.13	0.76 ± 0.04	0.25 ± 0.04	3.12 ± 0.13	1.11 ± 0.14	0.33 ± 0.06	0.36 ± 0.05	
	75	2.10 ± 0.11	1.32 ± 0.12	1.11 ± 0.06	0.35 ± 0.06	3.20 ± 0.13	1.67 ± 0.13	0.32 ± 0.06	0.52 ± 0.05	
	100	2.60 ± 0.14	1.59 ± 0.15	0.96 ± 0.05	0.96 ± 0.07	3.56 ± 0.15	2.55 ± 0.17	1.00 ± 0.09	0.72 ± 0.06	
	200	3.21 ± 0.16	1.89 ± 0.17							
	400					3.15 ± 0.16	2.43 ± 0.07		0.77 ± 0.05	
	650					2.73 ± 0.14	2.20 ± 0.07		0.81 ± 0.05	

Station	Depth (m)	Dissolved (dpm 100L^{-1}) ^{210}Pb	Dissolved (dpm 100L^{-1}) ^{210}Po	Particulate (dpm 100L^{-1}) ^{210}Pb	Particulate (dpm 100L^{-1}) ^{210}Po	Total (dpm 100L^{-1}) ^{210}Pb	Total (dpm 100L^{-1}) ^{210}Po	^{210}Po/^{210}Pb Particulate	^{210}Po/^{210}Pb Total	^{210}Pb/^{226}Ra
S3										
279	10	3.63 ± 0.19	1.9 ± 0.2	1.28 ± 0.07	0.56 ± 0.07	4.9 ± 0.2	2.5 ± 0.2	0.44 ± 0.06	0.51 ± 0.05	0.74 ± 0.03
	25	1.40 ± 0.07	0.80 ± 0.08	0.72 ± 0.04	0.26 ± 0.04	2.12 ± 0.09	1.06 ± 0.09	0.35 ± 0.06	0.50 ± 0.05	
	50	1.17 ± 0.06	0.53 ± 0.06	0.75 ± 0.04	0.31 ± 0.04	1.92 ± 0.07	0.84 ± 0.08	0.41 ± 0.06	0.44 ± 0.04	
	75	1.63 ± 0.08	0.94 ± 0.09	1.07 ± 0.05	0.79 ± 0.06	2.70 ± 0.10	1.73 ± 0.11	0.74 ± 0.07	0.64 ± 0.05	
	100	1.94 ± 0.10	1.07 ± 0.11	0.98 ± 0.05	0.76 ± 0.05	2.92 ± 0.11	1.83 ± 0.12	0.78 ± 0.07	0.63 ± 0.05	
	200	0.90 ± 0.05	0.67 ± 0.05	0.74 ± 0.04	0.21 ± 0.04	1.64 ± 0.06	0.88 ± 0.06	0.28 ± 0.05	0.54 ± 0.04	
	320	0.55 ± 0.03	0.47 ± 0.03	1.50 ± 0.07	1.54 ± 0.09	2.06 ± 0.07	2.01 ± 0.10	1.02 ± 0.08	0.98 ± 0.06	
285	10	3.9 ± 0.2	2.1 ± 0.2							
290	10	6.6 ± 0.3	2.9 ± 0.3							
295	10	5.8 ± 0.3	2.6 ± 0.3	0.046 ± 0.003	0.160 ± 0.006	5.9 ± 0.3	2.8 ± 0.3	3.5 ± 0.2	0.47 ± 0.05	
299	10	5.9 ± 0.3	2.6 ± 0.3	0.062 ± 0.003	0.175 ± 0.008	5.9 ± 0.3	2.8 ± 0.3	2.81 ± 0.19	0.48 ± 0.06	0.91 ± 0.05
301	10	6.0 ± 0.3	2.4 ± 0.3	0.152 ± 0.009	0.119 ± 0.010	6.1 ± 0.3	2.5 ± 0.3	0.78 ± 0.08	0.41 ± 0.05	0.91 ± 0.04
	25	3.01 ± 0.15	1.10 ± 0.15	0.200 ± 0.011	0.038 ± 0.011	3.21 ± 0.15	1.13 ± 0.16	0.19 ± 0.06	0.35 ± 0.05	
	50	2.07 ± 0.10		0.56 ± 0.03	0.49 ± 0.03	2.63 ± 0.11		0.88 ± 0.07		
	75	2.34 ± 0.12	1.43 ± 0.13	0.61 ± 0.03	0.56 ± 0.04	2.95 ± 0.13	1.98 ± 0.14	0.92 ± 0.07	0.67 ± 0.05	
	100	2.12 ± 0.11	1.45 ± 0.12	0.51 ± 0.03	0.70 ± 0.04	2.64 ± 0.11	2.15 ± 0.12	1.38 ± 0.10	0.82 ± 0.06	
	150	1.82 ± 0.09	1.66 ± 0.11	0.46 ± 0.02	0.48 ± 0.03	2.28 ± 0.10	2.14 ± 0.11	1.05 ± 0.09	0.94 ± 0.06	
	200	3.04 ± 0.16	2.05 ± 0.17	0.65 ± 0.03	0.53 ± 0.03	3.70 ± 0.16	2.58 ± 0.17	0.81 ± 0.07	0.70 ± 0.06	
	300	4.5 ± 0.2	2.7 ± 0.3							
	500	3.19 ± 0.16	2.35 ± 0.17	0.72 ± 0.03	1.00 ± 0.05	3.91 ± 0.16	3.36 ± 0.18	1.38 ± 0.10	0.86 ± 0.06	
	1000					4.3 ± 0.2	2.45 ± 0.08		0.57 ± 0.04	
	1500					4.3 ± 0.2	3.86 ± 0.11		0.89 ± 0.05	
	2000					5.2 ± 0.3	5.04 ± 0.16		0.98 ± 0.06	
	3000					5.2 ± 0.3	5.32 ± 0.15		1.03 ± 0.06	
	3680					6.4 ± 0.3	4.99 ± 0.13		0.77 ± 0.04	
303	10	6.7 ± 0.3	2.6 ± 0.4	0.51 ± 0.03	*<0.004*	7.2 ± 0.3	2.6 ± 0.4	-	0.36 ± 0.05	1.10 ± 0.05
306	10	4.6 ± 0.2	1.6 ± 0.2	0.39 ± 0.02	0.24 ± 0.02	5.0 ± 0.2	1.8 ± 0.3	0.62 ± 0.07	0.36 ± 0.05	

Station	Depth (m)	Dissolved (dpm 100L^{-1})		Particulate (dpm 100L^{-1})		Total (dpm 100L^{-1})		^{210}Po/^{210}Pb		^{210}Pb/^{226}Ra
		^{210}Pb	^{210}Po	^{210}Pb	^{210}Po	^{210}Pb	^{210}Po	Particulate	Total	
309	10	4.0 ± 0.2	1.8 ± 0.2	0.37 ± 0.02	0.26 ± 0.02	4.4 ± 0.2	2.0 ± 0.2	0.70 ± 0.07	0.46 ± 0.05	0.64 ± 0.03
	25	3.00 ± 0.16	1.82 ± 0.17	0.324 ± 0.018	0.090 ± 0.019	3.32 ± 0.16	1.91 ± 0.17	0.28 ± 0.06	0.57 ± 0.06	
	50	1.79 ± 0.09	0.98 ± 0.10	0.59 ± 0.03	0.20 ± 0.03	2.39 ± 0.10	1.18 ± 0.10	0.34 ± 0.05	0.49 ± 0.05	
	75	1.65 ± 0.08	0.74 ± 0.09	0.57 ± 0.03	0.27 ± 0.03	2.22 ± 0.09	1.01 ± 0.09	0.48 ± 0.05	0.46 ± 0.04	
	100	1.60 ± 0.08	1.77 ± 0.10	0.49 ± 0.03	0.25 ± 0.03	2.09 ± 0.09	2.02 ± 0.10	0.50 ± 0.07	0.97 ± 0.06	
	150	1.36 ± 0.07	1.01 ± 0.08	0.40 ± 0.02	0.21 ± 0.03	1.76 ± 0.08	1.22 ± 0.08	0.52 ± 0.07	0.69 ± 0.06	
	200	1.85 ± 0.10	1.23 ± 0.11	0.39 ± 0.02	0.34 ± 0.02	2.25 ± 0.10	1.57 ± 0.11	0.85 ± 0.08	0.70 ± 0.06	
	300	1.89 ± 0.10	1.87 ± 0.12	0.60 ± 0.03	0.56 ± 0.04	2.49 ± 0.11	2.43 ± 0.12	0.93 ± 0.08	0.98 ± 0.07	
	500	2.70 ± 0.15	2.13 ± 0.16	0.56 ± 0.03	0.56 ± 0.04	3.26 ± 0.15	2.69 ± 0.17	1.01 ± 0.08	0.83 ± 0.06	
	1000					2.59 ± 0.14	2.21 ± 0.07		0.85 ± 0.05	
	1500					4.3 ± 0.2	3.27 ± 0.10		0.76 ± 0.05	
	2000					4.1 ± 0.2	3.56 ± 0.11		0.86 ± 0.05	
	2750	4.2 ± 0.2	2.2 ± 0.2	1.09 ± 0.06	1.23 ± 0.07	5.3 ± 0.2	3.5 ± 0.2	1.12 ± 0.09	0.65 ± 0.05	
	4365	5.7 ± 0.3	5.9 ± 0.3							
312	10	3.9 ± 0.2	1.8 ± 0.2	0.234 ± 0.015	0.87 ± 0.03	4.1 ± 0.2	2.6 ± 0.2	3.7 ± 0.3	0.64 ± 0.06	0.65 ± 0.03
S4										
320	10	4.2 ± 0.2	1.6 ± 0.2	1.21 ± 0.07	0.33 ± 0.07	5.4 ± 0.2	2.0 ± 0.2	0.28 ± 0.06	0.36 ± 0.05	
328	10	4.7 ± 0.3	2.0 ± 0.3	0.97 ± 0.05	0.27 ± 0.05	5.7 ± 0.3	2.3 ± 0.3	0.28 ± 0.05	0.41 ± 0.05	0.71 ± 0.03
	25	1.74 ± 0.09	0.76 ± 0.09	0.39 ± 0.02	0.07 ± 0.02	2.14 ± 0.09	0.83 ± 0.09	0.18 ± 0.06	0.39 ± 0.05	
	50	1.08 ± 0.06	0.85 ± 0.07	0.278 ± 0.015	0.144 ± 0.016	1.36 ± 0.06	1.00 ± 0.07	0.52 ± 0.06	0.73 ± 0.06	
	75	1.40 ± 0.07	0.90 ± 0.08	0.96 ± 0.06	0.14 ± 0.06	2.35 ± 0.09	1.04 ± 0.10	0.15 ± 0.06	0.44 ± 0.04	
	100	1.01 ± 0.05	0.60 ± 0.06	0.61 ± 0.03	0.17 ± 0.03	1.62 ± 0.06	0.77 ± 0.07	0.27 ± 0.06	0.47 ± 0.04	
	150	1.49 ± 0.08	1.20 ± 0.09	0.63 ± 0.04	0.26 ± 0.04	2.12 ± 0.08	1.46 ± 0.09	0.41 ± 0.06	0.69 ± 0.05	
	200	1.95 ± 0.10	1.41 ± 0.11	0.52 ± 0.03	0.28 ± 0.03	2.47 ± 0.10	1.69 ± 0.11	0.53 ± 0.07	0.68 ± 0.05	
	300	2.60 ± 0.13	2.57 ± 0.15	0.81 ± 0.05	0.53 ± 0.05	3.41 ± 0.14	3.10 ± 0.16	0.66 ± 0.07	0.91 ± 0.06	
	500	3.17 ± 0.16	2.65 ± 0.18	0.94 ± 0.06	0.85 ± 0.06	4.11 ± 0.17	3.50 ± 0.19	0.91 ± 0.08	0.85 ± 0.06	
	1000					4.6 ± 0.2	4.24 ± 0.12		0.93 ± 0.05	
	1500					6.4 ± 0.3	4.49 ± 0.14		0.71 ± 0.04	
	2500					8.7 ± 0.5	7.6 ± 0.2		0.87 ± 0.05	
	3900					12.2 ± 0.6	11.5 ± 0.3		0.95 ± 0.05	

Station	Depth (m)	Dissolved (dpm 100L^{-1})		Particulate (dpm 100L^{-1})		Total (dpm 100L^{-1})		^{210}Po/^{210}Pb		^{210}Pb/^{226}Ra
		^{210}Pb	^{210}Po	^{210}Pb	^{210}Po	^{210}Pb	^{210}Po	Particulate	Total	
333	10	4.4 ± 0.2	1.4 ± 0.2	0.66 ± 0.03	0.29 ± 0.03	5.1 ± 0.2	1.7 ± 0.2	0.43 ± 0.06	0.33 ± 0.05	0.58 ± 0.03
338	10	6.9 ± 0.4	1.9 ± 0.4	1.92 ± 0.12	0.77 ± 0.12	8.8 ± 0.4	2.7 ± 0.4	0.40 ± 0.07	0.30 ± 0.04	0.95 ± 0.04
	25	4.0 ± 0.2	1.3 ± 0.2	1.58 ± 0.10	0.53 ± 0.10	5.6 ± 0.2	1.9 ± 0.2	0.33 ± 0.07	0.33 ± 0.05	
	50	2.92 ± 0.16	1.28 ± 0.16	0.91 ± 0.05	*<0.004*	3.83 ± 0.16	1.28 ± 0.16	-	0.33 ± 0.04	
	75	1.41 ± 0.08	0.92 ± 0.08	0.87 ± 0.05	0.12 ± 0.05	2.28 ± 0.09	1.04 ± 0.10	0.14 ± 0.06	0.46 ± 0.05	
	100	1.38 ± 0.08	0.87 ± 0.08	0.92 ± 0.05	0.48 ± 0.05	2.30 ± 0.09	1.35 ± 0.10	0.52 ± 0.06	0.59 ± 0.05	
	150			0.95 ± 0.05	0.30 ± 0.05			0.31 ± 0.06		
	200	2.24 ± 0.12	2.02 ± 0.14	0.79 ± 0.04	0.63 ± 0.05	3.03 ± 0.13	2.65 ± 0.15	0.81 ± 0.08	0.87 ± 0.06	
	300	3.15 ± 0.17	2.12 ± 0.19	1.09 ± 0.06	0.90 ± 0.06	4.24 ± 0.18	3.0 ± 0.2	0.82 ± 0.07	0.71 ± 0.06	
	500	4.3 ± 0.2	2.6 ± 0.2	1.14 ± 0.06	1.50 ± 0.08	5.4 ± 0.2	4.1 ± 0.3	1.32 ± 0.10	0.75 ± 0.06	
	1000					5.7 ± 0.3	4.05 ± 0.12		0.71 ± 0.04	
	1500					7.7 ± 0.4	5.02 ± 0.14		0.66 ± 0.04	
342	10	8.9 ± 0.5	3.8 ± 0.5	0.89 ± 0.05	0.73 ± 0.05	9.8 ± 0.5	4.5 ± 0.5	0.82 ± 0.08	0.46 ± 0.06	1.07 ± 0.05
	25	3.89 ± 0.19	1.6 ± 0.2	0.57 ± 0.03	0.34 ± 0.03	4.5 ± 0.2	2.0 ± 0.2	0.60 ± 0.07	0.44 ± 0.05	
	50	3.05 ± 0.16	1.36 ± 0.16	1.05 ± 0.06	0.19 ± 0.06	4.10 ± 0.17	1.56 ± 0.17	0.18 ± 0.06	0.38 ± 0.04	
	75	2.40 ± 0.13	1.17 ± 0.14	1.04 ± 0.06	0.30 ± 0.06	3.44 ± 0.14	1.47 ± 0.15	0.29 ± 0.06	0.43 ± 0.05	
	100	2.14 ± 0.11	0.95 ± 0.12	0.55 ± 0.03	0.17 ± 0.03	2.69 ± 0.12	1.13 ± 0.12	0.31 ± 0.06	0.42 ± 0.05	
	150	1.20 ± 0.06	0.95 ± 0.07							
	200	1.90 ± 0.10	1.45 ± 0.11	0.79 ± 0.04	0.44 ± 0.05	2.69 ± 0.11	1.89 ± 0.11	0.55 ± 0.07	0.70 ± 0.05	
	300	3.12 ± 0.17	1.83 ± 0.18	0.83 ± 0.04	0.78 ± 0.06	3.95 ± 0.17	2.61 ± 0.19	0.94 ± 0.08	0.66 ± 0.06	
	500	3.64 ± 0.19	2.1 ± 0.2	1.19 ± 0.06	1.42 ± 0.08	4.8 ± 0.2	3.5 ± 0.2	1.19 ± 0.09	0.73 ± 0.05	
	1000					4.3 ± 0.2	4.06 ± 0.14		0.95 ± 0.06	
	1500					5.0 ± 0.3	3.91 ± 0.13		0.78 ± 0.05	
	2185					5.7 ± 0.3	3.96 ± 0.13		0.70 ± 0.05	
349	10	4.7 ± 0.3	1.9 ± 0.3	0.74 ± 0.03	0.51 ± 0.04	5.5 ± 0.3	2.4 ± 0.3	0.69 ± 0.06	0.44 ± 0.05	0.58 ± 0.03
352	10	4.2 ± 0.2	1.5 ± 0.2	0.266 ± 0.014	0.129 ± 0.015	4.5 ± 0.2	1.6 ± 0.2	0.49 ± 0.06	0.36 ± 0.06	0.52 ± 0.03
358	10	4.3 ± 0.2	1.8 ± 0.2	0.44 ± 0.02	0.15 ± 0.02	4.8 ± 0.2	1.9 ± 0.2	0.33 ± 0.05	0.40 ± 0.05	0.68 ± 0.03
363	10	3.58 ± 0.19	1.8 ± 0.2							
S5										
371	10	4.5 ± 0.2	2.0 ± 0.2	0.88 ± 0.04	0.33 ± 0.04	5.4 ± 0.2	2.3 ± 0.2	0.38 ± 0.05	0.43 ± 0.05	0.83 ± 0.04

Station	Depth (m)	Dissolved (dpm 100L^{-1})		Particulate (dpm 100L^{-1})		Total (dpm 100L^{-1})		^{210}Po/^{210}Pb		^{210}Pb/^{226}Ra
		^{210}Pb	^{210}Po	^{210}Pb	^{210}Po	^{210}Pb	^{210}Po	Particulate	Total	
377	10	2.67 ± 0.14	1.73 ± 0.15	1.59 ± 0.07	0.56 ± 0.08	4.25 ± 0.16	2.28 ± 0.17	0.35 ± 0.05	0.54 ± 0.04	0.67 ± 0.03
379	10	2.69 ± 0.15	1.49 ± 0.16							
382	10	2.16 ± 0.11	1.38 ± 0.12	2.42 ± 0.11	0.49 ± 0.11	4.58 ± 0.16	1.88 ± 0.16	0.20 ± 0.05	0.41 ± 0.04	0.73 ± 0.03
383	10	1.91 ± 0.10	1.65 ± 0.12	2.54 ± 0.12	0.48 ± 0.12	4.44 ± 0.16	2.13 ± 0.17	0.19 ± 0.05	0.48 ± 0.04	
384	10	2.32 ± 0.12	1.68 ± 0.14							
385	10	3.16 ± 0.17	1.91 ± 0.19	2.43 ± 0.15	0.55 ± 0.15	5.6 ± 0.2	2.5 ± 0.2	0.23 ± 0.06	0.44 ± 0.05	0.83 ± 0.04
	25	1.70 ± 0.09	0.82 ± 0.09	1.08 ± 0.07	7.08 ± 0.15	2.78 ± 0.11	7.89 ± 0.18	6.5 ± 0.4	2.84 ± 0.13	
	50	1.55 ± 0.08	0.68 ± 0.08	1.09 ± 0.06	0.12 ± 0.06	2.64 ± 0.10	0.80 ± 0.10	0.11 ± 0.05	0.30 ± 0.04	
	75	1.30 ± 0.07	0.72 ± 0.07	0.88 ± 0.05	0.20 ± 0.05	2.18 ± 0.08	0.92 ± 0.09	0.23 ± 0.05	0.42 ± 0.04	
	100	1.55 ± 0.08	0.90 ± 0.08	0.85 ± 0.05	0.27 ± 0.05	2.40 ± 0.09	1.17 ± 0.10	0.32 ± 0.06	0.49 ± 0.04	
	150	2.55 ± 0.14	0.22 ± 0.14	0.90 ± 0.05	0.41 ± 0.05	3.45 ± 0.15	0.63 ± 0.15	0.46 ± 0.06	0.18 ± 0.04	
	200	2.92 ± 0.17	2.23 ± 0.19	0.87 ± 0.05		3.78 ± 0.18				
	300	3.15 ± 0.17	2.14 ± 0.19	0.97 ± 0.05	0.61 ± 0.06	4.11 ± 0.18	2.75 ± 0.19	0.63 ± 0.07	0.67 ± 0.06	
	500	2.92 ± 0.15	2.03 ± 0.17	0.75 ± 0.04	0.52 ± 0.05	3.67 ± 0.16	2.55 ± 0.17	0.70 ± 0.07	0.69 ± 0.06	
	1000					3.53 ± 0.18	2.06 ± 0.06		0.58 ± 0.03	
	2000					4.4 ± 0.2	3.15 ± 0.09		0.71 ± 0.04	
	3000					6.1 ± 0.3	3.77 ± 0.10		0.62 ± 0.03	
	3455					4.5 ± 0.2	3.29 ± 0.10		0.73 ± 0.05	
387	10	5.0 ± 0.3	1.3 ± 0.3	1.88 ± 0.09	0.42 ± 0.09	6.9 ± 0.3	1.8 ± 0.3	0.22 ± 0.05	0.25 ± 0.04	
391	10	5.1 ± 0.3	1.3 ± 0.3	2.81 ± 0.14	0.49 ± 0.14	7.9 ± 0.3	1.8 ± 0.3	0.18 ± 0.05	0.23 ± 0.04	

Station	Depth (m)	Dissolved (dpm 100L^{-1})		Particulate (dpm 100L^{-1})		Total (dpm 100L^{-1})		^{210}Po/^{210}Pb		^{210}Pb/^{226}Ra
		^{210}Pb	^{210}Po	^{210}Pb	^{210}Po	^{210}Pb	^{210}Po	Particulate	Total	
400	10	4.6 ± 0.2	5.6 ± 0.3	1.31 ± 0.07	0.40 ± 0.07	5.9 ± 0.2	6.0 ± 0.3	0.31 ± 0.06	1.01 ± 0.06	0.92 ± 0.04
	25	0.55 ± 0.03	0.22 ± 0.03	0.83 ± 0.05	0.17 ± 0.05	1.38 ± 0.06	0.39 ± 0.06	0.21 ± 0.06	0.28 ± 0.05	
	50	3.33 ± 0.17	0.56 ± 0.17	0.51 ± 0.03		3.83 ± 0.18				
	75	0.50 ± 0.03	0.46 ± 0.03	0.46 ± 0.03	0.18 ± 0.03	0.96 ± 0.04	0.63 ± 0.04	0.39 ± 0.06	0.66 ± 0.05	
	100	0.35 ± 0.02	0.43 ± 0.02	0.61 ± 0.03	0.13 ± 0.03	0.96 ± 0.04	0.56 ± 0.04	0.22 ± 0.06	0.59 ± 0.05	
	150	0.67 ± 0.04	0.48 ± 0.04	0.99 ± 0.05	0.37 ± 0.05	1.66 ± 0.06	0.85 ± 0.07	0.37 ± 0.06	0.51 ± 0.04	
	200	0.68 ± 0.04	1.16 ± 0.05	1.28 ± 0.06	0.42 ± 0.07	1.96 ± 0.07	1.58 ± 0.09	0.33 ± 0.05	0.81 ± 0.05	
	300	1.41 ± 0.07	1.31 ± 0.08	0.82 ± 0.04	0.69 ± 0.05	2.23 ± 0.08	2.00 ± 0.10	0.84 ± 0.08	0.90 ± 0.05	
	500	0.78 ± 0.04	0.70 ± 0.05	1.03 ± 0.05	0.39 ± 0.06	1.82 ± 0.07	1.10 ± 0.07	0.38 ± 0.06	0.60 ± 0.05	
	1000	0.50 ± 0.02	0.35 ± 0.02							
	1015					1.89 ± 0.10	1.34 ± 0.04		0.71 ± 0.04	
404	10	3.9 ± 0.2	1.5 ± 0.2	1.24 ± 0.06	0.25 ± 0.06	5.2 ± 0.2	1.7 ± 0.2	0.20 ± 0.05	0.34 ± 0.05	
407	10	2.92 ± 0.17	1.24 ± 0.17	2.42 ± 0.12	0.75 ± 0.12	5.3 ± 0.2	2.0 ± 0.2	0.31 ± 0.05	0.37 ± 0.04	1.10 ± 0.05
	25	0.41 ± 0.02	1.99 ± 0.09	0.316 ± 0.017	0.029 ± 0.017	0.72 ± 0.03	2.02 ± 0.09	0.09 ± 0.05	2.79 ± 0.17	
409	10	10.3 ± 0.6	1.7 ± 0.6	1.30 ± 0.07		11.6 ± 0.6				3.27 ± 0.18
411	10	6.5 ± 0.4	1.6 ± 0.4							
	25	0.24 ± 0.01	0.29 ± 0.02							
	40	0.24 ± 0.01	0.22 ± 0.02	2.70 ± 0.12	2.24 0.14	2.94 ± 0.13	2.46 ± 0.14	0.83 ± 0.06	0.83 ± 0.06	

Quan d'un cel blau del nord somriguin
núvols blancs i bufi el vent
i els teus pulmons s'inflin com veles
i el sol t'escupi raigs al front.
Quan els pit-rojos i les caderneres,
els gaigs, les garses i els mussols
refilin a l'unís on una melodia
que tens al cor, potser comencis
a sospitar

Tot torna a començar, Mishima